

1-1-2015

Development of Manufacturing Systems for Nanocrystalline and Ultraine Grain Materials Employing Indexing Equal Channel Angular Pressing

Michael Wayne Hester

Follow this and additional works at: <https://scholarsjunction.msstate.edu/td>

Recommended Citation

Hester, Michael Wayne, "Development of Manufacturing Systems for Nanocrystalline and Ultraine Grain Materials Employing Indexing Equal Channel Angular Pressing" (2015). *Theses and Dissertations*. 1465. <https://scholarsjunction.msstate.edu/td/1465>

This Dissertation - Open Access is brought to you for free and open access by the Theses and Dissertations at Scholars Junction. It has been accepted for inclusion in Theses and Dissertations by an authorized administrator of Scholars Junction. For more information, please contact scholcomm@msstate.libanswers.com.

Development of manufacturing systems for nanocrystalline and ultra-fine grain materials
employing indexing equal channel angular pressing

By

Michael Wayne Hester

A Dissertation
Submitted to the Faculty of
Mississippi State University
in Partial Fulfillment of the Requirements
for the Degree of Doctor of Philosophy
in Engineering
in the Department of Industrial and Systems Engineering

Mississippi State, Mississippi

May 2015

Development of manufacturing systems for nanocrystalline and ultra-fine grain materials
employing indexing equal channel angular pressing

By

Michael Wayne Hester

Approved:

John M. Usher
(Director of Dissertation)

Stanley F. Bullington
(Committee Member)

Oliver J. Myers
(Committee Participant)

Kari Babski-Reeves
(Graduate Coordinator / Committee Member)

Jason M. Keith
Interim Dean
Bagley College of Engineering

Name: Michael Wayne Hester

Date of Degree: May 8, 2015

Institution: Mississippi State University

Major Field: Engineering

Major Professor: Dr. John M. Usher

Title of Study: Development of manufacturing systems for nanocrystalline and ultra-fine grain materials employing indexing equal channel angular pressing

Pages in Study: 288

Candidate for Degree of Doctor of Philosophy

Nanotechnology offers significant opportunities in providing solutions to existing engineering problems as well as breakthroughs in new fields of science and technology. In order to fully realize benefits from such initiatives, nanomanufacturing methods must be developed to integrate enabling constructs into commercial mainstream. Even though significant advances have been made, widespread industrialization in many areas remains limited. Manufacturing methods, therefore, must continually be developed to bridge gaps between nanoscience discovery and commercialization.

A promising technology for integration of top-down nanomanufacturing yet to receive full industrialization is equal channel angular pressing, a process transforming metallic materials into nanostructured or ultra-fine grained materials with significantly improved performance characteristics. To bridge the gap between process potential and actual manufacturing output, a prototype top-down nanomanufacturing system identified as indexing equal channel angular pressing (Ix-ECAP) was developed. The unit was designed to capitalize on opportunities of transforming spent or scrap engineering elements into key engineering commodities.

A manufacturing system was constructed to impose severe plastic deformation via simple shear in an equal channel angular pressing die on 1100 and 4043 aluminum welding rods. 1/4 fraction factorial split-plot experiments assessed significance of five predictors on the response, microhardness, for the 4043 alloy. Predictor variables included temperature, number of passes, pressing speed, back pressure, and vibration. Main effects were studied employing a resolution III design. Multiple linear regression was used for model development. Initial studies were performed using continuous processing followed by contingency designs involving discrete variable length work pieces.

IX-ECAP offered a viable solution in severe plastic deformation processing. Discrete variable length work piece pressing proved very successful. With three passes through the system, 4043 processed material experienced an 88.88% increase in microhardness, 203.4% increase in converted yield strength, and a 98.5% reduction in theoretical final grain size to 103 nanometers using the Hall-Petch relation. The process factor, number of passes, was statistically significant at the 95% confidence level; whereas, temperature was significant at the 90% confidence level. Limitations of system components precluded completion of studies involving continuous pressing. Proposed system redesigns, however, will ensure mainstream commercialization of continuous length work piece processing.

DEDICATION

To: Regina Tapp Hester, my wife and greatest soul mate in life.

Dayton Michael Hester, my son and greatest hero.

Franklin Douglas Hester, my father and greatest inspiration.

Mary Clemmons Hester, my mother and greatest supporter.

Edward Emmitt Tapp, my father in law and greatest of the “Greatest Generation”.

Mildred Hester Tapp, my mother in law and greatest lady.

ACKNOWLEDGEMENTS

This dissertation was only made possible through a shared collective effort at a very special place through a very special process by some very special people. A lengthy discourse could be written about each one; however, written word and even spoken word are woefully inadequate in capturing the true essence of contribution and specialness. Recognition, however, is appropriate and from this perspective I sincerely express my heartfelt appreciation and indebtedness. The very special place, of course, is the treasured Mississippi State University; whereas, the very special educational process that afforded me this opportunity at this point in my life is the MSU distance learning program. Most importantly are the very special people who became the enablers, challengers, and encouragers at every step of the journey. First, is my dissertation committee who will forever be considered mentors of epic proportion, and to whom I would like to thank Dr. John Usher (Committee Chair), Dr. Stanley Bullington, Dr. Kari Babski-Reeves, and Dr. Oliver Myers. Secondly, there are always the unsung heroes who made major contributions in minor ways or minor contributions in major ways. Your efforts are truly appreciated and your names forever written in my heart and mind. Lastly, to my family sincere appreciation goes to my beloved parents, Doug and Mary Hester, and my son and best friend in life, Dayton. Foremost, I thank my endeared wife, Gina, whom I have known and loved since fifth grade. This task is complete only because of your unwavering love, support, patience, and constant “cheerleading”.

TABLE OF CONTENTS

DEDICATION	ii
ACKNOWLEDGEMENTS	iii
LIST OF TABLES	vii
LIST OF FIGURES	xi
CHAPTER	
I. INTRODUCTION AND MOTIVATION	1
II. RESEARCH.....	6
Primary Research Goal	6
Problem Description	10
Hypotheses and Objectives	13
Objective 1: Manufacturing Process Development	14
Objective 2: Statistical Experimental Design	15
Objective 3: Materials Development and Characterization	15
Primary Assumptions.....	16
Specific Aim	17
Primary Hypothesis.....	17
III. REVIEW OF RELEVANT LITERATURE	18
Nanotechnology	18
Overview of Nanotechnology	18
Nanomanufacturing Approaches	19
Traditional versus Nanostructured Materials.....	20
Severe Plastic Deformation Processing	23
Overview of Severe Plastic Deformation	23
Equal Channel Angular Pressing	27
Accumulated Roll Bonding.....	28
High Pressure Torsion.....	30
Equal Channel Angular Pressing Review	31
Methods.....	32
Rotary Die ECAP.....	33
Con-Shearing ECAP	33

Equal Channel Angular Rolling.....	34
Conform Process.....	35
Incremental Equal Channel Angular Pressing.....	35
Work Piece Forms.....	36
Materials.....	36
Parameters.....	37
Die Design.....	38
Number of Passes.....	40
Processing Route.....	41
Pressing Temperature.....	42
Pressing Speed.....	43
Friction.....	43
Back Pressure.....	43
Aspect Ratio.....	44
Punch Force.....	44
Material Properties.....	45
Vibrational Energy.....	45
IV. EXPERIMENTAL METHODS AND MATERIALS.....	47
Experimental Development Rationale.....	47
Method - Indexing Equal Channel Angular Pressing.....	49
Facilities and Equipment.....	54
Die Design.....	61
Die Insert and Holding Block.....	63
Pressing Die.....	66
Clamping Die.....	68
Reinforcing Guides.....	70
Heat Treatment.....	71
Hydraulic Force Systems.....	76
Pressing Force.....	76
Clamping Force.....	82
Cylinder Speed and Motion Control.....	88
Hydraulic Power Unit.....	91
Vibration System.....	91
Back Pressure.....	94
Heating System.....	98
Materials - Alloy Selection and Work Piece Form.....	102
Materials Characterization.....	108
Mechanical Properties.....	108
Grain Size and Morphology.....	108
V. EXPERIMENTAL DESIGN.....	110
Fractional Factorial Split-Plot (FFSP).....	110
Multiple Regression Analysis.....	115

VI.	RESULTS AND DISCUSSION	119
	Continuous Length Processing	120
	Variable Length Discrete Processing.....	127
	Variable Length Discrete Rods.....	128
	Face Plate Redesign	132
	Clamping System and Plunger Redesign	133
	Heating System Redesign	134
	Back Pressure Mechanism Redesign	138
	Pressing Speed	140
	Vibration	146
	Preliminary Feasibility Trials	150
	Fractional Factorial Split-Plot (FFSP) Experimental Trials	153
	4043 Aluminum Alloy	158
	Materials Development.....	185
	4043 Aluminum	188
	1100 Aluminum	200
VII.	SUMMARY AND CONCLUSIONS	201
	Summary.....	201
	Conclusions.....	202
	Manufacturing Process Development.....	202
	Statistical Methods.....	204
	Materials Development.....	205
	Future Research	206
	Manufacturing Methods and Procedures	206
	Statistical Methods.....	207
	Materials Development.....	207
	REFERENCES	210
	ADDITIONAL BIBLIOGRAPHY.....	217
	APPENDIX	
A.	EXPERIMENTAL DATA.....	230
	4043 Aluminum Alloy - Research Data Sheets	231
	1100 Aluminum Alloy - Research Data Sheets	256
B.	THERMAL REQUIREMENTS	281
	Process Description.....	282
	Considerations.....	283
	Wattage Requirement Calculations.....	284

LIST OF TABLES

3.1	Materials processed by equal channel angular pressing.....	37
4.1	Chemical compositions of D2 tool steel and 1018 carbon steel	62
4.2	Chemical compositions of D2 tool steel and 1018 carbon steel	62
4.3	Die component heat treatments	75
4.4	Hydraulic cylinder size versus extension force.....	86
4.5	Hydraulic pressing speed versus flow rate for four inch cylinder.....	89
4.6	Chemical compositions of 1100 and 4043 aluminum and AWS 5.27 copper alloy	104
4.7	Room temperature mechanical properties of annealed 1100 and 4043 aluminum and AWS 5.27 copper alloy	104
4.8	Chemical composition of 316L stainless steel	105
4.9	Room temperature mechanical properties of annealed 316L stainless steel.....	105
4.10	Heat treat schedules for 1100 and 4043 aluminum, brass, and 316L stainless steel baseline materials	106
5.1	Initial DOE experimental factors	112
5.2	Design table for fractional factorial split-plot experiment (randomized).....	114
6.1	Processing strain rates for 1100 and 4043 alloys at low and high pressing speeds	146
6.2	DOE experimental factors	154
6.3	Design table for fractional factorial split-plot experiment (randomized).....	156
6.4	Design matrix and data display for split-plot ¼ fraction factorial for 4043 aluminum.....	159

6.5	Analysis of variance for hardness (coded units) for 4043 aluminum	164
6.6	Estimated effects and coefficients for hardness for 4043 aluminum	166
6.7	Error sum of squares for multivariate regression adding predictor variables for 4043 aluminum.....	167
6.8	Coefficients of partial determination for multivariate regression adding predictor variables for 4043 aluminum	168
6.9	Residuals table for 4043 aluminum using the full model regression equation	171
6.10	Hardness conversions of 4043 baseline and processed samples from Vickers to Brinell	191
6.11	Brinell hardness and yield strength values for O, H14, and H18 tempers for 4043 aluminum	192
6.12	Hall-Petch calculated yield strength for 4043 baseline aluminum sample	196
6.13	Hall-Petch calculated grain size, d, for 4043 processed maximum hardness aluminum sample	198
6.14	Hall-Petch grain size determination for 4043 aluminum mean hardness.....	199
A.1	Research data sheet – 4043 – sample 1	232
A.2	Research data sheet – 4043 – sample 2	233
A.3	Research data sheet – 4043 – sample 3	234
A.4	Research data sheet – 4043 – sample 4	235
A.5	Research data sheet – 4043 – sample 5	236
A.6	Research data sheet – 4043 – sample 6	237
A.7	Research data sheet – 4043 – sample 7	238
A.8	Research data sheet – 4043 – sample 8	239
A.9	Research data sheet – 4043 – sample 9	240
A.10	Research data sheet – 4043 – sample 10	241
A.11	Research data sheet – 4043 – sample 11	242

A.12	Research data sheet – 4043 – sample 12	243
A.13	Research data sheet – 4043 – sample 13	244
A.14	Research data sheet – 4043 – sample 14	245
A.15	Research data sheet – 4043 – sample 15	246
A.16	Research data sheet – 4043 – sample 16	247
A.17	Research data sheet – 4043 – sample 17	248
A.18	Research data sheet – 4043 – sample 18	249
A.19	Research data sheet – 4043 – sample 19	250
A.20	Research data sheet – 4043 – sample 20	251
A.21	Research data sheet – 4043 – sample 21	252
A.22	Research data sheet – 4043 – sample 22	253
A.23	Research data sheet – 4043 – sample 23	254
A.24	Research data sheet – 4043 – sample 24	255
A.25	Research data sheet – 1100 – sample 1	257
A.26	Research data sheet – 1100 – sample 2	258
A.27	Research data sheet – 1100 – sample 3	259
A.28	Research data sheet – 1100 – sample 4	260
A.29	Research data sheet – 1100 – sample 5	261
A.30	Research data sheet – 1100 – sample 6	262
A.31	Research data sheet – 1100 – sample 7	263
A.32	Research data sheet – 1100 – sample 8	264
A.33	Research data sheet – 1100 – sample 9	265
A.34	Research data sheet – 1100 – sample 10	266
A.35	Research data sheet – 1100 – sample 11	267
A.36	Research data sheet – 1100 – sample 12	268

A.37	Research data sheet – 1100 – sample 13	269
A.38	Research data sheet – 1100 – sample 14	270
A.39	Research data sheet – 1100 – sample 15	271
A.40	Research data sheet – 1100 – sample 16	272
A.41	Research data sheet – 1100 – sample 17	273
A.42	Research data sheet – 1100 – sample 18	274
A.43	Research data sheet – 1100 – sample 19	275
A.44	Research data sheet – 1100 – sample 20	276
A.45	Research data sheet – 1100 – sample 21	277
A.46	Research data sheet – 1100 – sample 22	278
A.47	Research data sheet – 1100 – sample 23	279
A.48	Research data sheet – 1100 – sample 24	280

LIST OF FIGURES

2.1	Traditional equal channel angular pressing (ECAP).....	7
2.2	Equal channel angular pressing dies	8
2.3	Grain size reductions for interstitial free steels after subsequent passes of ECAP.	9
3.1	Accumulated roll bonding process	29
3.2	High pressure torsion process	30
3.3	Equal channel angular pressing process.....	32
3.4	Rotary die ECAP	33
3.5	Con-shearing ECAP	34
3.6	Equal channel angular rolling – ECAR.....	34
3.7	ECAP conform process	35
3.8	Incremental ECAP.....	36
3.9	ECAP die angles.....	39
3.10	Channel angel, Φ , versus strain, ε	40
3.11	Schematic of varying die Angle, Φ , and Ψ	40
3.12	Processing routes.....	42
3.13	Effect of back pressure	44
4.1	Research progression flow chart	49
4.2	Step 1 of I _X -ECAP conceptual design.....	51
4.3	Step 2 of I _X -ECAP conceptual design.....	52
4.4	Step 3 of I _X -ECAP conceptual design.....	53

4.5	Step 4 of I _X -ECAP conceptual design.....	54
4.6	Cross-sectional view of concept design of the I _X -ECAP process	56
4.7	Front view of manufacturing unit.....	57
4.8	Rear view of manufacturing unit.....	58
4.9	Close-up view of pressing components of the system	59
4.10	Close-up view of clamping components of the system.....	59
4.11	View of completed manufacturing unit.....	60
4.12	Unassembled die components	61
4.13	Die inserts.....	64
4.14	Die inserts ready for process runs	65
4.15	Die insert being removed from holding block with a hand held magnet tool during processing	66
4.16	Pressing die	67
4.17	Horizontally parted clamping die	69
4.18	Clamping die with horizontally mounted chuck component	70
4.19	Reinforcing guides	71
4.20	Heat treatment facilities for D2 tool steel dies	72
4.21	D2 tool steel dies packed in cast iron chips to minimize surface oxidation.....	73
4.22	Clamping die during surface heat treatment.....	74
4.23	Pressing forces for 0.125-inch diameter 316 stainless steel rod with 0.25 tons of back pressure force (m = 0.125).....	81
4.24	Pressing forces for 0.15625-inch diameter 316 stainless steel rod with 0.25 tons of back pressure force (m = 0.125).....	81
4.25	Horizontally mounted hydraulic cylinder for pressing force	82
4.26	Conventional friction force analysis	83

4.27	Friction force analysis for clamping die.....	83
4.28	Clamping die conceptual design cross section.....	85
4.29	Hydraulic cylinder performance curves.....	86
4.30	Vertically mounted hydraulic cylinder.....	88
4.31	Dual-control mono-block directional 8-gpm 4-way/3-position spring center flow control valve.....	90
4.32	Flow control valves mounted in manufacturing unit.....	91
4.33	Miniature pneumatic vibrator.....	92
4.34	Vibrator air supply.....	93
4.35	Concept design of cross section view of back pressure components.....	94
4.36	Back pressure spring force.....	97
4.37	Back pressure components mounted to the die insert holding block.....	97
4.38	Temperature controllers for clamping and pressing dies.....	99
4.39	Cartridge heaters.....	99
4.40	Cartridge heaters and thermocouple inserted into pressing die.....	100
4.41	Envirotrol® thermal insulation coating applied to die components.....	100
4.42	Thermally insulated pressing and clamping dies placed in manufacturing unit.....	101
4.43	Thermal images of pressing die.....	101
4.44	Sample rods ready for processing.....	107
6.1	Basic components of original Ix-ECAP process.....	120
6.2	Continuous rod inserted through back side of clamping chuck and die ready for pressing.....	121
6.3	Close-up view of aluminum rod extending through die face plates.....	124
6.4	Copper rod extending through die face plates.....	125

6.5	Pressed aluminum rod extending through pressing die face plate after continuous pressing	126
6.6	Continuous and discrete length work pieces	129
6.7	4043 aluminum rods showing 1, 2, and 3 presses through the system	130
6.8	1100 aluminum rods showing 1, 2, and 3 presses through the system	131
6.9	Clamping and pressing die face plates redesign.....	132
6.10	Ejector pin used as plunger	133
6.11	Infrared thermal image of front side of die insert holding block and face plates during 4043 aluminum rod processing	134
6.12	Infrared thermal image of rear view of die insert holding block and face plates prior to 4043 aluminum rod processing	135
6.13	Infrared thermal image of rear view of die insert holding block and face plates during 4043 aluminum rod processing	135
6.14	Temperature curves for 4043 and 1100 aluminum die heating system for DOE blocks 1, 2, and 3	136
6.15	Statistical summary of high temperature capability of heating system.....	137
6.16	Spring loaded back pressure mechanism	138
6.17	Static loaded back pressure mechanism	139
6.18	Back pressure rod and slip collar	140
6.19	Flow control valves for pressing speed.....	142
6.20	Statistical and graphical summary of slow pressing speeds.....	144
6.21	Statistical and graphical summary of fast pressing speeds	145
6.22	Pneumatic vibrator and air supply.....	147
6.23	Vibration monitoring instrument.....	148
6.24	Regulated air pressure and vibration analysis	149
6.25	Pressing unit during actual experimental runs	157

6.26	4043 aluminum rods showing 1 pass through the system for run order #2	161
6.27	4043 aluminum rods showing 3 passes through the system for run order #1	162
6.28	4043 aluminum rods sectioned and mounted in epoxy for micro hardness and metallographic analysis	163
6.29	Main effects plot for response variable, hardness, for 4043 aluminum	165
6.30	Plot of full model fitted values versus actual hardness for observation runs of 4043 aluminum	172
6.31	Normal probability plot of residuals for 4030 aluminum	173
6.32	Histogram of residuals for 4043 aluminum.....	173
6.33	Plot of residuals versus run order for 4043 aluminum	174
6.34	Plot of residuals versus actual hardness for 4043 aluminum	175
6.35	Plot of residuals versus fits for 4043 aluminum.....	175
6.36	Plot of residuals versus temperature for 4043 aluminum.....	176
6.37	Plot of residuals versus number of passes for 4043 aluminum	177
6.38	Plot of residuals versus back pressure for 4043 aluminum.....	177
6.39	Plot of residuals versus pressing speed for 4043 aluminum	178
6.40	Plots of residuals versus vibration for 4043 aluminum.....	178
6.41	Tests for equal variances of residuals for A (Temperature) for 4043 aluminum.....	180
6.42	Tests for equal variances of residuals for B (Number of Passes) for 4043 aluminum.....	181
6.43	Tests for equal variances of residuals for C (Back Pressure) for 4043 aluminum.....	182
6.44	Tests for equal variances of residuals for D (Speed) for 4043 aluminum.....	183
6.45	Tests for equal variances of residuals for E (Vibration) for 4043 aluminum.....	184

6.46	Aluminum – silicon phase diagram.....	186
6.47	Microstructure of 1100 (commercial purity) aluminum alloy. Insoluble particles of aluminum-iron and aluminum-iron-silicon (dark) in aluminum matrix (light)	187
6.48	Microstructure of 4043 aluminum alloy. Silicon particles (gray) in aluminum matrix (light)	187
6.49	Individual value plot of Vickers microhardness versus number of passes at low and high temperatures for 4043 aluminum.....	188
6.50	Flowchart for the materials development analysis of 4043 aluminum processed by the manufacturing system.....	190
6.51	Yield strength versus Brinell hardness for 4043 aluminum	193
6.52	Microstructures of un-pressed 4043 aluminum. Sections from longitudinal and transverse directions (sample #A4B2)	194
6.53	Etched microstructure of transverse section of un-pressed baseline 4043 aluminum rod (sample #A4B2) color tinted to reveal grain boundaries	195
6.54	Scatter plot of Hall-Petch grain size versus number of passes at low and high temperature for 4043 aluminum based on converted mean hardness.....	199
6.55	Microstructures of un-pressed 1100 aluminum. Sections from longitudinal and transverse directions (sample #A1B1)	200
B.1	Pressing and clamping die dimensions.....	283
B.2	Cartridge heater	288

CHAPTER I

INTRODUCTION AND MOTIVATION

Success of engineered systems, whether simple or complex, depends not only on the application of proven methodologies but also the integration of new and innovative technologies (Kossiakoff and Sweet, 2003). This criterion is especially true in today's rapidly developing modern era. To attain success in system efficiency and effectiveness, scientists, engineers, and technologists representing many key disciplines have played pivotal roles in the design, development, and optimization of manufacturing processes. A continuation of the successes of these roles, however, is dramatically impacted by technological innovation and contingent on the ability of personnel to understand and integrate these new technologies into existing or newly developed systems (Kuo, 2007).

One such innovation providing challenges as well as significant opportunities is the intentioned application of nanoscale science and technology. Nanotechnology affords the design, development, and manipulation of matter, components, and structures at dimensions approaching billionths of a meter with the potential realization of non-traditional or novel properties or characteristics (Poole and Owens, 2003). Within this burgeoning field is found both incremental as well as radical departure opportunities for system improvements providing exciting insight towards resolution of future, existing, traditional, and even legacy engineering problems.

For example, one of the oldest and more traditional industries is the iron casting industry dating back over 2,000 years. Even with advances throughout this storied history, the basic manufacturing constructs of melting, molding, and casting of iron into useful components remains essentially the same (Huang, 2010). A significant problem in recent years as experienced in other industrial sectors is the increasing price of raw materials. Specifically for the iron casting industry, the primary energy source for melting iron is foundry coke used in cupola furnaces. During a six year period from 2002 to 2008 the commodity price of foundry coke increased 450 % (Huang, 2010). Survival, therefore, hinged on the development of an alternative or supplemental fuel. Limited success efforts addressing this problem had been underway since the early 1970's focusing on innovative methods to use waste anthracite or foundry coke fines as agglomerated briquettes as the replacement fuel source. The major problem inhibiting success involved the lack of sufficient binding strength for the agglomerated fines at elevated temperatures. During the iron melting process, the weight of charge materials in the furnace stack crushed the briquettes to inefficient and unusable fines. Recent discoveries employing nanotechnology constructs validated within actual manufacturing settings provided the critical breakthrough (Huang, 2010). Based on development of coordinated growth and natural interlocking of silicon dioxide nanowires on anthracite surfaces, the binding strength was dramatically improved to levels previously unattainable, thereby, enabling successful use of anthracite briquettes in cupola operations. These initial discoveries based on new insights from nanotechnology provided the technological pathway whereby foundries could reduce their dependency on

foundry coke as the predominant fuel source within their respective manufacturing processes by 25 to 40 percent (Huang, 2010).

With many engineering systems being comprised of assemblies, sub-assemblies, components, and individual parts, a major decisive contributor to successful operation of such systems is the material performance characteristics of the respective elemental components comprising the system. For example, a biomedical engineering system comprised of titanium parts used in total hip replacements serves to ameliorate negative effects of degenerative joint diseases. Such systems are based on the surgical procedure identified as total joint replacement (TFR) arthroplasty. Even though successful in most instances, re-current surgeries were required in 12.8% of the 152,000 cases reported in the year 2000 (Colombo, 2010). This equates to almost 20,000 persons needing follow-up invasive procedures. A primary cause of mechanical failure of hip replacements results from an intriguing phenomenon of stress shielding due to differences in stiffness or modulus values between bone and implanted material. Modulus values of available biocompatible alloys possessing the necessary strength levels required for hip replacements are much greater than the modulus values of bone. Therefore, during physical activity, stresses are carried by the titanium components possessing the greater stiffness. This effect results in an un-equal distribution of loads between bone and implant. Based on the principle of Wolff's Law whereby additional bone mass is transferred to highly stressed areas and removed from low stressed areas, a degeneration of bone takes place at the hip which transfers additional loads to the implant. The end result, therefore, is subsequent premature failure of the titanium implants. A solution to the problem is found in utilizing alloys with lower stiffness. Reducing the stiffness of

traditional metallic materials, however, is achieved with concomitant decreases in strength. As a result, various β -type titanium alloys with good biocompatibility and lower moduli possess insufficient strength required for hip applications (Colombo, 2010). The answer to the problem, therefore, is dependent on the development of technologies that allow improvements in strength of metal alloys with only minor increases in stiffness or no commensurate increases at all. One such method with the potential to achieve non-traditional performance characteristics is the top-down nanomanufacturing process referred to as Equal Channel Angular Pressing (ECAP). During this process, titanium rods are pressed through a die with intersecting entrance and exit channels having equal cross sections. Even though the size of the component remains unchanged, the extreme straining of the metal as it passes through the die produces ultra-fine or nanocrystalline grains. Resulting novel microstructures enable titanium components to be manufactured offering opportunities of modified material properties for use as medical implants (Latysh, Krallics, Alexandrov, and Fodor, 2006).

These examples representing totally different problem resolutions across disciplines, fields, and industries provide insight to the contribution of nanotechnology in helping ensure the survival of entire industries as well as enhancing the quality of life. Advancement and integrated application of nanoscale science and technology plays a vital role in continued societal development. Actual industrialization and commercialization in many nanotechnology areas, however, remains in the infancy stage of life cycle development (Salerno, Landoni, and Verganti, 2008). Therefore, design and development of economic manufacturing processes in these respective areas is crucial

towards enabling the realization and application of such technologies. Contributing to this process of nanotechnology progression provides the motivation for this research.

CHAPTER II

RESEARCH

Primary Research Goal

Throughout the history of materials development, especially metallic systems, the quest has been directed at attaining the highest performance characteristics per unit weight of material. This scenario is especially critical to industries such as transportation which includes aerospace, automotive, rail, and maritime. Each of these respective applications requires high performance materials of lightweight construction (Azushima, Kopp, Korhonen, Yang, Micari, Lohoti, Groche, Tanagimoto, Tsuji, Rosochowski, and Hanagida, 2008). One of the key parameters is the attainment of even higher material strength while at the same time retaining excellent ductility. Typically, these two performance characteristics are mutually exclusive; increasing strength is achieved at the expense of ductility and vice versa. However, with a focus on performance gains from diverse applications of nanotechnology, these mutually exclusive restrictions are being challenged and overcome (Valiev, Alexandrov, Zhu, and Lowe, 2002).

One particular method which has proven successful in overcoming traditional materials performance barriers is referred to as Equal Channel Angular Pressing (ECAP). Originally developed by Segal in Russia during the 1970s, this process has proven capable of achieving significant improvements in performance characteristics in numerous metallic systems (Segal, 1999). For example, without altering the external

dimensions of the submitted work piece, metal components have experienced 323 percent increases in yield strength while retaining elongations of 34 percent after only one pass through ECAP (Qu, Huang, Gao, Yang, Wu, Zang, and Zhang, 2008). One of the main advantages of the process is simplicity. As shown conceptually in Figure 2.1, a metal sample or work piece is inserted into the entrance channel and simply pushed or pressed through the die using a plunger. Instead of flowing through the die, the metal is sheared under intense strain as it traverses the turn at the bend with angle, Φ . These intense strains impose extreme distortion or severe plastic deformation in the region depicted by angle, Ψ , subsequently, reducing the metal's internal microstructural grain size into the ultra-fine (100 to 1,000 nanometers) or nanoscale (≤ 100 nanometers) regimes (Zhu, Valiev, Langdon, Tsuji, and Lu, 2010).

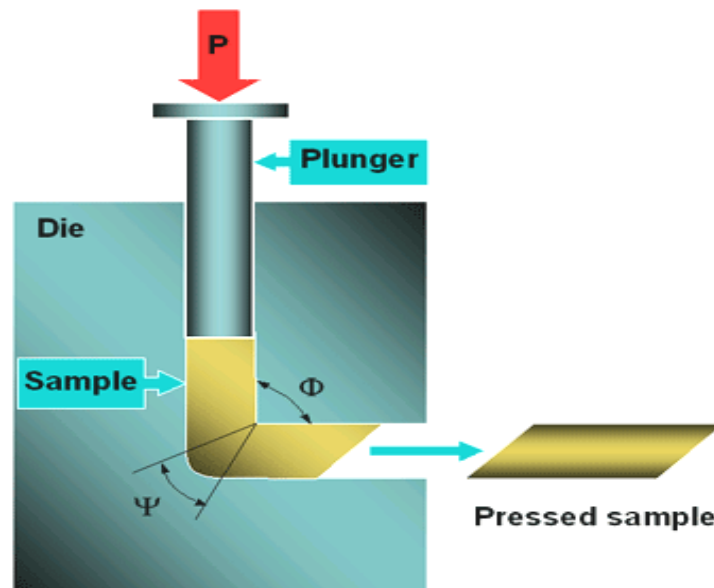


Figure 2.1 Traditional equal channel angular pressing (ECAP)

Reference: <http://www.ame-www.usc.edu>

To provide further clarification of the methodology, actual ECAP dies with pressed work pieces are illustrated in Figure 2.2.

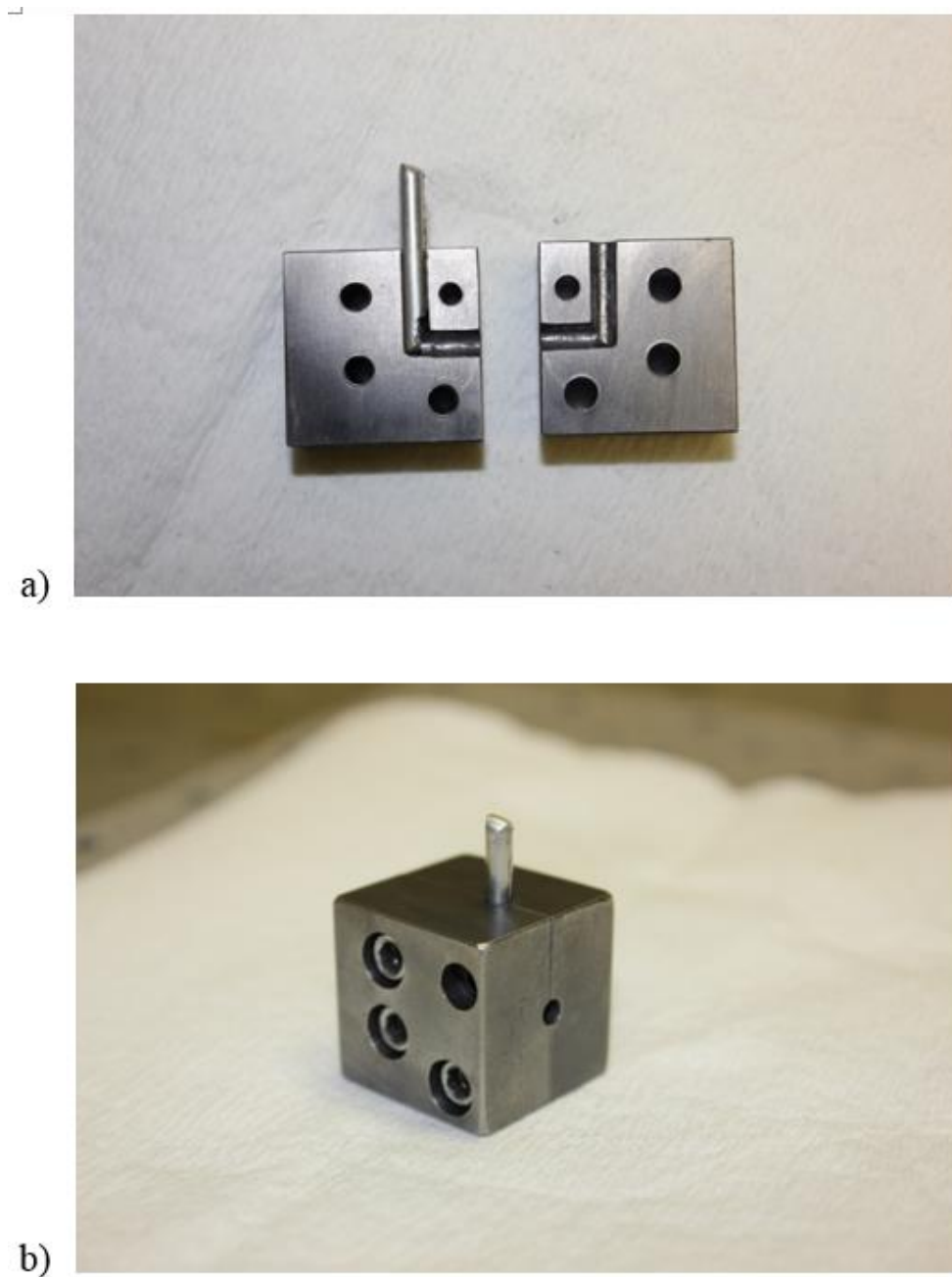


Figure 2.2 Equal channel angular pressing dies

- a) Unassembled ECAP die with pressed sample in exit channel
- b) Assembled ECAP die with pressed sample exiting the die

Using equal channel angular pressing, samples can be processed repeatedly through the die since the work piece dimension remains unchanged, thereby, allowing progressive reductions in the microstructural grain size as illustrated in Figure 2.3 (Yoon, Yoo, Kim, Baik, and Kim, 2010).

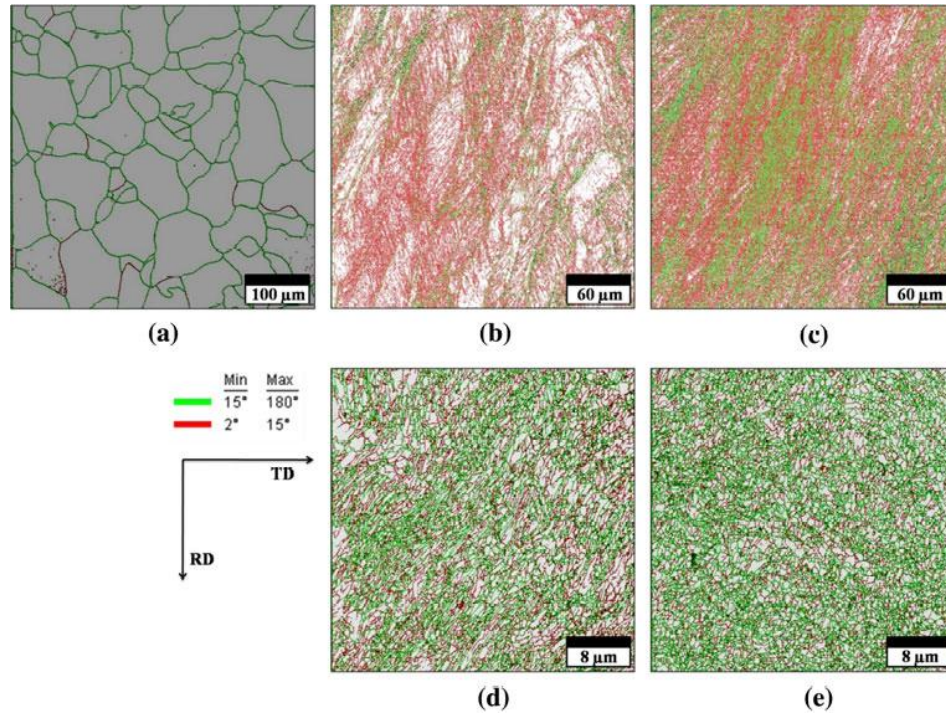


Figure 2.3 Grain size reductions for interstitial free steels after subsequent passes of ECAP.

- a) Initial material
- b) 1 pass
- c) 2 passes
- d) 4 passes
- e) 8 passes

These efforts are motivated by a primary objective of reducing the grain size of the internal microstructure into ultra-fine grain or nanoscale dimensions. Attainment of this goal affords significant potential material property enhancements primarily

prescribed by the Hall-Petch relationship which defines an inverse dependence between a material's grain size and the resulting yield strength at room temperature. As grain size is reduced, yield strength of the material increases as follows (Valiev and Langdon, 2006):

$$\sigma_y = \sigma_0 + k_y d^{-1/2} \quad (2.1)$$

where,

σ_y is the material's yield strength

σ_0 is the material's friction stress

k_y is a material constant for yielding

d is the material's internal grain size

This important theoretical construct provides the generalized relationship between grain size of a material and its respective strength. However, as grains become progressively smaller towards the ultra-fine and nanoscale regime, departures from the Hall-Petch relation have been reported (Haouaoui, 2005). In other words, at some limiting grain size, reportedly 10 nanometers and smaller, the strength of the material decreases as the grain size decreases.

Problem Description

Substantial research has been conducted on the process of equal channel angular pressing since the original works of Segal. These endeavors have resulted in well documented substantiations of processing advantages, disadvantages, parameters, and material performance outcomes (Valiev and Langdon, 2006). A general consensus related to these findings is the consensus that ECAP is one of the most promising technologies for integration of top-down nanomanufacturing into industrial

commercialization mainstream (Zhu, Lowe, and Langdon, 2004). In lieu of this prediction, however, widespread acceptance and realization of manufacturing processes supporting such an initiative is still lacking. Even though numerous ECAP modifications have been proposed or patented, a dominant design for ECAP manufacturing has yet to be realized (Lowe, 2006). Primary obstacles to industrial commercialization are related to cost and economies of scale. For example, one of the key obstacles is the fact that basic ECAP is a batch process, i.e., a work piece is inserted into the die, pressed, and then removed. Repeated processing to achieve even finer grain sizes and enhanced properties requires labor intensive re-insertion of the work piece into the die. A second major limitation of traditional ECAP is the length dimension of potential work pieces. As can be seen from the die set up, the plunger presses the sample through the length of the entrance channel. A major factor of concern is related to buckling of the plunger as the pressing force is applied. As a result, limitations on the aspect ratio (length/width or diameter) of the entrance channel must be enforced. Therefore, traditional ECAP is limited to relatively short work pieces.

Even though scale up to extremely large components is viable with proper design and development of manufacturing equipment, limitations of batch processing and work piece dimensions must be overcome. Solutions to these respective issues have been addressed through design of continuous ECAP processes (Xu, Schroeder, Berbon, and Langdon, 2010). However, these methods typically employ complex roller and/or die systems requiring more extensive ancillary equipment. A simple manufacturing system employing traditional ECAP dies with modifications to facilitate continuous or semi-continuous processing of variable length work pieces is needed. A new method is

proposed within this research referred to as Indexing Equal Channel Angular Pressing (I-ECAP).

This research, therefore, is based on the primary goal of substantiating the realization that ultra-fine grained or nanocrystalline structural materials can be economically produced in commercialized quantities and appropriate sizes at scale-up manufacturing process levels. As noted previously, research has identified metallic materials possessing nanoscale and ultra-fine grain microstructural typologies exhibiting orders of magnitude improvements in critical performance characteristics. Producing such materials requires considerations of potentially significant changes in processing parameters, performance characterizations, and manufacturing methods. Therefore, the hypothesis is proposed that differences exist between performance characteristics and processing parameters for traditional and nanocrystalline or ultra-fine grained structural materials employing the Indexing Equal Channel Angular Pressing method. A study based on the equal channel angular pressing (ECAP) process will manufacture rods employing a newly developed top down nano-manufacturing approach.

The objective of this research will be to identify and quantify the differences between performance characteristics for baseline traditional versus nanoscale or ultra-fine grain metallic rods using severe plastic deformation manufacturing methodologies. Equipped with knowledge contributions gained from this research, the ultimate long-term goal is the development of comprehensive systems providing enabling constructs ensuring capable, reproducible, and optimal large-scale production of ultra-fine grain (UFG) or nanocrystalline (NC) components.

Hypotheses and Objectives

The integration of traditional methods for control of processes during the manufacture of nanostructured materials provides enabling technologies allowing the transition from laboratory investigations to industrial manufacture of nanostructured materials, components, and systems. Specifically, in the case of equal channel angular pressing, traditional dies and ancillary equipment can be modified to accomplish nanomanufacturing constructs (Osman, Rardon, Friedman, and Vega, 2006). From a scientific and engineering multi-disciplinary perspective, a plethora of research has focused on the basic science and characterization of nanostructured materials, and limited research is available which addresses individually applied statistical techniques or procedures required for manufacturing process conditions within a nanomanufacturing environment. From a holistic viewpoint whereby a manufacturing system is designed, developed, and implemented specifically for nanostructured materials processing based on nanoscience constructs, research is even more limited. Given the astounding total projected U.S. market growth rate exceeding thirty percent annually for industrial integration of nanotechnology through the year 2020, further advances in research that develop engineering systems congruent with the foundations of nanoscale science and technology will greatly enhance eclectic nanotechnological contributions to society (Osman et al., 2006). The long-term goal of this research, therefore, is the development of manufacturing constructs enabling capable, reproducible, and optimal large-scale production of ultra-fine grain or nanocrystalline components. Three objectives associated with the proposed research include the following:

Objective 1: Manufacturing Process Development

The first objective is to design and develop a new manufacturing process with defined parameters for production of ultra-fine grain (UFG) or nanocrystalline (NC) structural materials. Several manufacturing methods, specifically equal channel angular processing, have successfully been employed using severe plastic deformation to achieve UFG or NC materials. However, continuous production of product forms such as metal rods in varying lengths is a limiting factor in transfer of technology to industrial settings and commercial viability. Indexing Equal Channel Angular Pressing (Ix-ECAP) reported within this research represents a new method intended to overcome this aforementioned limitation. A detailed discussion of the design of the proposed manufacturing method along with process parameterization is presented to help further the development of new and advanced manufacturing methodologies.

To warrant further scientific, technical, and economic interest and justification, an application of the technology towards resolution of a sustainable engineering problem is proposed. For example, one of the most common methods for joining structural components involves welding. A significant proliferation of this manufacturing process is found in notable industries such as general construction, economic infrastructures, chemical processing, aviation, and nuclear. The consequent nature of the welding process itself produces spent electrodes or scrap metal lengths of unused rods. These remaining pieces are typically discarded or recycled as scrap. However, implementation of the newly developed Indexing Equal Channel Angular Pressing (Ix-ECAP) process provides a critical alternative in transforming welding scrap into vital engineering materials with mechanical properties of vast potential importance. The feasibility of

inducing severe plastic deformation and subsequent strain hardening within these recycled product forms employing I_X-ECAP manufacturing methodologies is presented and discussed.

Objective 2: Statistical Experimental Design

The second primary objective involves the design and development of statistical experimentation to assess manufacturing process parameters within the newly developed Indexing Equal Channel Angular Pressing (I_X-ECAP) method. Manufacturing feasibility employing indexing equal channel angular pressing is dependent on the proper selection and combinatorial settings of the defined parameters for the process. This respective feasibility is measured by the outputs of the process, that being metallic rods possessing acceptable structural integrity and significantly improved material properties. Statistical design of experiments will be employed for process development involving fractional factorial split-plot (FFSP) designs and subsequent multiple linear regression predictor models. With indexing equal channel angular pressing being a newly developed manufacturing process, iterative application of statistical techniques during process development for I_X-ECAP extends previous statistical design of experimental efforts employed with traditional ECAP. Therefore, detailed analysis of statistical experimental design methodologies used during development of the new process are reported within the research analyses.

Objective 3: Materials Development and Characterization

A third major objective is to identify and quantify resulting material performance characteristics for traditional versus ultra-fine grain or nanocrystalline components

produced by the newly developed I_X-ECAP process. Commercial acceptance and economic integration is profoundly dependent on the resulting material properties attained offering potentially significant improvements to existing products and components or the discovery of unrealized product offerings. Material systems utilized in this research represent mainstream industrial metals, i.e., aluminum alloys, reflecting traditional familiarity and widespread acceptance within economic commerce. Therefore, research findings regarding metallurgical alterations, subsequent mechanical properties, and constitutive relationships are reported to provide a basis for prediction and reliability of material performance characteristics.

Primary Assumptions

Primary assumptions supporting the initiatives within this research include the following: 1) traditional or classical materials and metallurgical theory provides a systematic framework for material processing, methodologies, and constructs, 2) industrial enabling technologies exist providing manufacturing constructs for successful implementation of top-down nanomanufacturing viability, 3) nanoscience operates according to scientifically based principles of physics, and 4) stochastic systems are active and operate according to the laws of statistics and probability theory.

The proposed research is industrial and laboratory based whereby selected materials were studied for ultra-fine grain (UFG) or nanocrystalline (NC) manufacture in a small-scale production-oriented facility and, subsequently, characterized in research and/or commercial laboratory facilities. Secondary goals for this research are to provide manufacturing information regarding processing variables and to contribute to materials

databases regarding the structure-property relationships for the respective materials produced.

Specific Aim

The specific aim is to identify and quantify the material performance characteristics in terms of mechanical properties and grain size for traditional and nanocrystalline or ultra-fine grain rods produced via the Indexing Equal Channel Angular Pressing (IX-ECAP) process.

Primary Hypothesis

The primary hypothesis is the premise that traditional and nanocrystalline or ultra-fine grain rods differ in material performance characteristics in terms of mechanical properties (microhardness) and grain size as produced using the Indexing Equal Channel Angular Pressing (IX-ECAP) process.

CHAPTER III
REVIEW OF RELEVANT LITERATURE

Nanotechnology

Overview of Nanotechnology

Comprehensive integration of nanoscale science and technology (NST) offers a foundational premise for the realization of a technological and industrial revolution with implications for significant global and societal enhancements. In recognition and support of such initiatives, developing countries have committed substantial resources towards research and development within NST constructs. Recognized as a world leader, the United States enacted a National Nanotechnology Initiative (NNI) in January, 2000 with a budgetary commitment of \$270 million (Roco, 2001). For the fiscal year 2009, the U.S. Federal Government announced the NNI budget at \$1.5 billion representing a 455% increase in nanotechnology research funding during this nine-year period. Within the developmental initiative, eight component research specializations have been identified with 51% of the budgetary funding being directed to the areas of nanomaterials and fundamental phenomena and processes. Only 4% of total funding is dedicated to nanomanufacturing with no specific categorization relating to industrial engineering, quality deployment, statistical methodologies, or systems management (National Nanotechnology Initiative, 2008). Consequently, proposed research extending laboratory

processing to semi-production manufacturing identifying differences in structural traditional and nanocrystalline materials performance characteristics is needed.

Recognizing the substantial efforts accomplished within the preceding two to three decades, an assessment of nanotechnology realization indicates infant and limited industrial integration and standardization (Salerno et al., 2008). Specifically within the confines of this dissertation, antecedent research is significantly limited regarding the delineation of comparable traditional and nanostructured component manufacturing for structural materials applications. Therefore, research that delineates these differences and, subsequently, develops effective manufacturing constructs supporting nanomanufacturing initiatives is warranted.

Nanomanufacturing Approaches

With the intent of producing elemental components at the nanoscale dimension, two primary manufacturing routes have been established within the nanotechnology community to attain the intended objectives, that being the bottom-up and top-down approaches. The first method, bottom-up, relies on the precisioned manipulation of individual atoms or molecules through attainment, segmenting, and structuring into desired final shapes (Poole and Owens, 2003). These structures or components typically result from nucleation or growth outcomes based on chemical reactions involving liquid, gas, or solid pre-cursors (Sengul, Theis, and Ghosh, 2008). From an industrial commercialization perspective producing larger bulk quantities of nanostructured materials, however, the top-down approach is more amenable. With this method, large structures undergo unique manufacturing steps or phases resulting in a reduction of overall dimensions or microstructural feature sizes yielding a final product with

nanostructured characteristics (Poole and Owens, 2003). One such top-down approach that is the focus of this research is the application of equal channel angular pressing (ECAP) which will be discussed in subsequent sections.

Traditional versus Nanostructured Materials

With significant global emphasis and funding during the last two decades, nanotechnology research and development has substantiated profound differences between various traditional and nanostructured materials, thereby, resulting in a transformation towards technological revolution. Vernacular exposition provides insight to the precepts of nanotechnology. Simply stated, nanotechnology involves the intentioned manipulation or design of materials, structures, machines, or systems at very small dimensions resulting in novel performance characteristics due to the reduced size (Mukundan, 2004). The dimensions are described as nanometers and represent one billionth of a meter which is approximately $1/50,000^{\text{th}}$ to $1/75,000^{\text{th}}$ the diameter of a human hair (Rue, 2006; Dasgupta, Joseph, Wang, and Wu, 2008). Traditional materials reflect a collective averaging of component properties and discontinuities; whereas, nanomaterials retain the individual or elemental power of properties according to the physics of quantum mechanics. For example, researchers have produced a well-established pioneering material referred to as carbon nanotubes offering significantly superior properties to traditional structural steel. Intriguingly, the material is 100 times stronger than steel with only one-sixth the weight (Mamalis, 2007; Lau and Hue, 2002). From a superficial perspective, this may sound insignificant; however, consideration of this difference translated to other engineering systems represents profound implications towards industrial and technological change. For example, nanotechnology is also

directed towards energy initiatives. A consideration of an automobile that derives 100 times more miles per gallon (mpg) in fuel efficiency at one-sixth the weight would engender profound implications for U.S. dependency on foreign oil. A fuel efficiency rating of 2,000 mpg represents a technological paradigm shift. Furthermore, carbon nanotubes possess 100,000 times greater electrical conductivity than one of the most commonly used industrial conductors, copper (Mamalis, 2007). Extensive research regarding synthesis parameters and characteristics for these respective nanomaterials has been documented; however, limited research is available regarding scale-up development of supporting manufacturing processes (Andrews and Weisenberger, 2004).

Additional studies involving other representative component research specializations reveal a primary focus on material development and characterization explicitly delineating traditional and nanostructured differences, but with limited application of large-scale manufacturing methodologies. For example, research has been conducted documenting parametric realization of nanostructured cryomilled aluminum, a process representing one of the most promising transitions from laboratory processing to full-scale industrial production (Witkin and Lavernia, 2006). The research provided exhaustive coverage of parameter development and processing; however, ancillary engineering constructs critical to manufacturing processes such as statistical analysis, experimental design, or inclusion of quality methodologies were outside the scope of the intended specific research. An additional example involves the study of the synthesis of magnetic field mediated nanocomposites, a process that produced coatings with novel performance enhancing characteristics (Sun, Keshoju, and Xing 2008). Once again, a common theme relating the absence of statistical or quality methodologies was evident.

A research study by Dasgupta et al. (2008), however, investigated statistical modeling to determine robust parameter synthesis of cadmium selenide nanostructures. This investigation represented one of the limited research efforts involving an application of statistical methodologies and revealed explicit limitations of traditional statistical methods within nanotechnology processing. A comprehensive development of large-scale manufacturing constructs, however, was outside the scope of the research. Additional research was reported by Rue (2006) in discussing the overall elements assuring product quality during production of nanoelectronic components. No laboratory study or industrial processing was conducted involving nanocomponent manufacture, only descriptive generalized discussions of the potential ramifications of the application of traditional quality system methodologies within the nano environment. As proposed by the author for this research, differences in traditional and nanostructured materials provide knowledge towards the development and implementation of appropriate manufacturing systems in bringing nanotechnology and its subsequent societal benefits to fruition. Based on the aforementioned literature review, additional research is needed to further develop and extend the knowledge base regarding delineation of processing parameters, possible scale-up manufacturing methods, and characteristic differences between traditional and nanoscale or ultra-fine grain engineered materials. Transfer of this technology, therefore, contributes to the development and realization of industrial nano-based manufacturing systems.

Material and performance characteristics, as well as process manufacturing parameterization within nanotechnology constructs, represent potentially progressive radical departures from traditional methodologies and constraints. Based on confirmation

of this hypothesis (differences do exist in the processing and performance characteristics between selected structural nano and traditional materials), comprehensive manufacturing processes can be effectively developed whereby controls, techniques, and methodologies are employed to ensure capable, reproducible, and optimal manufacture. The potential societal benefits of such realization as well as significant global research funding indicate driving forces necessitating the efforts proposed within this research. Investigations that focused on statistical analysis of nanomaterials processing provided preliminary insight to the disjoint between successful implementation of traditional statistical techniques within nano environments. Further research identified generically induced differences between traditional and nano quality constructs such as standardization, metrology, process capabilities, and robustness of parameter design (Gould, 2006; Heilmann, Chen, Konkola, and Schattenberg, 2004). However, based on antecedent research and infancy of nanotechnology's industrial commercialization, significant opportunities exist within the literature to provide objective and subjective evidence concerning the implication of differences between structural traditional and nano materials processing and performance characteristics regarding the development of appropriate manufacturing systems and supporting engineering constructs such as statistical methodologies and quality standardizations. This research is intended to fill such a void and contribute to the progressive life-cycle development of nanoscale science and technology initiatives.

Severe Plastic Deformation Processing

Overview of Severe Plastic Deformation

Based on an understanding of the vast potential of nanotechnology across many scientific fields and applications, a question arises as to whether the constructs and

benefits of nanotechnology can be effectively, economically, and simply integrated into existing enabling technologies of today's manufacturing processes. One area of manufacturing that offers such potential involves the metal working process identified as severe plastic deformation (SPD) (Valiev, Lowe, and Mukherjee, 2000). Within this method, extremely large plastic strains or distortions are introduced into large, moderate, or small work pieces in order to produce an ultra-fine or nanocrystalline internal microstructure. Based on this altered microstructure, one main objective of SPD is the attainment of unusually high strengths allowing smaller or more lightweight components to be substituted in comparable engineering applications (Azushima et al., 2008).

Even though origins of modern day SPD methods date back to the 1950s, the purest form of SPD has its roots in India, ancient China, and the Middle East during the crafting of Damascus steel, Wootz steel, and the famed Japanese Samurai sword. Paralleling modern day engineering efforts, these early manufacturers endeavored and attained dramatic improvements in material performance characteristics that have intrigued scientists throughout the course of history (Valiev and Langdon, 2006). Unknowingly, these early workers employed nanotechnology constructs during the repeated folding and hammering of steel to produce exotic blades of Damascus swords. Recent scientific investigations discovered microstructures containing unique iron carbide nanowires within these materials which enable highly novel mechanical responses. For example, upon bending 90°, Damascus swords can be straightened to their original shape without loss of elasticity and toughness, and without cracking or distortion. (Kochmann, Riebold, Goldberg, Hauffe, Levin, Meyer, Stephan, Muller,

Belger, and Paufler, 2004). Even today, such superplastic behaviors would be of significant value in many engineering applications.

As with most inquiries in science and technology, combinations of incremental and quantum successes and failures yields progression. Contributions from severe plastic deformation processes are no exception. The origins of modern day SPD methods stems from the initial classic works of Bridgmann in the 1950s. His work involved the application of high pressure in conjunction with torsional loading to attain large plastic straining in metal disks with the intention of achieving significantly improved material properties. Even though improvements were made, unknowingly, his working pressures lacked sufficient magnitude to dramatically alter the material's performance characteristics. The methodologies he used, however, are today considered technologically well grounded traditional severe plastic deformation processes (Valiev and Langdon, 2006). During the decades of the 1980s and 1990s, progressive heightened interests regarding possibilities stemming from nanotechnology brought forth resurgent activity in severe plastic deformation processes (Valiev and Langdon, 2006). These efforts were significantly fueled by the development of equal channel angular pressing (ECAP) by V. M. Segal in Russia in 1972, a process introduced to the international community during the 1990s, providing substantiated development of nanocrystalline and ultra-fine grain structures in conventional materials (Segal, 1999). Even though significant developments have been realized in characterizing materials performance within severe plastic deformation processes primarily in laboratory settings, universal industrial commercialization based on the establishment of manufacturing constructs of

these processes is yet to be realized. Therefore, further work in developing SPD manufacturing methods is needed.

Severe plastic deformation processes offer a significant advantage over traditional metalworking methods in producing ultra-fine grain or nanocrystalline materials. Even though large plastic deformations or straining can be achieved in common manufacturing methods such as rolling, bending, swaging, forging, and extrusion, the upper limit of straining is limited. Specifically, for these processes the ability to attain a degree of strain greater than 2.0 requires the dimensions of the work pieces to be reduced significantly from the original dimension. Therefore, the ability to achieve ultra-fine grain or nanocrystalline microstructures is limited in producing components for structural applications employing these traditional methods. Consequently, SPD processing was created to allow unlimited or very large degrees of straining to be imposed within a material with work piece dimension remaining unchanged (Azushima et al., 2008).

With a long history of traditional metalworking processes, numerous SPD efforts have been newly created, emerged from, or been modified as a result of these methods. Examples of SPD techniques include the following: equal channel angular pressing (ECAP), accumulative roll bonding (ARB), high pressure torsion (HPT), repetitive corrugation and straightening (RCS), cyclic extrusion compression (CEC), torsion extrusion, severe torsion straining (STS), cyclic closed-die forging (CCDF), and super short multi-pass rolling (SSMR) applications. Of the numerous SPD methods currently available, three of the processes are more widely studied and receive prominent consideration. These dominating processes include equal channel angular pressing (ECAP), accumulated roll bonding (ARB), and high pressure torsion (HPT) (Azushima et

al., 2008). General descriptions of each of these methods are presented in the subsequent sections.

Equal Channel Angular Pressing

Equal channel angular pressing (ECAP) represents a metal working process whereby a work piece is forced through entrance and exit channels of a die with equal cross sections in order to impose extremely large plastic strains or distortions through simple shearing of the material. Instead of experiencing laminar-like fluid flow through a piping system, the metal actually passes through the die until shearing takes place at the intersection of the entrance and exit channels. The intersection angle ranging from 65° to 135° establishes the severity of strain imposed into the work piece and, therefore, the resultant degree of microstructural refinement and strain hardening. With the cross sectional dimensions being unchanged, repeated pressing of the work piece can be performed providing a significant advantage in achieving extremely high strains.

Additional processing parameters, such as rotations of the work piece and back pressure, have been identified contributing to exceptional material performance regarding homogeneity of the work pieces and attainment of novel performance characteristics. One of these key parameters includes the processing route. In other words, the work piece can be rotated during repeated pressings in varying configurations to induce greater equiaxed straining of the microstructural features (Valiev and Langdon, 2006).

Noted advantages of ECAP include the following: 1) simplicity in concept, design, development, and ease of use, 2) very high strains can be attained through repeated pressings or die modifications to achieve higher strains for each pass through the die, 3) flexibility in scaling-up or scaling-down for industrial applications, 4) flexibility in

work piece forms such as rod, wire, bar, plate, and sheet, and 5) ECAP is readily incorporated into traditional methods such as extrusion, rolling, etc. (Langdon, 2007).

Likewise, traditional equal channel angular pressing exhibits the following disadvantages: 1) conventional ECAP is considered a discontinuous or batch process; however, numerous methods have been employed to address this limitation and will be discussed in a subsequent section, 2) limitations on work piece length for batch processes, i.e., critical aspect ratios must be less than 10 and typically smaller, 3) excessive material waste of the work piece; typical material yield is approximately 54.3% homogeneous uniform flow of the work piece for batch conventional ECAP, and 4) low process efficiency resulting from the need for repetitive passes through the die (Xu et al., 2010).

Accumulated Roll Bonding

Accumulated roll bonding (ARB) represents a very unique and conceptually simple process with capabilities of producing extremely large strains in metals and successful attainment of nanocrystalline microstructures. However, the application of this method is restricted to sheet forms. In the accumulated roll bonding manufacturing process (refer to Figure 3.1), metal sheets are fed through two horizontal rolls to achieve a 50% reduction in sheet thickness. As the sheets exit the rolls, a transverse cut is made, whereby, the sheet is now comprised of two equal pieces. The pieces are cleaned and prepped to facilitate bonding, stacked on top of each other, and re-rolled again to another 50% thickness reduction. Cycles are repeated until the required degree of strain and resultant microstructure is obtained.

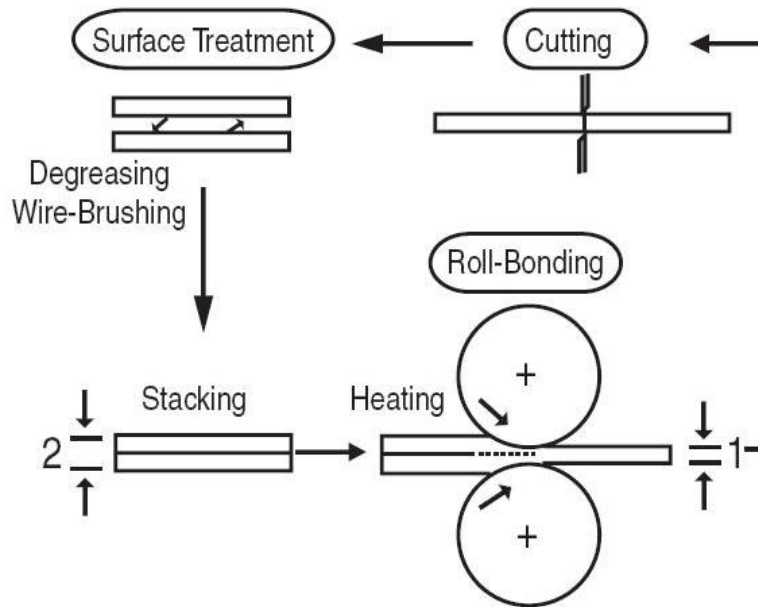


Figure 3.1 Accumulated roll bonding process

Reference: <http://www.materialsminded.wordpress.com>

ARB offers significant advantage over traditional rolling for producing nanocrystalline microstructures. In conventional rolling, a maximum strain of approximately 4.0 to 5.0 represents a limiting factor since a continued thinning in material thickness takes place as the process is repeated. ARB, however, can incur essentially unlimited amounts of strain, thereby offering unparalleled potential for microstructural and material property enhancements (Zhu et al., 2010). The major advantage of ARB is the ability to continuously process large or small metal sheets. With only ten passes through the rolls, the resulting sheet metal is comprised of 1,024 layers and experiences a total strain of 8.0 while maintaining the original thickness (Azushima et al., 2008). Conversely, the primary disadvantage of ARB is the fact that the process is limited to sheet metal forms. Even though invented in 1998 by Saito and Tsuji, only very limited industrial commercialization of ARB has been reported (Zhu et al., 2010).

High Pressure Torsion

High pressure torsion (HPT) is truly an SPD process that attains nanoscale dimensions in the resulting micro-constituents at 50 to 100 nanometers (Zhu et al., 2010). Processing via HPT consists of thin circular material samples being held in place by machined offsets and concurrently compressed between two anvils applying extremely high pressure (refer to Figure 3.2). The uniqueness of HPT is based on the application of loading, that being high axial loads applied with one anvil in conjunction with torsional loads applied from a rotating second anvil (Zhu et al., 2010). Once again, the concept of HPT is straightforward with the complexities being derived from the design and development of satisfactory equipment to provide the required extreme pressures and torsion for loading. However, this simplicity also offers one of the few advantages of HPT, that being the effect of combined axial pressure and torsion on degree of material straining. In other words, nanocrystalline microstructural response to SPD is more easily and directly determined using HPT methods (Valiez, 2001).

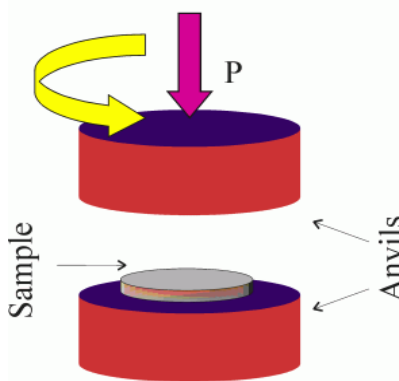


Figure 3.2 High pressure torsion process

Reference: <http://www.materialsminded.wordpress.com>

Limitations, however, have precluded widespread commercialization of HPT. For example, the main imposition of HPT is very small work piece dimensions. Typical sample sizes for HPT processing consist of circular samples approximately 10 to 20 millimeters in diameter by 0.8 millimeters thick. A second major disadvantage of the process inherently results from the torsional loading of the sample. Due to rotational loading, the total strain imposed on the sample is dependent on the location from the center axis of rotation (Azushima et al., 2008). In other words, the strain at the center would be vastly different from the strain at the outside of the sample resulting in a non-homogeneous microstructure throughout the sample. Even though continued processing of the sample results in an acceptable degree of saturation straining, various other microstructural anomalies have been identified (Zhu, et al., 2010). Industrial commercialization is being investigated utilizing larger cylindrical samples and various other applications for HPT processing.

Equal Channel Angular Pressing Review

Equal channel angular pressing uses the concept of severe plastic deformation to significantly alter the performance characteristics of materials, primarily metals. Typical metal working processes such as extrusion apply a force to a billet of larger form of solid metal to push or extrude it through a straight path die to form a smaller, similar, or alternate shaped product form. The ECAP process, however, applies a force to a form of solid metal such as a medium length rectangular bar to press it through an equally shaped cross sectional die. The pathway through the die, however, turns 90 degrees in typical applications. In other words, the metal is forced to make a sharp turn prior to exiting the die cavity. This manufacturing process induces extreme strain or plastic deformation in

the work piece resulting in grain refinement caused by imposition of simple shear and the response of resultant metallurgical microstructural reactions (Segal, 2004). Conventional ECAP is shown below in Figure 3.3.

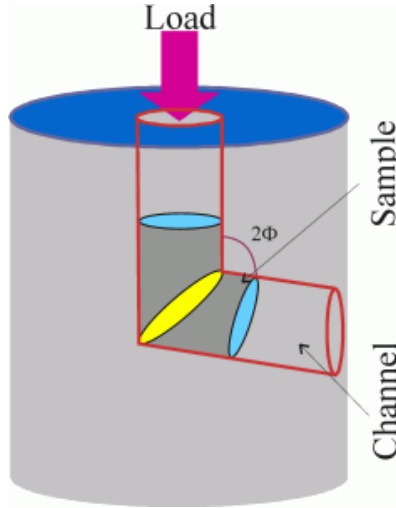


Figure 3.3 Equal channel angular pressing process

Reference: <http://www.ipam.ugatu.ac.ru>

In the following sections, a basic overview of the key engineering constructs of equal channel angular pressing is presented. Topics to be discussed include methods, work piece forms, materials, and parameters.

Methods

Throughout the years of development, several modifications have been introduced to traditional ECAP to overcome inherent limitations of the process. Several of the most prominent designs are presented to illustrate the simplicities as well as the complexities of the process. Selected designs reviewed include the following: rotary die ECAP, con-

shearing ECAP, equal channel angular rolling, conform process, and incremental equal channel angular pressing (I-ECAP).

Rotary Die ECAP

During rotary die equal channel angular pressing, multiple punches allow the die to be rotated through steps (a), (b), and (c) to repeatedly press the sample without removing the work piece (Valiev and Langdon, 2006).

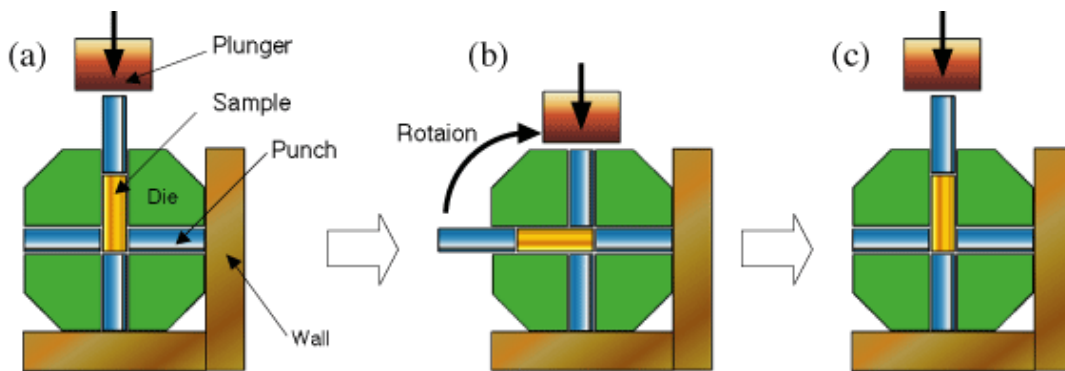


Figure 3.4 Rotary die ECAP

Reference: <http://www.aist.go.jp>

Con-Shearing ECAP

Con-shearing ECAP is designed to allow the work piece to travel around the periphery of a central roll, thereby allowing a strip of metal to be sheared from the bulk work piece and undergo straining through the equal channel angular (ECA) portion of the exit die (Azushima, et al., 2008). As can be seen and inferred from the illustration, this method would require more extensive ancillary supporting facilities and equipment for large scale manufacturing operations.

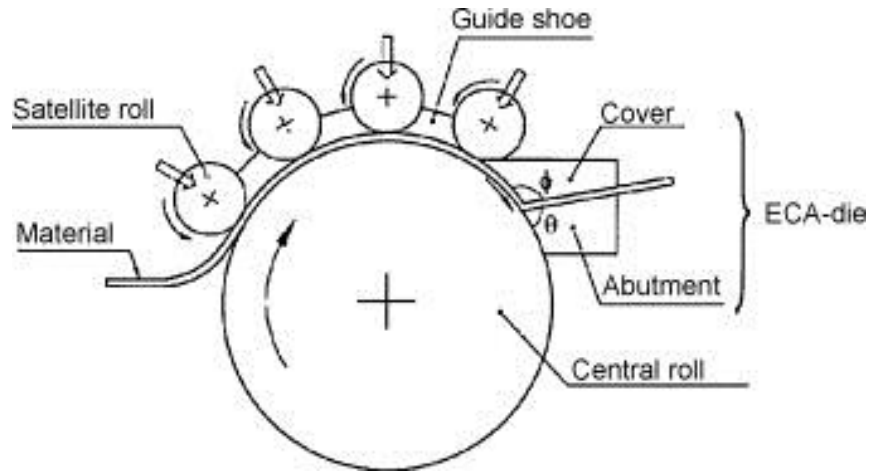


Figure 3.5 Con-shearing ECAP

Equal Channel Angular Rolling

Equal channel angular rolling (ECAR) represents a combination of traditional rolling and ECAP. Two large circular rolls feed and guide the work piece into the inlet and outlet channel of the dies to induce severe plastic deformation. The original thickness of the work piece is reduced during the rolling process prior to ECAP straining (Azushima, et al., 2008).

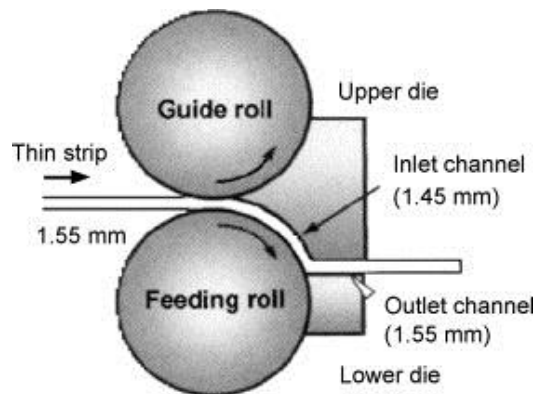


Figure 3.6 Equal channel angular rolling – ECAR

Conform Process

The conform process is very similar to ECAR; however, the work piece thickness in the conform process is not reduced as performed in the rolling ECAP process.

Frictional forces acting on the work piece feed the material into the exit channel of the ECAP portion of the die (Valiev and Langdon, 2006).

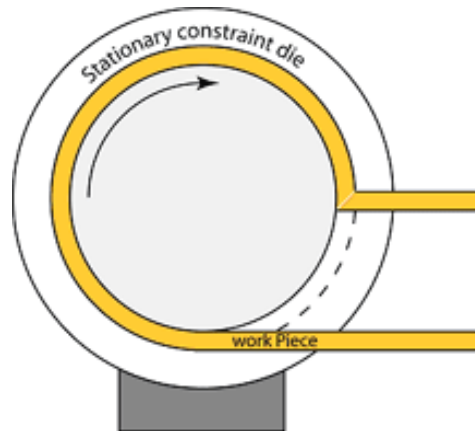


Figure 3.7 ECAP conform process

Reference: <http://www.nanospd.org>

Incremental Equal Channel Angular Pressing

Incremental equal channel angular pressing (I-ECAP) uses a split die to incrementally induce straining into the work piece. The component enters the entrance channel and is then pressed by the split die portion “C” acting along the distance of increment “b” as shown, thereby, forcing the work piece through the exit channel (Azushima, et al., 2008).

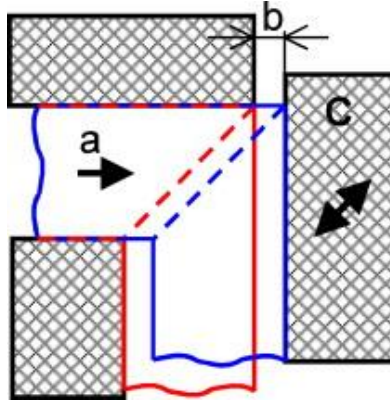


Figure 3.8 Incremental ECAP

Work Piece Forms

Work pieces successfully pressed using ECAP include wire, rod, bar, plate, sheet, chips, machining fines, tubing, sandwich sheets, and powders.

Materials

Early investigations using ECAP focused primarily on processing softer materials such as pure aluminum, copper, etc. However, material systems processed by ECAP now include an expanding list of both ferrous and non-ferrous commercial alloys, as well as high melting point and difficult to work metals such as tungsten. Composite materials are also being investigated for ECAP processing. To provide a general scope of material applications, a brief listing of material systems processed by equal channel angular pressing is provided in Table 3.1 (Stoica, 2001):

Table 3.1 Materials processed by equal channel angular pressing

Metallic System	Specific Alloys	
Aluminum	Al (pure aluminum)	Al-0.3Mn
	Al-1Mg	1050 Al
	Al-3Mg	3003 Al
	Al-3Mg-0.2 Sc	5056 Al
	Al-3Mg-0.2Zr	6061 Al
Copper	Cu-25Ag	CU-18Nb
Iron (Steel)	Low Carbon Steel	304 Stainless Steel
	AISI 4340	316 Stainless Steel
Magnesium	AZ31B	ZK-60
Titanium	Ti (commercially pure)	Ti-6AL-4V
	Ti-45.5Al-2Cr-2Nb	
Shape Memory Alloys	ZK60 533	

Parameters

Successful manufacture of critical engineering components employing either conventional equal channel angular pressing (ECAP) or a new design such as Indexing Equal Channel Angular Pressing (IX-ECAP) is dependent on identification and control of processing parameters. ECAP represents a unique manufacturing method with process parameters of vital importance in producing reproducible high quality reliable parts. The proposed Indexing Equal Channel Angular Pressing (IX-ECAP) process is described in detail in Chapter IV Experimental Methods and Materials; however, at this juncture it is important to note the parameters identified below represent well established key processing variables from traditional ECAP that are transferable and, therefore, provide requisite foundation for successful design and development of the new IX-ECAP process.

Ten process parameters providing the foundational premises within traditional ECAP are presented. These critical factors have been thoroughly researched and must be

understood to achieve success in equal channel angular pressing. However, to the best of the author's knowledge one additional process parameter is discussed which has not been researched in association with any of the variations of ECAP methodology, that being the application of vibrational energy to the die during pressing. Based on well defined benefits of vibrational energy to other engineering systems as subsequently discussed in following sections, the integration of this parameter to indexing equal channel angular pressing will be studied for the first time.

As such, an introduction to the key process control parameters identified for successful processing of materials utilizing equal channel angular pressing technology is provided in the following sections.

Die Design

Die design is at the core of ECAP processing since it is within this component that severe plastic strain is imposed on the work piece. Naturally, the die material must be of sufficient strength and dimension to withstand the impending stresses as the work piece traverses the channels. The primary research focus in die design, however, has been associated with dimensional lay-out of the die interiors. Several key factors are noted as follows in conjunction with Figures 3.9, 3.10, and 3.11 (Valiev and Langdon, 2006):

- Die angle, Φ , is the single most critical process parameter since this value determines the amount of strain imposed for each pass through the die (refer to Figure 3.10).

- Curvature angle, Ψ , is important as it influences flow through the channels and the development of a potential “dead zone” where no strain is imposed.
- Channel diameters and lengths are, likewise, of importance as these attributes impact pressing forces and strain distributions in the work piece.

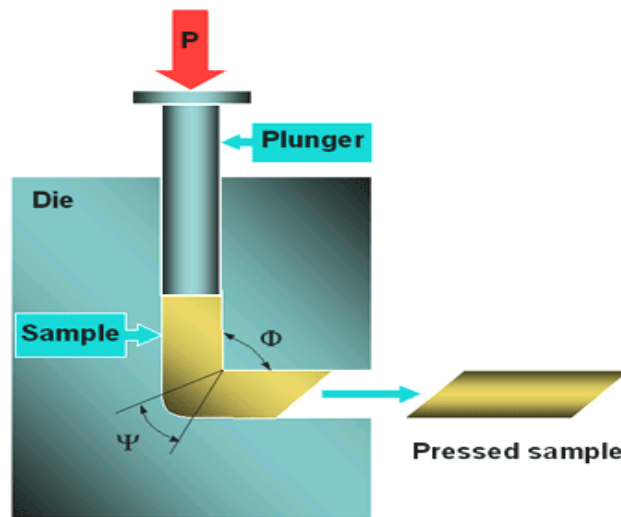


Figure 3.9 ECAP die angles

Reference: <http://www.ame-www.usc.edu>

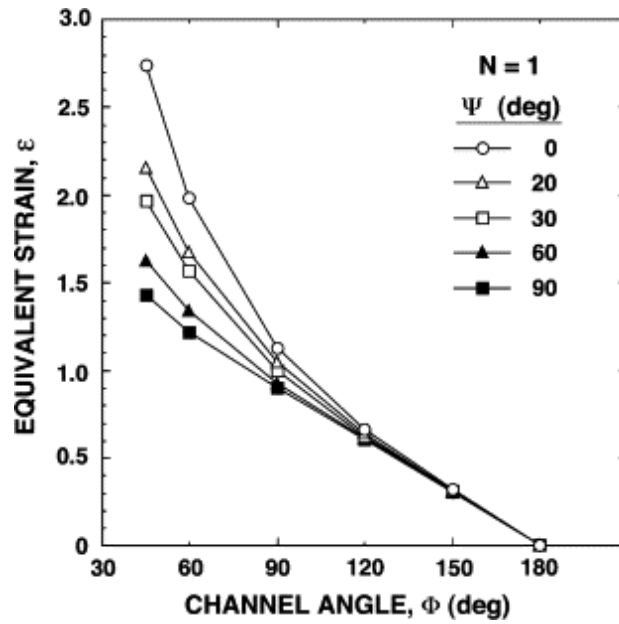


Figure 3.10 Channel angle, Φ , versus strain, ϵ

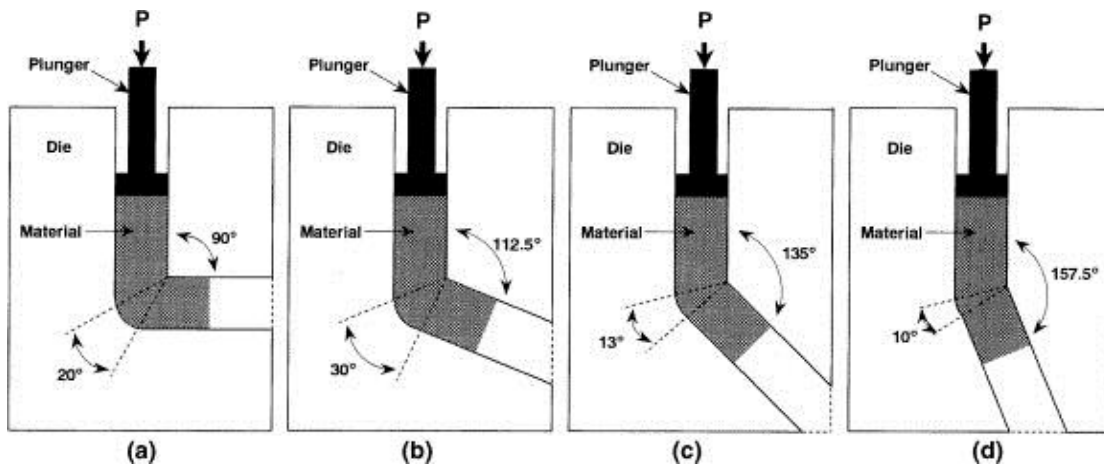


Figure 3.11 Schematic of varying die Angle, Φ , and Ψ

Number of Passes

The total amount of strain is cumulative; therefore, increasing the number of passes increases the total cumulative impact of strain towards refining the grain size to

the ultra-fine or nanocrystalline dimensions (Jin, Son, and Im, 2010). Equivalent strain for each pass through the process is determined as follows (Valiev and Langdon, 2006):

$$\varepsilon_N = \frac{N}{\sqrt{3}} \left[2 \cot \left(\frac{\Phi}{2} + \frac{\Psi}{2} \right) + \Psi \operatorname{cosec} \left(\frac{\Phi}{2} + \frac{\Psi}{2} \right) \right] \quad (3.1)$$

where: ε_N = equivalent strain
 N = number of passes
 Ψ = angle at outer arc of curvature at intersection of channels
 Φ = channel intersection angle

For the simplified case where $\Psi = 0$ and the channel intersection angle is represented as $\Phi = 2\varphi$ the following relationship applies (Valiez et al., 2006):

$$\varepsilon_N = \frac{2N}{\sqrt{3}} \cot \varphi \quad (3.2)$$

where: ε_N = equivalent strain
 N = number of passes
 φ = half angle at the channel intersection

Therefore, equivalent strains for 1, 2, 3, 4, and 5 passes through the system at a 90° channel angle with $\Psi = 0$ are 1.15, 2.31, 3.46, 4.62, and 5.77, respectively.

Processing Route

As work pieces are repeatedly pressed through the die, the orientation of the samples can be altered or changed prior to re-insertion into the die. These rotations have a profound impact on the degree of homogeneity and anisotropy within the work piece upon completion of processing. Four basic routes, as illustrated in Figure 3.12, have been defined as A, B_A, B_C, and C. Extensive research has identified processing route B_C as

the optimum route producing equiaxed homogeneous microstructures in a pressed work piece (Valiev and Langdon, 2006).

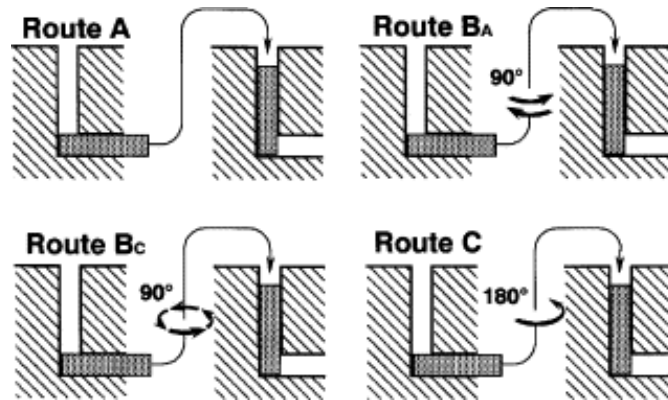


Figure 3.12 Processing routes

Pressing Temperature

Pressing temperature also plays a key role in ECAP in several ways. One of the most important contributions is the impact on flow stress of the work piece material and the required pressing force. As the temperature is increased, material flow stress decreases enabling a softer material to be processed, thereby reducing the required pressing loads. This aspect also helps improve die life since less stresses are placed on the die. Secondly, lower temperatures typically result in smaller grain sizes. Close temperature control is critical in order to preclude the occurrence of deleterious high temperature metallurgical reactions (Yamashita, Yamaguchi, Horita, and Langdon, 2000).

Pressing Speed

Various pressing speeds studied in severe plastic deformation processes range from ballistic to extremely slow. However, speed is a critical factor in applicable ECAP processing and is conventionally in the range of 1 to 20 millimeters per second. It is noted that a slower speed allows adequate straining to occur more readily at the shearing zone in the die, thus providing a more homogeneous microstructure (Langdon, 2007). Also, excessive speeds contribute to defect structures such as surface cracking of the work piece.

Friction

Two primary influences of friction during ECAP processing include the effect on required pressing loads and work piece strain inhomogeneities. For example, as friction factors along the die walls increase, the required pressing loads to move the work piece through the die increase substantially. These higher forces within the manufacturing system require more costly mechanical equipment, increased possibilities of plunger buckling, and increased wear and galling in the die. Likewise, frictional drag on the work piece surfaces strongly influences strain distributions in the pressed sample leading to increased variability in material performance (Balasundar and Raghu, 2010).

Back Pressure

Recent research has substantiated significant benefits in applying back pressure to the exiting work piece during ECAP processing. One of the most important factors is the elimination of work piece cracking as illustrated for the magnesium alloy in Figure 3.13 (Lapovok, 2005).

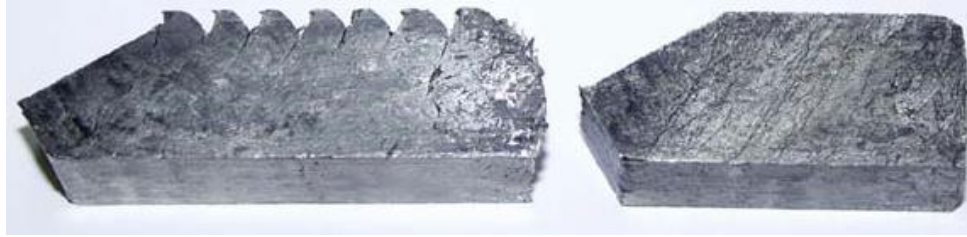


Figure 3.13 Effect of back pressure

Notes: Without back pressure (left). Sample with back pressure (right).

Most importantly, recent research findings reveal ECAP pressing performed with back pressure using a magnesium-aluminum alloy resulted in significant increases in both strength and ductility of the work piece (Kang, Liu, Wang, and Zhao, 2010).

Aspect Ratio

For traditional ECAP processes utilizing a punch or plunger to move the work piece through the die, the ratio of longitudinal dimension to the cross-sectional dimension becomes critical due to the potential of buckling. Aspect ratios reported for successful pressing during conventional ECAP is less than ten and, typically, in the range of four to eight. This aspect ratio limitation, likewise, restricts the work piece dimensions available from batch type ECAP processing (Segal, 2004).

Punch Force

Required loads for ECAP manufacturing is a critical factor in the design of ancillary mechanical equipment comprising the system. Punch force is a function of such factors as die design, friction, pressing speed, and work piece material properties (Segal, 2004).

Material Properties

Work piece material properties play a vital role in the ultimate performance outcomes and, therefore, must be evaluated in consideration of design and development of the ECAP manufacturing system. Numerous material factors such as flow stress, strain hardening rate, recrystallization temperature, and inherent metallurgical reactions represent only a few of the important criteria to be considered (Dobatkin, Zrnik, and Mamuzic, 2006).

Vibrational Energy

The entire process of ECAP is based on an eclectic derivation and distribution of energy sources throughout the elements of the system. For example, mechanical energy must be supplied to press the work piece through the channels and overcome the effects of material flow stress and friction forces acting along the die walls. Additionally, internal energy must be available to allow severe plastic straining of the work piece material and to initiate metallurgical reactions such as dislocation motion and rearrangement. Manufacturing systems throughout industry routinely employ vibrational energy from many different sources to assist process effectiveness. For example, vibrating conveyors transfer raw materials or finished parts. Other examples have demonstrated very significant positive effects of vibrational energy in reducing grain size of component microstructures during the solidification of castings (Miller, 1982).

Based on a review of the literature by the author of this proposed research, no reports of the use of vibrational energy have yet been located. Therefore, it is purported that ECAP manufacturing could realize gains in process performance outputs through the application of externally applied vibrational energy. For example, distribution of

lubricants throughout die channels could be improved to reduce pressing loads and facilitate heat transfer to reduce adiabatic heating. Furthermore, metallurgical reactions promoting development of refined nanocrystalline or ultra-fine grains could be enhanced.

Therefore, vibration was employed within this proposed research to fill the identified knowledge gap. As noted in subsequent sections detailing experimental methods, externally applied vibrational energy was identified as a main factor studied in designed experiments for I_x-ECAP.

CHAPTER IV

EXPERIMENTAL METHODS AND MATERIALS

Experimental Development Rationale

This research investigates the design of a new manufacturing approach, whereby differences in traditional and ultra-fine grain (UFG) and/or nanocrystalline (NC) material property processing and performance is assessed. A new methodology based on modifications of traditional ECAP constructs representing foundational nanotechnology manufacturing which employs a top-down approach using bulk pressing with the objective of producing ultra-fine grain and/or nanocrystalline aluminum rods. These investigations involve a single manufacturing process referred to as Indexing Equal Channel Angular Pressing (IX-ECAP). To the best of this author's knowledge, this method along with the descriptive, "Indexing Equal Channel Angular Pressing", is being used for the first time. Resultant product outcomes from the nanomanufacturing process is compared and contrasted to baseline conventionally produced bulk aluminum alloys.

The primary objective of this research is to identify and quantify the differences between material properties of product forms produced in comparable traditional production processes and those employing IX-ECAP. The attainment of ultra-fine grain and/or nanocrystalline morphologies is investigated through the application of severe plastic deformation (SPD) via IX-ECAP manufacturing. The research involves processing bulk solid pieces of types 1100 and 4043 aluminum alloy rods. Material

property assessments representing each of these respective experiments were made from mechanical property characterizations based on transverse section hardness measurements, as well as microstructural delineations based on average grain size. Material surface integrity for cracking and distortion was assessed for both alloys based on visual examinations of longitudinal and transverse sections of processed work pieces.

Selection of the ECAP process for this research is based on factors contributing to the transition from laboratory to industrial manufacture. First, the respective manufacturing method is based on existing and available enabling technologies represented by traditional extrusion methods, equipment, and materials which equates to comparable cost structures. Secondly, based on previous research studies, moderate as well as significant gains in material performance characteristics have been reported, which translates into lower initial risk or anticipated higher expectations associated with integration of produced materials in engineering structures and components. Lastly, ECAP represents a manufacturing process offering one of the greatest potentials for scale-up producing bulk nanostructured product forms that can then be used for subsequent processing into other forms, such as wire drawing or metal stamping (Zhu et al., 2004). Outcomes from this research contribute towards extending the knowledge base in developing proper elements of process control used to support nanotechnology manufacturing operations.

Progression of the research proceeded along developmental phases consisting of system concept development and design, manufacturing unit build and testing, statistical experimentation, materials characterization, and analysis as illustrated in Figure 4.1.

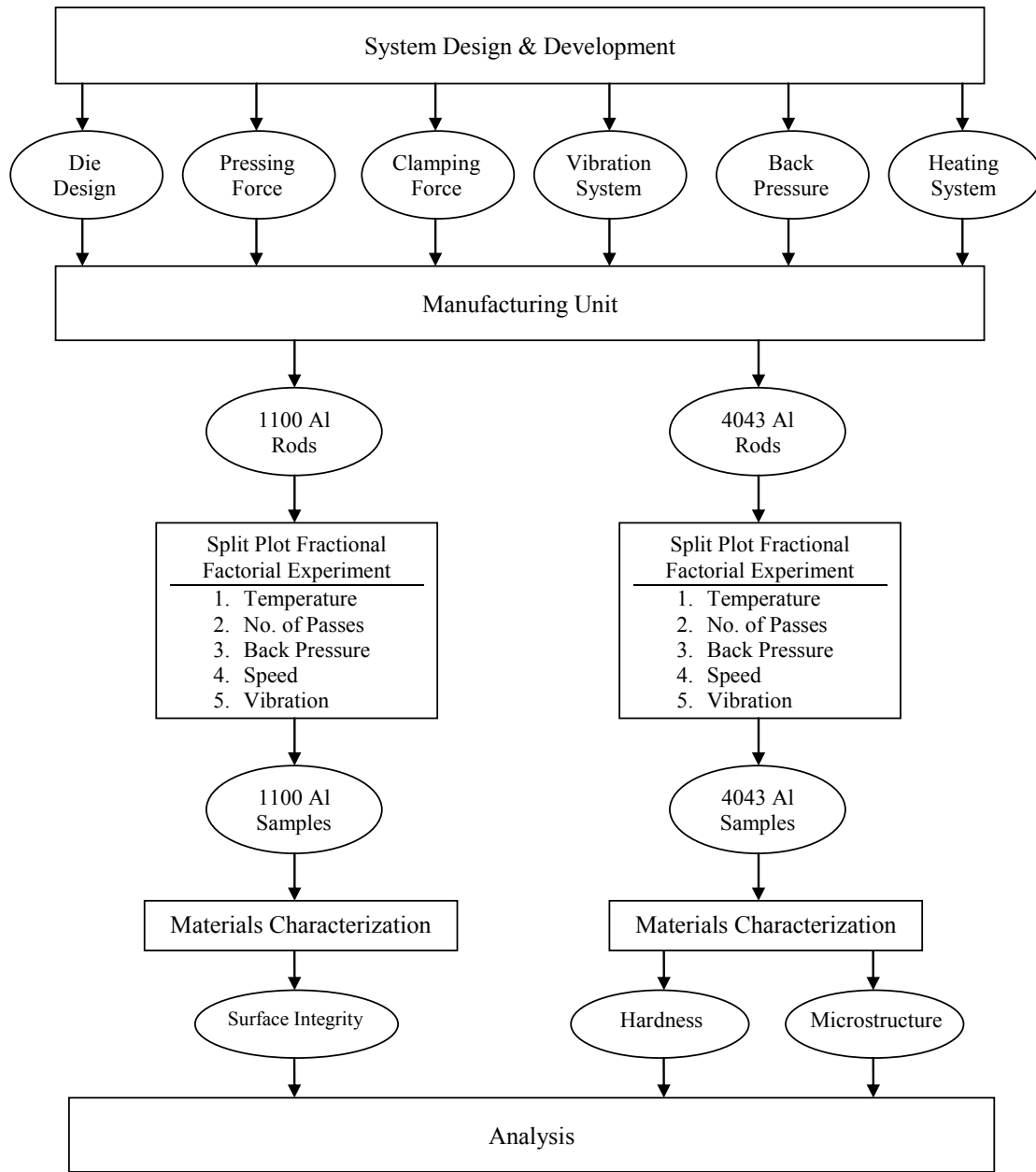


Figure 4.1 Research progression flow chart

Method - Indexing Equal Channel Angular Pressing

IX-ECAP represents a new approach in the application of severe plastic deformation processing. The design seeks to overcome significant barriers to

commercialization acceptance. First, the principles of I_X-ECAP focus on simplicity and an integration of currently available cost effective manufacturing enabling technologies. Second, even though the process is identified as “indexing” with an implication to batching, the process is truly a semi-continuous operation intended to produce continuous unlimited work piece lengths. Third, the I_X-ECAP design allows variable work piece lengths with minimal restrictions concerning dimensional lengths. This capability seeks to overcome the significantly limiting constraint in traditional ECAP regarding short work pieces and associated critical aspect ratios for die punches or plungers. Fourth, process simplicity of I_X-ECAP is conducive to manufacturing flexibility allowing the development of manufacturing cells comprised of parallel or series systems. ECAP processing routes and number of pressings can readily be accommodated by I_X-ECAP. Fifth, the basic constructs of the process reveal realistic implications for up-scaling or down-scaling to industrial applications involving very large or small work pieces. Lastly, since I_X-ECAP integrates basic constructs of traditional ECAP the potential of achieving ultra-fine grain or nanocrystalline microstructural characteristics across diverse material systems is favored. The intended research, therefore, investigated the realization of bringing these intended gains to fruition.

Design and development of the I_X-ECAP process is an integration of traditional constructs of equal channel angular pressing, modified ECAP processes, and alternative considerations aimed at overcoming commercialization barriers. Conceptual layout and processing steps associated with I_X-ECAP are illustrated in the subsequent pages. One of the main notable differences between conventional ECAP and even the modified versions to date is related to relative motion of die and work piece. (Note: work piece refers to

the material product form being processed through the die, i.e., aluminum rods, bar stock, etc.) In traditional and modified ECAP methods, the die is typically in a stationary location or plane, whether rotating or fixed, in order to accommodate work piece material that is being fed into the die. I_x-ECAP, however, relies on a movable die indexing along the longitudinal axis of the work piece to feed the material through the die. The basic steps are illustrated in Figures 4.2 – 4.5.

As shown in Figure 4.2 (a), the work piece is first inserted through the clamping die into the entrance channel of the pressing die. The rod is then secured with a clamping force using the clamping die as shown in (b). The pressing die is located in the backward starting position.

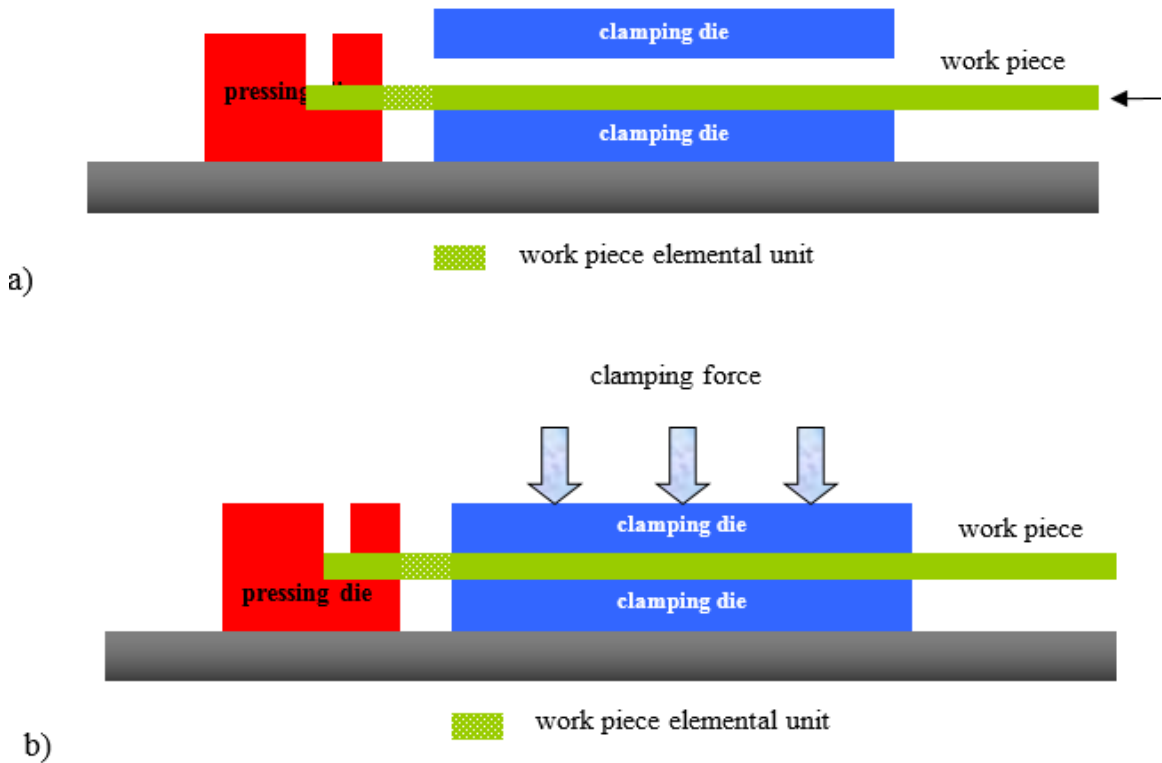


Figure 4.2 Step 1 of I_x-ECAP conceptual design

The pressing die is then indexed forward with an indexing force until contact is made with the clamping die as illustrated in Figure 4.3 (a). Directional indexing travel of the pressing die feeds the work piece through the pressing die as shown by the work piece elemental unit. Next, the clamping force on the work piece is released as illustrated in (b).

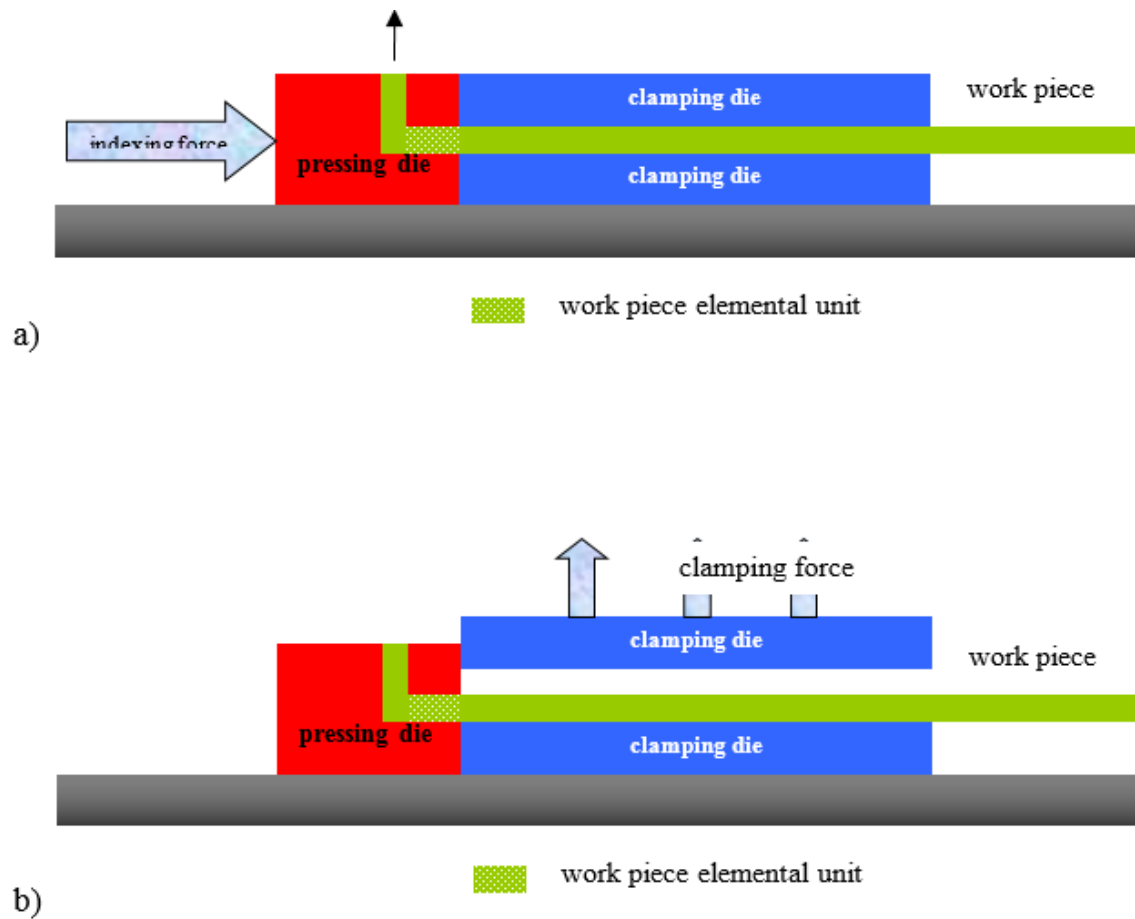


Figure 4.3 Step 2 of Ix-ECAP conceptual design

The pressing die is then allowed to travel backwards as shown Figure 4.4 a). This step also serves to pull additional work piece material into the clamping die. The work piece is once again secured in the clamping die with the clamping force as noted in (b).

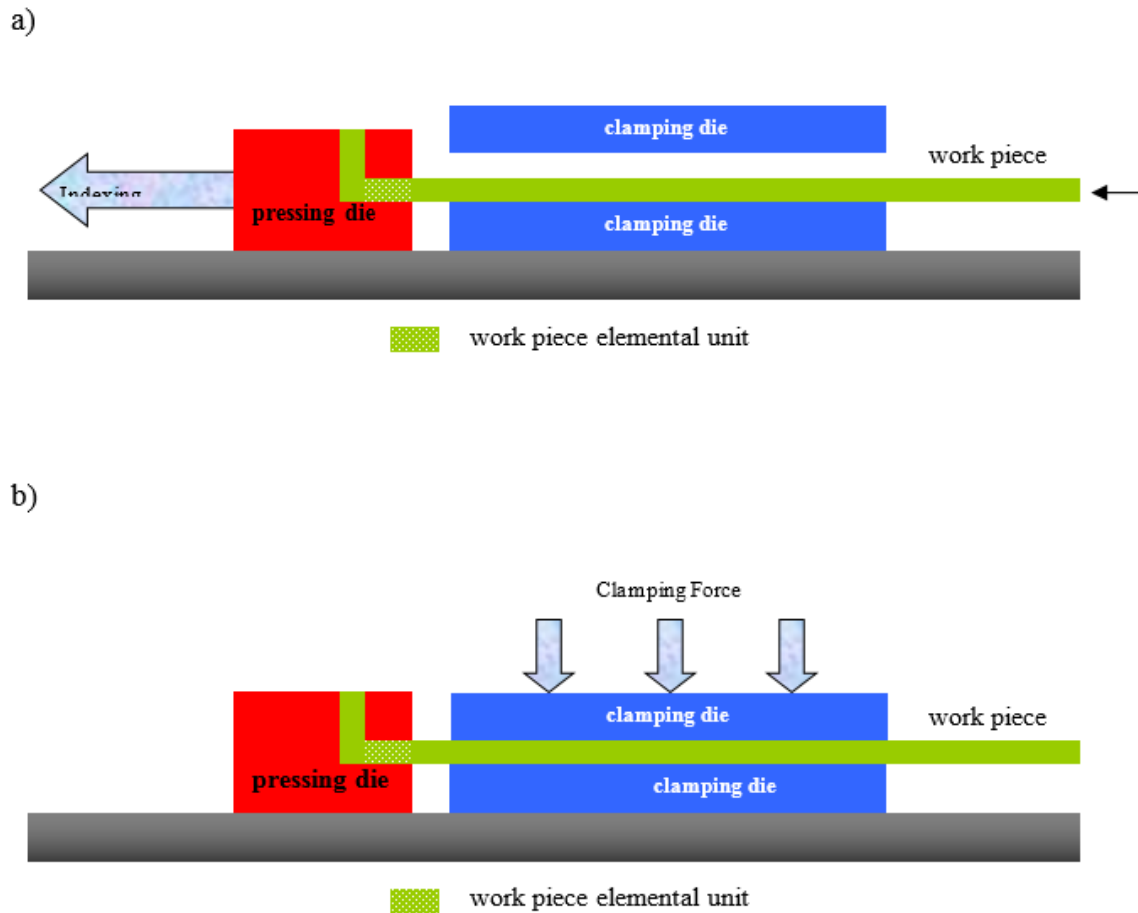


Figure 4.4 Step 3 of IX-ECAP conceptual design

As a final step, the pressing die is indexed forward making contact with the clamping die to continue feeding the rod through the system. Pressed rod leaves the pressing die through the exit channel as illustrated in Figure 4.5.

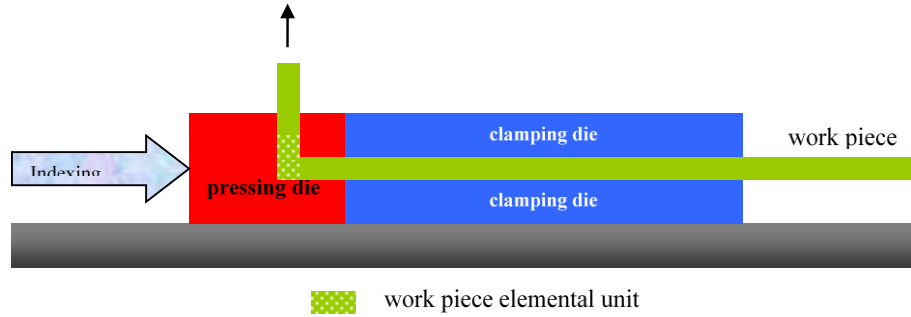


Figure 4.5 Step 4 of Ix-ECAP conceptual design

Sequencing of continuous rods through the process starts over as illustrated in the previous steps. Once material has been loaded into the system, Ix-ECAP is essentially a four-step process continuously indexing work piece material through the die as follows: 1) clamp the work piece, 2) index the pressing die forward, 3) unclamp the work piece, and 4) retract the pressing die pulling additional material into the system. Processing parameters were studied for technology transfer to industrial manufacturing.

Facilities and Equipment

As noted in the research flow chart in Figure 4.1, several design elements were required to build a prototype manufacturing unit. These respective elements consisted of the pressing and clamping force hydraulic systems, back pressure components, vibration elements, thermal system, and various die components. Development of the manufacturing system involved an intense focus from two primary perspectives, that being the detailed elements comprising the die components through which the metal rods would pass and, secondly, supporting or ancillary equipment which provided the drivers and support structures for the die components. For example, in this system the dies were comprised of two basic halves, the pressing die and the clamping die. However,

supporting elements of the system that actually made the process functional included such items as a steel mounting table to hold the dies, hydraulic pump to drive the hydraulic cylinders, cartridge heaters with relays and a controller to maintain proper temperature, an air operated miniature piston vibrator to provide vibrational energy, and an air supply compressor used to drive the vibrator, etc.

Each of the respective system components are described as entities within themselves in order to explain the contribution to and criticality in controlling the five process factors evaluated in this dissertation. These five factors included the following: 1) pressing temperature, 2) number of passes through the process, 3) back pressure applied to the exit end of the work piece, 4) pressing speed, and 5) vibration applied to the pressing die. A more detailed conceptual side view of the I_x-ECAP process is shown in Figure 4.6 on the next page. Details of system components are described in the following sections.

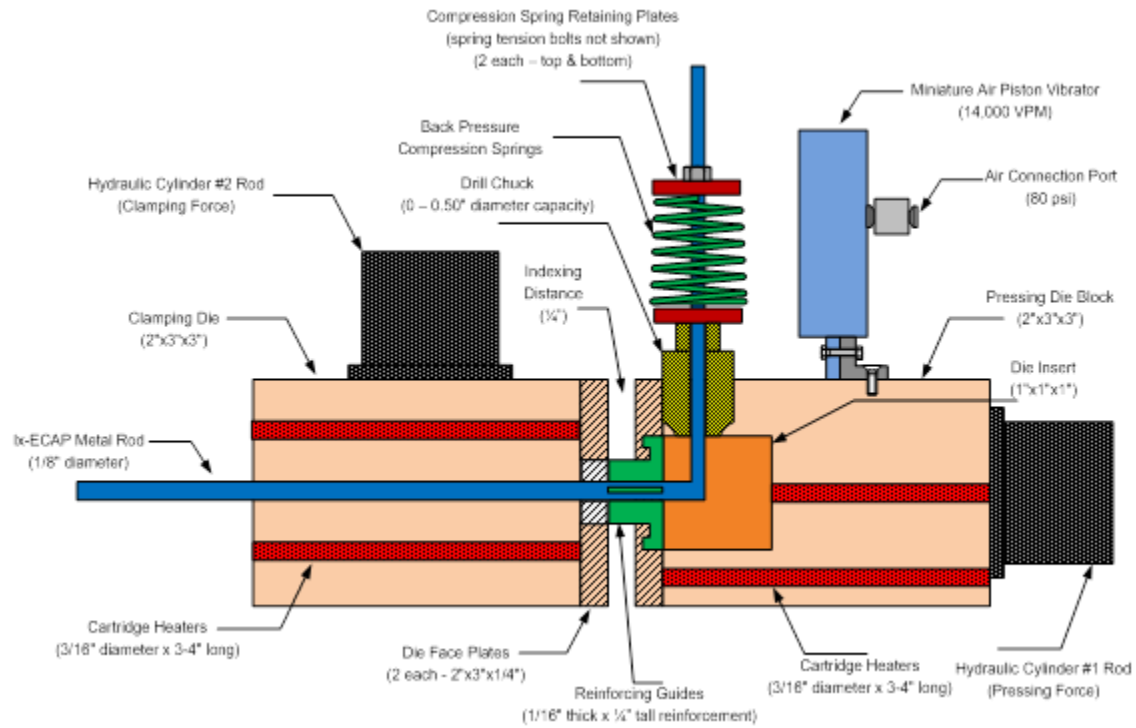


Figure 4.6 Cross-sectional view of concept design of the IX-ECAP process

(Not to scale)

In transitioning from a conceptual perspective to an understanding of the actual manufacturing unit that was designed and built, full views of the completed system are provided on the following pages in Figures 4.7 through 4.11.

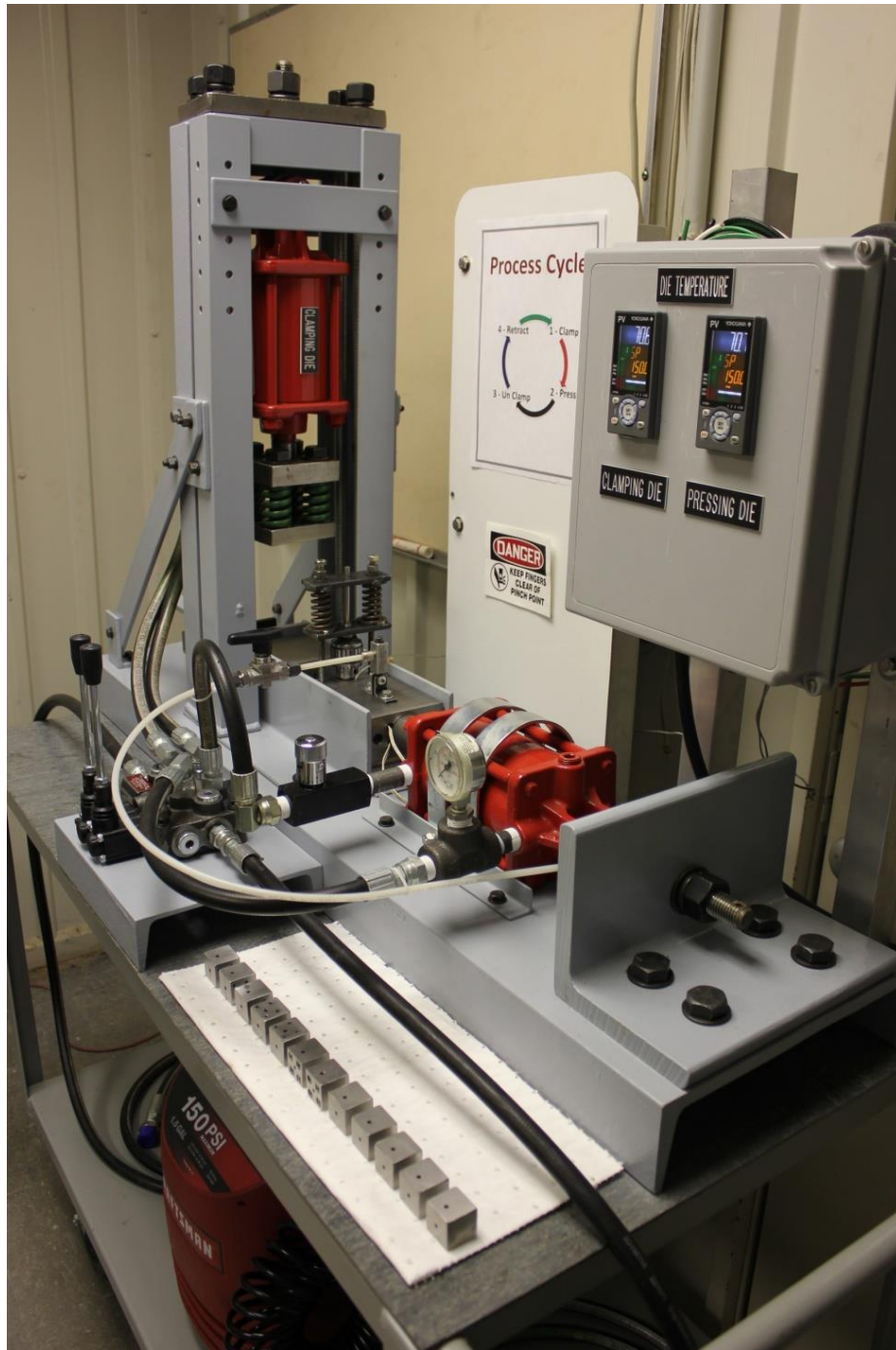


Figure 4.7 Front view of manufacturing unit



Figure 4.8 Rear view of manufacturing unit.

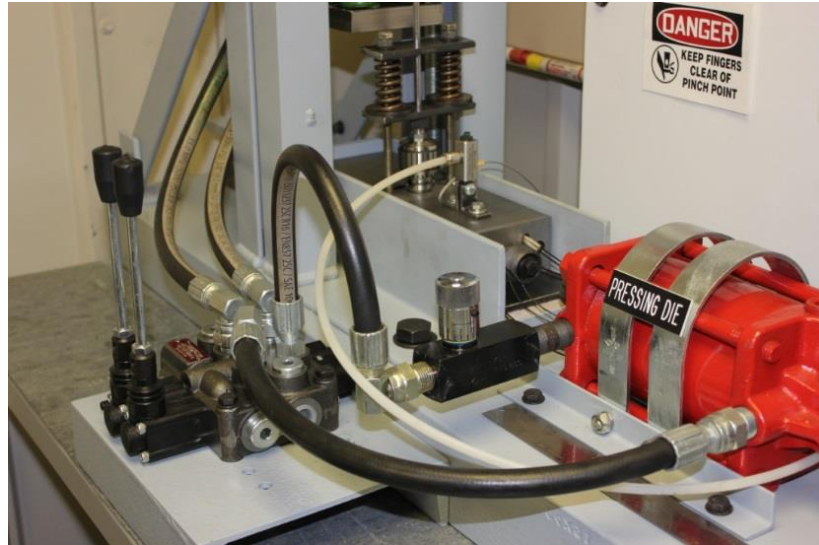


Figure 4.9 Close-up view of pressing components of the system

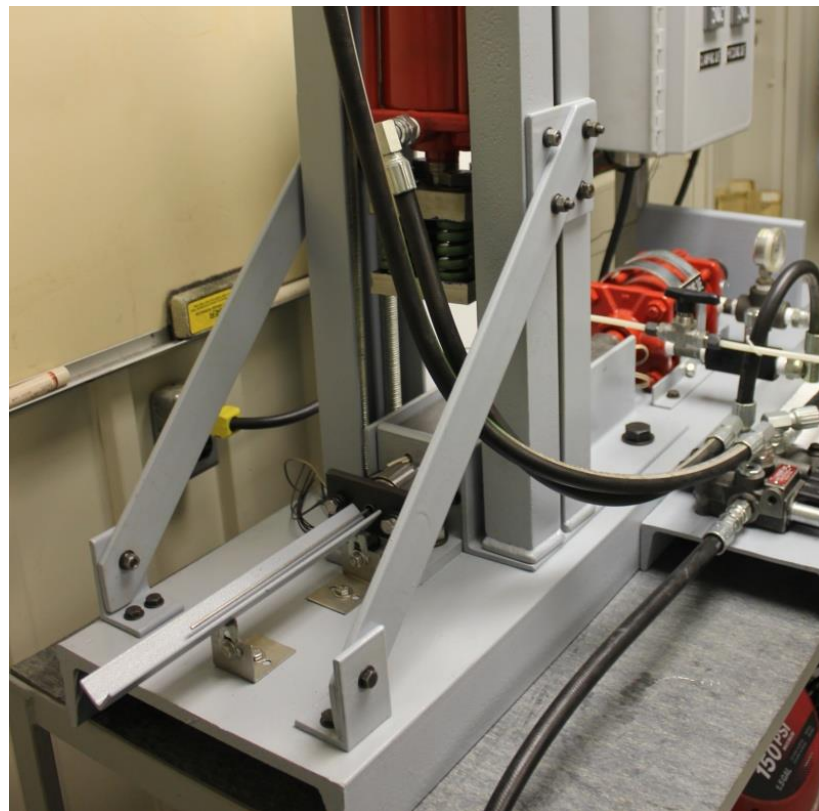


Figure 4.10 Close-up view of clamping components of the system

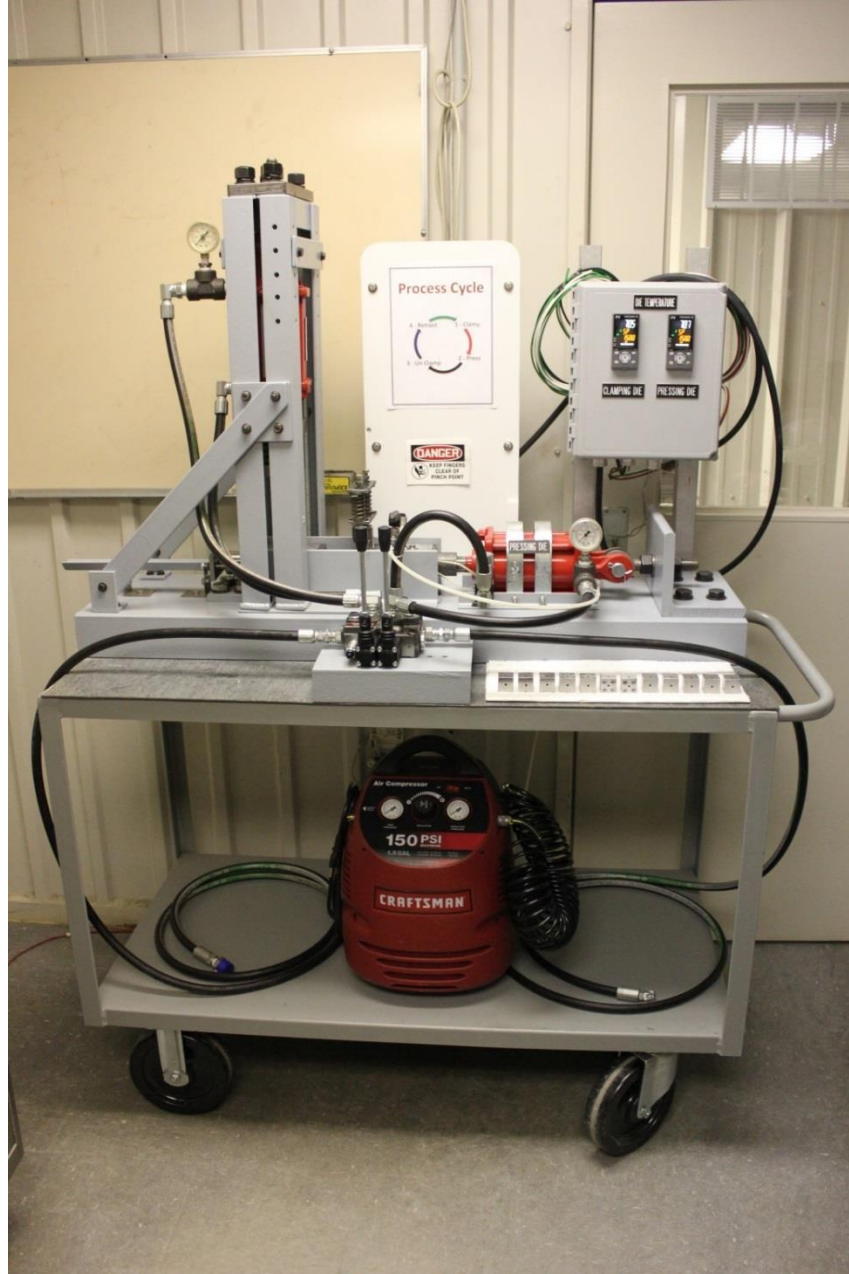


Figure 4.11 View of completed manufacturing unit

Die Design

Die design and fabrication involved construction of components providing both direct and supporting roles in the manufacturing unit. Specifically, system die elements consisted of the following: 1) die insert, 2) die insert holding block, 3) pressing die, 4) pressing die face plates, 5) clamping die, 6) clamping die face plates, and 7) reinforcing guides. Unassembled die components are shown below and described in the following sections. Tables identifying the materials of construction for each of the respective die components are presented on the next page.

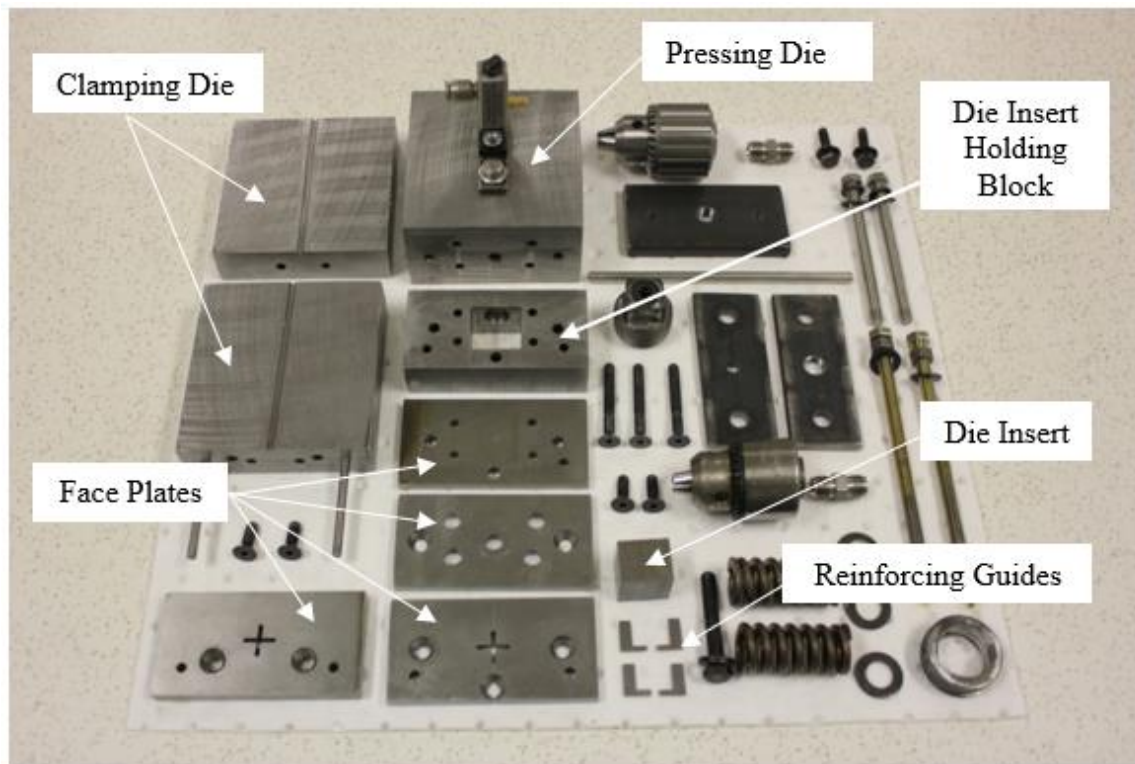


Figure 4.12 Unassembled die components

Table 4.1 Chemical compositions of D2 tool steel and 1018 carbon steel

Die Component	Material of Construction
Die Inserts	D2 Tool Steel
Pressing Die Face Plates	D2 Tool Steel
Clamping Die Face Plates	D2 Tool Steel
Reinforcing Guides	D2 Tool Steel
Clamping Die	1018 Carbon Steel
Pressing Die	1018 Carbon Steel
Die Insert Holding Block	1018 Carbon Steel

Table 4.2 Chemical compositions of D2 tool steel and 1018 carbon steel

Element	D2 Tool Steel (wt. %)	1018 Carbon Steel (wt. %)
Carbon	1.40 – 1.60	0.14 – 0.20
Manganese	0.60 max	0.60 – 0.90
Phosphorus	0.030 max	0.040 max
Sulfur	0.030 max	0.050 max
Silicon	0.60 max	-
Chromium	11.00 – 13.00	-
Nickel	0.30 max	-
Molybdenum	0.70 – 1.20	-
Tungsten	N/A	-
Vanadium	1.10 max	-
Cobalt	1.00 max	-

Reference: <http://www.matweb.com/search/DataSheet>

Die Insert and Holding Block

The primary die component of the system consisted of metal inserts whereby aluminum rods would pass through a 90° angle at the intersection of the entrance and exit channels of the die. For this investigation, D2 tool steel was used to fabricate 1 x 1 x 1 inch cubes containing 0.125-inch diameter entrance and exit channels as shown in Figure 4.13. The length of the entrance channel was 0.250 inch; whereas, the exit channel length was 0.500 inch. Parting line dies were held together using size #8-32 threaded alloy steel socket head cap screws as shown.

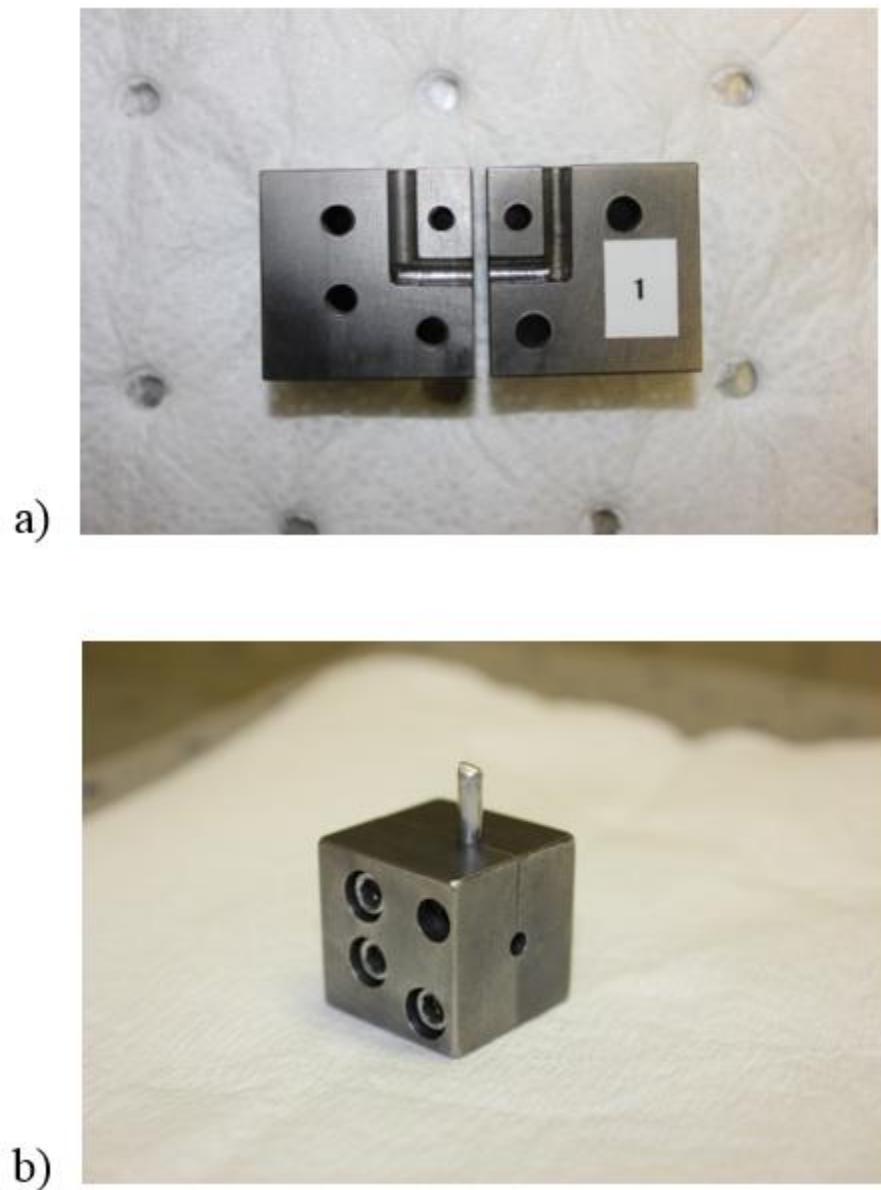


Figure 4.13 Die inserts

- a) Unassembled die insert with parting line
- b) Assembled die insert with aluminum rod exiting the die after pressing

To ensure a sufficient number of die inserts were available for process runs, twelve die inserts were fabricated to compensate for unexpected die failures. Within these twelve dies, four designs were constructed. The first design was a two-piece

vertical parting line die. A second design consisted of a two-piece horizontal parting line die. Third was a unique three-piece vertical parting line die, and the fourth design consisted of a solid one-piece cube. Intersecting channels of the die inserts were drilled using 0.125 inch diameter 135° point drill bits and, progressively polished using 240, 400, and 600 grit silicon carbide paper. Each of these designs is shown in Figure 4.14.

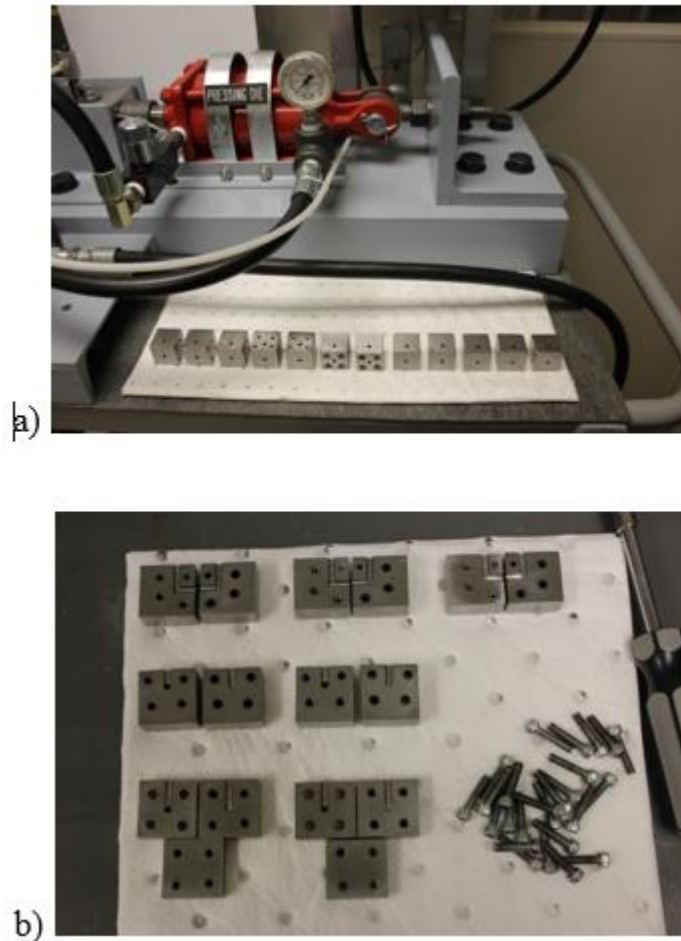


Figure 4.14 Die inserts ready for process runs

- a) Die inserts ready for process runs
- b) Unassembled die inserts with parting lines

A second die component directly associated with the die insert is identified as the die insert holding block. Instead of fabricating the equal channel angular die from a single large piece of expensive tool steel, an alternative was to fabricate a smaller 1 x 1 x 1 inch tool steel die cube and then insert the cube into a holding block constructed of less expensive carbon steel. In the event of failure within the channels, replacement would only involve a simple die insert replacement instead of an entire piece of much larger tool. A picture of a die insert being removed from the holding block with a magnet during actual processing is shown in Figure 4.15.



Figure 4.15 Die insert being removed from holding block with a hand held magnet tool during processing

Pressing Die

A third die component consisted of the pressing die block which attached to the pressing force hydraulic cylinder rod to provide horizontal movement of the die. This die element was fabricated from 1018 carbon steel and measured 3.875 x 3.875 x 2.000

inches as shown in Figure 4.16. The die insert holding block with the die insert in place was attached to the pressing die. To provide resistance to deformation from stresses generated during the pressing operation, D2 tool steel face plates were attached to each end of the pressing die as well as one face plate sandwiched between the die holding block and pressing die.

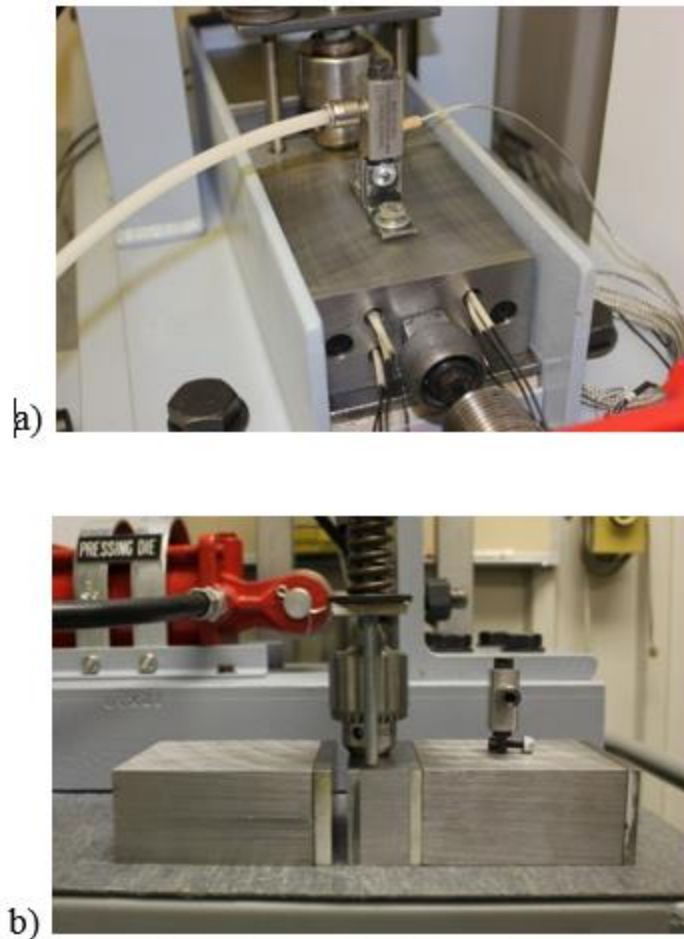
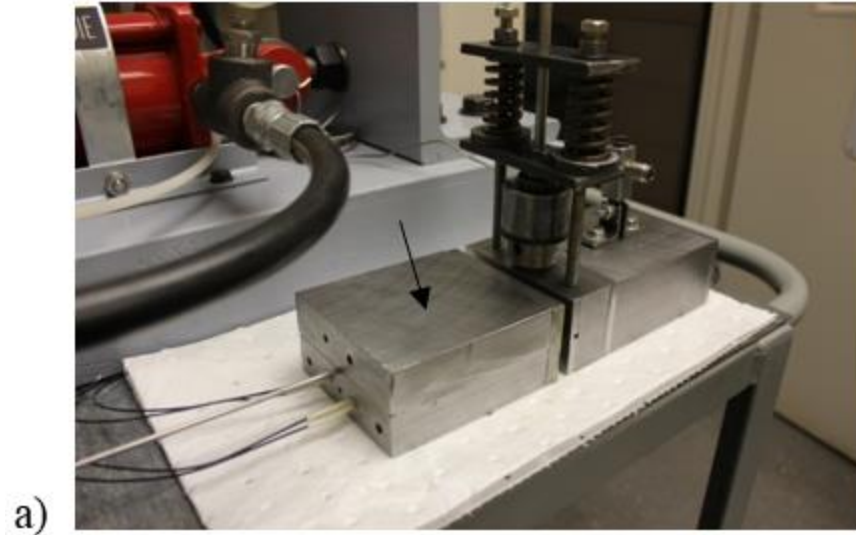


Figure 4.16 Pressing die

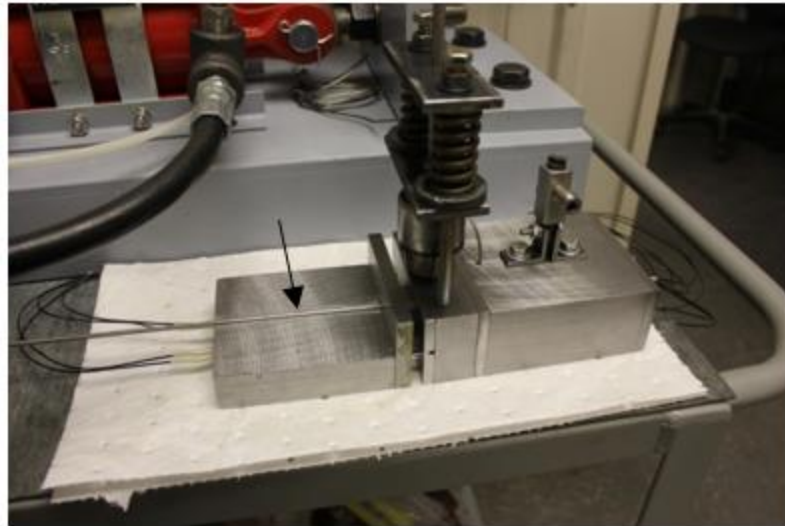
- a) Pressing die mounted in guide rails of the system
- b) Side view of pressing die with face plates and die insert holding block shown

Clamping Die

The next component consisted of the clamping die and clamping die face plates. The clamping die served to hold the aluminum rod in place during pressing. This component consisted of two carbon steel horizontally parted die halves each measuring 3.875 x 3.875 x 1.000 inches with a 0.109375 inch center hole drilled along the parting line. One 3.875 x 2.000 x 0.375 inch D2 tool steel face plate was attached to the die insert holding block side of the clamping die as shown in Figure 4.17.



a)



b)

Figure 4.17 Horizontally parted clamping die

a) Clamping die with both halves in place

b) Clamping die with top half removed

To provide additional clamping capacity to the work piece rods during pressing, an additional component was added to the system as illustrated in Figure 4.18. This component consisted of a clamping chuck mounted in a horizontal position on the rear side of the clamping die retaining plate. After the rods were inserted through the chuck

into the clamping die prior to pressing, the chuck was tightened to provide additional clamping force.

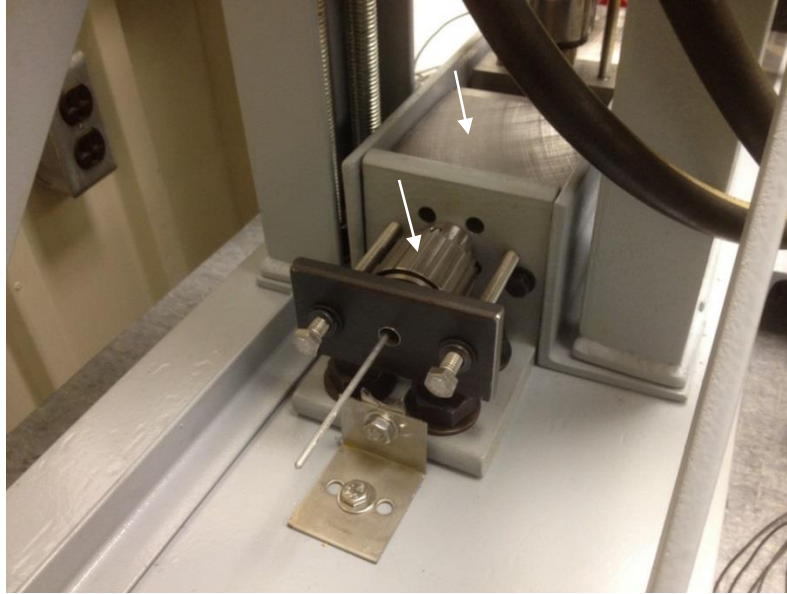


Figure 4.18 Clamping die with horizontally mounted chuck component

Reinforcing Guides

A final die component consisted of four reinforcing guides held in place by the clamping and pressing die face plates to prevent buckling of the rod within the indexing gap during processing. These die pieces were constructed of 0.0625 inch thick D2 tool steel.

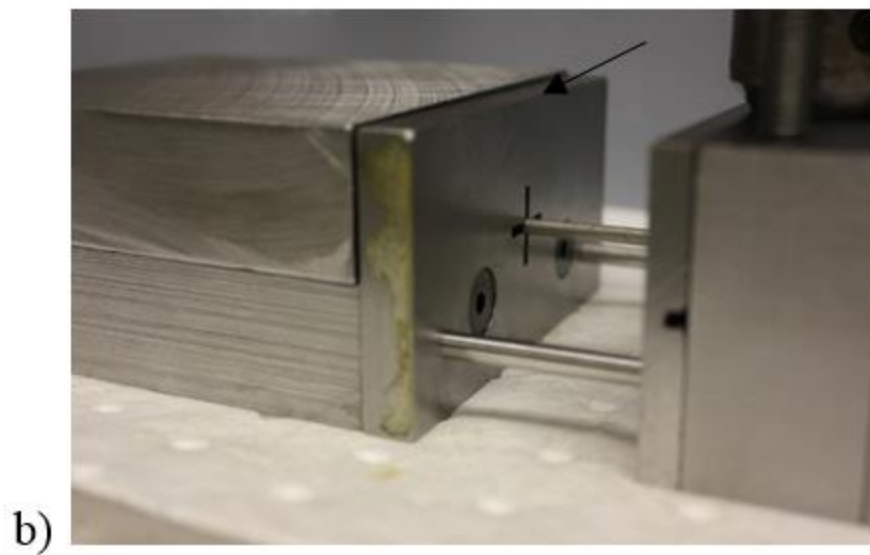
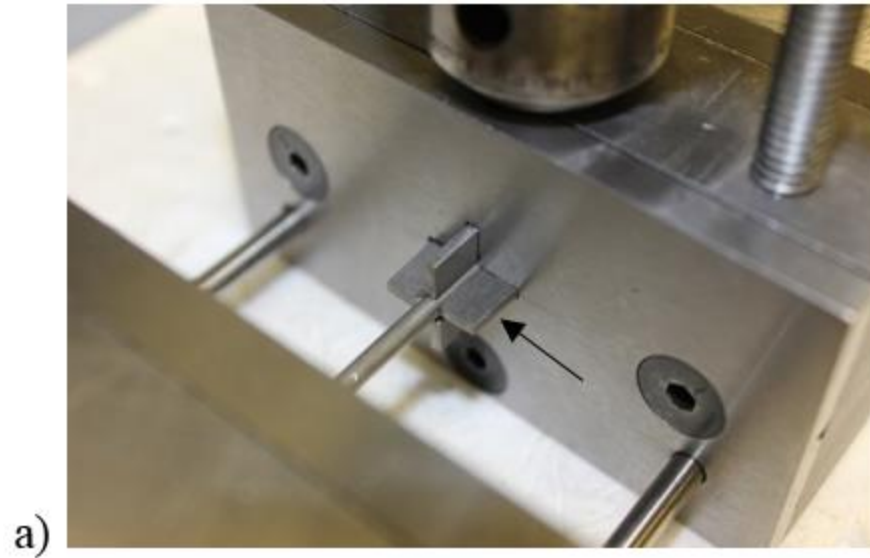


Figure 4.19 Reinforcing guides

- a) Reinforcing guides in pressing die face plate
- b) Reinforcing guide slots in clamping die face plate

Heat Treatment

Fabrication of die components not only required drilling, cutting, tapping, polishing, etc., but also subsequent heat treating to develop sufficient hardness. Heat

treatment for the D2 tool steel was performed in a Fisher Scientific isotemp programmable forced draft laboratory furnace as shown in Figure 4.20.

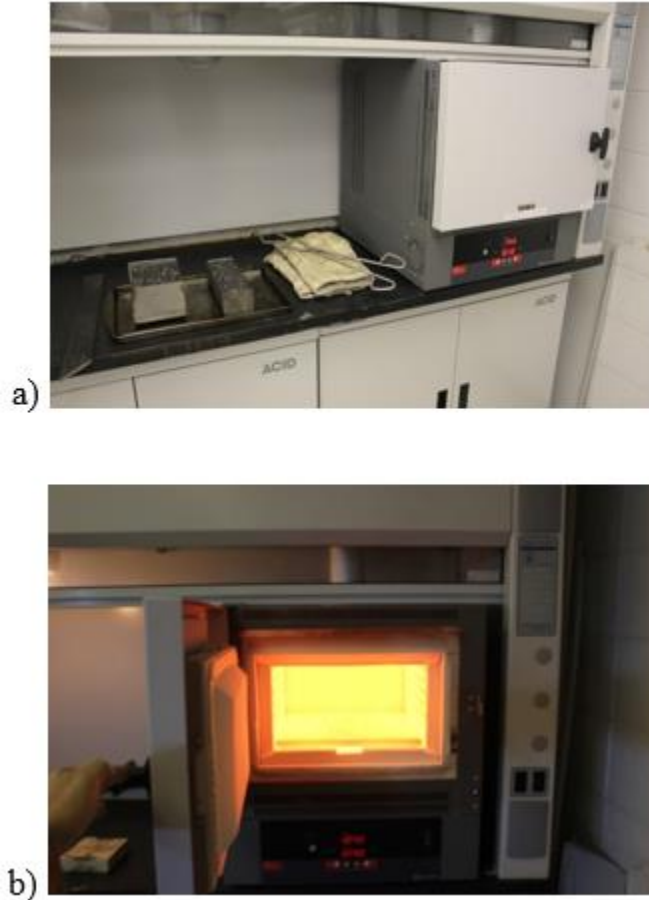


Figure 4.20 Heat treatment facilities for D2 tool steel dies

- a) Oven and die components ready for heat treating
- b) Oven during tool steel heat treating

For tool steel hardening heat treatment, the oven was pre-heated to an austenizing temperature of 1850 °F and allowed to stabilize. Die pieces were placed in cast iron chips to minimize surface oxidation as illustrated in Figure 4.21. Die components were placed in the oven for 25 minutes at the austenizing temperature after which the tools

were removed from the oven and allowed to air cool. Oven was re-set to a tempering temperature of 450 °F and allowed to stabilize. Dies were then placed back into the oven for two hours. Pieces were then removed from the oven and allowed to air cool. Tools were tempered twice using this respective procedure.

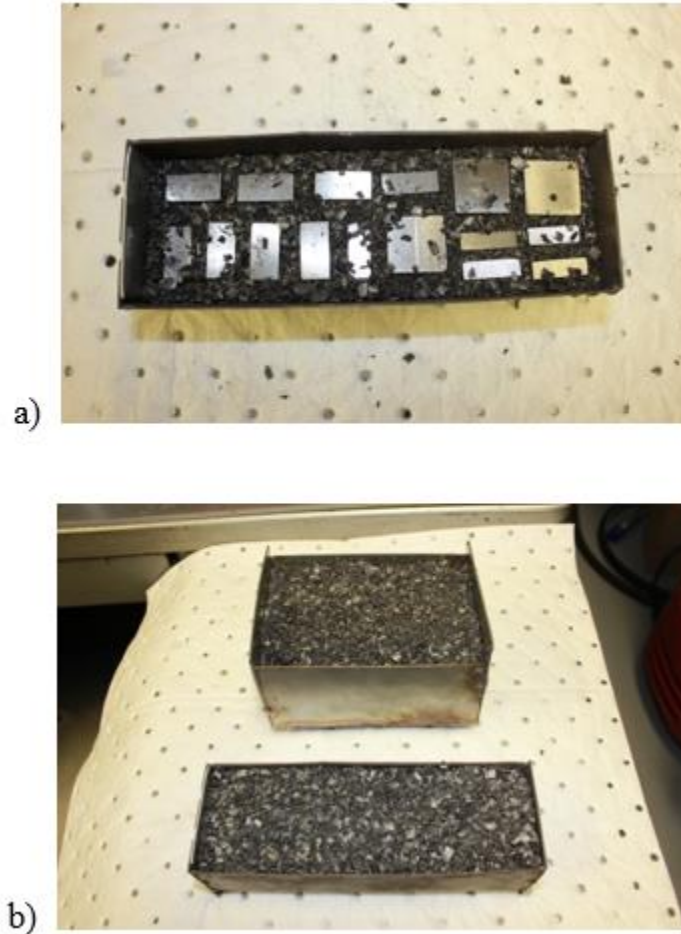


Figure 4.21 D2 tool steel dies packed in cast iron chips to minimize surface oxidation

- a) Uncovered die components in cast iron chips
- b) Covered die components in cast iron chips ready for heat treatment

Since the clamping die was made of soft carbon steel, the channel along which the aluminum rod would be securely held required a case hardening heat treatment. One inch

areas on each side of the channel along the entire length of the die halves were heated to 1450 °F and immediately covered with carburizing powder. The powder was then allowed to cool to ambient temperature. Powder covered areas were then re-heated to 1450 °F and immediately allowed to cool to room temperature as illustrated in Figure 4.22.

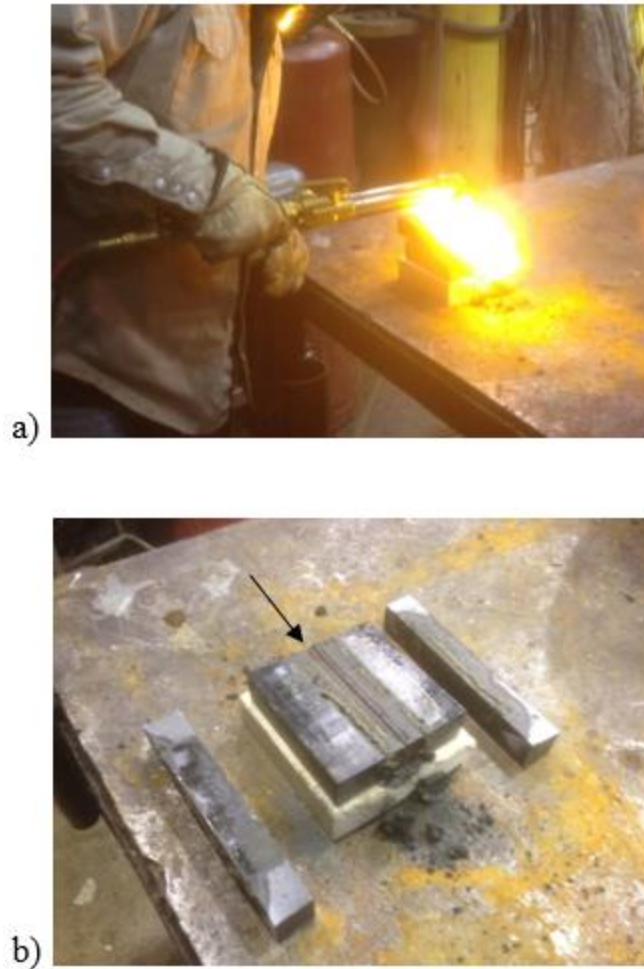


Figure 4.22 Clamping die during surface heat treatment

- a) Flame heating of clamping die
- b) Clamping die center line after surface hardening heat treatment prior to cleaning

After removal of residual powder and surface cleaning, hardness readings were taken along the channel on the top and bottom die halves using a Phase II MET-U1A50 hardness tester per ASTM A-1038-05 Standard Practice for Portable Hardness Testing by the Ultrasonic Contact Impedance Method (ASTM A 1038, 2005). Results were compared to readings taken prior to heat treatment. A summary of the heat treatments for each of the respective die components are provided in Table 4.3.

Table 4.3 Die component heat treatments

Die	Material	Heat Treatment	Description	Average Hardness (Before HT)	Average Hardness (After HT)
Die Inserts	D2 Tool Steel	<ul style="list-style-type: none"> ▪ Austenize at 1850 °F (20 min.) ▪ Air cool to ambient ▪ Temper at 450 °F (2 hrs) ▪ Air cool to ambient ▪ Temper at 450 °F (2 hrs) ▪ Air cool to ambient 	Through hardening of die.	22.5 HR _C	55.6 HR _C
Face Plates	D2 Tool Steel	<ul style="list-style-type: none"> ▪ Austenize at 1850 °F (20 min.) ▪ Air cool to ambient ▪ Temper at 450 °F (2 hrs) ▪ Air cool to ambient ▪ Temper at 450 °F (2 hrs) ▪ Air cool to ambient 	Through hardening of tool.	19.5 HR _C	55.9 HR _C
Reinforcing Guides	D2 Tool Steel	<ul style="list-style-type: none"> ▪ Austenize at 1850 °F (20 min.) ▪ Air cool to ambient ▪ Temper at 450 °F (2 hrs) ▪ Air cool to ambient ▪ Temper at 450 °F (2 hrs) ▪ Air cool to ambient 	Through hardening of tool.	42.8 HR _C	61.3 HR _C
Clamping Die	Carbon Steel	<ul style="list-style-type: none"> ▪ Heat to 1450 °F ▪ Apply hardening compound ▪ Re-heat to 1450 °F ▪ Air cool to ambient ▪ Remove hardening compound 	Carburizing case hardening along work piece channel axis.	161 HB	268 HB
Pressing Die	Carbon Steel	N/A	No thermal treatment.	N/A	N/A
Die Insert Holding Block	Carbon Steel	N/A	No thermal treatment.	N/A	N/A

Hydraulic Force Systems

Pressing Force

One of the most critical aspects of the entire process involved determining the forces required to press metal rods through the die. This aspect is vitally important since all remaining elements of the system were designed and built to accommodate these required pressing forces. For example, size selection of the hydraulic cylinder mounted in the horizontal position behind the pressing die was determined by this force requirement. Likewise, the clamping force and subsequent size of the hydraulic cylinder mounted in the vertical position used to hold the rod in the clamping die was based on this pressing force. Ultimately, the combination of these two hydraulic cylinders dictated the size of the hydraulic pump and power unit required to drive each of these cylinders. Supporting steel structures holding each of these hydraulic cylinders in place were then designed according to the hydraulic cylinder sizes which depended singularly on the pressing forces required within the system. These factors were not only important from a machine design standpoint, but also from an economic consideration. Machine elements are notably expensive and were designed accordingly to minimize project costs.

In order to determine the maximum pressing force from which the remaining elements of the system were built involved two alternatives, only one of which was selected due to economic constraints. The first and most preferable approach involved the use of finite element simulation software. This software has been used for several years in analyzing traditional ECAP processes to determine pressing forces, die forces, and even microstructure prediction of pressed components. The software has extensive

materials databases easily incorporating material properties of dies and pressed components. Versions of the software have been used extensively in academic work involving ECAP processes. However, no applications to the modifications employing Ix-ECAP have been noted. In order to further support the premise of this research, that being a simplistic approach to using existing enabling technologies to construct nanomanufacturing processes, an alternative was pursued which ultimately provided a very economical and viable solution in determining the pressing forces from which the entire system was built. This solution was provided by Perez and Luri, whereby, a method was developed with the primary purpose of providing practicing engineers and scientists an analytical solution that predicts required pressing forces for strain hardening circular cross section components in SPD processes such as ECAP (Perez and Luri, 2010). Analytical equations as noted on the following page were developed using the Upper Bound Method (UBM) which predicted required pressing forces. In using the method within this dissertation, parameters representing the Ix-ECAP process were entered into Excel using the analytical expressions for the extrusion pressure. The required pressing forces were then obtained using the extrusion pressures applied to the cross sectional areas of the rods used in the Ix-ECAP process. Analytical expressions as proposed by Perez and Luri are presented on the following pages. Once the equations were programmed into Excel, the effects of changes to various parameters such as pressing temperature, die design variables, rod diameters, and material properties were readily analyzed with regards to required pressing forces with subsequent implications to process design.

$$\begin{aligned} \sigma = & \sigma_{\text{mean}} \cdot \frac{1}{\sqrt{3}} \left[\frac{\pi - \emptyset}{\sin\left(\frac{\emptyset - \varphi}{2}\right)} \right] + \sigma_y \cdot \frac{2m}{\sqrt{3}} \left[\frac{2L_{\text{entrance}}}{D} + \cot\left(\frac{\emptyset - \varphi}{2}\right) \right] \\ & + \sigma_{\text{mean}} \cdot \frac{2m}{\sqrt{3}} \cdot \frac{(\pi - \emptyset)}{\sin\left(\frac{\emptyset - \varphi}{2}\right)} \left(\frac{R_{\text{internal}} + R_{\text{external}}}{D} \right) \\ & + \sigma_f \cdot \left[\left(\frac{2L_{\text{initial}}}{D} \right) - \cot\left(\frac{\emptyset - \varphi}{2}\right) - \frac{(\pi - \emptyset)}{\sin\left(\frac{\emptyset - \varphi}{2}\right)} \cdot \left(\frac{R_{\text{internal}} + R_{\text{external}}}{D} \right) - \frac{2L_{\text{entrance}}}{D} \right] \end{aligned} \quad (4.1)$$

$$\varphi = 2 \tan^{-1} \left\{ \left(\frac{2L_{\text{initial}}}{D} \right) 2 \tan^{-1} \left[\frac{\left(\frac{R_{\text{internal}} - R_{\text{external}}}{D} \right) \tan\left(\frac{\emptyset}{2}\right)}{1 + \left(\frac{R_{\text{internal}} - R_{\text{external}}}{D} \right) + \tan^2\left(\frac{\emptyset}{2}\right)} \right] \right\} \quad (4.2)$$

$$\varepsilon_f = \frac{1}{\sqrt{3}} \left\{ 2 \cot\left(\frac{\emptyset - \varphi}{2}\right) + (\pi - \emptyset) \left[1 - \cot\left(\frac{\emptyset - \varphi}{2}\right) \tan\left(\frac{\emptyset}{2}\right) \right] \right\} \quad (4.3)$$

$$\sigma_f = k(\varepsilon_f)^n \quad (4.4)$$

$$\sigma_{\text{mean}} = \frac{k(\varepsilon_f)^n}{n+1} \quad (4.5)$$

Where:

σ = pressing force

σ_{mean} = mean value of stress

σ_f = material yield or flow stress after one pressing

φ = angle between tangent points between channels and fillet radii

\emptyset = intersection angle between channels

ε_f = total equivalent plastic strain after one pressing

D = channel or rod diameter

m = shear friction coefficient

k = Hollomon model strength coefficient

n = Hollomon model strain hardening exponent

R_{internal} = Radius of the internal corner of the pressing channel

R_{external} = Radius of the external corner of the pressing channel

L_{entrance} = Length of rod in the entrance channel of the pressing channel

L_{initial} = Length of the rod prior to pressing

Designing the system to accommodate all possible factors to be studied depended on determining the maximum pressing force the system would experience. For example, even though the materials to be considered in this research were 1100 and 4043 aluminum alloys, the system was designed to handle much higher strength materials such as copper, carbon steel, and type 316 stainless steel to accommodate future research. Naturally, steel is much stronger than aluminum; therefore, the pressing force for 316 stainless steel was the controlling design consideration for sizing and selecting hydraulic cylinders. Also, the maximum force had to take into consideration pressing temperatures. Two temperatures were selected to accommodate the aluminum trials at ambient and 175 °F. Since high temperature offers a softening effect or decrease in flow stress to the metal rods, the lower temperature pressing force represented the design criteria. Furthermore, a back pressure force was an additional process factor consideration. As a result, a predetermined 0.25-ton force was added to the maximum pressing force. Another primary factor is the number of passes the rods were pressed through the die. As the number of passes increases, additional strain is induced into the metal components, thereby, increasing the strength of the material and required pressing forces. Thus, the pressing force for system design was obtained from an analysis using eight passes to configure the system for margins of safety and potential future investigations. Lastly, die channel surface finish and lubrication is important from the standpoint of the effect on the shear friction coefficient. As the friction coefficient is reduced through a smooth surface

finish and exceptional lubricant, pressing forces can be reduced significantly. Therefore, higher friction coefficients can be compared to lower or anticipated values to assess the impact on increased pressing force.

Based on the aforementioned considerations, the stroke versus pressing force curves for 0.125- and 0.15625-inch diameter rods are shown in Figures 4.23 and 4.24, respectively, on the following pages. Even though 0.125-inch diameter rods are the focus of this research, 0.15625-inch diameter rods will also be considered as a contingency for process development. Of special note is the fact that analytical expressions for pressing forces given by Perez and Luri only applies to one pass through the die. Force curves for four and eight passes are based on values obtained from actual pressing of 316 stainless steel as reported experimentally (Ueno, Kakihata, Kaneko, Hashimoto, and Vinogradov, 2011). Based on knowledge of the strain hardening behavior and resulting mechanical properties obtained from similar equal channel angular pressing studies, pass #4 and #8 curves were calculated as multiples of the pass #1 values. As reflected by each of the respective graphs, the maximum pressing force for a 0.125-inch diameter 316 stainless steel rod is 3.7 tons; whereas, the value for the 0.15625-inch rod at full stroke through the die and pass #8 is 5.2 tons. Values were based on a shear friction coefficient of 0.125 and a back pressure force of 0.25 tons.

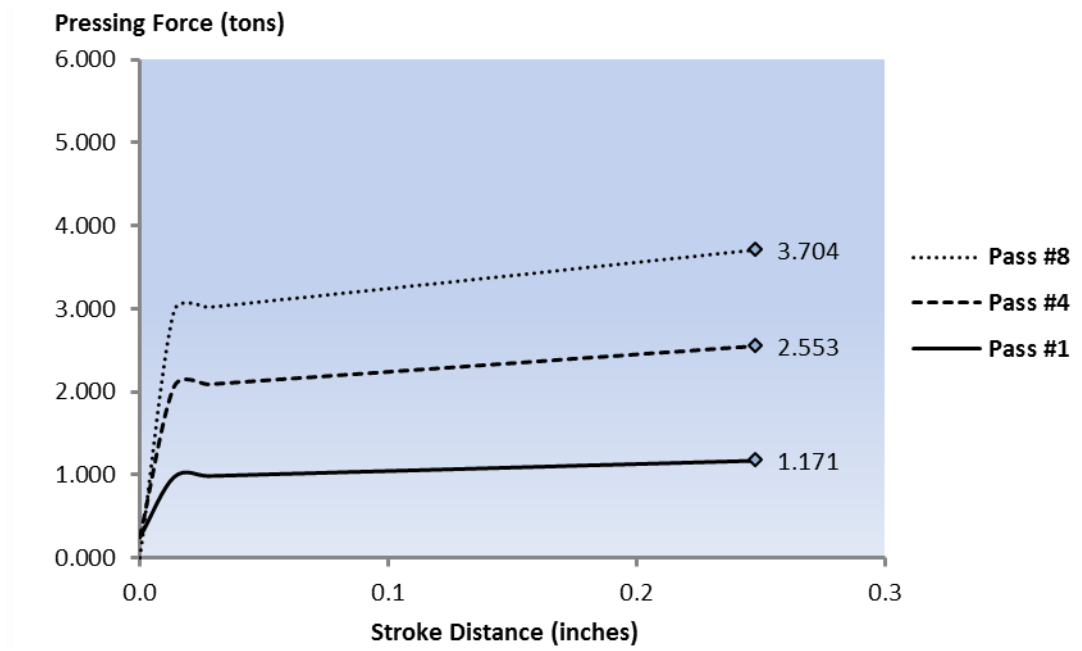


Figure 4.23 Pressing forces for 0.125-inch diameter 316 stainless steel rod with 0.25 tons of back pressure force ($m = 0.125$)

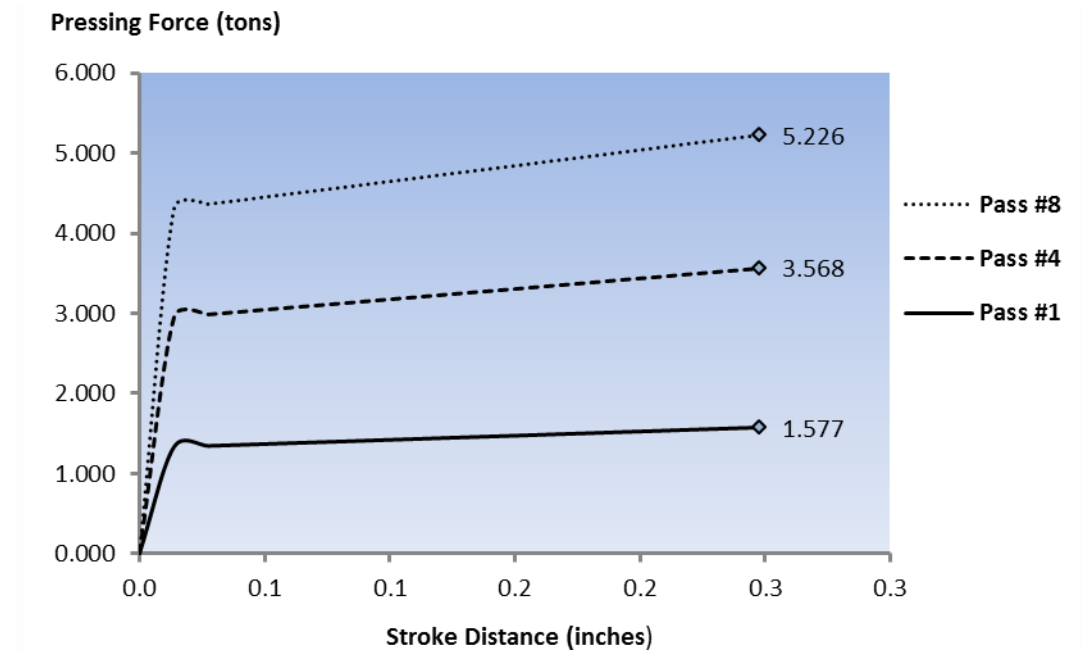


Figure 4.24 Pressing forces for 0.15625-inch diameter 316 stainless steel rod with 0.25 tons of back pressure force ($m = 0.125$)



Figure 4.25 Horizontally mounted hydraulic cylinder for pressing force

Clamping Force

Once values for the maximum pressing force were determined, the next critical step was to determine the clamping force required by the vertically mounted hydraulic cylinder located over the clamping die. Conventional friction force system analysis was used to calculate this required force. For example, the block with weight, W , resting on the zero inclined plane shown in Figure 4.26 is pulled by a force, P . However, static friction, μ , between the block and the plane resists such forward motion by an opposing friction force. The opposing friction force relationship using the nomenclature described above is defined as (Higdon, Stiles, Davis, and Evces, 1976) :

$$F_f = \mu W \quad (4.6)$$

Where:

F_f = opposing friction force

μ = static friction

W = block weight

Therefore, equilibrium will be maintained and the block will not move as long as the opposing friction force is equal to the pulling force, i.e. $F_f = P$.

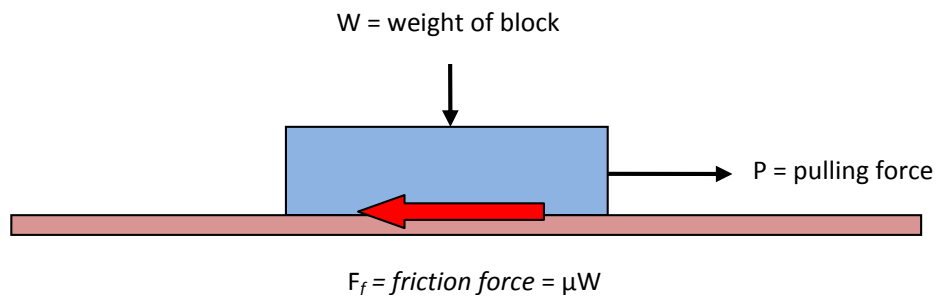


Figure 4.26 Conventional friction force analysis

Extending this analysis in determining the clamping force for the IX-ECAP process was obtained by considering the weight of the block to be negligible. The block is now assumed to be the metal rod in the clamping die with negligible weight. With this scenario, an additional plane will be placed on top of the block with a clamping force, C, applied to the top plane as illustrated in Figure 4.27.

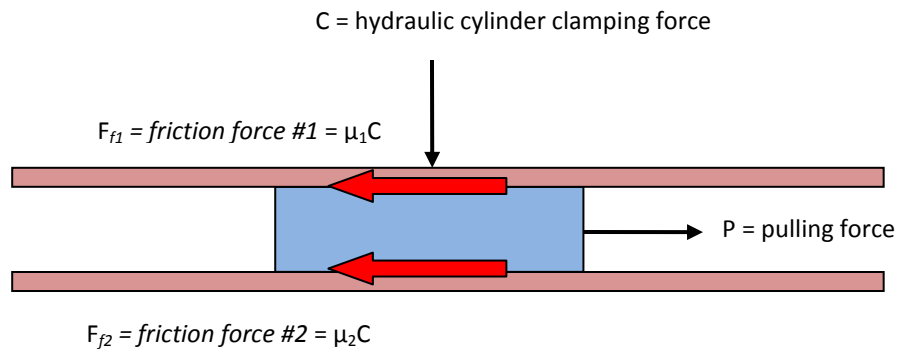


Figure 4.27 Friction force analysis for clamping die.

The opposing friction forces are defined as follows:

$$F_{f1} = \mu_1 C \quad (4.7)$$

$$F_{f2} = \mu_2 C \quad (4.8)$$

Summing forces in the horizontal or x-direction gives:

$$P = F_{f1} + F_{f2} = \mu_1 C + \mu_2 C \quad (4.9)$$

Assuming equal friction conditions exists for both planes, $\mu_1 = \mu_2 = \mu$, gives:

$$P = F_{f1} + F_{f2} = \mu_1 C + \mu_2 C = \mu C + \mu C = 2\mu C \quad (4.10)$$

Therefore, solving for the required clamping force, C, gives:

$$C = \frac{P}{2\mu} \quad (4.11)$$

Using a static coefficient of friction of 0.75 and values obtained for pressing forces of the 0.125- and 0.15625-inch diameter stainless steel rods, 3.7 and 5.2 tons respectively, gives the following required clamping forces:

$$C = \frac{P}{2\mu} = \frac{3.7 \text{ tons}}{2(0.75)} = 2.5 \text{ tons} \quad (4.12)$$

$$C = \frac{P}{2\mu} = \frac{5.2 \text{ tons}}{2(0.75)} = 3.5 \text{ tons} \quad (4.13)$$

Therefore, the hydraulic cylinder located in the vertical position over the clamping die must be designed to exert a minimum of 3.5 tons. It is noteworthy to consider the effect of a decrease in the friction coefficient. In the event μ is reduced to 0.50, then the clamping forces as noted above now reflect values of 3.7 and 5.2 tons, respectively. A conceptual design view of the cross section of the clamping die is illustrated in Figure 4.28.

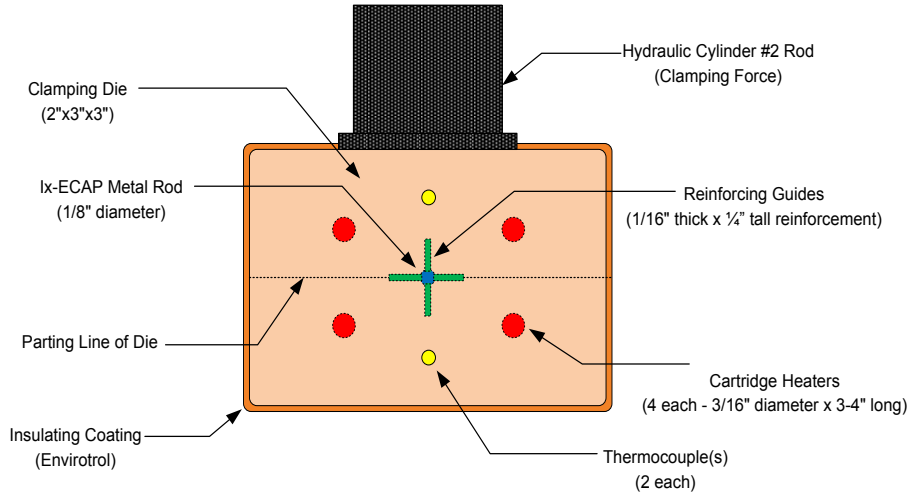


Figure 4.28 Clamping die conceptual design cross section

Proper size selection of the two hydraulic cylinders ensured adequate pressing force, clamping force, and pressing speed. As discussed previously in determining the required pressing and clamping forces to process the metal rods through the Ix-ECAP machine, at least 5.2 tons (10,400 lbs.) of both pressing and clamping force capacities were needed based on contingencies for 316 stainless steel. Therefore, hydraulic cylinders were sized accordingly. Hydraulic cylinder force capabilities were readily determined by the following relationship which is illustrated in Figure 4.29:

$$F = p(A_p) \quad (4.14)$$

Where: F = extension force of hydraulic cylinder, lbs. of force
 A_p = hydraulic piston area, in.²
 p = pressure of the hydraulic fluid applied to the piston, psi

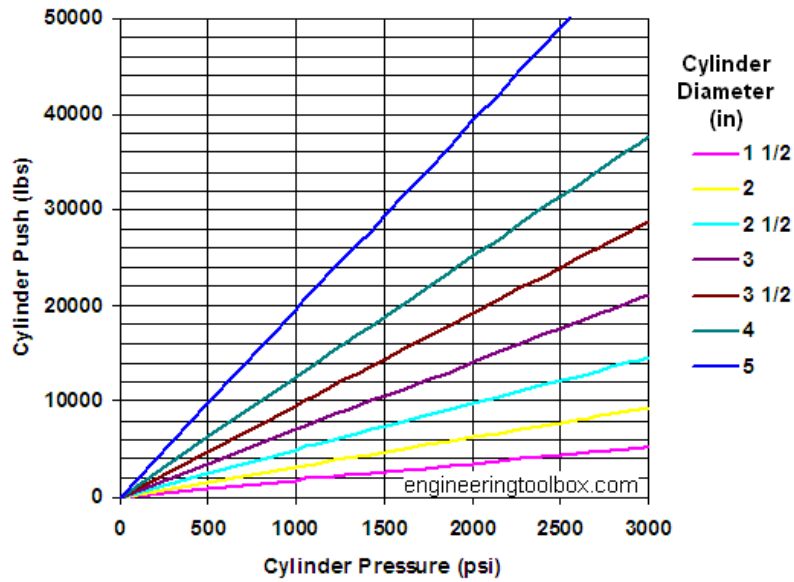


Figure 4.29 Hydraulic cylinder performance curves

Reference: http://www.engineeringtoolbox.com/hydraulic-force-calculator-d_1369.html

Using a system hydraulic pressure of 2,300 psi, the following cylinder sizes produce the extension forces as shown in Table 4.4.

Table 4.4 Hydraulic cylinder size versus extension force

Hydraulic Cylinder Size (inches)	Extension Force (tons)
2.50	5.7
3.25	9.6
4.00	14.5

Therefore, to ensure sufficient forces were available to process the material with additional contingencies that may be encountered during process development, 4-inch bolted hydraulic cylinders rated at a maximum pressure of 2,500 psi were selected for

both the pressing and clamping dies. This type cylinder is shown in Figure 4.30 on the following page.

Protection against potential damage to the clamping dies, support structures, and underlying components such as the insulating firebrick was added to the system. This was accomplished by attaching two parallel mounted clamping steel plates separated by four extra heavy duty chrome silicon steel compression springs to the clamping die hydraulic cylinder rod as shown in Figure 4.30. Load rate for each spring was 4,085 pounds per inch. With a maximum deflection of 25%, the springs allowed a clamping force of 4.085 tons to be applied with dampening protection to the clamping die and support structures.



Figure 4.30 Vertically mounted hydraulic cylinder

Cylinder Speed and Motion Control

Two levels of pressing speed were used to process the metal rods. The fast speed was 762 mm/minute (30 inches/minute); whereas, the slower speed was 25.4 mm/minute (1.0 inch/minute). The extension speed of the hydraulic piston rod is based on two primary factors, that being the area of the piston rod and flow rate of the hydraulic fluid through the system. These relationships are expressed mathematically as follows (http://www.engineersedge.com/fluid_flow/cylinder_piston_velocity.html):

$$V_E = \frac{[231(Q)]}{A_P} \quad (4.15)$$

Where: V_E = extension rate of the piston rod = pressing speed, in./minute

A_P = hydraulic piston area, in.²

$$A_P = \frac{\pi(D_P)^2}{4} \quad (4.16)$$

D_P = hydraulic piston diameter, in.

Q = flow rate of the pressurized fluid, gpm

231 = numerical constant representing the number of in.³ per gallon

To design the hydraulic system components supporting the hydraulic cylinders, specifically the hydraulic pump and flow control valves, the relationships noted above were rearranged to determine the required flow rate, Q , of the hydraulic fluid since the pressing speeds had already been pre-selected. These speeds were based on knowledge of traditional ECAP and its extension to the IX-ECAP process as identified in the literature reviews.

Therefore, rearranging Equation 18 gives the required flow rates of the hydraulic system as follows:

$$Q = \frac{V_E(A_P)}{231} \quad (4.17)$$

Flow rate requirements in gallons per minute (gpm) for a four inch cylinder at the two pressing speeds are shown in Table 4.5.

Table 4.5 Hydraulic pressing speed versus flow rate for four inch cylinder

Pressing Speed (inches / minute)	Flow Rate (gallons / minute)
-------------------------------------	---------------------------------

30	1.6312
1	0.0544

The small flow rates reflect the comparatively slow pressing speeds employed in the I_X-ECAP process. Industrial applications using hydraulic cylinders with four-inch piston rods have capabilities to operate at much faster extension speeds. This particular prototype system, therefore, utilized flow control valves and hydraulic pumps with small flow ratings. Scale up to larger manufacturing settings would require much higher flow rate capacities in flow control valves and pumps. In order to run the I_X-ECAP process, a dual-control mono-block directional 8-gpm 4-way/3-position spring center flow control valve was used to activate both hydraulic cylinders as shown in Figure 4.31.

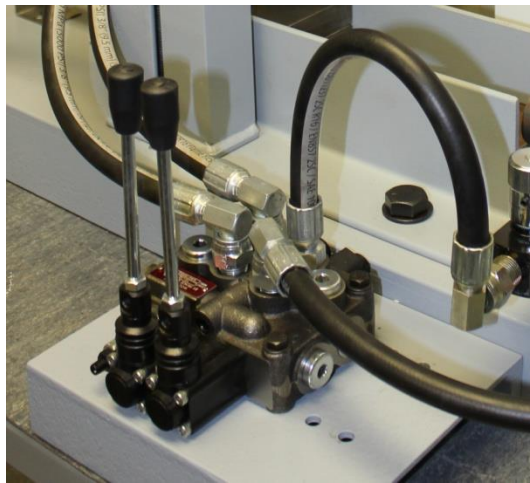


Figure 4.31 Dual-control mono-block directional 8-gpm 4-way/3-position spring center flow control valve

As shown in Figure 4.32 (a), use of the directional control valve allowed the pressing and clamping cylinders to be controlled individually during the indexing cycles. To provide additional precision in controlling pressing speed, an adjustable inline flow

control valve rated at 3,000 psi maximum pressure and 15 gpm was installed at the pressing die hydraulic cylinder as shown in Figure 4.32 (b).

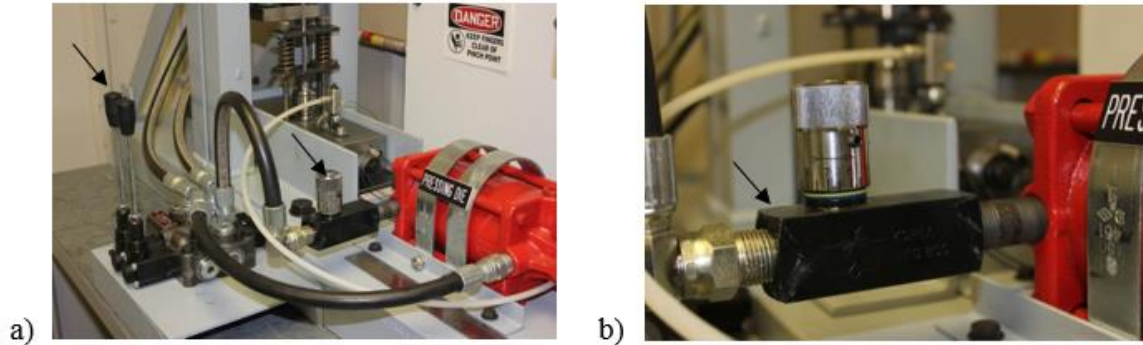


Figure 4.32 Flow control valves mounted in manufacturing unit

- a) Bidirectional and inline valve mounted in manufacturing unit
- b) Adjustable inline valve close up view

Hydraulic Power Unit

Another critical component of the system is the hydraulic pump supplying necessary fluid pressures and flows to the cylinders. These two criteria, in conjunction with cylinder size, determine whether the required pressing forces and speeds would be achieved. Based on design requirements of the IX-ECAP process as discussed previously, specifically pressure cylinders operating at 2,500 psi and flow rates at less than 1 gallon per minute, a heavy-duty two-stage hydraulic pump rated at 3,000 psi maximum pressure with high and low flow capacities of 11 and 1.1 gallons per minute, respectively, was selected. The pump was driven by a 160 cc OHV Honda gasoline powered engine.

Vibration System

The addition of vibrational energy to the process offers a unique approach. Within this research vibration will be considered at two levels, that being no vibration

and vibration applied. A miniature pneumatic vibrator based on high output frequencies and moderate force loads was selected. The unit selected was a Cleveland miniature pneumatic vibrator model number VM-25 which performs at 14,000 vibrations per minute with a 12-pound force or impact load. The Cleveland vibrator required 60 psig of air pressure minimum, 1.6 cfm capacity, and was mounted to the top of the pressing die as shown in Figures 4.33 and 4.34.

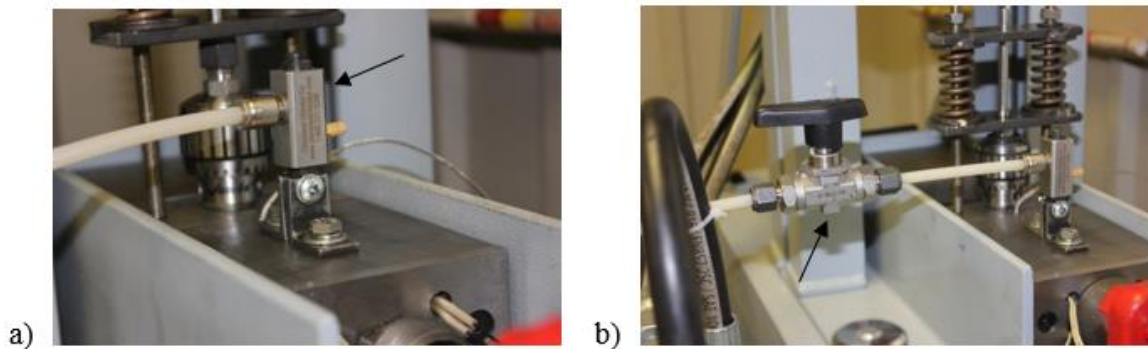


Figure 4.33 Miniature pneumatic vibrator

- a) Miniature pneumatic vibrator mounted on top of pressing die
- b) Vibrator with air flow control valve



a)



b)

Figure 4.34 Vibrator air supply

a) Vibrator mounted to pressing die with airline attached.

b) Compressor providing air supply

Back Pressure

Without question, the most challenging aspect of the design process involved determining a simple, economical, safe, and appropriate method to apply a back pressure force to the metal rod upon exit from the die. This criterion was especially difficult considering the use of continuous length rods. However, after extensive designs and re-designs the mechanism illustrated in Figure 4.35 was selected for the initial trial runs.

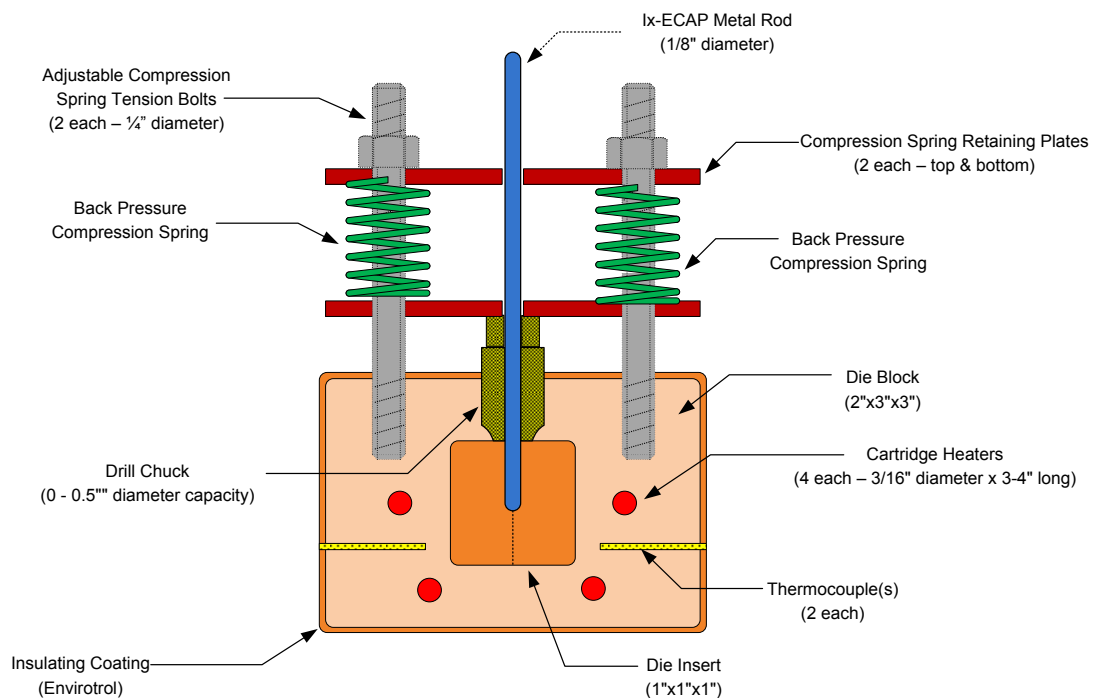


Figure 4.35 Concept design of cross section view of back pressure components

As previously reported in the literature review, back pressure applied in ECAP processes has shown to offer significant advantages in overcoming limitations of the ECAP process. For example, surface cracking in pressed components was eliminated through back pressure by changing the surface stress state from tensile to compressive in

certain areas of the work piece. Also, the anomaly of increasing strength in conjunction with increasing a material's elongation was overcome in some alloy systems with the application of back pressure. Therefore, the motivation to include back pressure within this research was substantial.

As illustrated in Figure 4.35, back pressure was initially applied to the exiting rod by the use of two compression springs held between two retaining plates. The springs and plates were held in place by two studs placed through the center of the springs and threaded into the high strength steel pressing die. Adjusting nuts were then attached to the studs on the top retaining plate. The metal rod passed through circular openings in both retaining plates. From a safety standpoint, securing the springs by placing the rods through the center of the springs was critical. Compressed springs inadvertently released during the I_x-ECAP cycle would pose a serious potential for injury.

To apply back pressure during indexing, the exiting metal rod fed through a manual drill chuck located below the bottom compression spring retaining plate. Prior to indexing the die, the drill chuck was manually tightened, gripping the rod. As the rod exited the die, the drill chuck clamping the rod pushed the bottom retaining plate upwards, compressing the springs. At the end of the 0.250-inch indexing stroke, the drill chuck was carefully and manually released allowing the springs to force the chuck back down to the exit channel of the die insert. The chuck was then manually tightened around the exiting metal rod ready for another indexing cycle. In future industrial integration, automated pneumatic or hydraulic chuck collars would provide better alternatives to manual operation.

Medium and heavy load high performance chrome-silicon die steel springs were used to apply 0.25 to 0.43 tons of total back pressure force. Medium load springs were used to ensure no surface cracking occurred on the work piece; however, as a contingency for the application of additional pressure, medium load springs could easily be changed to heavy load springs. As shown in Figure 4.36 on the following page, medium load springs provide a spring load rate of 400 pounds/inch; whereas, the heavy load spring load rate is 900 pounds/inch. With a maximum deflection as per manufacturer's specification, the medium load spring can only be compressed 37% of its length. Therefore, the springs were pre-compressed 0.500 inches by tightening the nuts on the top retaining plates prior to the start of the indexing cycle to give a back pressure force of 0.200 tons. The rod was indexed through the die for an additional distance of 0.250 inches giving a total compressed die spring distance of 0.750 inches. At this final compressed distance, the springs exerted a total of 0.300 tons on the rod. Similarly, heavy load springs may only be compressed 30%; therefore, the spring could be compressed from 0.350 to 0.600 inches giving a back pressure force of 0.315 to 0.540 tons during the indexing cycle.

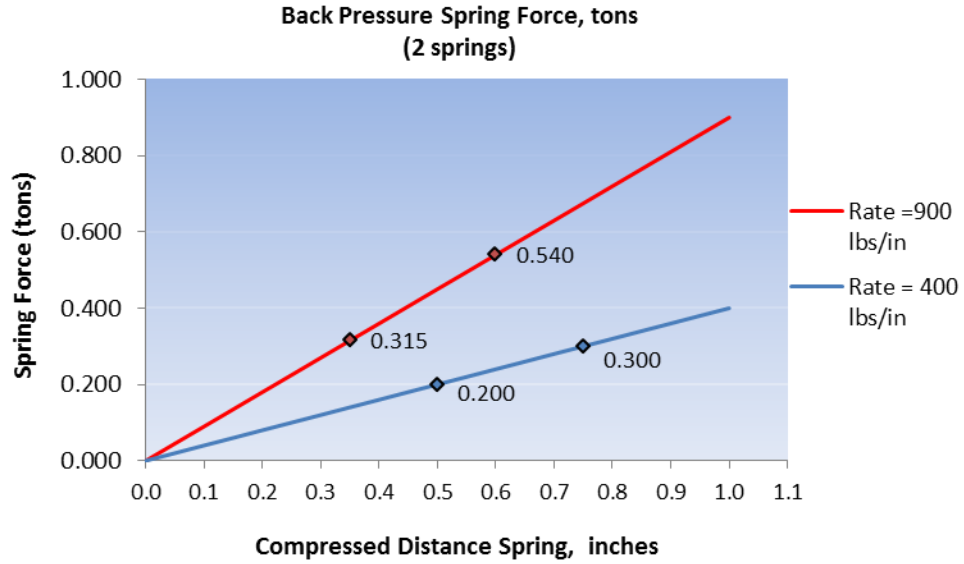


Figure 4.36 Back pressure spring force

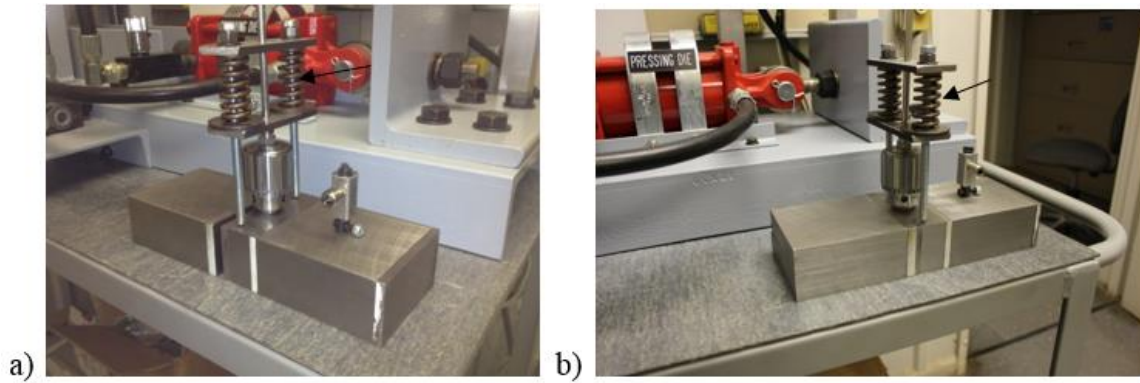


Figure 4.37 Back pressure components mounted to the die insert holding block

- a) Front view of back pressure spring mechanism
- b) Back view of back pressure spring mechanism

Heating System

Metal working processes often require elevated temperatures due to reductions in work piece flow stress resulting in lower pressing forces for equipment, less opportunities for damage mechanisms in pressed components, etc. As such, anticipated use and potential benefits of high temperatures in the I_x-ECAP process is no exception. This research, therefore, studied processing temperatures at two levels, that being an ambient temperature of 25 °C (77 °F) and a higher level at 79.4 °C (175 °F). However, as stated previously, designs of heating systems were made to accommodate contingencies for future research using both non-ferrous and ferrous materials such as 316 stainless steel. Therefore, pressing temperatures to 302 °F was the thermal design upper limit. In order to attain the higher 302 °F temperatures, circular cartridge heaters were designed for insertion into both the clamping and pressing dies. These heating elements were connected to electrical relays which, subsequently, were connected to a temperature controller. Thermocouples were inserted into each die to provide feedback to the controller. The temperature control unit to be used in this research was a Yokogawa model #UT52A controller. Controllers and cartridge heaters are shown in Figures 4.38 and 4.39 on the following page. Maintaining an elevated temperature in the clamping die would serve as a pre-heat prior to actual pressing; whereas, heating the pressing die would establish the metal forming temperature. A 1.0-mm thick thermal insulating Envirotrol[®] ceramic coating was applied to the exterior surfaces of the clamping die, pressing die, and face plates to minimize heat loss as shown in Figures 4.41 and 4.42. Thermal images illustrating heat distribution throughout the dies are shown in Figure 4.43.

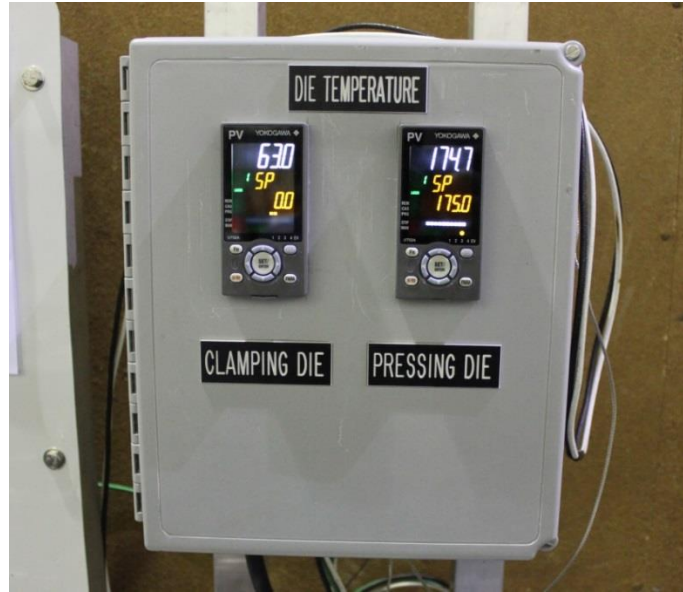


Figure 4.38 Temperature controllers for clamping and pressing dies

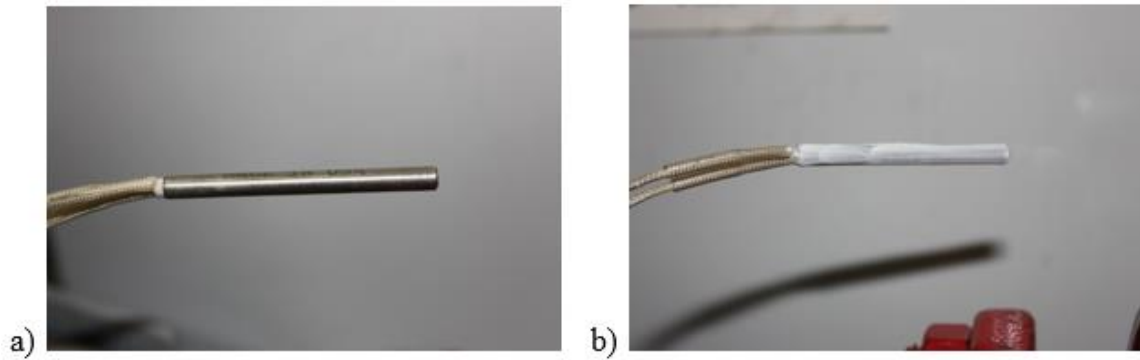


Figure 4.39 Cartridge heaters

- a) Uncoated cartridge heater
- b) Cartridge heater with anti-seize coating

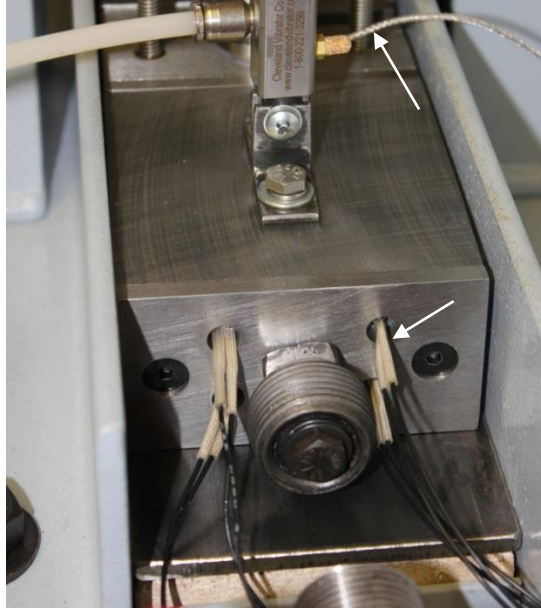


Figure 4.40 Cartridge heaters and thermocouple inserted into pressing die

Note: Pressing die placed on 0.250-inch steel wear plate mounted on fire brick for thermal protection to bottom base frame of the system

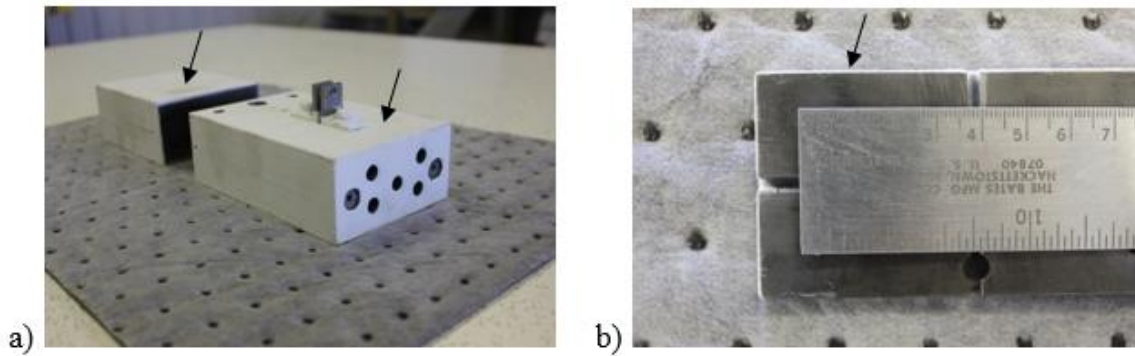


Figure 4.41 Envirotrol® thermal insulation coating applied to die components

- a) Pressing and clamping dies with thermal insulation coating
- b) End view of pressing die face plate showing thickness of thermal insulation coating



Figure 4.42 Thermally insulated pressing and clamping dies placed in manufacturing unit

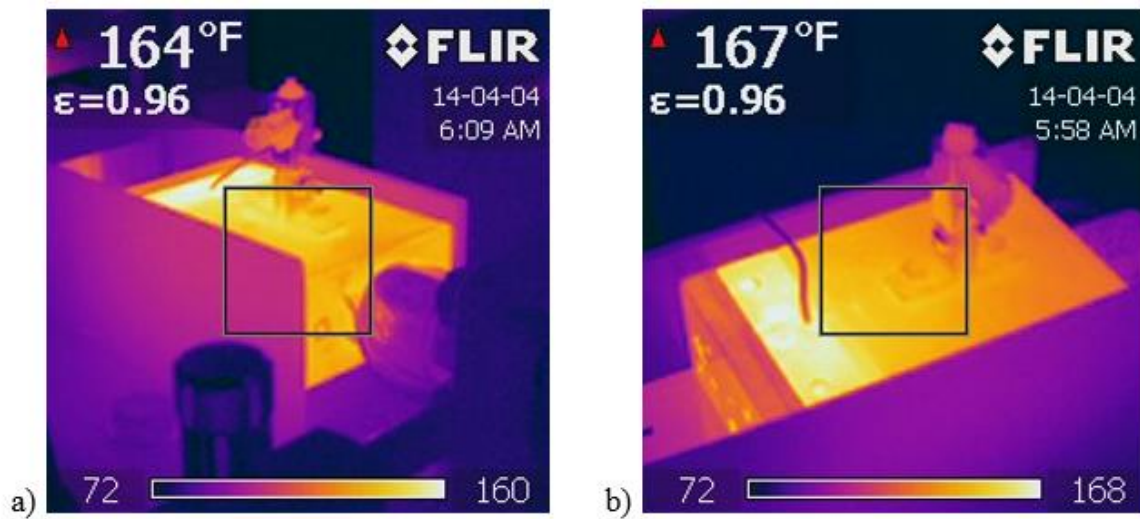


Figure 4.43 Thermal images of pressing die

- a) Infrared thermal image of back view of pressing die
- b) Infrared thermal image of front top view of pressing die

Materials - Alloy Selection and Work Piece Form

Proper sample selection through metallurgical alloy considerations plays a vital role in the success of the research study. This assessment also contributes towards commercial viability and promotion of nanostructured materials ensuring universal acceptance within the engineering community. Several factors contribute to the selection of types 1100 and 4043 aluminum for this research. A first consideration is the extension of knowledge to existing research regarding SPD processes producing nanocrystalline materials. For ECAP, severe plastic deformation involves the inducement of significant strains within a solid component through mechanical means without subsequent changes in cross-sectional dimensions. Research studies involving ECAP and cryomilling have provided detailed analyses involving non-ferrous metals such as aluminum and copper (Zhu et al., 2004; Brochu, Zimmerly, Ajdelsztajn, Lavernia, and Kim, 2007; Haouaoui, 2005). A continuation of research promoting the transfer of such processes and materials from laboratory to commercialization is warranted.

Of foremost importance, however, are the inherent properties of the material itself in conduciveness to nanocrystalline propensity and response to plastic deformation. Specifically, aluminum alloys 1100 and 4043 are relatively soft metals possessing good ductility making these materials ideal for consideration in mechanical forming operations such as ECAP. Additionally, the metals possess inherent properties whereby microstructures remain stable as single-phase alloys from room temperature to elevated temperatures, thereby providing continuity within processing operations. Based on this aforementioned consideration, these materials do not respond to hardening through heat effects or thermal treatment, but can be hardened due to mechanical working. This

hardening effect promotes increases in strength, but with possible reductions in ductility or toughness. However, this provides opportunistic response beyond traditional materials through investigations of nanocrystalline processing. Another inherent property related to aluminum is the low stacking fault energy of the crystal structure which provides an indication of the degree of response to mechanical forming. It is reported that low stacking fault materials respond to plastic deformation by possessing a greater responsiveness to hardening and retention of fine stable grains within the metal (Hertzberg, 1996; Haouaoui, 2005). Each of these respective aspects of 1100 and 4043 aluminum contributes favorably to improvements in mechanical properties and increased probabilities of attaining nanocrystalline features. From a commercial familiarity perspective, it is important to note that aluminum represents the most available metallic element found on earth (Smith, 1993; Smith, 1993). Therefore, a commonality and familiarity with these respective materials within the industrial community further encourages commercial acceptance of IX-ECAP products.

One work piece form and two metal alloys were used for analysis in this research. Work piece form consisted of 0.125-inch diameter welding rods. Materials selected for investigation were 1100 and 4043 aluminum. However, contingency materials for possible future use or system performance trials were also selected and prepared. These materials included 316L stainless steel and AWS 5.27 copper alloy welding rods. Alloy chemical compositions and typical room temperature mechanical properties in the fully annealed condition are provided in Tables 4.6, 4.7, 4.8 and 4.9 on the following pages.

Table 4.6 Chemical compositions of 1100 and 4043 aluminum and AWS 5.27 copper alloy

Element	1100 Aluminum wt. %	4043 Aluminum wt. %	AWS 5.27 Copper wt. %
Aluminum	99.00 min	Remainder	0.01
Copper	0.05 – 0.20	0.30 max	56.0 – 60.0
Manganese	0.10 max	0.05 max	0.01 – 0.50
Zinc	0.05 max	0.10 max	-
Beryllium	0.0008 max	0.0008 max	-
Silicon	1.0 max (Si + Fe)	4.5 – 6.0	0.04 – 0.15
Iron	1.0 max (Si + Fe)	0.80 max	0.25 – 1.20
Titanium	-	0.20 max	-
Lead	-	-	0.05
Tin	-	-	0.80 – 1.10
Others	0.15 max total	0.05 max each	-

Table 4.7 Room temperature mechanical properties of annealed 1100 and 4043 aluminum and AWS 5.27 copper alloy

Property	1100 Aluminum	4043 Aluminum	AWS 5.27 Copper (As-Welded)
Tensile Strength, MPa (ksi)	90 (13)	115 (17)	386 (56)
Yield Strength, MPa (ksi)	34 (5)	55 (8)	-
Elongation, %	35 (1/16 inch thick specimens)	31 (3.2 mm diameter rods)	-
Hardness (Brinell)	23	N/A	80 - 110

Reference(s):

American Society for Metals, 1979

<http://www.inweldcorporation.com/datasheets/Inweld%20LFB%20&%20LFBFC.pdf>

Table 4.8 Chemical composition of 316L stainless steel

Element	316L Stainless Steel wt. %
Carbon	0.030 max
Chromium	16 - 18
Iron	61.9 – 72.0
Manganese	2.00 max
Molybdenum	2.0 – 3.0
Nickel	10 - 14
Phosphorous	0.045 max
Silicon	1.0 max
Sulfur	0.030 max

Table 4.9 Room temperature mechanical properties of annealed 316L stainless steel

Property	316L Stainless Steel (Annealed Bar)
Tensile Strength, MPa (ksi)	515 (74.7)
Yield Strength, MPa (ksi)	205 (29.7)
Elongation, %	60
Hardness (Brinell)	149

Reference: American Society for Metals, 1979

Traditional material assessed for material property characterization consisted of bulk solid 0.125 inch diameter circular stock that was available in 36.000-inch length pieces in the as-received condition.

To establish a baseline from which to assess the impact of processing metal rods through the I_x-ECAP process, welding rods were heat treated to the annealed condition prior to being run through the system. Rods were sectioned and annealed for extended

times to achieve a fully softened state. Heat treating was performed in a Fisher Scientific isotemp programmable forced draft laboratory furnace. Heat treat schedules are detailed as follows:

Table 4.10 Heat treat schedules for 1100 and 4043 aluminum, brass, and 316L stainless steel baseline materials

Alloy	Heat Treatment	Description
1100 Aluminum	<ul style="list-style-type: none"> ▪ Heat at 662 °F (20 min.) ▪ Air cool to ambient 	Full anneal
4043 Aluminum	<ul style="list-style-type: none"> ▪ Heat at 662 °F (20 min.) ▪ Air cool to ambient 	Full anneal
Copper (AWS 5.27)	<ul style="list-style-type: none"> ▪ Heat at 1112 °F (20 min.) ▪ Air cool to ambient 	Full anneal
316L Stainless Steel	<ul style="list-style-type: none"> ▪ Heat at 1904 °F (20 min.) ▪ Air cool to ambient 	Full anneal

An additional requisite of utmost importance regarding material selection and processing through the I_X-ECAP process and subsequent transition to commercial mainstream involves confirmation of work piece alloy chemistry. During research efforts, materials confirmation is based on materials supplier certifications and purchase order documentation. However, during actual industrial processing employing work pieces such as spent or scrap welding rods, etc., other means are required for alloy verification to ensure I_X-ECAP parameters are appropriate for successful manufacturing as well as to ensure adherence to customer and engineering specification. Enabling technologies such as hand-held or stationary x-ray fluorescence (XRF) positive materials identification (PMI) analyzers offer a fast, efficient, and reliable means to ensure alloy specifications are met.

Rods heat treated, sectioned, and ready for processing are shown below as well as the die inserts which were to be used to process selected work pieces.

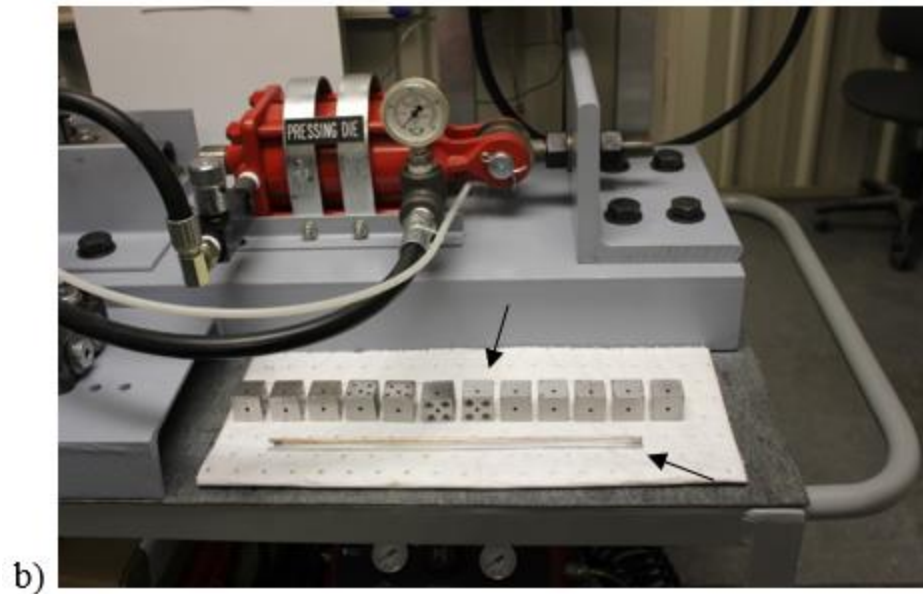
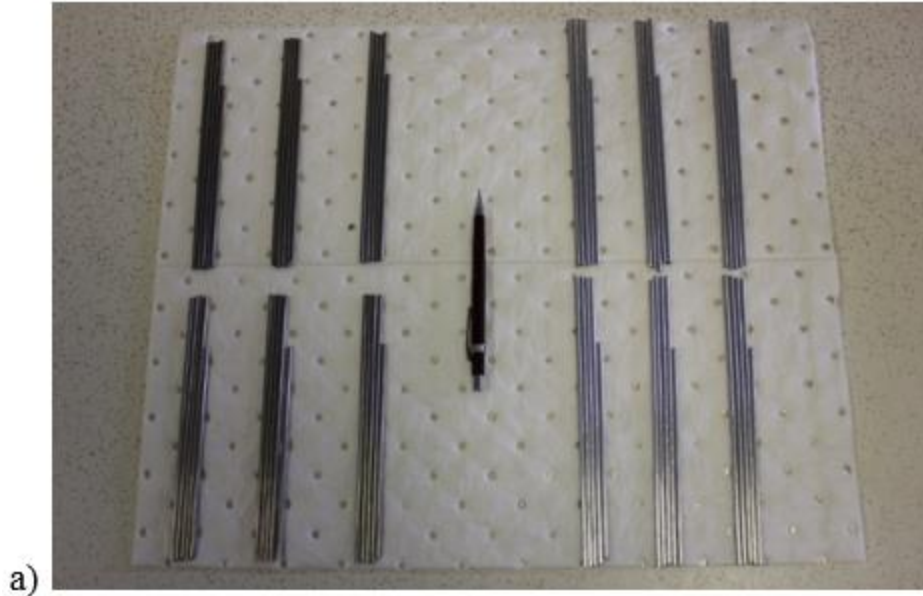


Figure 4.44 Sample rods ready for processing

- a) Rods ready for heat treatment and processing
- b) Die inserts and aluminum rods ready for processing

Materials Characterization

Assessment of differences between traditional and ultra-fine grain or nanocrystalline alloy of 4043 aluminum was quantified through material characterization techniques involving mechanical property performance measures and evaluation of microstructural grain size. As noted previously, only surface integrity was assessed for the 1100 alloy during initial feasibility trials.

Mechanical Properties

One of the important determinants delineating traditional and nanoscale materials involves an assessment of performance measures that are inherently descriptive of metal components. Within this study, standard mechanical properties were measured using micro-hardness techniques. Test coupons for hardness testing were obtained along the pressed transverse cross section of work pieces. Consideration of three-dimensional mechanical anisotropy was not explored within this research. To assess IX-ECAP work piece homogeneity, however, micro-hardness measurements were taken along the transverse axis cross sections at the midpoint of the pressed sample. Testing was performed in accordance with ASTM E384, Standard Test Method for Microhardness of Materials and E92 Standard Test Method for Vickers Hardness of Metallic Materials (ASTM E 384 and E 92, 1997).

Grain Size and Morphology

Initial baseline grain sizes were determined for unprocessed samples. This assessment was performed using optical light microscopy, a method which involved metallographic sample preparation and subsequent analysis using an optical metallurgical

light microscope having a resolution of approximately 1,000 nanometers. This technique was used for grain size determinations and general morphology existing within the aforementioned optical resolution capabilities. Cross sections of the unpressed rods were cut for analysis. During sectioning of samples, coolant such as water or cutting fluid was employed to ensure samples did not excessively overheat. Samples were prepared metallographically according to standardized procedures as identified in ASTM standard E 3, Standard Practice for Preparation of Metallographic Specimens and standard E 407, Standard Practice for Microetching Metals and Alloys. Upon completion of sample preparation, microstructural assessments were conducted referencing ASTM standards E 112, Standard Test Method for Determining Average Grain Size (ASTM E3, E112, and E407, 1997). Length and width grain size measurements were obtained on cross diagonals of microstructures as well as counting grain intercepts to obtain a mean lineal intercept distance to determine an average grain dimension.

Final grain sizes for pressed samples were determined theoretically based on application of the Hall-Petch relationship employing known material constants and conversions from microhardness values.

CHAPTER V
EXPERIMENTAL DESIGN

Fractional Factorial Split-Plot (FFSP)

This research employs $\frac{1}{4}$ fractional factorial split-plot design of experiments (DOEs) using five factors at two levels to assess statistical significance of processing parameters selected for the study. The required number of runs for a 2^5 full factorial experiment is thirty two runs. However, based on the constraints associated with randomizing factor level combinations (FLCs) in the I_x-ECAP process, a $\frac{1}{4}$ fraction factorial split-plot experimental design was selected, requiring eight runs. For example, four of the factors were quite easily changed to provide randomization. These include pressing speed, number of passes through the die, back pressure applied to the pressed rod, and vibrational energy. However, one factor, pressing temperature, was more difficult to change and required stabilization time for thermal equilibrium in the die and work pieces. Therefore, pressing temperature at two treatment levels was randomized within whole plots with the remaining four factors randomized at two levels within sub-plots. Based on available resources in actually running the process as well as subsequent product analysis, the split plot $\frac{1}{4}$ fraction factorial was the final design selection. Three replicates were run in blocks at the whole plot high and low temperatures in order to account for experimental noise. Therefore, a total of 24 observations were produced and analyzed for each respective alloy system, 1100 and 4043 aluminum.

An important clarification regarding the experimental trials that were performed involves the two aluminum alloy systems selected and subsequent analysis. With I_x-ECAP being a new process, the 1100 aluminum alloy was run through the complete ¼ fractional factorial split plot design with three replicates at the whole plot level. However, the 1100 material served to only substantiate the feasibility of actually running the manufacturing unit successfully and producing output rods of acceptable surface integrity. As a result, no statistical analysis was conducted on the 1100 alloy. Assessing process performance involving analysis of variance and regression model development was conducted only for the 4043 material.

A multi-factorial fixed effects split-plot experimental design was used to statistically validate the impact of key process predictor variables on the output response for the I_x-ECAP process. Five processing predictor variables or factors include: 1) pressing temperature, 2) number of passes through the die, 3) back pressure, 4) pressing speed, and 5) externally applied vibrational energy. The dependent variable or output response was microhardness on the transverse cross section of the 4043 work pieces. Selected microstructures (average grain size) were also analyzed. Based on the results of experimentation, Minitab® was used to identify statistical significance at $\alpha = 0.05$. Factors to be studied for the aluminum alloys as well as the experimental design, defining relation, alias structure, and design table are presented as follows:

Table 5.1 Initial DOE experimental factors

Factor ID	Experimental Factors	1100 Aluminum		4043 Aluminum	
		Low Level (-1)	High Level (+1)	Low Level (-1)	High Level (+1)
A	Pressing Temperature (HTC)	77 °F	175 °F	77 °F	175 °F
B	No. of Passes	1	3	1	3
C	Back Pressure Force	0 lbs.	600 lbs.	0 lbs.	600 lbs.
D	Speed	0.9 in./min.	30 in./min.	0.9 in./min.	30 in./min.
E	Vibrational Energy	0 cpm	14,000 cpm	0 cpm	14,000 cpm

Note: HTC = hard-to-change factor

Fractional Factorial Split-Plot Design:

Fraction:	1/4
Resolution:	III
Factors:	5
Hard-to-change factors:	1
Whole plots:	6
Runs per whole plot:	4
Whole-plot replicates:	3
Subplot replicates:	1
Blocks:	3
Runs:	24
Design Generators:	D = ABC, E = AB
Hard-to-change factor(s):	A

Whole Plot Generators:	A
Defining Relation:	$I = ABCD = ABE = CDE$
Alias Structure:	$I + ABE + CDE + ABCD$ $A + BE + ACDE + BCD$ $B + AE + BCDE + ACD$ $C + ABCE + DE + ABD$ $D + ABDE + CE + ABC$ $E + AB + CD + ABCDE$ $AC + BCE + ADE + BD$ $AD + BDE + ACE + BC$

As noted from the alias structure and the design being Resolution III, main effects are confounded with two-way interactions as well as higher-order interactions. Likewise, additional two-way interactions are confounded with higher-order interactions.

Table 5.2 Design table for fractional factorial split-plot experiment (randomized)

Run Order	Block	Whole Plot	A	B	C	D	E
1	1	1	-	+	+	-	-
2	1	1	-	-	-	-	+
3	1	1	-	+	-	+	-
4	1	1	-	-	+	+	+
5	1	2	+	+	-	-	+
6	1	2	+	+	+	+	+
7	1	2	+	-	-	+	-
8	1	2	+	-	+	-	-
9	2	3	-	+	-	+	-
10	2	3	-	-	+	+	+
11	2	3	-	-	-	-	+
12	2	3	-	+	+	-	-
13	2	4	+	-	-	+	-
14	2	4	+	-	+	-	-
15	2	4	+	+	-	-	+
16	2	4	+	+	+	+	+
17	3	5	-	+	+	-	-
18	3	5	-	-	-	+	+
19	3	5	-	-	-	-	+
20	3	5	-	+	-	+	-
21	3	6	+	+	-	-	+
22	3	6	+	-	+	-	-
23	3	6	+	+	+	+	+
24	3	6	+	-	-	+	-

A = Temperature

B = Number of Passes

C = Back Pressure

D = Speed

E = Vibration

Multiple Regression Analysis

Regression analysis was performed for model generation. The multiple linear regression model representing the relationship between regressor and response variables is as follows (Montgomery and Runger, 2007):

$$Y = \beta_0 + \beta_1x_1 + \beta_2x_2 + \dots + \beta_kx_k + \epsilon \quad (5.1)$$

Where:

Y = response variable

β = regressor coefficients

x = independent regressor variables

ϵ = random error term

Proper selection of predictor variables used in regression models represents a critical element in the overall success and credibility of experimental design methodologies employed in research initiatives. Naturally, a very important selection criterion is based on the knowledge contribution of the experimenter regarding critical factors and possible interactions. In lieu, however, of such technical expertise and expectation of contributory effects of predictor variables, the experimenter must statistically validate experimental outcomes and be guided based on proper evaluation and use of alternative variable selection methods. Several notable methods available include the ANOVA regression model, forward selection, backward selection, and stepwise selection.

An assessment of data sets generated from this study provides improvement opportunities to the research involving IX-ECAP. Even though two-factor and higher-order interaction effects were excluded from model development, their inclusion would

have made the number of predictor variable possibilities extremely large. This represents a comparable implication to an experimental design whereby a full factorial split plot design for five factors at two levels with one hard-to-change factor may be considered requiring a total of 96 runs for three whole plot replicates. Such an experiment represents a full-resolution design allowing the effects of all main factors and all interactions to be studied. Simply focusing on main factors and two-factor interactions involves a total of fifteen possible predictor variables from which the regression model could be constructed. Therefore, a systematic statistically validated method for variable selection is requisite to a professional approach in data analysis.

Based on results obtained using the variable selection methods used in this inquiry, valuable insights are realized offering significant improvements to the validity of the research. Specifically, the first major implication involves the use of a pre-defined systematic approach to regression model building. For example, if an experimental design results in an extremely large number of predictor variables from which to choose, then simply trying to review the ANOVA table for significant variables could be very tedious. However, properly selecting a method such as forward, backward, or stepwise selection could quite easily be implemented within the data analysis process using statistical software such as Minitab[®]. Once data input is completed, Minitab[®] readily generates the regression equations.

Another major implication relates to the actual selection of predictor variables. Developing the regression model from an ANOVA involves identifying the significant variables from the variance table and then using the respective tabulated predictor coefficients to generate the equation. However, as noted previously, if the number of

factors and interactions are large, this could be an involved task with potential for error. Also, a simple manual review and selection of variables warrants more statistically valid considerations.

Alternative methods include forward selection, backward selection, and step-wise selection algorithms discussed as follows. Forward selection starts with no predictor variables in the model and progressively adds variables based on individually assessing each new predictor's significance as compared to a pre-defined significance level. Conversely, backward selection begins with all predictor variables initially in the model and progressively eliminates predictors based on a comparison of their respective significance levels to a pre-defined alpha level. However, the most often used method, stepwise selection, involves a combination of both forward and backward selection. Using this method, the procedure is started in the same manner as forward selection by adding a predictor variable; however, the model is re-fitted each iteration to determine if any variables could be eliminated based on the defined criteria noted above. Therefore, stepwise selection overcomes the limitations in forward and backward selection of precluding the effects of prior variables added or eliminated during requisite steps in the process. With stepwise selection, predictors are continually assessed for inclusion or exclusion in the regression model.

Based on a consideration of experimental design constraints used in this research, however, the ANOVA regression model was required due to the complexities of the $\frac{1}{4}$ fraction factorial split plot design. Employing the stepwise, forward, or backward selection methods would generate efficient regression equations; however, the algorithms would analyze the experimental design as a factorial without inclusion of the impacts

from a split-plot design incorporating blocking due to necessities of running the experiments over a three-day period, randomizations within whole plots for the hard-to-change factor associated with temperature changes, and randomizations within sub-plots for the remaining factors. Regression coefficients would be generated; however, p-values for main effects would be incorrectly reported. Employing a fractional factorial split plot design analysis, the ANOVA regression equation provided in Minitab® correctly asserts the predictor coefficients and associated p-values. With this analysis, however, all regressors would be included in the model equation. With this research representing an initial screening experiment for a newly developed prototype system, only five main factors and no interactions are being studied, which reflects minimal complexity in selecting regressors and regressor coefficients. Therefore, the ANOVA regression equation is appropriate for the initial stages of manufacturing system design and development. Practical technical knowledge offered by the experimenter should, also, be applied not only to the development of the actual process but to question and discern the validity of the regression outputs.

With the development of a new process, complete knowledge of all factors impacting the output of the system represents valuable information. However, a progressive approach in designing proper experimentation within available resources is very important. Investigating and determining significant factors of interest with the IX-ECAP system, likewise, required an experimental plan within economic and physical constraints of the system. As a result, a $\frac{1}{4}$ fraction factorial split plot design was selected which readily and economically accommodated data generation, acquisition, and analysis.

CHAPTER VI

RESULTS AND DISCUSSION

This research investigates the development of a simplified top-down nanomanufacturing method to transform traditional materials such as spent or scrap welding rods into nanocrystalline or ultra-fine grain materials with improved metallurgical characteristics available for industrial use. The manufacturing method developed was based on reconfigurations of traditional ECAP constructs to induce severe plastic deformation into selected work pieces. A primary objective was to design and build a system based on indexing continuous length material through the process. Contingency objectives considered the viability of processing variable length discrete work pieces. Based on results of initial trials of continuous length work pieces through the IX-ECAP process, the contingency of processing variable length discrete metal rods was required in order to successfully run fractional factorial split-plot designed experiments for study of selected process factors.

Discussion of the results is considered from four perspectives: continuous length processing, variable length discrete processing, statistical experimentation and analysis, and materials development.

Continuous Length Processing

The original conceptual design of indexing equal channel angular pressing consisted of clamping a 0.125-inch diameter rod between two die halves and then pressing one end of the rod through a 90-degree turn in a die insert mounted in a pressing die holder. A 0.250-inch indexing gap between the clamping and pressing die face plates was reinforced with four sliding steel guides to prevent buckling of the rod as it traveled through the indexing gap. To reduce flow stress required for pressing, the metal rod work piece would be preheated using cartridge heaters inserted into both the clamping and pressing dies. Hydraulic cylinders provided necessary clamping and pressing forces for the system. Additional elements consisted of a spring loaded back pressure mechanism and pneumatic vibrator. These basic components are illustrated in Figures 6.1 and 6.2.

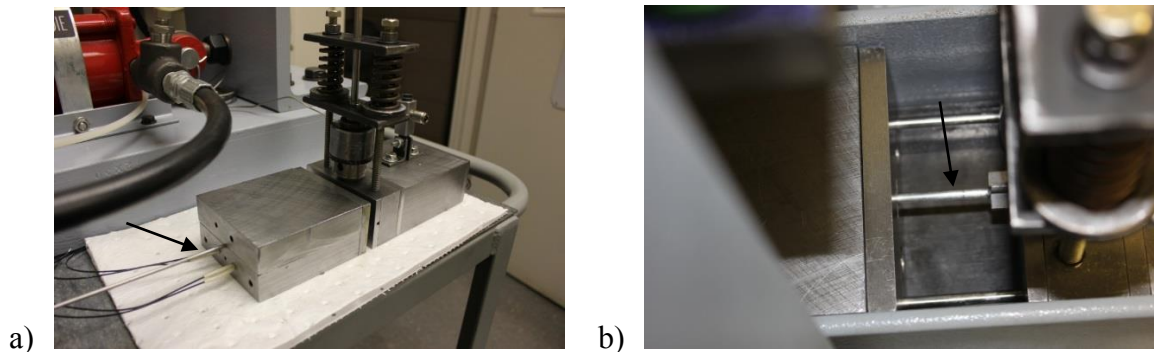


Figure 6.1 Basic components of original IX-ECAP process

- a) Rod is inserted into back of clamping die. Cartridge heaters, back pressure springs, and vibrator are also shown
- b) Indexing gap opened showing guide pins, rod work piece, and reinforcing guides

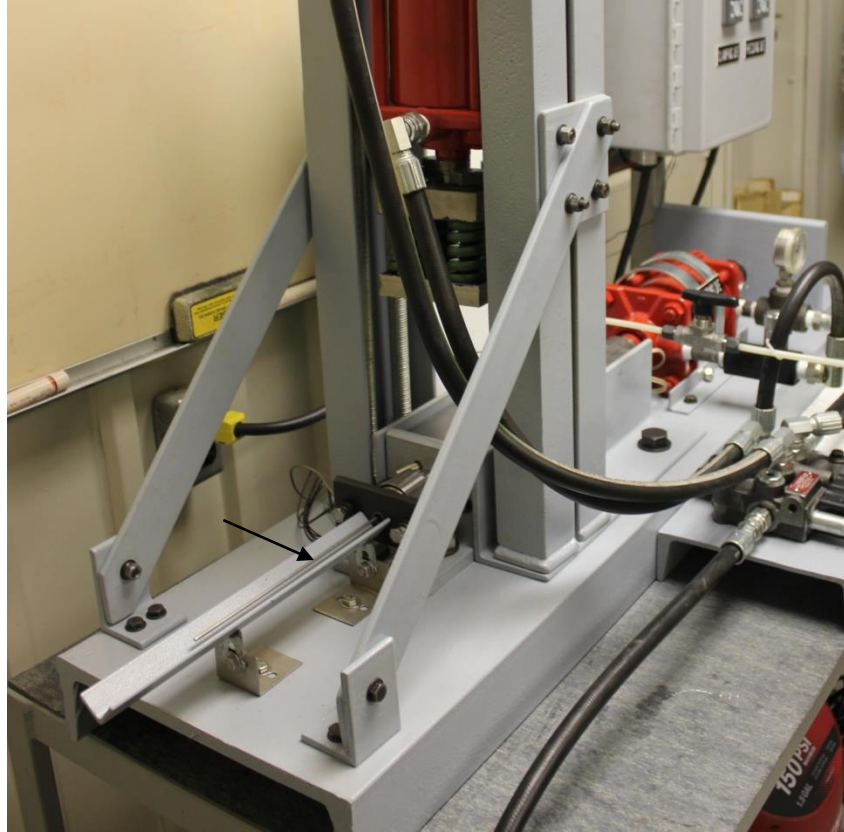


Figure 6.2 Continuous rod inserted through back side of clamping chuck and die ready for pressing

To test the initial performance of the system, trial runs were made using fully annealed 1100 aluminum alloy 0.125-inch diameter rods of 3-inch length. In order to investigate the stability of the overall machine structures as well as higher pressing capabilities, fully annealed AWS 5.27 copper alloy welding rods with a 0.125-inch diameter were also tested.

Initial trials consisted of the following procedure:

- Die insert entrance and exit channels were lubricated with 10W-30 motor oil,

- 0.125-inch aluminum rod was inserted through the clamping die through the indexing gap and reinforcing guides into the die insert mounted in the pressing die,
- 0.125-inch diameter steel rod was inserted through the clamping chuck at the rear of the clamping die and placed behind the work piece rod for support during pressing,
- Die components were then placed in the guide rails of the I_x-ECAP machine,
- Hydraulic cylinders were positioned and attached as appropriate,
- Indexing gap was opened to 0.250 inch, and
- Rod was pressed through the entrance channel of the die insert.
- Initial trials were run without employing elevated temperatures, back pressure, or vibration during processing.

Experimental results from these initial trials provided significant insight to processing variables and procedures required for successful implementation of both continuous and discrete fixed length pressing. From a perspective of five key process factors, initial trials considered the most likely settings deemed crucial to successful pressing of acceptable rod integrity such as surface finish, dimensional stability, etc. For example, pressing was performed at the slow speed of 0.9 inches per minute with only one pass through the system. Back pressure would be considered in later trials since increased pressing stresses are imposed on the work piece as a result of the applied back pressure. Non-elevated temperatures were selected in order to reduce the likelihood of lateral volumetric expansion in the indexing gap since preheated work pieces have lower

rigidity. During initial trials with the original design, cartridge heaters were placed in both the clamping and pressing dies which could be activated to preheat the rod prior to entering the indexing gap and die insert as needed in subsequent trials. Vibration would, likewise, be applied during subsequent trials.

Results of the initial trials revealed several limitations adversely impacting success of processing continuous length rods as well as opportunities for overcoming such obstacles. A critical consideration from a practical standpoint involves lateral stresses imposed on the rod as the pressing force is applied. Lack of close tolerance fit between the reinforcing guides and die face plate slots allowed volumetric lateral expansion of the rod during pressing which prevented passage of the rod through the 90-degree turn in the die insert. As can be seen in Figure 6.3, the reinforcing guides prevented buckling of the aluminum rod; however, radial or normal stresses during pressing caused the aluminum work piece to fill any voids resulting from the loose tolerance fits between reinforcing guides and die face plates.

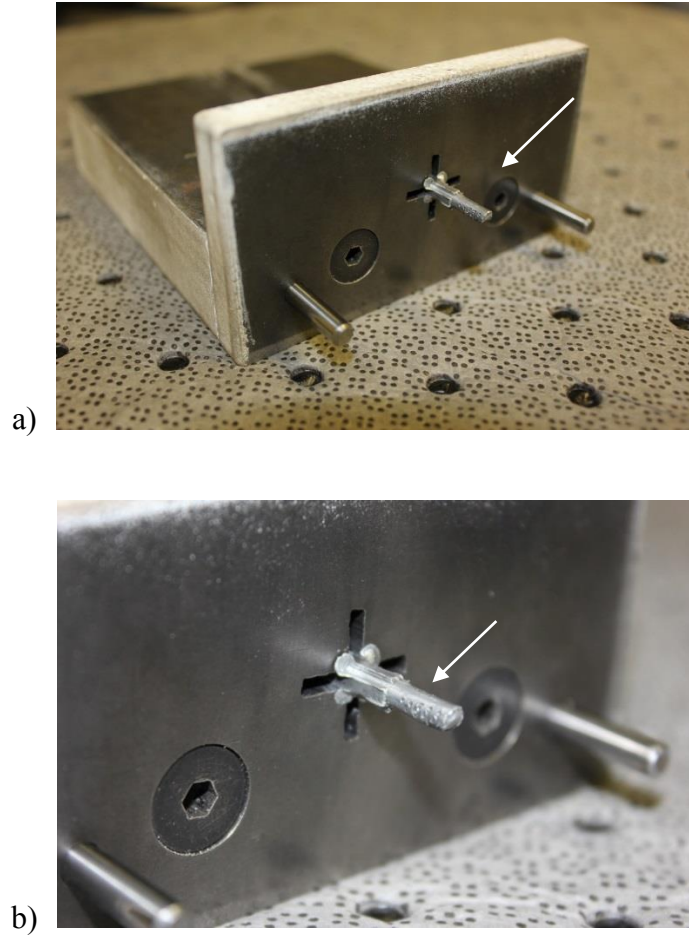


Figure 6.3 Close-up view of aluminum rod extending through die face plates

- a) Rod extending through clamping die face plate
- b) Close up view of flared aluminum rod at indexing gap

To test the integrity of the support structures of the manufacturing unit as well as elemental components of the system, higher strength yet fully annealed copper (AWS 5.27) welding rods were processed through the system. As with aluminum rods, the copper also experienced volumetric lateral expansion due to the lack of close fit between reinforcing guides and face plate slots. Additionally, the higher material flow stresses for copper required higher pressing forces. As a result, insufficient close tolerance fit

allowed misalignment and non-equilibrium stress distribution and loading causing fracture of the reinforcing guides as shown in Figure 6.4.

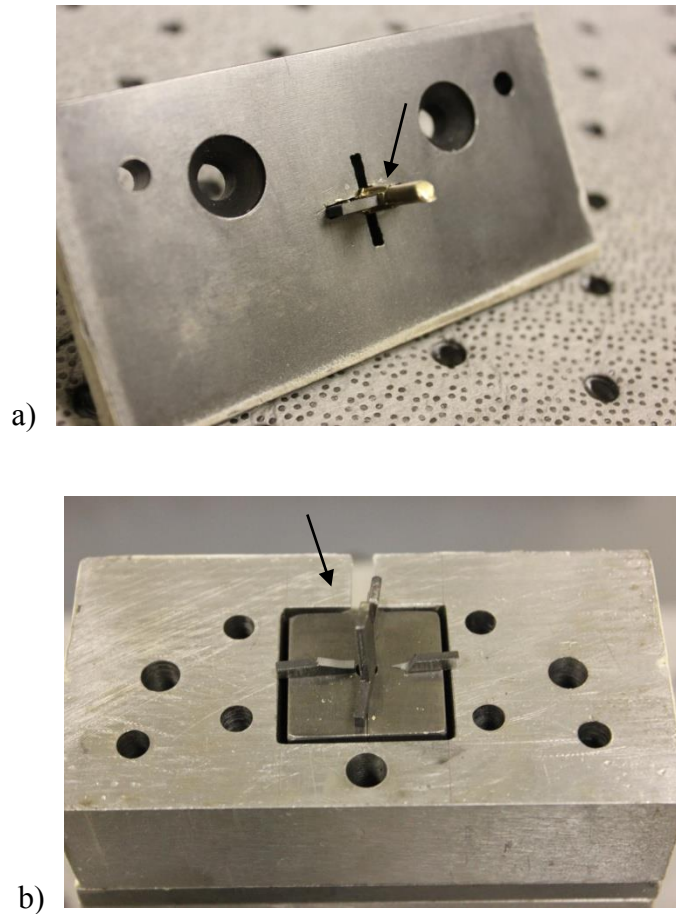


Figure 6.4 Copper rod extending through die face plates

- a) Rod extending through clamping die face plate with fractured reinforcing guides
- b) Fractured reinforcing guides at die insert in die holding block

Even though the initial premise appears to preclude the success of indexing equal channel angular pressing of continuous length work pieces, a closer examination of the aluminum work piece within the die insert entrance channel at the point of contact with the exit channel reveals additional insight. As shown in Figure 6.5, the rod end which was originally sharpened at a 45-degree angle to initiate pressing has since flattened to

90-degrees. Additionally, the rod end has subsequently filled the die channel and experienced further straining with volumetric changes equivalent to the die interfaces. Lastly, circumferential strain striations indicating movement through the die can be seen on the exterior section of the rod which entered the die insert entrance channel.

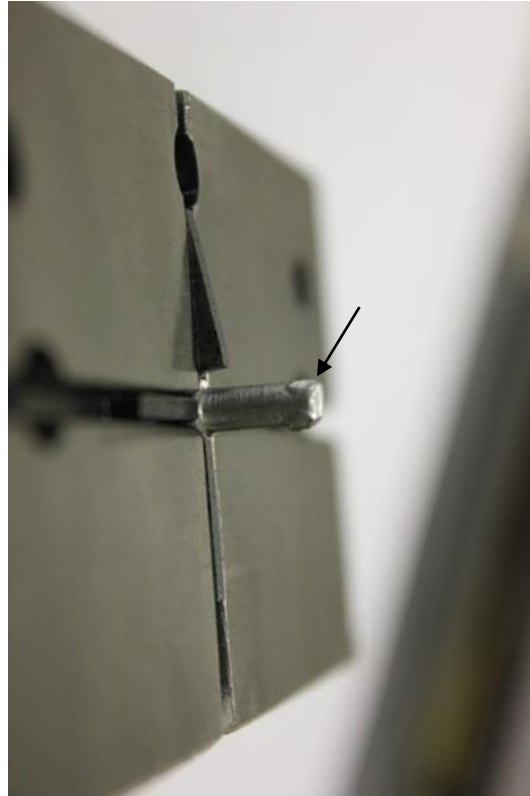


Figure 6.5 Pressed aluminum rod extending through pressing die face plate after continuous pressing

Based on results of the initial trials, a critical assessment was made based on available resources which identified limiting factors that would preclude continued experimentation using continuous length rods or allow system redesign to facilitate pressing of variable length discrete work pieces. The most important limiting factor to

continuous processing involved the requirement for close tolerance fit tools, specifically the reinforcing guides and die face plate slots through which the guides would fit. The guides not only needed to be machined to closer tolerances but also redesigned to allow a curved and increased contact area between the rod work piece and reinforcing guides. These two redesign considerations would limit lateral volumetric expansion of the rod work piece, thereby allowing flow through the die insert entrance and exit channels. Hardening heat treatments would, once again, be required upon completion of rebuild of the guides and face plates.

Since resources were unavailable for additional precision machining of reinforcing guides and die face plates, experimentation was continued with redesigns that accommodated the contingency of discrete pressing of variable length rod work pieces. The possibility of fracture of reinforcing guides and other system components was eliminated, and success of performing fractional factorial split-plot experimentation studying the five process factors selected for the manufacturing unit was improved. Process redesign required the following changes: use of discrete variable length rods, addition of 0.125-inch diameter ejector pin plunger, modification and addition of face plates with center holes without reinforcing guides, back pressure mechanism changed from spring load to static weight load, and reconfiguration of heating elements. Each of these redesigns is discussed in the following sections.

Variable Length Discrete Processing

In order to accommodate a continuation of processing samples, the manufacturing unit required system redesign. This redesign resulted in the ability of the system to

process variable length discrete aluminum rods very successfully. Modifications to the system included the following:

- Variable length discrete rods were processed.
- Reinforcing guides were eliminated and face plates modified to contain only a center hole through which the rod would pass.
- Clamping chuck and die were used to secure a 1/8-inch diameter tool steel ejector pin with 10-inch length which served as the plunger for the aluminum rod.
- Heating system employed cartridge heaters only in the pressing die and die insert holding block instead of heating both the clamping and pressing dies.
- Back pressure mechanism was changed from a spring loaded apparatus to a static dead weight system.

Each of these modifications along with the resultant outcomes is described in the following sections.

Variable Length Discrete Rods

With elimination of reinforcing guides and slotted face plates, a mandatory transition from continuous to discrete variable length work pieces was required since unstrained portions of the rod located within the indexing gap between pressing and clamping dies would result in buckling of the work piece. Examples of continuous and discrete length work pieces are illustrated in Figure 6.6.



a)



b)

Figure 6.6 Continuous and discrete length work pieces

a) Continuous rods of 36- and 12-inch lengths

b) Discrete rods of 0.875- and 0.625-inch lengths

A system which readily accommodated variable length rods was required since reductions in work piece length occurred during each subsequent pass through the system when three passes were required. These respective dimensional changes resulted from flashing of metal around the plunger and radial expansion of the rod during passage through the exit channel as shown in Figures 6.7 and 6.8 on the following pages.

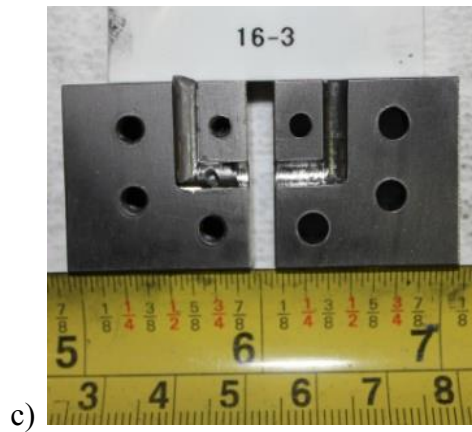
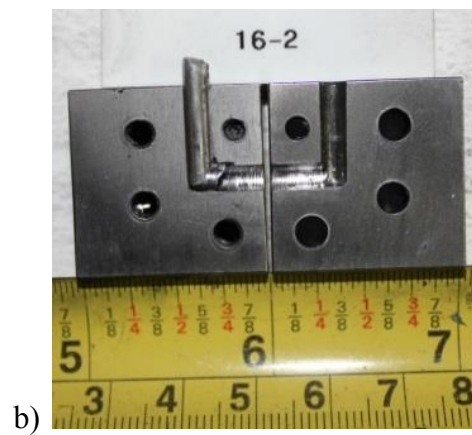
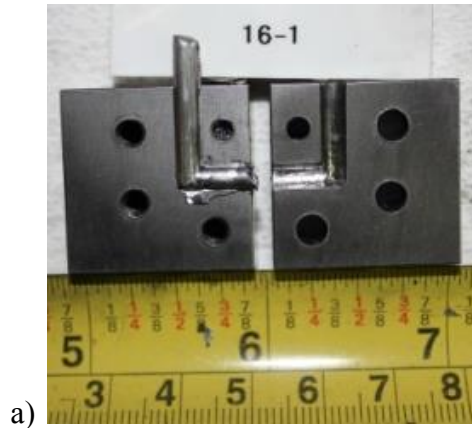


Figure 6.7 4043 aluminum rods showing 1, 2, and 3 presses through the system

- a) Pass #1
- b) Pass #2
- c) Pass #3

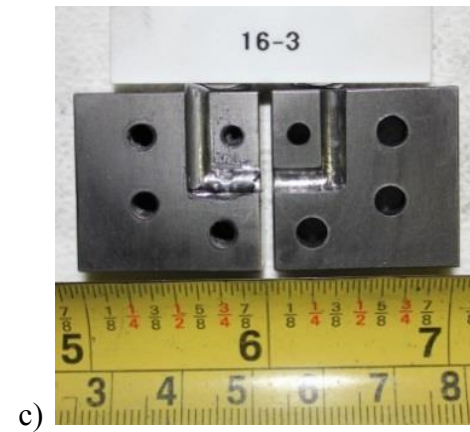
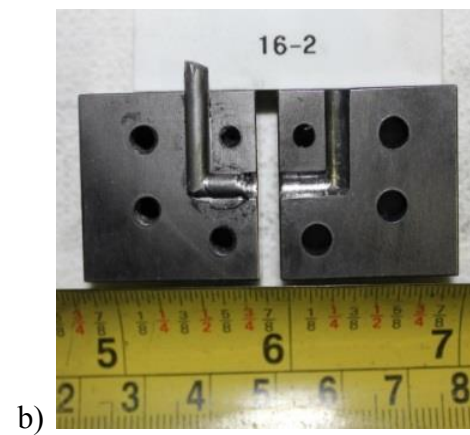
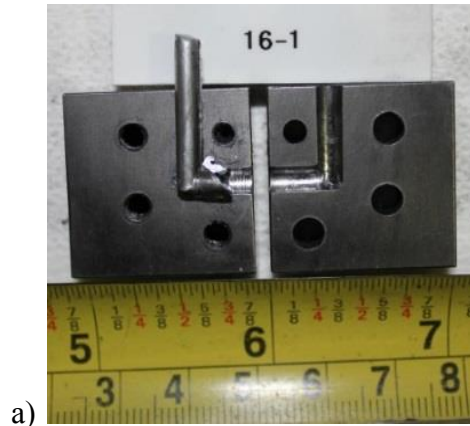


Figure 6.8 1100 aluminum rods showing 1, 2, and 3 presses through the system

- a) Pass #1
- b) Pass #2
- c) Pass #3

Face Plate Redesign

Reinforcing guides were eliminated and face plates modified to contain only a center hole through which the rod would pass. New face plates were constructed for both the clamping and pressing dies which, once again, required subsequent hardening heat treatments. The clamping die was fitted as in the original design with a single 0.375-inch thick face plate; however, two face plates were added to the pressing die as compared to a single face plate in the original design. These respective face plates consisted of one 0.250-inch and one 0.375-inch thick plates fitted to the pressing die insert holding block. Modifications are shown in Figure 6.9.

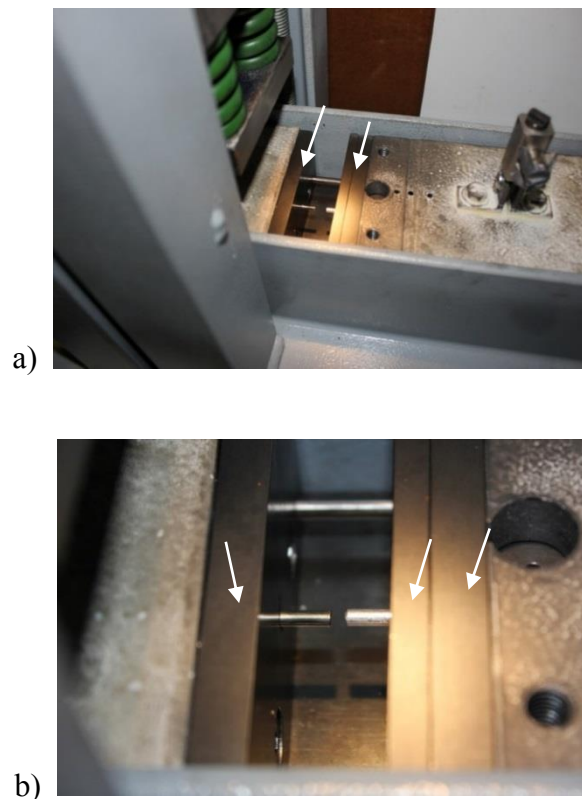


Figure 6.9 Clamping and pressing die face plates redesign

- a) View of redesigned face plates attached to dies installed in guides of the machine
- b) Close-up view of face plates for both clamping and pressing dies

Clamping System and Plunger Redesign

Processing discrete length rods now required the use of a plunger to press the work pieces through the die. This was accomplished by inserting a 0.125-inch diameter tool steel ejector pin 10 inches in length through the clamping chuck and clamping die (see Figure 6.10 below). As shown on the previous page in Figure 6.9, the plunger contacts the rod and presses the work piece through the die as the pressing die is indexed forward.

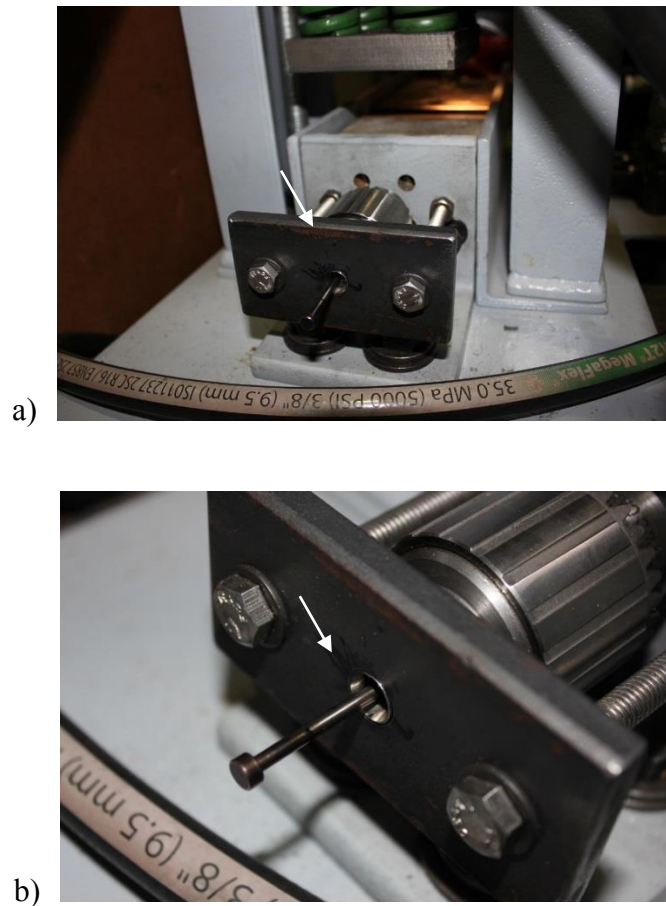


Figure 6.10 Ejector pin used as plunger

- a) Overall view of ejector pin through clamping chuck and clamping die
- b) Close-up view of ejector pin inserted into clamping chuck

Heating System Redesign

Original design of the heating system provided pre-heating of the rod work pieces in both the clamping die and pressing die components. However, since continuous rods would not be passing through the clamping die, cartridge heaters in this part of the system were no longer warranted. After further review of the system, an important consideration was made to provide added thermal protection to prevent the pneumatic vibrator and hydraulic cylinder rod from excessive temperatures. This protection was achieved by inserting 2-inch long cartridge heaters into the die insert holding block instead of 4-inch length heaters. This redesign provided thermal input that was concentrated within the area of the die face plates and die insert. As shown in Figure 6.11 by the white colored area in the center of the thermal image, the highest temperatures were concentrated within the die insert where actual severe plastic deformation of the rods occurred.

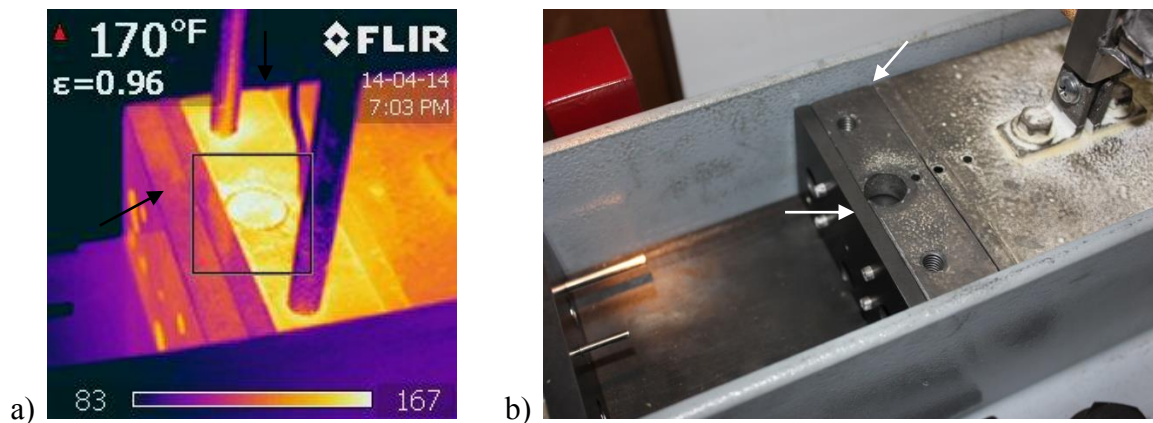


Figure 6.11 Infrared thermal image of front side of die insert holding block and face plates during 4043 aluminum rod processing

- a) Infrared image of die insert holding block
- b) Normal photograph of die insert holding block portion of the pressing die with cartridge heaters visible

Additional thermal images of the heating system are provided in Figures 6.12 and 6.13 below illustrating the concentration of heat input at the die insert areas of the pressing die.

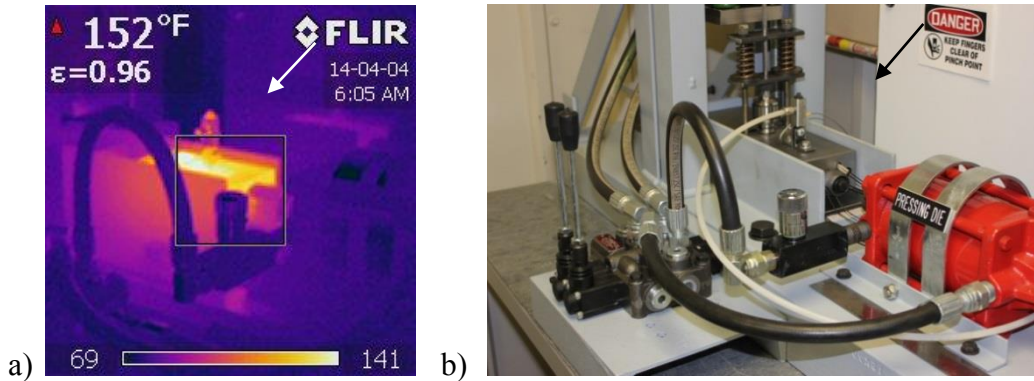


Figure 6.12 Infrared thermal image of rear view of die insert holding block and face plates prior to 4043 aluminum rod processing

- a) Infrared image of die insert holding block
- b) Normal photograph of die insert holding block portion of the pressing die

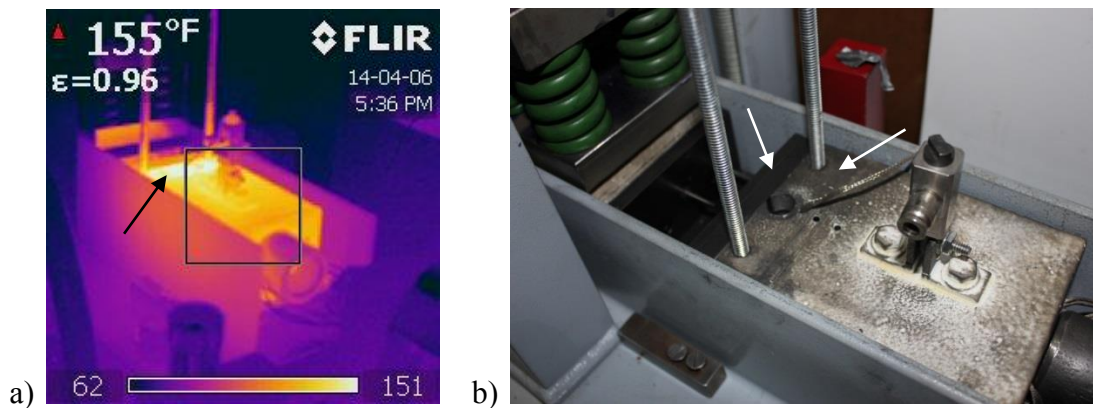


Figure 6.13 Infrared thermal image of rear view of die insert holding block and face plates during 4043 aluminum rod processing

- a) Infrared image of back view of pressing die
- b) Normal photograph of back view of pressing die

An important aspect of the heating system was the ability of the thermal unit to provide sufficient response during transition to higher level temperature settings. As illustrated in Figure 6.14, the system performed extremely well in providing proper response to thermal heating upon demand. For example, all experimental DOE runs involving both the 4043 and 1100 aluminum samples are shown. Each time the temperature was changed for each respective higher temperature whole plot as dictated by the DOE design matrix, the system required a consistent 30-minute time duration to transition from initial ambient temperature to the higher factor level setting.

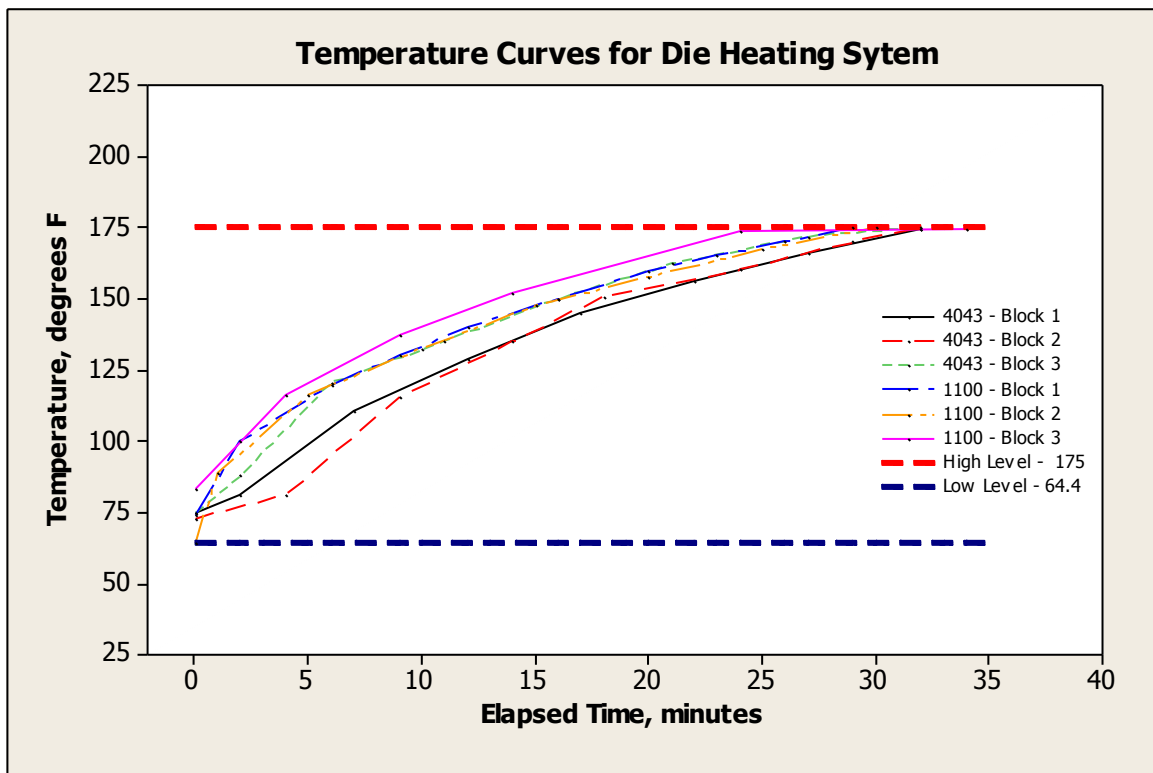


Figure 6.14 Temperature curves for 4043 and 1100 aluminum die heating system for DOE blocks 1, 2, and 3

Another important characteristic of the thermal unit involves the capability of the system to control temperatures at the desired factor level. As illustrated in Figure 6.15, 95% confidence intervals for the means for the 4043 and 1100 alloy trials were 175.19 to 175.37 and 174.63 to 175.11, respectively for the high temperature set point of 175 °F.

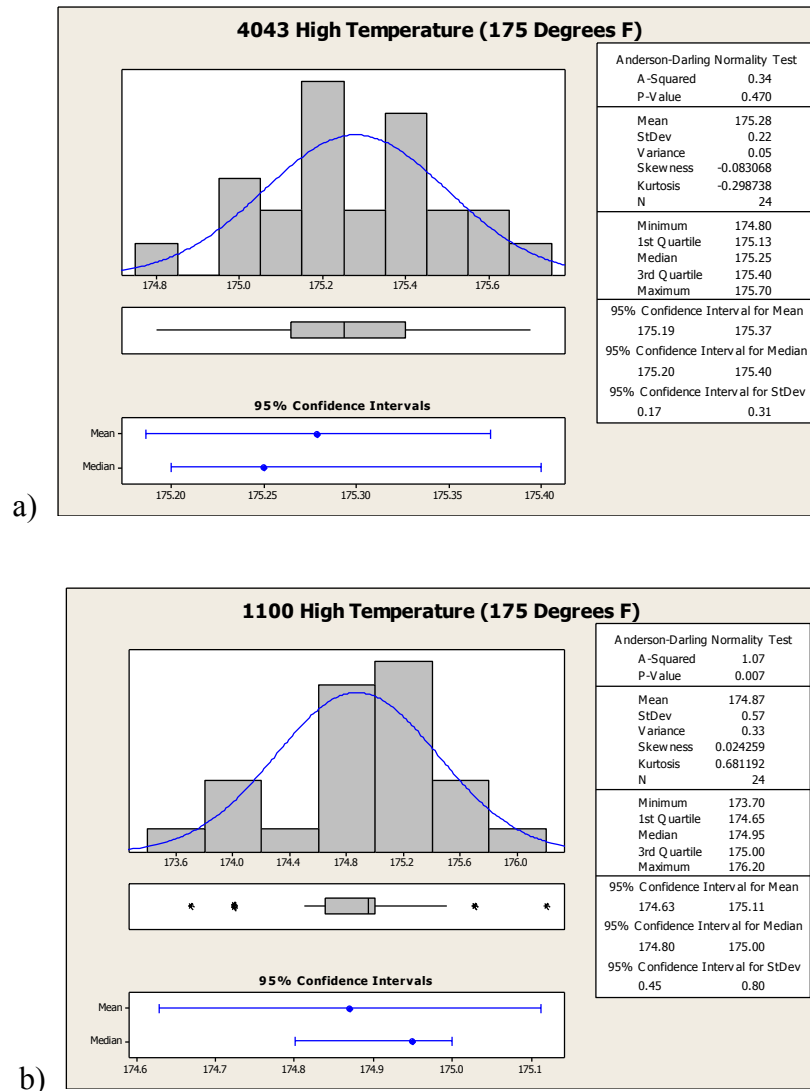


Figure 6.15 Statistical summary of high temperature capability of heating system

a) High temperature of 4043 experimental trials. Mean temperature is 175.28

b) High temperature of 1100 experimental trials. Mean temperature is 174.87

Back Pressure Mechanism Redesign

Based on initial test runs of the process, one additional redesign involved modifying the back pressure mechanism from a dynamic spring loaded design to a static weight system. Dual medium load springs supplied an initial and final force of 0.2 to 0.3 tons based on a pre-compression of 0.500 inches and a subsequent indexing compression of an additional 0.250 inches. As shown in Figure 6.16, these back pressure forces resulted in extensive flashing of the aluminum rod at the parting line as well as an inability to successfully press the work piece through the entirety of the exit channel of the die. Using dual medium load springs resulted in a back pressure stress of 48,918 psi being applied to the cross section of the work piece.

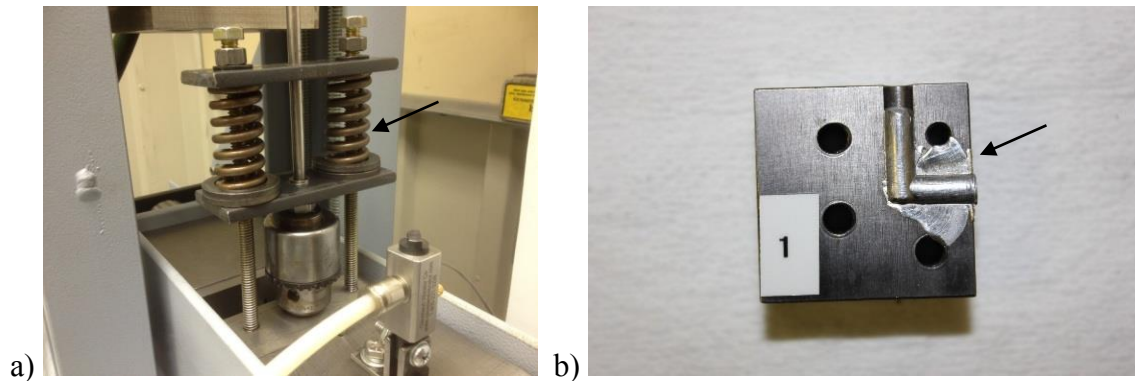


Figure 6.16 Spring loaded back pressure mechanism

- a) High force spring loaded back pressure design
- b) 1100 aluminum rod showing excessive flashing at parting line and lack of pressing

To provide a constant and less extreme back pressure force to the work piece, a 1.75 x 1.75 x 8-inch carbon steel square block was used in place of the medium load springs. Total weight of the redesigned back pressure mechanism was 10 pounds which supplied a back pressure stress of 815 psi to the rod cross section. A follow-up test using

the redesigned back pressure mechanism is illustrated in Figure 6.17 which shows minimal flashing at the parting line and complete pressing of the rod into the exit channel of the die.

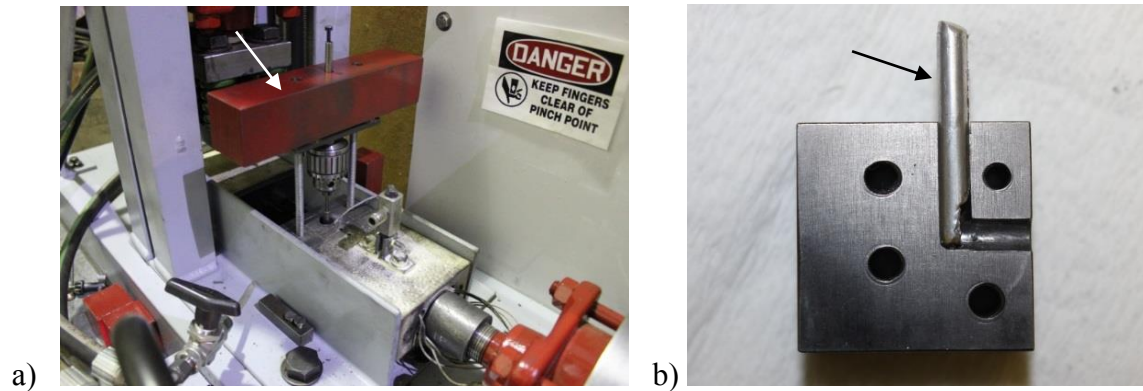


Figure 6.17 Static loaded back pressure mechanism

a) Low force static loaded back pressure design

b) 1100 aluminum rod showing no flashing at parting line and complete pressing of the workpiece

The back pressure mechanism employed a 0.125-inch diameter steel rod inserted through the clamping chuck into a slip collar guide located on top of the exit channel of the die insert as shown in Figure 6.18. Prior to pressing, the steel rod was inserted into the exit channel of the die insert and clamped with the vertically mounted drill chuck. As the work piece emerged from the die insert exit channel, the slip collar allowed rigid alignment and, subsequently, back pressure to be applied to the pressed aluminum rod.



Figure 6.18 Back pressure rod and slip collar

Pressing Speed

Pressing speed represents a critical factor from several perspectives in the design of indexing equal channel angular pressing. For example, pressing speed is vitally important in determining the economic viability of the proposed process. Cycle times are directly related to the speed with which the machine is able to press work pieces through the unit. Additionally, pressing speed directly impacts required forces for work piece plastic deformation which plays a pivotal role in selecting hydraulic and structural components of the system. Altering the pressing speed impacts the material's flow stress according to the relationship of strain rate versus flow stress at constant strain and temperature as follows (Dieter, 1986):

$$\sigma = C(\dot{\epsilon})^m \quad (6.1)$$

Where:

σ = material flow stress

C = material constant

$\dot{\epsilon}$ = strain rate

m = material strain rate sensitivity

Additional responses to the system based on differences in pressing speed include work piece integrity such as propensity for surface cracking and dimensional distortions, impacts on microstructural grain refinement, and thermal heating of die components due to mechanical work imposed.

As noted previously in Chapter V, components were designed and selected to provide pressing speeds at two levels, that being 1 and 30 inches per minute, respectively. System components consist of hydraulic flow control valves, cylinders, and a power unit to provide motion control of the pressing and clamping dies. System motion design, therefore, was based on positional control and direct settings of flow valves as shown in Figure 6.19.

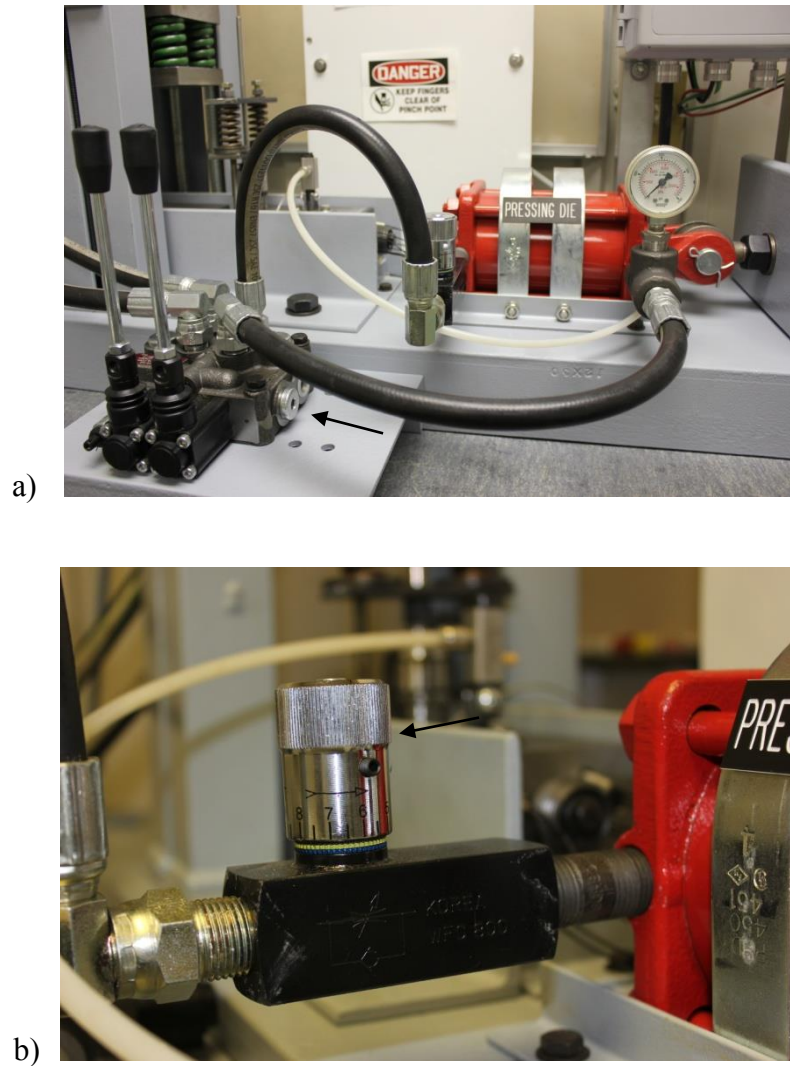


Figure 6.19 Flow control valves for pressing speed

- a) Bidirectional flow control valve for pressing and clamping cylinders
- b) Adjustable inline flow control valve for pressing cylinder

As illustrated in Figure 6.20 and 6.21 on the following pages, slow pressing speeds were controlled with significantly less variability than faster speeds. Statistical summaries for slow pressing speeds for both the 4043 and 1100 aluminum experimental trials provides 95% confidence intervals for the mean of 0.865 to 0.951 and 1.039 to 1.212 inches per minute, respectively. Likewise, means for slow speeds are 0.908 for the

4043 trials and 1.125 for the 1100 aluminum trials. Conversely, 95% confidence intervals for the mean of fast speeds indicated much wider intervals. For example, the 4043 intervals were 23.470 to 28.879, and the 1100 intervals were 25.145 to 32.714. Means were 26.179 and 28.929 inches per minute, respectively.

The greater variability in the higher pressing speeds can be explained by the method whereby the speeds were obtained. Specifically, pressing speeds were determined by measuring the indexing distance traveled during pressing based on manual stop watch actuation using 1/100 second increments. At the slower speeds of 1 inch per minute, manual actuation of the stop watch was more accurate. However, at the higher pressing speeds of 30 inches per minute, manual stop watch actuation was more difficult resulting in greater variability. However, experimental settings were selected at two levels which reflected pressing speeds that were multiples of magnitude different for each of the respective high and low levels. Resources for automated motion sensing were unavailable for this research.

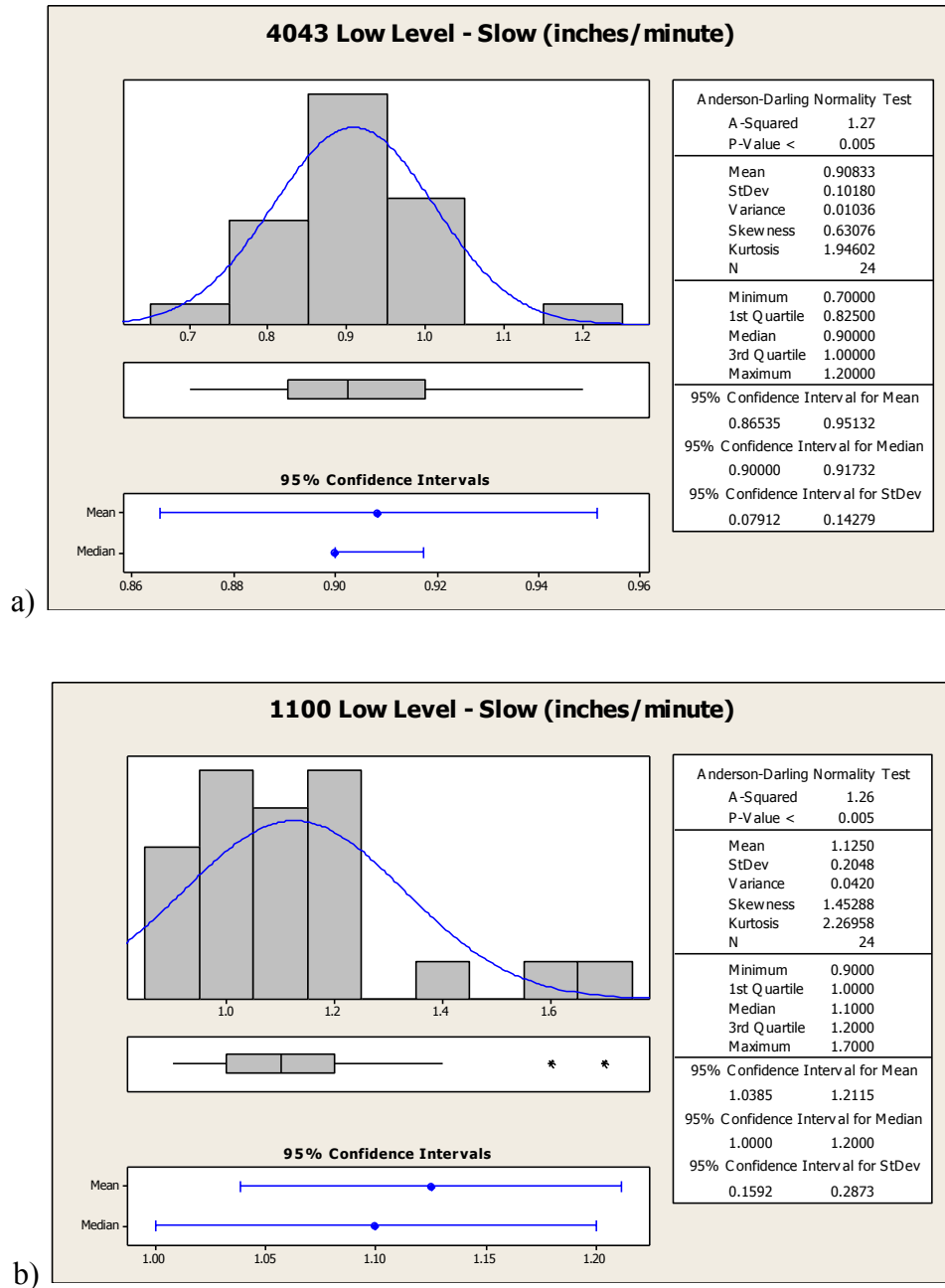


Figure 6.20 Statistical and graphical summary of slow pressing speeds

- a) 4043 statistical summary. Mean slow speed is 0.908 inches/minute
 b) 1100 statistical summary. Mean slow speed is 1.125 inches/minute

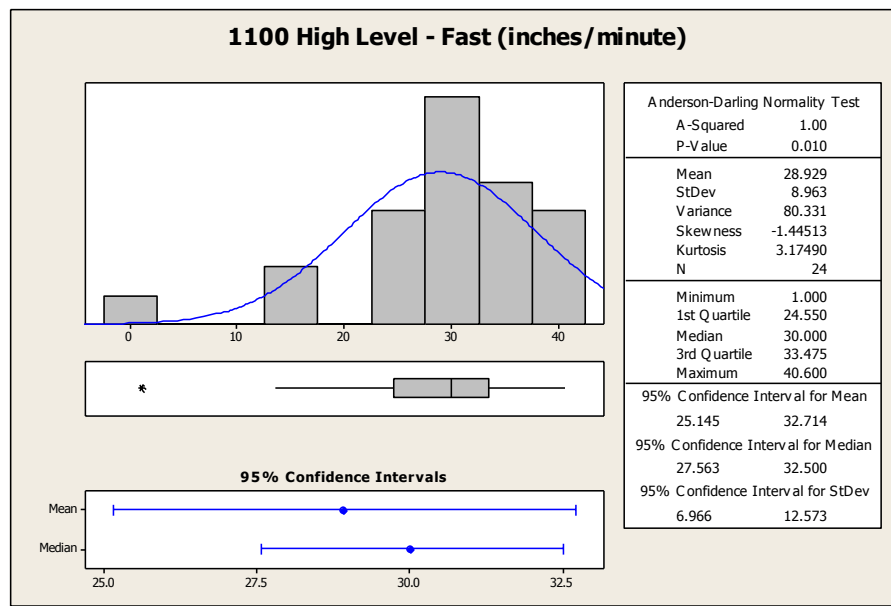
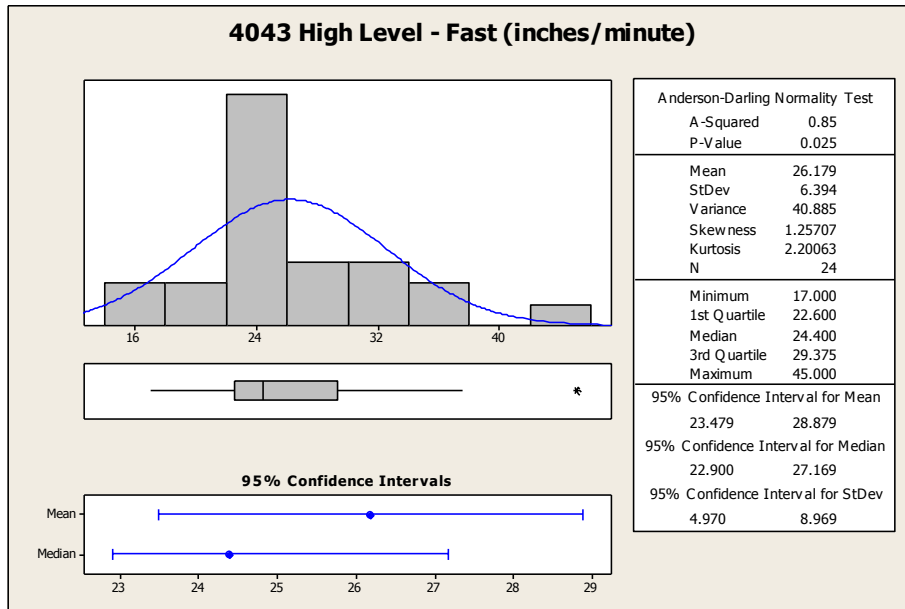


Figure 6.21 Statistical and graphical summary of fast pressing speeds

- a) 4043 statistical summary. Mean fast speed is 26.179 inches/minute
- b) 1100 statistical summary. Mean fast speed is 28.929 inches/minute

Using the pressing speeds illustrated previously for the 1100 and 4043 alloys at both the high and low levels, the processing strain rates can be determined. For equal

channel angular pressing the strain rate is defined as follows (Gutierrez-Urrutia, Munoz-Morris, Puertas, Luis, Morris, 2008):

$$\dot{\epsilon} = \frac{20V \cos \theta}{a} \quad (6.2)$$

Where:

$\dot{\epsilon}$ = processing strain rate = strain per second

V = extrusion speed

2θ = tool angle = 90°

a = work piece (rod) thickness = 0.125 inches = 3.175 mm

Processing strain rates for the slow and fast pressing speeds for the 1100 and 4043 aluminum are tabulated as follows:

Table 6.1 Processing strain rates for 1100 and 4043 alloys at low and high pressing speeds

Strain Rate	1100 Aluminum		4043 Aluminum	
	Slow Speed	Fast Speed	Slow Speed	Fast Speed
$\dot{\epsilon}$	2.121 / second	54.549 / second	1.713 / second	49.364 / second

Vibration

Vibration was provided by a miniature pneumatic vibrator with an on/off air flow control valve attached to an air supply line from the air compressor as illustrated in Figure 6.22. During experimental trials, low factor settings for vibration were selected by simply closing the air supply control valve. High factor settings were selected by

setting the air compressor pressure regulator to 80 psi prior to opening the air supply control valve. The vibrator was allowed to actuate for one minute prior to pressing.

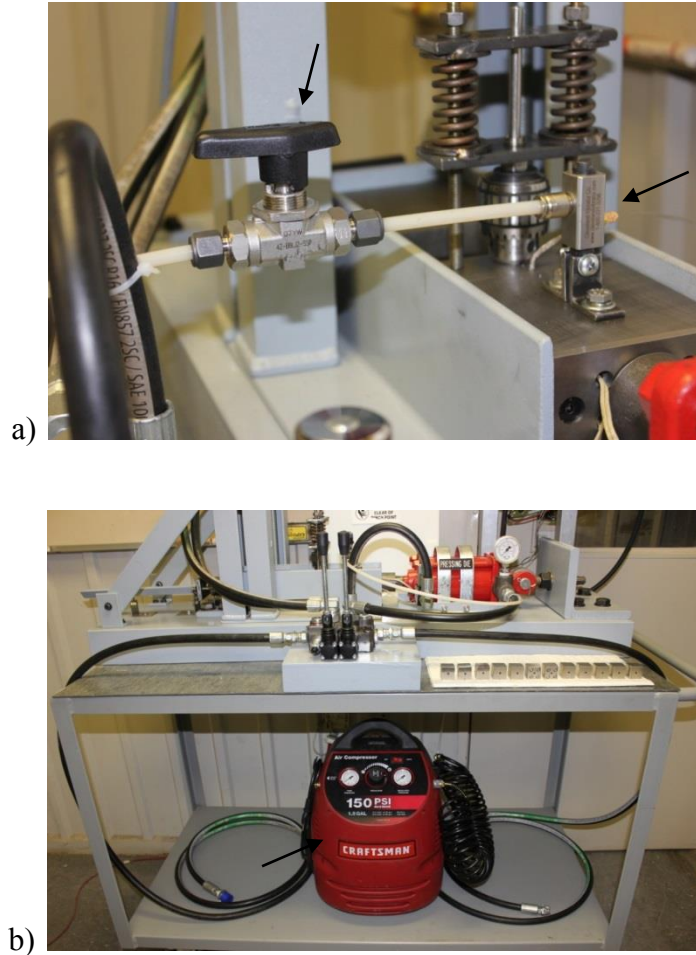


Figure 6.22 Pneumatic vibrator and air supply

- a) On/off air supply control valve and pneumatic vibrator
- b) Air compressor

A vibration monitoring instrument, the CSI RBM Consultant Model B2120A-1 vibration analyzer, quantified the vibration added to the system. The unit is shown in Figure 6.23. Use of this particular instrument offers the advantage of being able to

quantify the vibration inputs, thereby, providing a foundation for better understanding the Ix-ECAP process and defining opportunities for proposed future research.

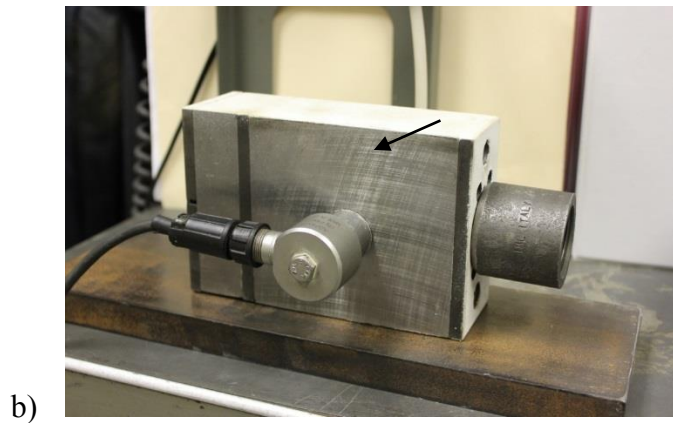


Figure 6.23 Vibration monitoring instrument

a) Vibration monitoring unit

b) Vibration transducer mounted to pressing die for analysis

At high experimental factor settings, the vibrator provided a frequency of 9,498.6 cycles per minute as analyzed at the base of the pressing die at an output pressure of 80

psi. Per manufacturer's specifications at 80 psi, the vibrator output is 14,000 vibrations per minute with an impact force of 12 pounds.

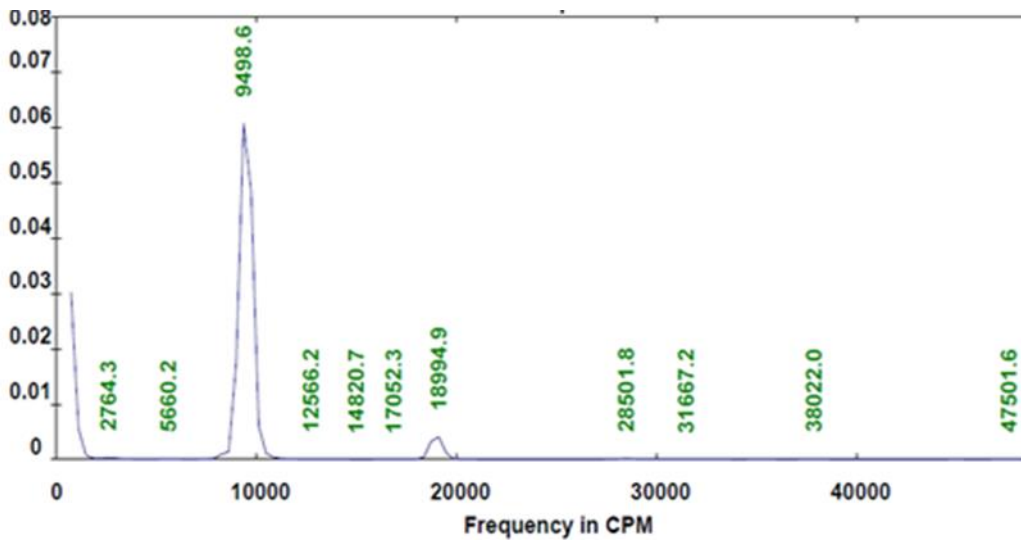


Figure 6.24 Regulated air pressure and vibration analysis

- a) Air pressure was set to 80 psi for each DOE run at the high vibration factor level
- b) Vibration analysis indicating 9,498.6 cycles per minute (cpm) at the bottom of pressing die

Preliminary Feasibility Trials

In order to assess the feasibility of running a new system to study the impact of selected process factors in subsequent fractional factorial split plot experiments, initial runs were performed employing the process redesigns described previously. A conservative approach was taken to ensure safety, minimize potential damage to the unit, and to identify potential failure modes of the system. As a result, initial factor settings were selected based on knowledge of severe plastic deformation processing provided in the literature review. The first trial, though unsuccessful in pressing samples, provided significant insight to the intricacies and limiting factors of the IX-ECAP process.

Selection of process variables were as follows:

- Material Processed: Fully annealed 1100 aluminum
- Work piece Form: 0.125 inch diameter rods 0.875 inch length
- Temperature: Ambient (70 degrees F)
- Pressing Speed: Slow (1 inch/minute)
- Indexing Distance: 0.250 inch
- Back Pressure: None
- Vibration: None
- Die Insert: Vertically parted two piece die insert #1
- Plunger: 0.125 inch diameter tool steel rod 10 inch length
- Die Lubrication: 10W-30 motor oil
- Clamping Force: Clamping die only. Clamping chuck not used.
- Number of Passes: 1
- Processing Route: B_c

To initiate the first trial, all die components were placed in the machine with hydraulics attached. Work pieces were prepared to the dimensions noted above. A single aluminum rod was selected, lubricated with oil, and placed in the entrance channel of the die insert. Both entrance and exit channels of the die insert were lubricated prior to pressing. The plunger was inserted through the clamping die into the pressing die face plate until contact was made with the end of the aluminum rod. Clamping force was applied with the clamping die, and the pressing die was then indexed forward 0.250 inches until contact was made by the clamping and pressing die face plates. The aluminum rod successfully entered the exit channel of the die insert, and the cycle was repeated. However, as the rod was further pressed into the exit channel during the next cycle, lateral distortion due to excessive compressive stresses and buckling of the steel plunger occurred even with a short indexing distance of 0.250 inches. Process changes were critically needed if continued experimentation was to be conducted.

The second trial was equally conservative in approach and included only one change in processing variables which led to ultimate success in pressing samples. Instead of using motor oil as a lubricant, an extreme pressure molybdenum disulfide graphite based lubricant was applied to the aluminum rod as well as the die insert and face plate entrance and exit channels. An air dryer was used to heat and dry the lubricant on each of the contact surfaces prior to pressing. Pressing was once again attempted as in the first trial; however, this time the sample rod was completely cycled through the process without buckling the plunger. Success during the second trial allowed a more aggressive approach to running additional feasibility trials in preparation for subsequent DOEs.

Based on prior success in the second trial, the remaining process factor settings were investigated. Performing additional experimental runs allowed an assessment to be made regarding the ability of the system to functionally process samples through the system and produce work pieces of acceptable quality in terms of product integrity such as absence of surface cracking, distortions, etc. These subsequent trials resulted in successful processing of work pieces employing any combination of the factors and process variables that would be required in the fractional factorial split plot experiments to be performed. Process factors and variables are detailed below.

- Materials Processed: 4043 and 1100 aluminum alloy
- Work Piece Form: 0.125 inch diameter rods from 0.250 to 0.875 inch lengths
- Temperature: Ambient (70 degrees F) and 175 degrees F
- Pressing Speed: Slow (1 inch/minute) and fast (30 inches/minute)
- Indexing Distance: 0.250 to 0.8125 inches
- Back Pressure: 0 and 10 pounds
- Vibration: 0 and 14,000 cpm
- Die Insert: Vertically parted two piece die insert #1
- Plunger: 0.125 inch diameter tool steel rod 10 inch length
- Die Lubrication: Molybdenum disulfide graphite based lubricant
- Clamping Force: Clamping die and chuck
- Number of Passes: 1, 2, and 3
- Processing Route: B_c

Progression towards performing fractional factorial split plot experiments was made possible by the success of the initial feasibility studies.

Fractional Factorial Split-Plot (FFSP) Experimental Trials

With the development of a new process, complete knowledge of all factors impacting the output of the system represents valuable information. However, a progressive approach in designing proper experimentation within available resources is very important. Investigating and determining significant factors of interest with the indexing equal channel angular pressing system, likewise, required an experimental plan within economic and physical constraints of the system. As a result, a $\frac{1}{4}$ fractional factorial split plot design was selected which studied the impact of five factors at two levels. The split plot design accommodated the hard-to-change factor, temperature, since the system heating elements required additional processing time to heat or cool the dies to high and low levels.

Factors to be studied for the 4043 and 1100 type aluminum alloys are identified once again in Table 6.2 as follows:

Table 6.2 DOE experimental factors

Factor ID	Experimental Factors	1100 Aluminum		4043 Aluminum	
		Low Level (-1)	High Level (+1)	Low Level (-1)	High Level (+1)
A	Pressing Temperature (HTC)	77 °F	175 °F	77 °F	175 °F
B	No. of Passes	1	3	1	3
C	Back Pressure	0 lbs. (0 psi)	10 lbs. (815.30 psi)	0 lbs. (0 psi)	10 lbs. (815.30 psi)
D	Speed	1 in./min.	30 in./ min.	1 in./min.	30 in./min.
E	Vibration	0 cpm	9,498.6 cpm	0 cpm	9,498.6 cpm

Note: HTC = hard-to-change factor

A critical prerequisite in actually running the split plot experiments involved proper planning of time constraints and a determination of available resources. To help illustrate this premise, the design matrix is provided in Table 6.3 on the following page. Based on the original plan, three replicates were to be conducted for the 1/4 fraction factorial split plot design. However, based on time constraints required to complete the eight runs required at the sub plot level, replicates or blocks had to be run on separate days of the week. Therefore, statistical analysis required the use of blocks in terms of days in order to complete the experiment. To provide options for selection of the final experimental design, randomly generated experimental designs from which to select were produced by Minitab®. The first randomizations occurred for the hard-to-change factor, temperature (A), at the whole plot level with subsequent randomizations generated for subplots within each whole plot for the remaining four easy-to-change factors. Upon review of the possible options, the design matrix in Table 6.3 was selected primarily due

to the randomized ordering of the temperature factor levels within each block which allowed four runs to be completed at the low temperature setting followed by four runs at the high setting within each block. This design facilitated physical constraints of experimentation for a process such as I_X-ECAP which involved thermal heating and cooling of system components while maintaining statistical validation through randomly generated design matrices.

As shown in Figure 6.25, a copy of the design matrix was attached to the machine's white board in easy view of the experimenter in order to complete each of the runs at the appropriate factor level settings.

Table 6.3 Design table for fractional factorial split-plot experiment (randomized)

Run Order	Block	Whole Plot	A (Temp)	B (No. Passes)	C (B/P)	D (Speed)	E (Vibration)
1	1	1	-	+	+	-	-
2	1	1	-	-	-	-	+
3	1	1	-	+	-	+	-
4	1	1	-	-	+	+	+
5	1	2	+	+	-	-	+
6	1	2	+	+	+	+	+
7	1	2	+	-	-	+	-
8	1	2	+	-	+	-	-
9	2	3	-	+	-	+	-
10	2	3	-	-	+	+	+
11	2	3	-	-	-	-	+
12	2	3	-	+	+	-	-
13	2	4	+	-	-	+	-
14	2	4	+	-	+	-	-
15	2	4	+	+	-	-	+
16	2	4	+	+	+	+	+
17	3	5	-	+	+	-	-
18	3	5	-	-	-	+	+
19	3	5	-	-	-	-	+
20	3	5	-	+	-	+	-
21	3	6	+	+	-	-	+
22	3	6	+	-	+	-	-
23	3	6	+	+	+	+	+
24	3	6	+	-	-	+	-

A = Temperature

B = Number of Passes

C = Back Pressure (B/P)

D = Speed

E = Vibration



a)



b)

Figure 6.25 Pressing unit during actual experimental runs

- a) Overall system showing experimental design matrix
- b) System being changed to different factor level settings

4043 Aluminum Alloy

Details of the fractional factorial split-plot design selected for study of the IX-ECAP process are provided below.

Fractional Factorial Split-Plot Design:

Factors:	5	Whole plots:	6	Resolution:	III
Hard-to-change:	1	Runs per whole plot:	4	Fraction:	1/4
Runs:	24	Whole-plot replicates:	3		
Blocks:	3	Subplot replicates:	1		
Design Generators:		D = ABC, E = AB			
Hard-to-change factors:		A			
Whole Plot Generators:		A			
Defining Relation:		I = ABCD = ABE = CDE			
Alias Structure:		I + ABE + CDE + ABCD			
		A + BE + ACDE + BCD			
		B + AE + BCDE + ACD			
		C + ABCE + DE + ABD			
		D + ABDE + CE + ABC			
		E + AB + CD + ABCDE			
		AC + BCE + ADE + BD			
		AD + BDE + ACE + BC			

Run order, blocks, whole plots, and sub plot treatments along with experimental values of the output response variable are provided in the design matrix in Table 6.4.

Table 6.4 Design matrix and data display for split-plot $\frac{1}{4}$ fraction factorial for 4043 aluminum

Run Order	Block	Whole Plot	A	B	C	D	E	Response Hardness (HV ₁₀₀)
1	1	1	-	+	+	-	-	66
2	1	1	-	-	-	-	+	63
3	1	1	-	+	-	+	-	65
4	1	1	-	-	+	+	+	60
5	1	2	+	+	-	-	+	64
6	1	2	+	+	+	+	+	60
7	1	2	+	-	-	+	-	59
8	1	2	+	-	+	-	-	60
9	2	3	-	+	-	+	-	67
10	2	3	-	-	+	+	+	64
11	2	3	-	-	-	-	+	60
12	2	3	-	+	+	-	-	66
13	2	4	+	-	-	+	-	61
14	2	4	+	-	+	-	-	57
15	2	4	+	+	-	-	+	59
16	2	4	+	+	+	+	+	63
17	3	5	-	+	+	-	-	67
18	3	5	-	-	+	+	+	61
19	3	5	-	-	-	-	+	61
20	3	5	-	+	-	+	-	68
21	3	6	+	+	-	-	+	61
22	3	6	+	-	+	-	-	62
23	3	6	+	+	+	+	+	68
24	3	6	+	-	-	+	-	61

A = Temperature, B = No. of Passes, C = Back Pressure, D = Pressing Speed, E = Vibration

With the construction of a newly designed manufacturing prototype, a Resolution III design provided efficient and economical statistical validation as an initial screening

experiment in studying the effects of main process factors. As seen from the alias structure on the following page, main effects are free from aliasing with other main effects, thereby allowing a statistical assessment of the primary factors controlling process performance. However, main effects are confounded with two-, three-, and higher-order factor interactions, some of which could be statistically significant. Additionally, some of the two-factor interactions are confounded with other higher-order interactions. Therefore, subsequent experimentation is an area of future research in validating factor interactions regarding I_x-ECAP processing.

Runs were completed based on run order from the design matrix. Each replicate consisting of eight runs, four at the low-temperature level and four at the high-temperature level with randomizations within sub plots for the remaining four factors, were completed in blocks during different days. Runs were completed as follows:

- Pressing temperatures were set as defined by the design matrix,
- Die insert and rod work piece were sprayed with molybdenum disulfide graphite based lubricant and dried with forced heated air,
- Die components were assembled and placed in the pressing unit,
- Work piece was inserted into the die insert,
- Vibration and/or back pressure mechanisms applied as per design matrix,
- Hydraulic system activated,
- Clamping systems activated, and lastly
- Pressing of the work piece was performed.

For pressings requiring three passes through the system, rod work pieces were polished prior to subsequent passes by external surface fine grinding to 600 grit. The procedure was then repeated for each of the respective runs within each block.

Representative samples from runs requiring one pass and three passes through the system, respectively, are shown in Figures 6.26 and 6.27.

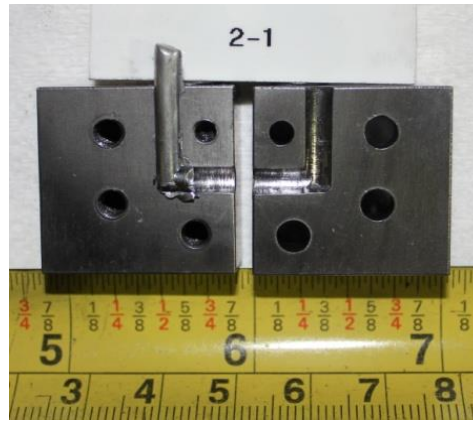


Figure 6.26 4043 aluminum rods showing 1 pass through the system for run order #2

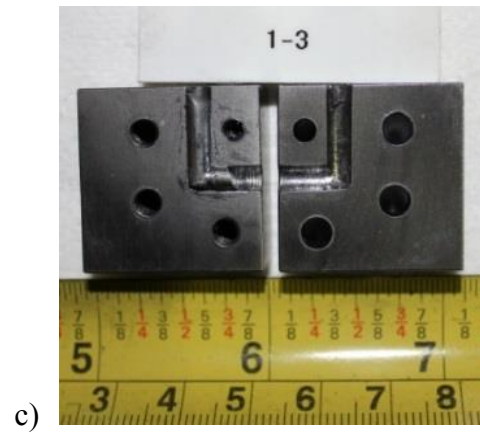
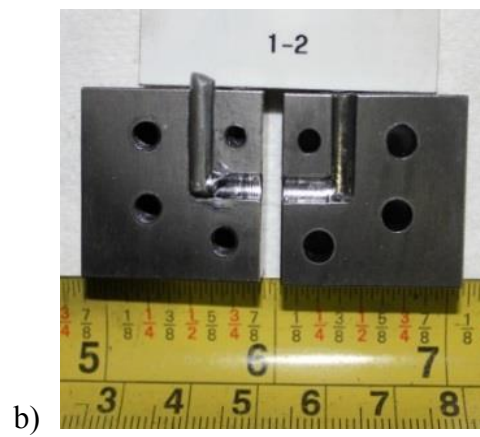
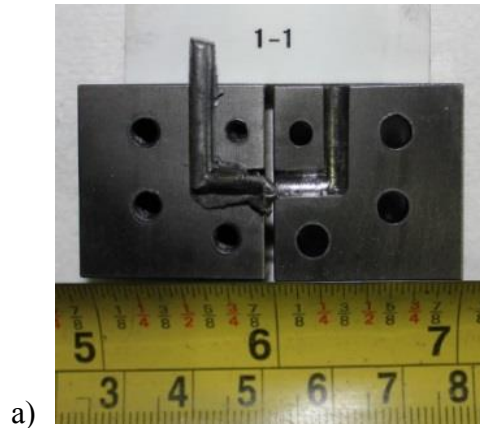


Figure 6.27 4043 aluminum rods showing 3 passes through the system for run order #1

- a) Pass #1
- b) Pass #2
- c) Pass #3

Upon completion of all experimental runs, rods were sectioned normal to the pressing direction at mid-length and mounted in epoxy sample molds in the transverse and longitudinal directions as shown in Figure 6.28. Vickers micro hardness readings were obtained on all transverse sections of un-pressed and pressed samples; whereas, microstructural analysis was performed on baseline transverse sections.

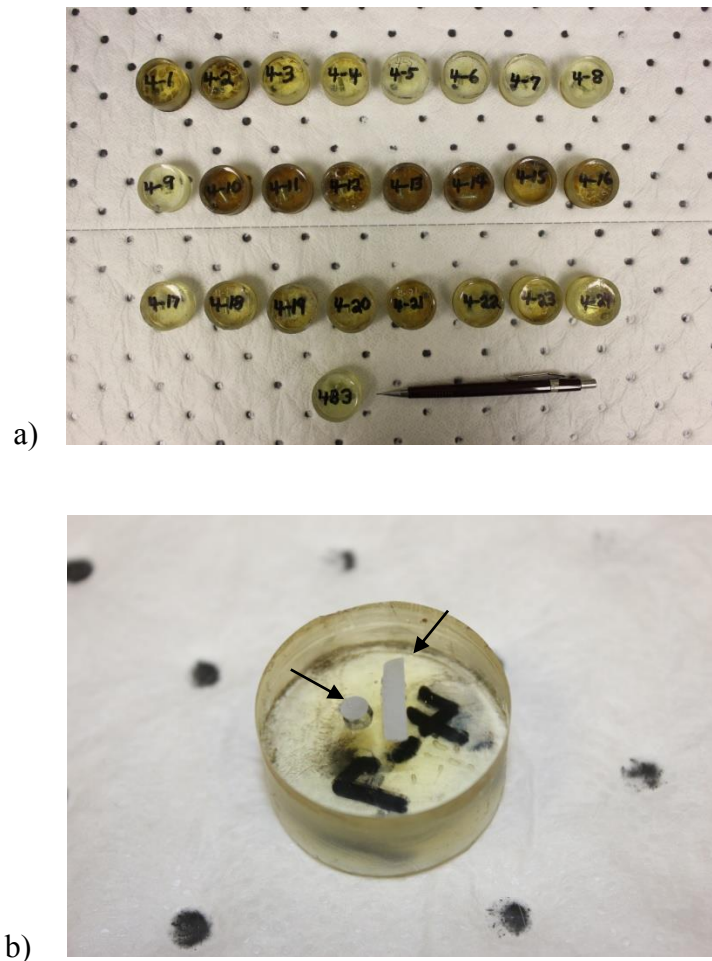


Figure 6.28 4043 aluminum rods sectioned and mounted in epoxy for micro hardness and metallographic analysis

- a) 24 pressed and 1 unpressed baseline samples mounted in epoxy
- b) Transverse and longitudinal pressed sample

Table 6.5 provides the analysis of variance (ANOVA) using Minitab® to draw conclusions regarding impact of process factors on the response variable, micro hardness. Statistical significance was determined at an alpha level of 5% ($\alpha=0.05$).

Table 6.5 Analysis of variance for hardness (coded units) for 4043 aluminum

Source	DF	Seq SS	Adj SS	Adj MS	F	P
Block	2	12.000	12.000	6.000	1.33	0.429
A[HTC] - Temp	1	45.375	45.375	45.375	10.08	0.086
WP Error	2	9.000	9.000	4.500	1.03	0.384
B - No. Passes	1	84.375	84.375	84.375	19.23	0.001
C - Back Pressure	1	1.042	1.042	1.042	0.24	0.634
D - Speed	1	5.042	5.042	5.042	1.15	0.302
E - Vibration	1	9.375	9.375	9.375	2.14	0.166
SP Error	14	61.417	61.417	4.387		
Total	23	227.625				

Based on a review of the p-values, one main factor was statistically significant in the effect on micro hardness. With a p-value of $0.001 < 0.05$, main factor B (number of passes through the system) was statistically significant. One very important consideration at the outset of experimental runs involved the possible impact of blocking as the three replicates were conducted over a three-day period. Initially, runs were scheduled to be conducted in sequential days; however, this could not be guaranteed based on resource and time constraints. Fortunately, replicates were able to be performed on sequential days and, based on the p-value of $0.429 > 0.05$, the variance contribution from runs on different days as noted by blocks was statistically insignificant. Even though not statistically significant with a p-value of 0.086, the impact of the hard-to-

change factor, temperature, is noteworthy. If the significance level was considered at $\alpha = 0.10$, temperature would be statistically significant.

Plots for main predictor variables versus the output response illustrate the effect of each of the respective factors as shown in Figure 6.29.

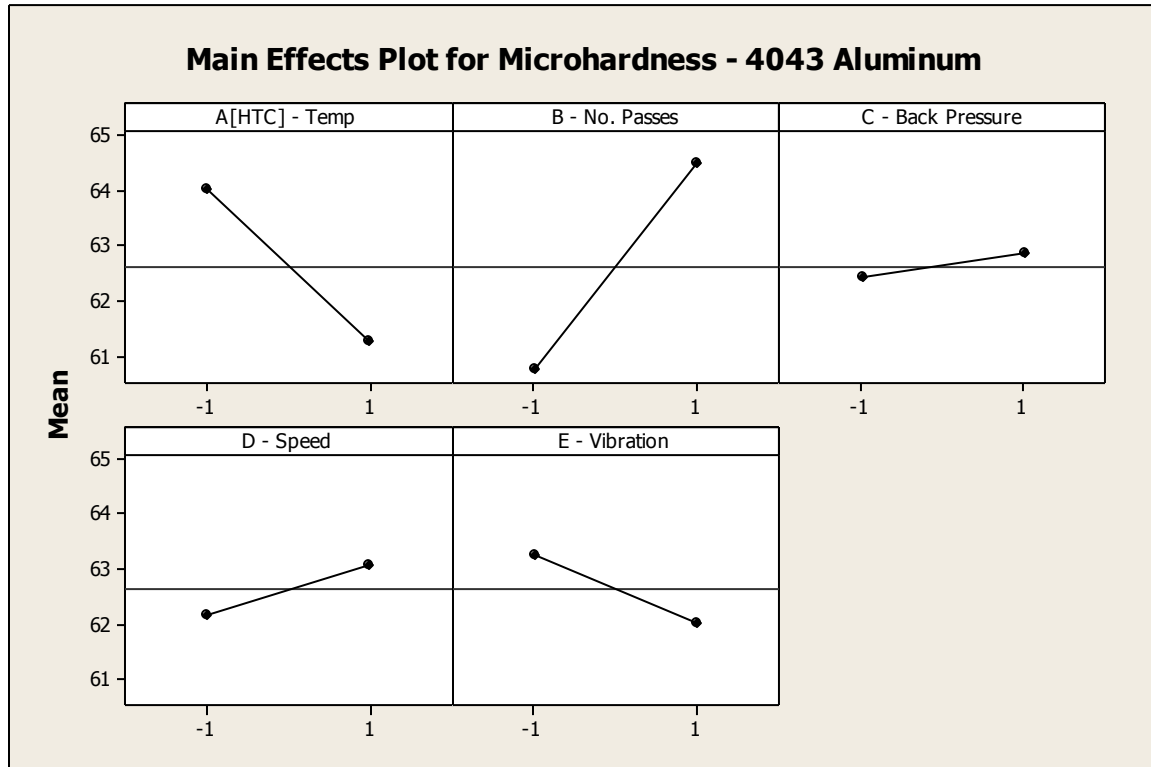


Figure 6.29 Main effects plot for response variable, hardness, for 4043 aluminum

To gain additional insight, regression analysis is provided which gives the estimated effects and coefficients for each of the regressor variables in developing a model for prediction of the response variable at factor levels established in the experimental design. Results of the ANOVA regression are provided in Table 6.6.

Table 6.6 Estimated effects and coefficients for hardness for 4043 aluminum

<u>Term</u>	<u>Effect</u>	<u>Coef</u>	<u>SE Coef</u>	<u>T</u>	<u>P</u>
Constant		62.625	0.4330	144.63	0.000
Block 1		-0.500	0.6124	-0.82	0.500
Block 2		-0.500	0.6124	-0.82	0.500
A[HTC] - Temp	-2.750	-1.375	0.4330	-3.18	0.086
B - No. Passes	3.750	1.875	0.4275	4.39	0.001
C - Back Pressure	0.417	0.208	0.4275	0.49	0.634
D - Speed	0.917	0.458	0.4275	1.07	0.302
E - Vibration	-1.250	-0.625	0.4275	-1.46	0.166
S = 2.09449 R-Sq (SP) = 61.91%					
S (WP) = 0.168148 R-Sq (WP) = 86.44%					

The regression equation provided by Minitab[®] employing all five factors is as follows:

$$\text{Hardness} = 62.625 - 1.375 [A] + 1.875[B] + 0.208 [C] + 0.458[D] - 0.625[E] \quad (6.3)$$

A consideration of the coefficients of partial determination for each factor provides additional insight to the development of the multivariate regression equation as each predictor variable is added to the model. For example, the five factors in order of progressive inclusion into the model based on the p-values noted in Table 6.6 are as follows: B -number of passes (p-value = 0.001), A – temperature (p-value = 0.086), E – vibration (p-value = 0.166), D - pressing speed (p-value = 0.322), and C – back pressure

(p-value = 0.634). With additions of each of the factors, the impacts on the error sum of squares (SSE) as well as the coefficients of partial determination for each predictor variable were assessed (Clark and Schkade 1979). The error sum of squares (SSE) is defined as follows: (Montgomery and Runger 2007):

$$SSE = \sum_{i=1}^n (y_i - \hat{y}_i)^2 \quad (6.4)$$

Where:

y_i = actual value of response variable, microhardness

\hat{y}_i = fitted value of response variable, microhardness

The error sum of squares and coefficients of partial determination were calculated based on progressively adding the five factors as summarized in Tables 6.7 and 6.8:

Table 6.7 Error sum of squares for multivariate regression adding predictor variables for 4043 aluminum

4043 Aluminum		
Error Sum of Squares for Model Containing X Factors	Model Factors	Error Sum of Squares, SSE
SSE(X_0)	No factors	227.625
SSE(X_B)	B	143.250
SSE(X_B, X_A)	B, A	99.000
SSE(X_B, X_A, X_E)	B, A, E	88.500
SSE(X_B, X_A, X_E, X_D)	B, A, E, D	83.458
SSE(X_B, X_A, X_E, X_D, X_C)	B, A, E, D, C	82.417

Table 6.8 Coefficients of partial determination for multivariate regression adding predictor variables for 4043 aluminum

4043 Aluminum		
Factors Contained in the Model	Factor Added	Coefficient of Partial Determination
No factors	B	0.371
B	A	0.309
B, A	E	0.106
B, A, E	D	0.057
B, A, E, D	C	0.013

Coefficients for each of the five factors are illustrated as follows:

- Factor B: Number of Passes

$R_{YB,0}^2$ = Partial coefficient of determination when factor B (number of passes) was added to the model containing only the intercept value and no factors.

$$R_{YB,0}^2 = \frac{SSE(X_0) - SSE(X_0, X_B)}{SSE(X_0)} = 0.371 \quad (6.5)$$

- Factor A: Temperature

$R_{YA,B}^2$ = Partial coefficient of determination when factor A (temperature) was added to the model containing factor B (number of passes).

$$R_{YA,B}^2 = \frac{SSE(X_B) - SSE(X_B, X_A)}{SSE(X_B)} = 0.309 \quad (6.6)$$

- Factor E: Vibration

$R_{YE,BA}^2$ = Partial coefficient of determination when factor E (vibration) was added to the model containing factors B (number of passes) and A (temperature).

$$R_{YE,BA}^2 = \frac{SSE(X_B, X_A) - SSE(X_B, X_A, X_E)}{SSE(X_B, X_A)} = 0.106 \quad (6.7)$$

- Factor D: Pressing Speed

$R_{YD,BAE}^2$ = Partial coefficient of determination when factor D (pressing speed) was added to the model containing factors B, A, and E.

$$R_{YD,BAE}^2 = \frac{SSE(X_B, X_A, X_E) - SSE(X_B, X_A, X_E, X_D)}{SSE(X_B, X_A, X_E)} = 0.057 \quad (6.8)$$

- Factor C: Back Pressure

$R_{YC,BAED}^2$ = Partial coefficient of determination when factor C (back pressure) was added to the model containing factors B, A, E, and D.

$$R_{YC,BAED}^2 = \frac{SSE(X_B, X_A, X_E, X_D) - SSE(X_B, X_A, X_E, X_D, X_C)}{SSE(X_B, X_A, X_E, X_D)} = 0.013 \quad (6.9)$$

As noted in Table 6.7, the error sum of squares is reduced from 143.250 to 88.500 when the factors B, A, and E are progressively added to the model. This represents a 38.22% reduction in the error sum of squares. Inclusion of the last two factors D and C, however, offers minimal improved performance of the regression equation since the error sum of squares is only reduced to 83.458 and 82.417, respectively. The coefficients of partial determination also provide insight to the contributions from each of the respective factors. For example, 37.1% of the remaining variation is explained by factor B (number of presses) when no other factors are present in the model. With factor B contained in the regression equation, the addition of factor A (temperature) is able to account for 30.9% of the remaining variation. Likewise, when factor E (vibration) is added to the model containing both factors B and A, 10.6% of the remaining variation is explained by factor E. Additional experimentation is warranted since factor E (vibration) with a p-value of 0.166 was not statistically significant. However, factor E was aliased with the AB two-

factor interaction. Either factor E (vibration) may ultimately impact the process at other factor levels or the AB interaction may also become statistically significant at other factor level settings of factors A and B. As a result, the multiple regression model representing the IX-ECAP process could be further investigated to assess the need for inclusion of main factors as well as two- or three-way interactions. With the ¼ fraction factorial split plot design serving as an initial screening experiment for a newly developed prototype manufacturing system investigating main factors at the exclusion of two-way and higher-order interactions, the inclusion of all main factors will be considered in the regression model in the initial assessment and subsequent analysis of process performance.

Fitted values calculated from the regression equation incorporating all terms are provided in the Minitab® output in Table 6.9.

Table 6.9 Residuals table for 4043 aluminum using the full model regression equation

<u>Obs</u>	<u>A[Temp]</u>	<u>Hardness</u>	<u>Fit</u>	<u>SE Fit</u>	<u>Residual</u>	<u>St Resid</u>
1	-1.00	66.000	66.250	1.070	-0.250	-0.13
2	-1.00	63.000	60.833	1.070	2.167	1.17
3	-1.00	65.000	66.750	1.070	-1.750	-0.94
4	-1.00	60.000	62.167	1.070	-2.167	-1.17
5	1.00	64.000	61.833	1.070	2.167	1.17
6	1.00	60.000	63.167	1.070	-3.167	-1.71
7	1.00	59.000	60.250	1.070	-1.250	-0.67
8	1.00	60.000	59.750	1.070	0.250	0.13
9	-1.00	67.000	66.750	1.070	0.250	0.13
10	-1.00	64.000	62.167	1.070	1.833	0.99
11	-1.00	60.000	60.833	1.070	-0.833	-0.45
12	-1.00	66.000	66.250	1.070	-0.250	-0.13
13	1.00	61.000	60.250	1.070	0.750	0.40
14	1.00	57.000	59.750	1.070	-2.750	-1.48
15	1.00	59.000	61.833	1.070	-2.833	-1.53
16	1.00	63.000	63.167	1.070	-0.167	-0.09
17	-1.00	67.000	66.250	1.070	0.750	0.40
18	-1.00	61.000	62.167	1.070	-1.167	-0.63
19	-1.00	61.000	60.833	1.070	0.167	0.09
20	-1.00	68.000	66.750	1.070	1.250	0.67
21	1.00	61.000	61.833	1.070	-0.833	-0.45
22	1.00	62.000	59.750	1.070	2.250	1.21
23	1.00	68.000	63.167	1.070	4.833	2.61R
24	1.00	61.000	60.250	1.070	0.750	0.40

R denotes an observation with a large standardized residual

A plot of the fitted values versus the actual hardness values from Table 6.9 based on observation number or run order is provided in Figure 6.30.

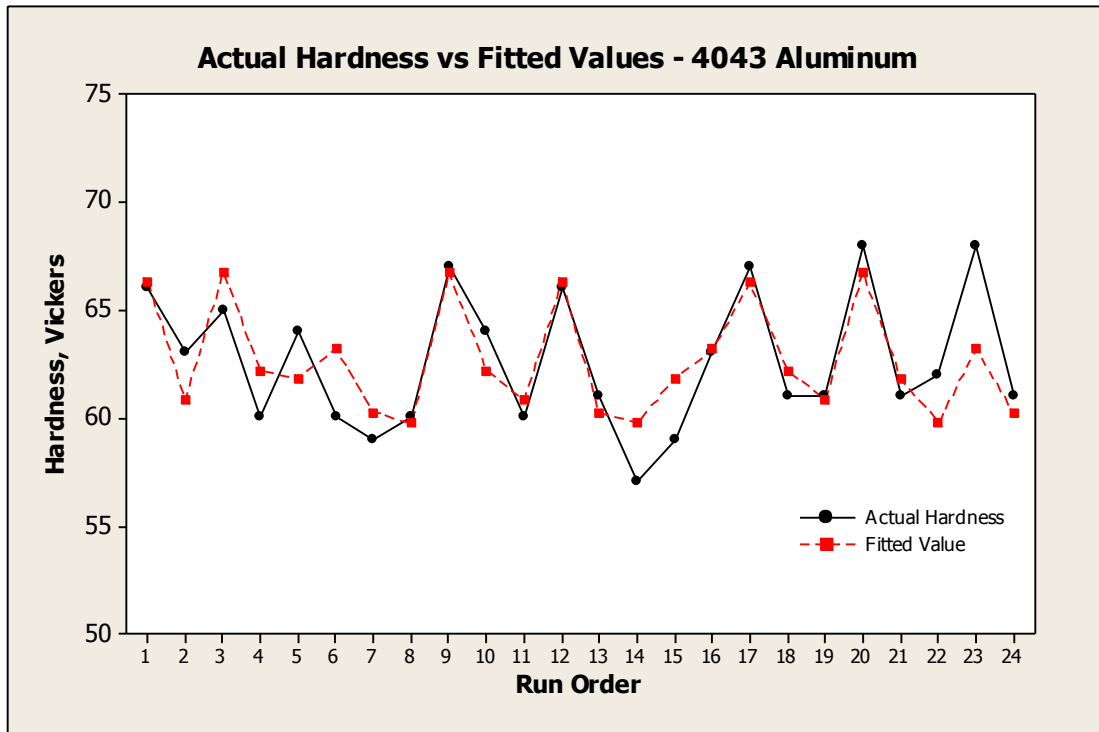


Figure 6.30 Plot of full model fitted values versus actual hardness for observation runs of 4043 aluminum

To verify model adequacy for the analysis of variance, residuals were examined to check underlying assumptions regarding normality, independence with mean equal to zero, and constant variance. As indicated in Figures 6.31 and 6.32 on the following page, the normal probability plot shows the residuals positioned along the straight line reflecting a closely approximated normal distribution while the histogram shows an overall normal (bell-shaped) distribution with minimal skewness to the left and maximum

frequency at (-1) instead of being centered at (0). The normality assumption, therefore, appears to be valid.

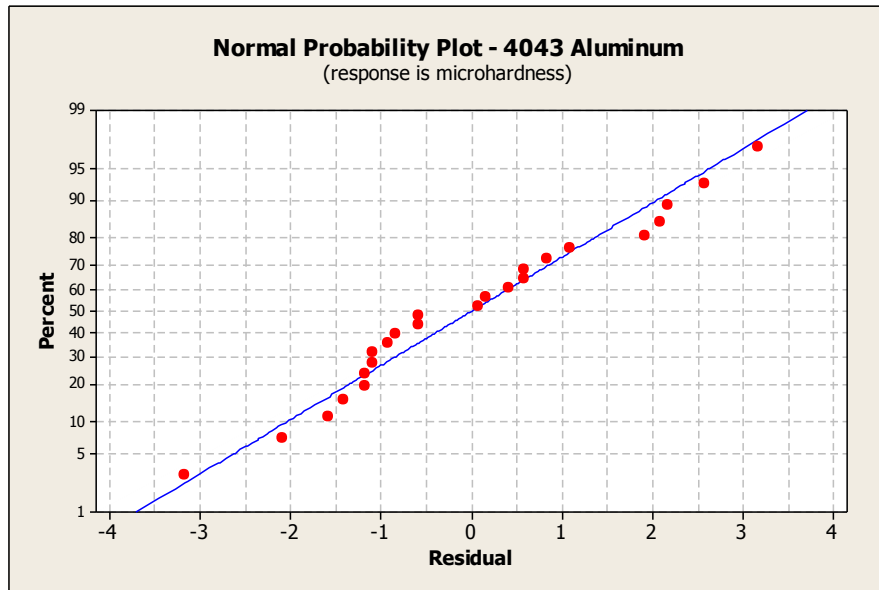


Figure 6.31 Normal probability plot of residuals for 4030 aluminum

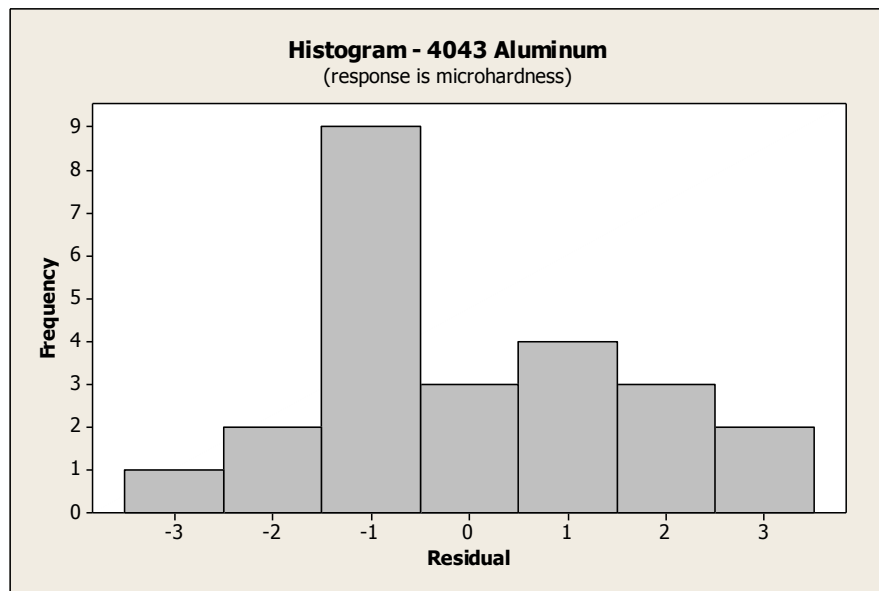


Figure 6.32 Histogram of residuals for 4043 aluminum

To verify the independence assumption, a plot of residuals versus observation order was performed. As illustrated in Figure 6.33, the independence assumption also appears to hold since a random distribution of points above and below the central line of zero is evident.

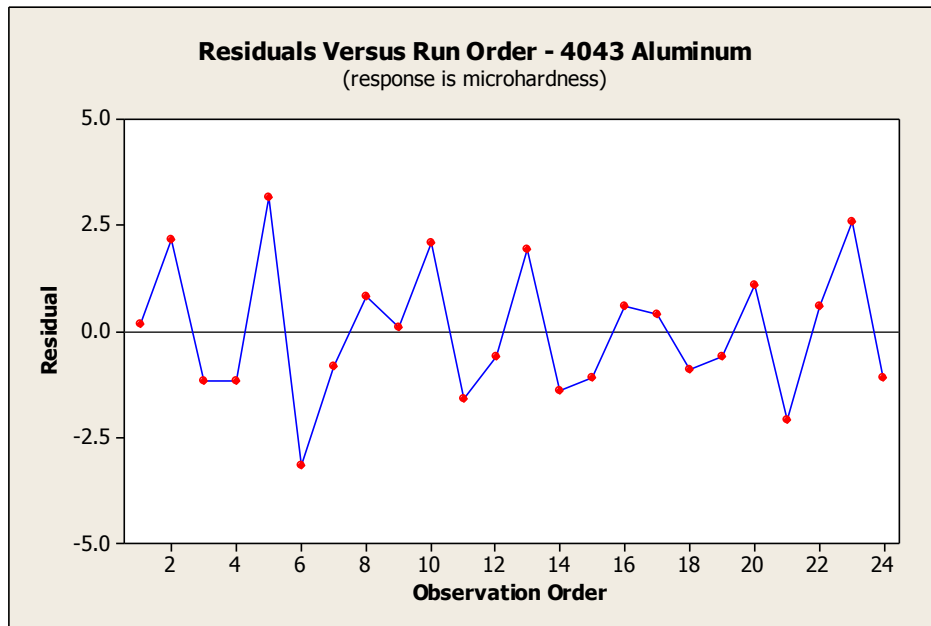


Figure 6.33 Plot of residuals versus run order for 4043 aluminum

The constant variance assumption was assessed based on plots of residuals versus output response variable (hardness), fitted values, and main factors. As shown in Figures 6.34 and 6.35 on the following page, plots of residuals versus hardness and fitted values indicated structureless patterns of points above and below the zero line regardless of the low to high values of hardness and fitted values. Therefore, based on these two respective plots, the constant variance assumption was supported. However, additional

insight regarding the assumption of constant variance was investigated based on plots of residuals versus main factors.

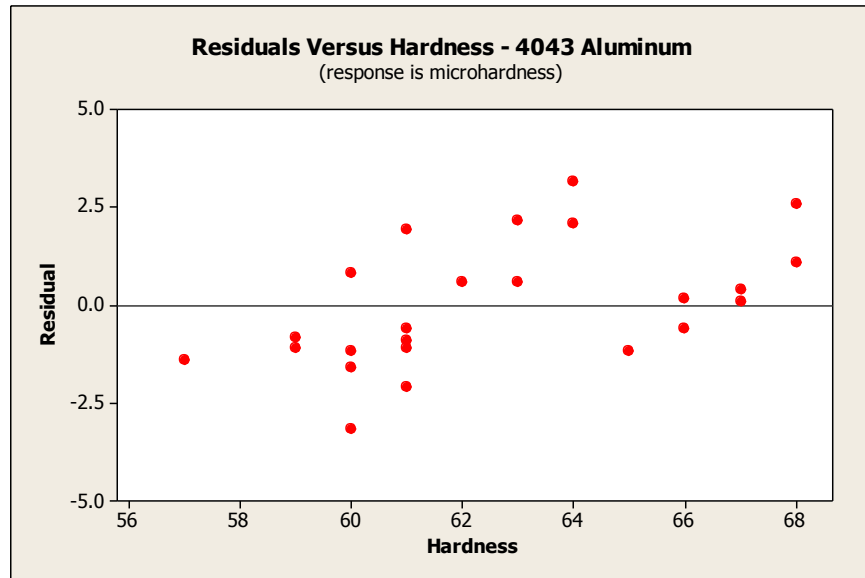


Figure 6.34 Plot of residuals versus actual hardness for 4043 aluminum

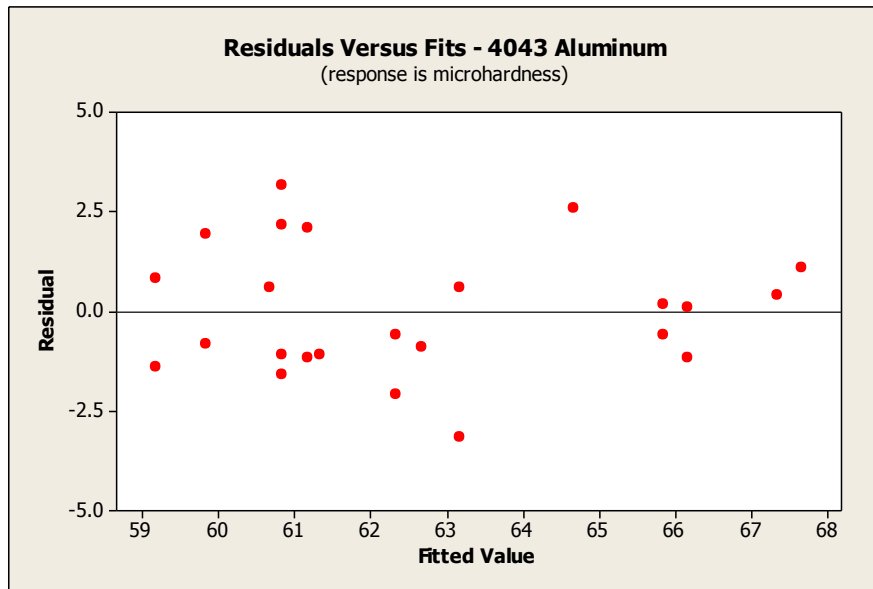


Figure 6.35 Plot of residuals versus fits for 4043 aluminum

To further check model adequacy regarding the constant variance assumption, residuals versus the regressors of temperature, number of passes, back pressure, pressing speed, and vibration were plotted. With the exception of the plot for residuals versus pressing speed and back pressure, each of the plots indicated a possible presence of non constant variance as the spread of the residual values at the low and high factor settings for temperature, number of passes, back pressure, and vibration appeared to differ. As shown in Figure 6.36 below, for example, the spread of the residuals at the low temperature factor setting was smaller than the the spread at the high factor setting. Refer to Figures 6.37 – 6.40 for the remaining plots.

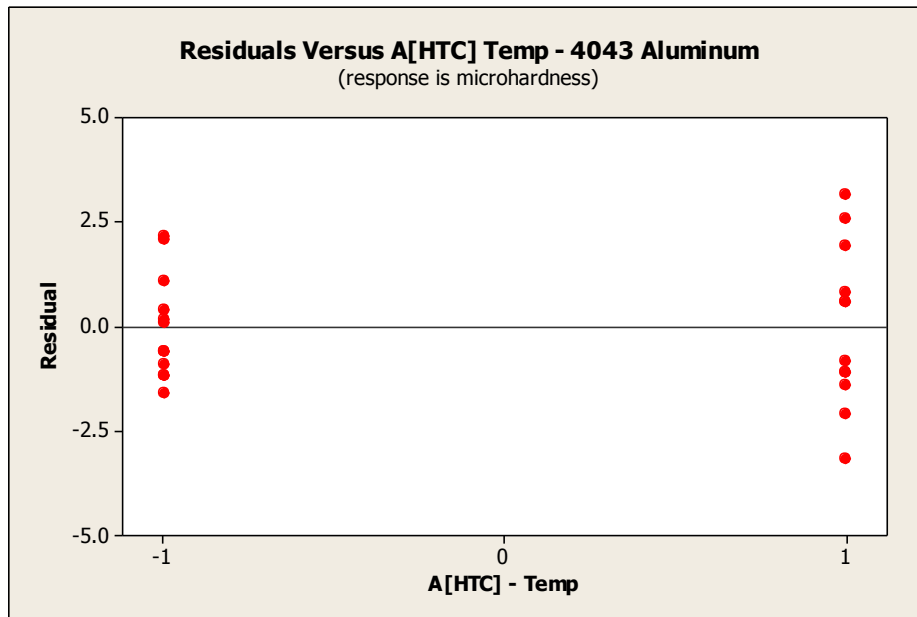


Figure 6.36 Plot of residuals versus temperature for 4043 aluminum

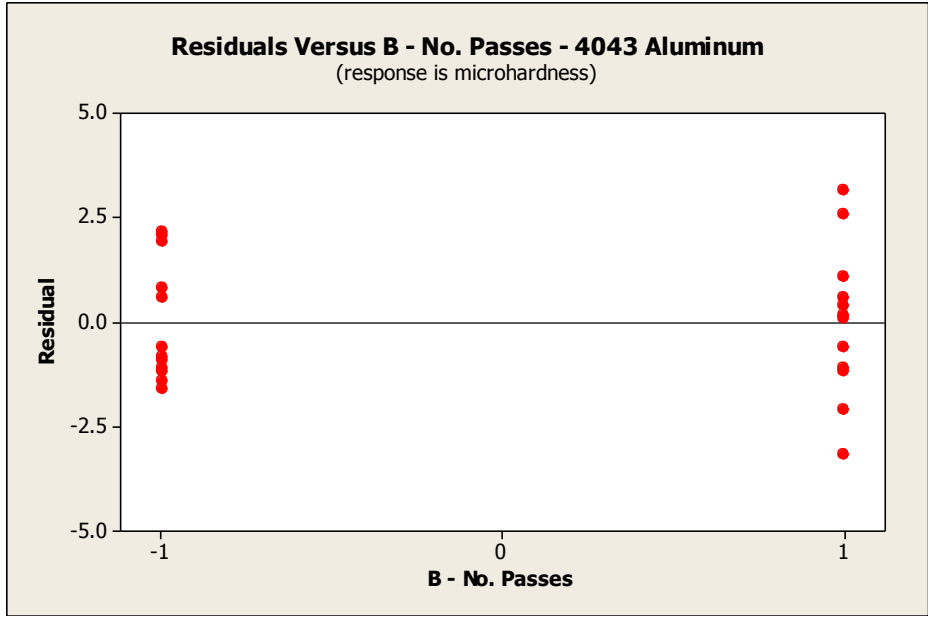


Figure 6.37 Plot of residuals versus number of passes for 4043 aluminum

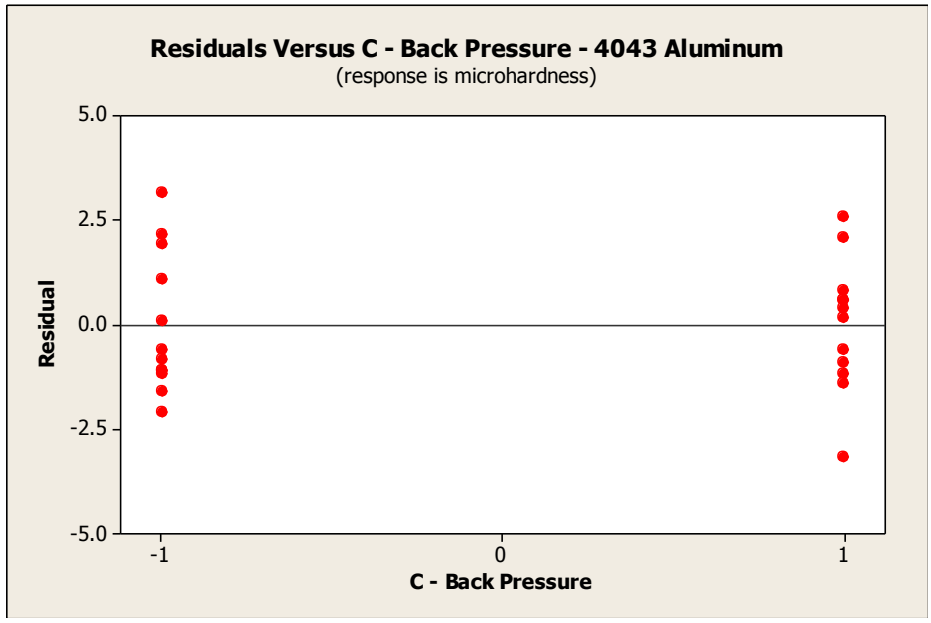


Figure 6.38 Plot of residuals versus back pressure for 4043 aluminum

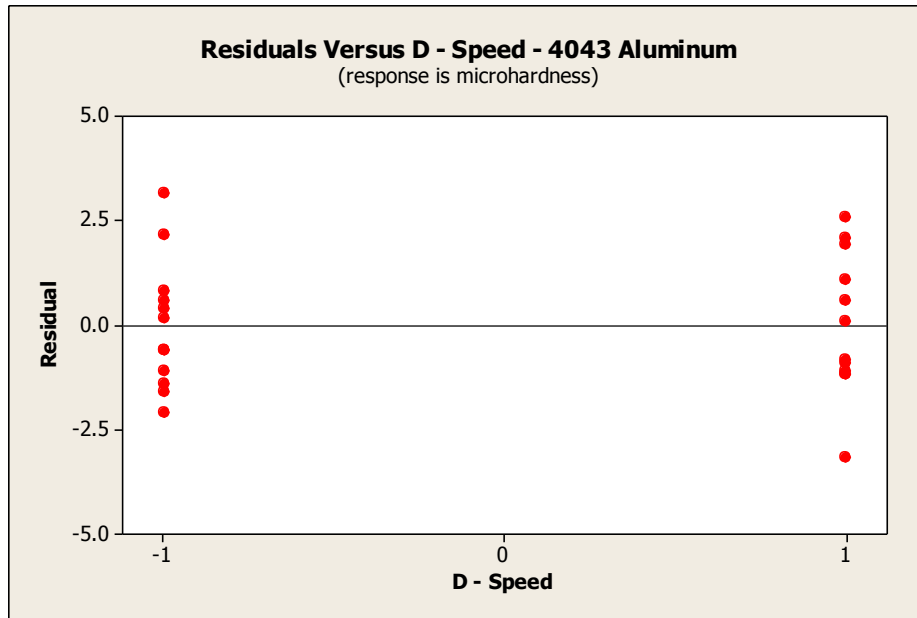


Figure 6.39 Plot of residuals versus pressing speed for 4043 aluminum

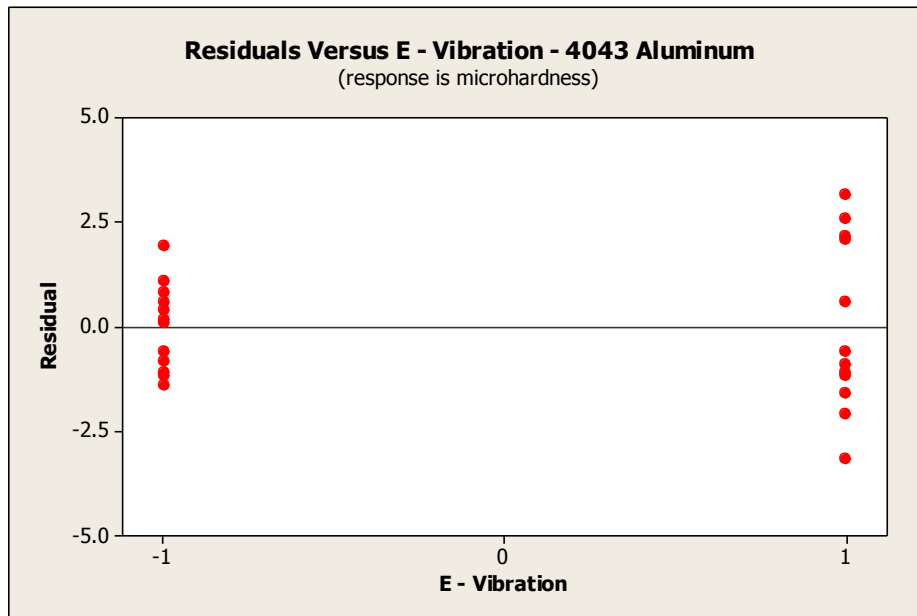


Figure 6.40 Plots of residuals versus vibration for 4043 aluminum

With possible invalidations regarding the constant variance assumption, formal tests were performed to assess statistical significance for equal variances on each of the regressor variables at the low and high factor levels. Specifically, Levene's test for equal variances was performed using a 5% significance level ($\alpha = 0.05$). Each of the analyses is presented subsequently; however, all tests indicated that differences in variances for each of the regressors were statistically insignificant (Levene p values > 0.05). However, main factor B (number of passes) with a Levene's p-value of 0.082 and main factor E (vibration) with a Levene's p-value of 0.054 were marginally statistically insignificant and could warrant further investigation. For example, this lack of potential equal variances for factor B (number of passes) makes intuitive sense due to the fact that Ix-ECAP is a strain hardening process resulting from simple shear imposed on the work pieces which alters the microstructures to develop finer grain sizes. As the number of passes through the system increases, the microstructures continue towards increased levels of homogeneity resulting in less variability in hardness and decreased residual variance. However, true homogeneity may not be reached at three passes through the system. Redistribution of the internal structures may be just beginning to become active at three passes. Additional passes through the system may be required prior to complete saturation of homogeneity in the microstructure and resulting hardness. Each of the tests for equal variances is provided on the following pages.

With R^2 values of 61.91 and 86.44 percent at the sub-plot and whole-plot levels, respectively, the model provides adequate insight to a first initial screening of the Ix-ECAP process.

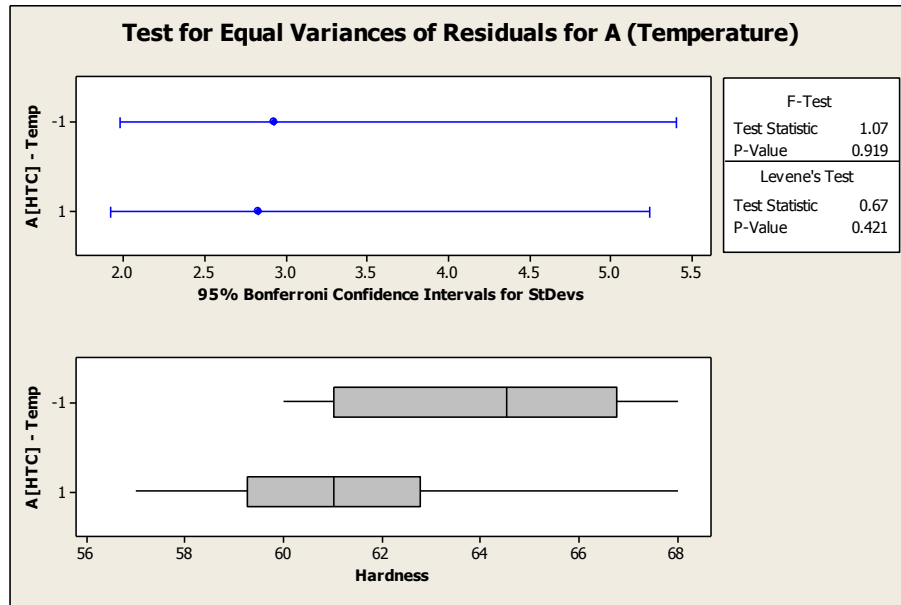


Figure 6.41 Tests for equal variances of residuals for A (Temperature) for 4043 aluminum

95% Bonferroni confidence intervals for standard deviations:

<u>A-Temp</u>	<u>N</u>	<u>Lower</u>	<u>StDev</u>	<u>Upper</u>
-1	12	1.97676	2.92326	5.40367
1	12	1.91535	2.83244	5.23579

F-Test (Normal Distribution):

Test statistic = 1.07, p-value = 0.919

Levene's Test (Any Continuous Distribution):

Test statistic = 0.67, p-value = 0.421

With p-values of 0.919 and 0.421 for the F-test and Levene's test, respectively, differences in the variances are not statistically significant. Therefore, the constant variance assumption is validated at the high and low temperature factor levels.

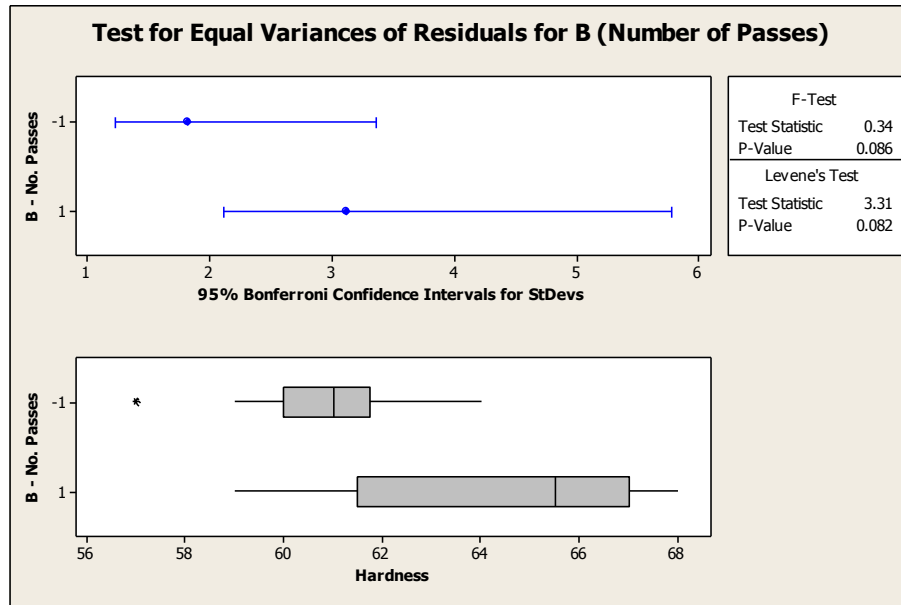


Figure 6.42 Tests for equal variances of residuals for B (Number of Passes) for 4043 aluminum

95% Bonferroni confidence intervals for standard deviations:

<u>B - No. Passes</u>	<u>N</u>	<u>Lower</u>	<u>StDev</u>	<u>Upper</u>
-1	12	1.22756	1.81534	3.35567
1	12	2.10903	3.11886	5.76524

F-Test (Normal Distribution):

Test statistic = 0.34, p-value = 0.086

Levene's Test (Any Continuous Distribution):

Test statistic = 3.31, p-value = 0.082

With p-values of 0.086 and 0.082 for the F-test and Levene's test, respectively, differences in the variances are not statistically significant. Therefore, the constant variance assumption is validated at the high and low factor levels for number of passes.

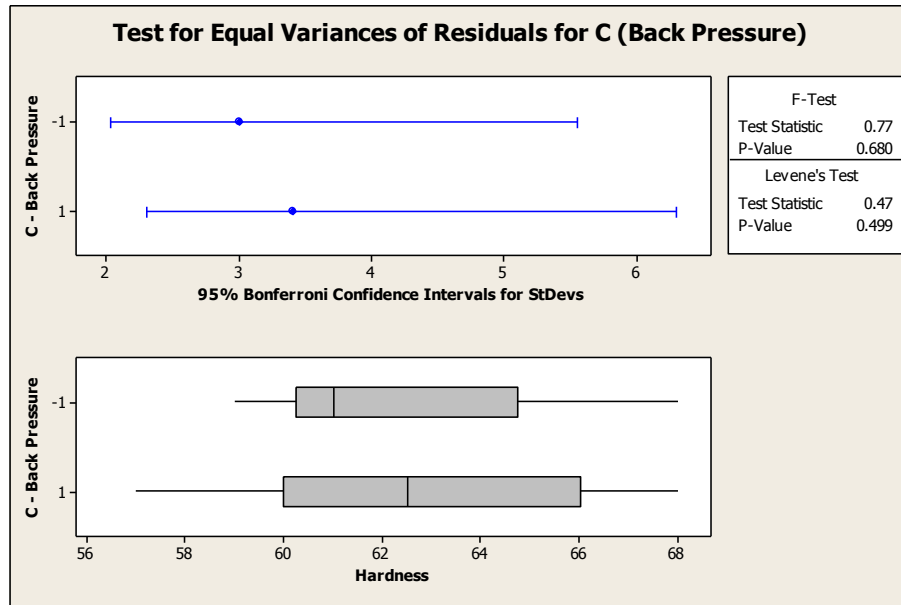


Figure 6.43 Tests for equal variances of residuals for C (Back Pressure) for 4043 aluminum

95% Bonferroni confidence intervals for standard deviations:

<u>C – Back Pressure</u>	<u>N</u>	<u>Lower</u>	<u>StDev</u>	<u>Upper</u>
-1	12	2.02780	2.99874	5.54319
1	12	2.30372	3.40677	6.29744

F-Test (Normal Distribution):

Test statistic = 0.77, p-value = 0.680

Levene's Test (Any Continuous Distribution):

Test statistic = 0.47, p-value = 0.499

With p-values of 0.680 and 0.499 for the F-test and Levene's test, respectively, differences in the variances are not statistically significant. Therefore, the constant variance assumption is validated at the high and low back pressure factor levels.

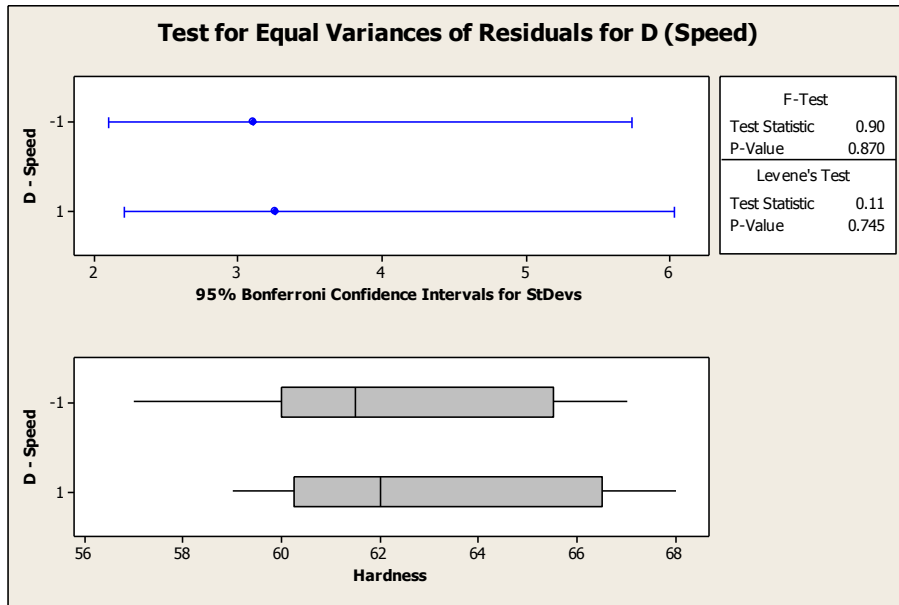


Figure 6.44 Tests for equal variances of residuals for D (Speed) for 4043 aluminum

95% Bonferroni confidence intervals for standard deviations:

<u>D - Speed</u>	<u>N</u>	<u>Lower</u>	<u>StDev</u>	<u>Upper</u>
-1	12	2.09584	3.09936	5.72920
1	12	2.20459	3.26018	6.02648

F-Test (Normal Distribution):

Test statistic = 0.90, p-value = 0.870

Levene's Test (Any Continuous Distribution):

Test statistic = 0.11, p-value = 0.745

With p-values of 0.870 and 0.745 for the F-test and Levene's test, respectively, differences in the variances are not statistically significant. Therefore, the constant variance assumption is validated at the high and low pressing speed factor levels.

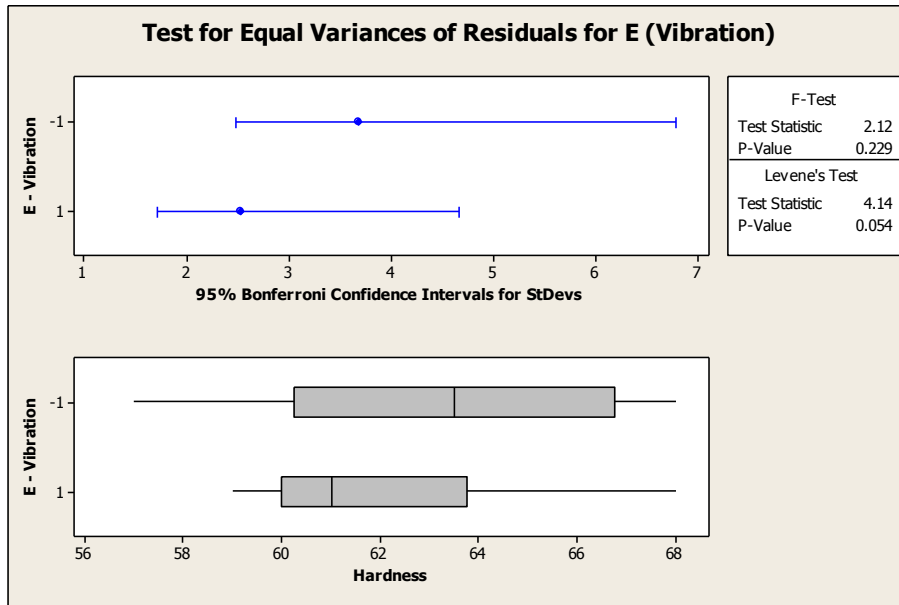


Figure 6.45 Tests for equal variances of residuals for E (Vibration) for 4043 aluminum

95% Bonferroni confidence intervals for standard deviations:

<u>E - Vibration</u>	<u>N</u>	<u>Lower</u>	<u>StDev</u>	<u>Upper</u>
-1	12	2.48249	3.67114	6.78614
1	12	1.70584	2.52262	4.66309

F-Test (Normal Distribution):

Test statistic = 2.12, p-value = 0.229

Levene's Test (Any Continuous Distribution):

Test statistic = 4.14, p-value = 0.054

With p-values of 0.229 and 0.054 for the F-test and Levene's test, respectively, differences in the variances are not statistically significant. Therefore, the constant variance assumption is validated at the high and low vibration factor levels.

Materials Development

As described in Chapter IV sub-sections entitled “Materials – Alloy Selection and Work Piece Form” and “Materials Characterization”, specified details of the type of materials being investigated as well as the characterization methods were discussed. Efforts were undertaken within this research to develop materials with enhanced performance characteristics to include refinements in grain structures and improved levels of strength via hardness increases while retaining moderate ductility and toughness. Material characterizations were performed to assess grain restructuring and changes in micro hardness. Further analysis regarding more comprehensive mechanical properties such as tensile strength, yield strength, ductility, toughness, fatigue, etc., represents an area for future studies.

Aluminum alloys 1100 and 4043 selected for this research offer a baseline of high purity aluminum and a binary alloy consisting of aluminum and silicon. The phase diagram representing each of these systems is provided on the following page in Figure 6.46. Series 1100 is a commercial purity alloy of 99% minimum aluminum; whereas, 4043 represents a binary alloy containing 4.5 – 6.0 % silicon with the remainder predominately aluminum. As noted from the diagram, the alloys remain single phase within the working temperature range of indexing equal channel angular pressing from 25 to 77 °C. Containing 4.5 - 6.0 % silicon, the 4043 alloy silicon solid solubility limit of 1.65% is exceeded and, therefore, reflects a two-phase hypoeutectic alloy consisting of primary silicon particles in an α -aluminum matrix (Hatch, 1984).

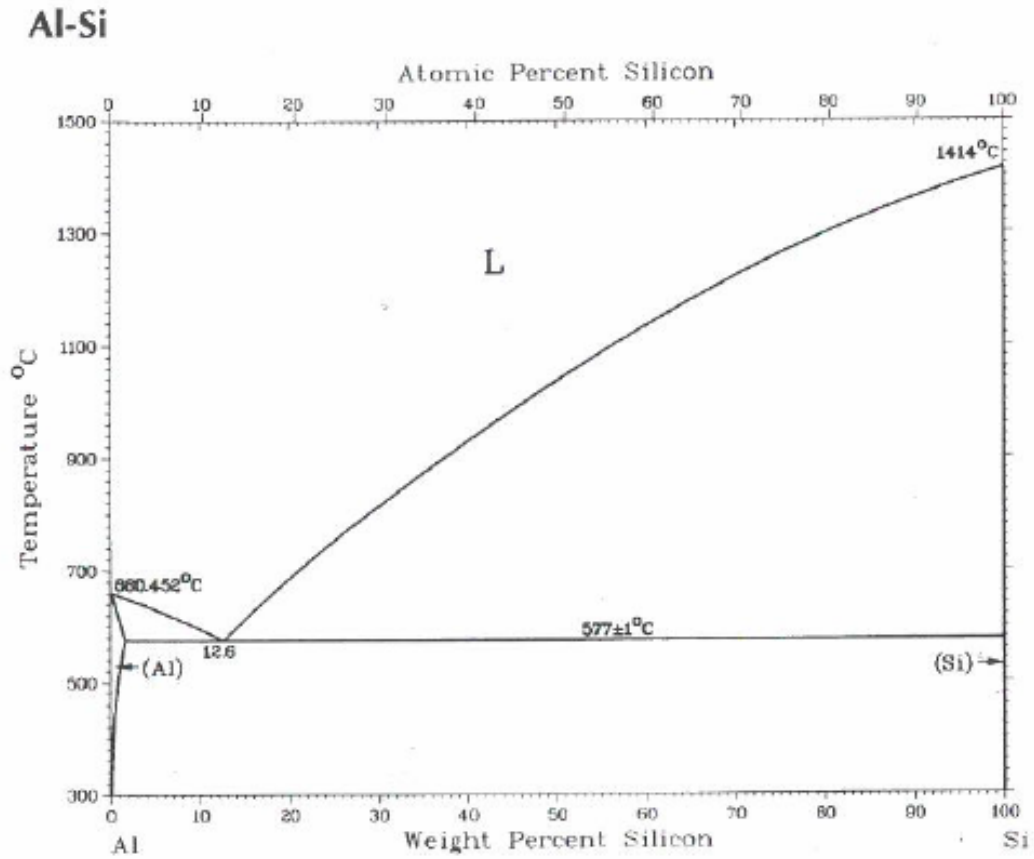


Figure 6.46 Aluminum – silicon phase diagram

Reference: ASM International, 1992

Representative microstructures for the 1100 and 4043 alloys are provided in Figures 6.47 and 6.48 on the following page.

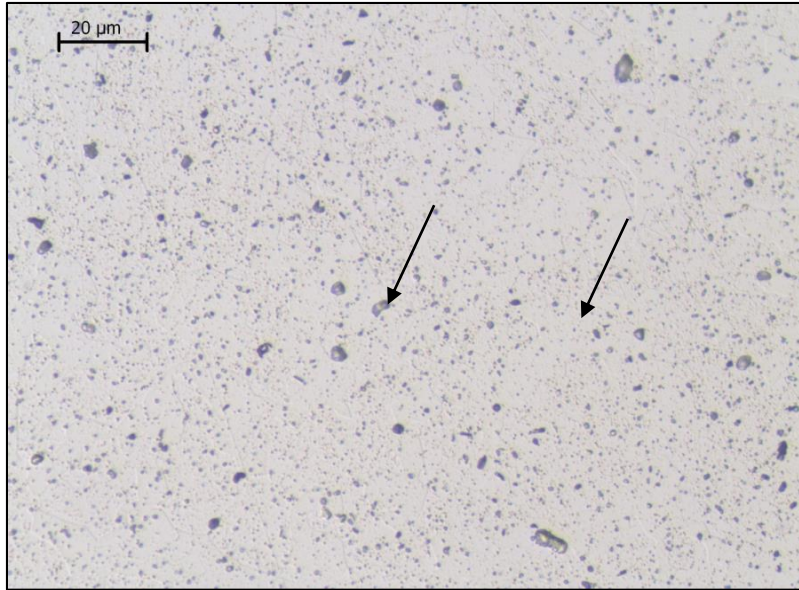


Figure 6.47 Microstructure of 1100 (commercial purity) aluminum alloy. Insoluble particles of aluminum-iron and aluminum-iron-silicon (dark) in aluminum matrix (light)

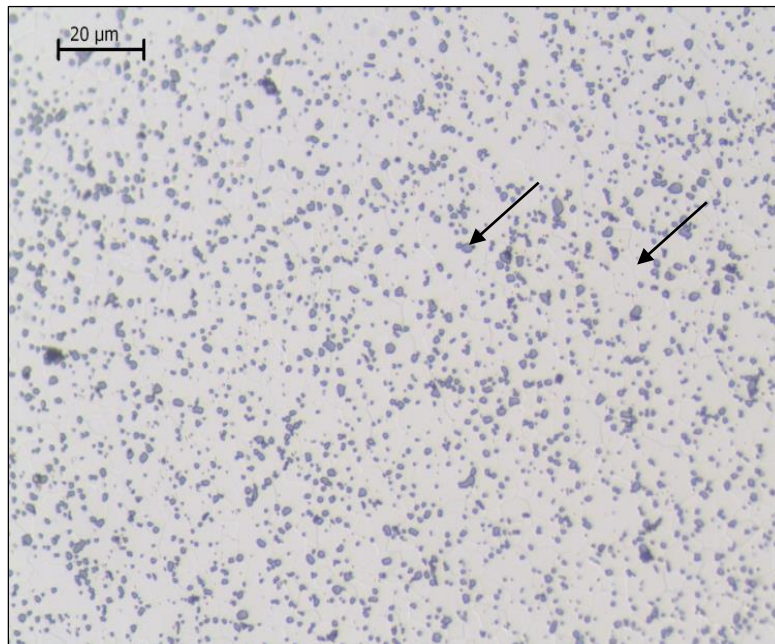


Figure 6.48 Microstructure of 4043 aluminum alloy. Silicon particles (gray) in aluminum matrix (light)

4043 Aluminum

With 4043 aluminum being a commercial alloy with widespread industrial use, the analysis focused on material property enhancements resulting from processing of 4043 discrete variable length rods using IX-ECAP. Figure 6.49 plots the individual and mean hardness values for all samples at both the low and high processing temperatures for each of the number of passes through the system. As illustrated, substantial increases in material hardness were obtained in transitioning through the system using a total of three passes.

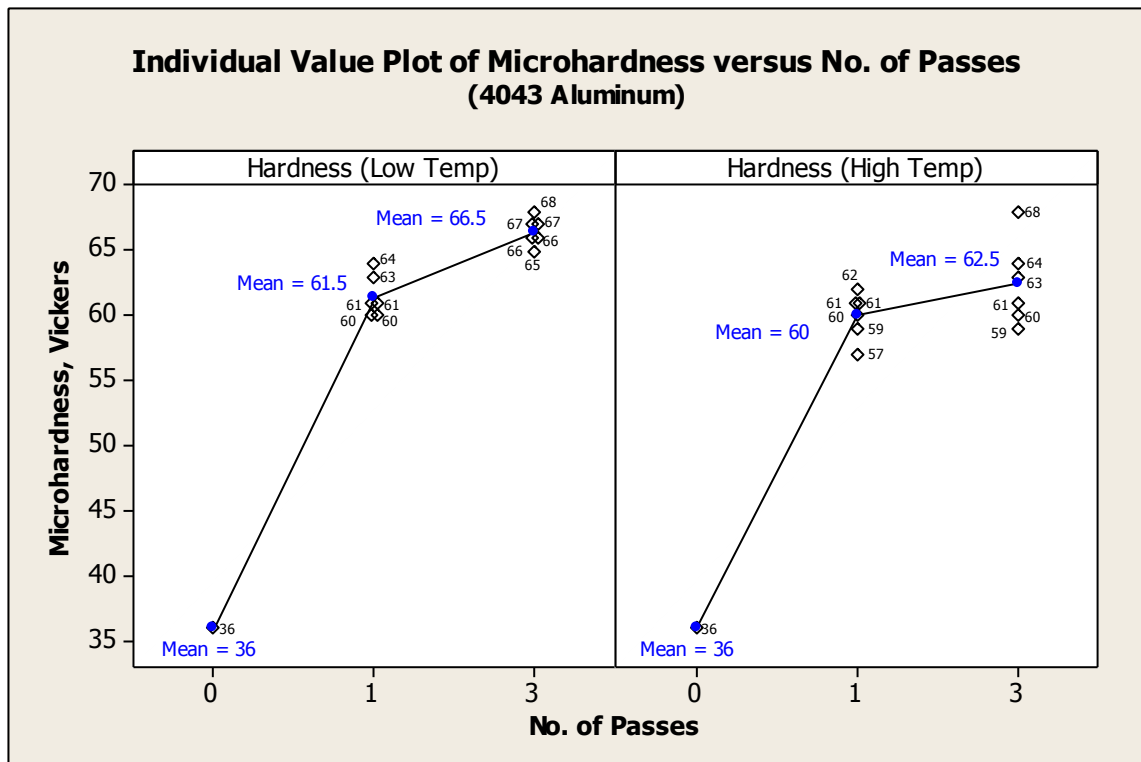


Figure 6.49 Individual value plot of Vickers microhardness versus number of passes at low and high temperatures for 4043 aluminum

As noted previously from the analysis of variance, the output response, microhardness, is primarily dependent on the number of passes through the system. However, processing temperature was also statistically significant at the 90% confidence level. Based on sample means, the microhardness increased 84.72% and 73.61% with three passes through the system at low and high temperatures, respectively. The improvements were more notable when considering individual samples. For example, at low temperature the maximum individual hardness obtained for three passes, Vickers hardness = 68, represented an 88.88% increase. Conversely, the maximum individual sample hardness at high temperature (with the exception of one outlier) was 64 which represented a 77.78% increase.

Assessing the ability of the system to achieve nanocrystalline or ultrafine grains involved the determination of associated changes in mechanical properties involving material yield strength in conjunction with assessing microstructural features involving grain size. The analysis involved the following steps: 1) micro hardness values for individual samples representing both the baseline and maximum hardness were converted from Vickers to Brinell in order to more readily obtain hardness versus yield strength relationships from existing literature, 2) based on data from material properties databases approximate conversions from Brinell hardness values to yield strength for both the baseline and processed samples were made, 3) metallographic analysis of the baseline sample was used to obtain direct measurements of initial grain size, 4) the baseline grain size along with the initial yield strength value were then used in the Hall-Petch relation to assess material constants for subsequent use in determining calculated values for final grain size in the processed sample, and 5) ultimately, the final grain size for the processed

sample exhibiting maximum hardness was obtained from calculated values using the Hall-Petch relation to evaluate system effectiveness in achieving nanocrystalline or ultrafine grains. A summary of the analysis steps is provided in Figure 6.50.

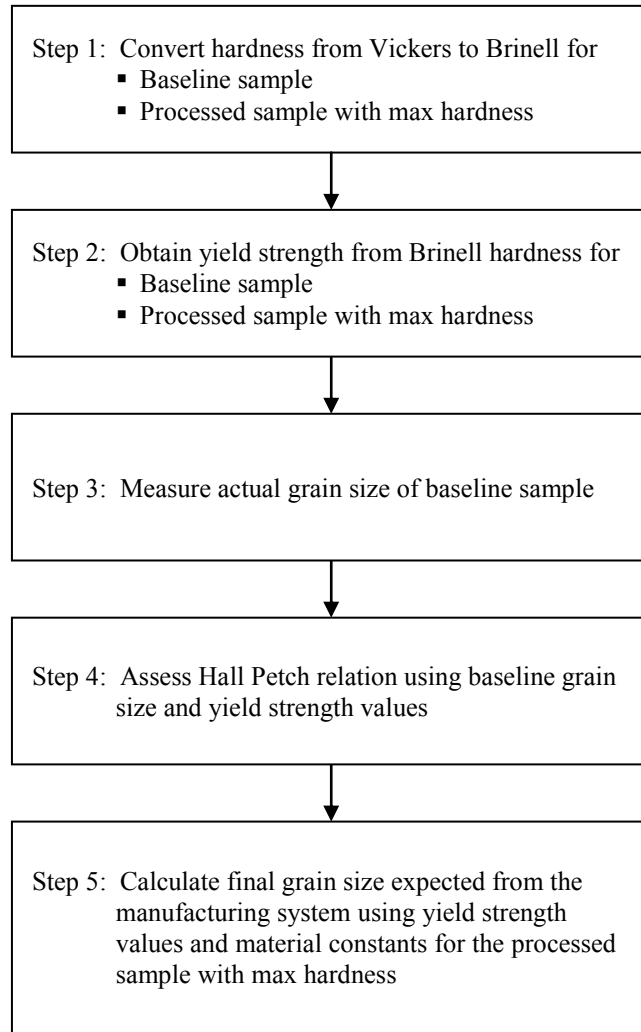


Figure 6.50 Flowchart for the materials development analysis of 4043 aluminum processed by the manufacturing system

As noted previously, the first step in the analysis was conversion of hardness values from Vickers to Brinell using Equation 6.10 as follows (ASTM E140, 1997):

$$\text{HBS } 10/500/15 = 3.7621 + 0.825368 (\text{HV}15) \quad (6.10)$$

where,

HBS 10/500/15 = converted Brinell hardness number based on a 10 mm diameter steel indenter using a 500 kgf load for 15 seconds

HV 15 = Vickers hardness number using a 15 kgf load

Results of the hardness conversions are summarized in Table 6.10. As discussed in ASTM E140, conversion approximations apply. For Equation 6.10, the coefficient of determination is $r^2 = 1$ for hardness values within the test range of 44 to 189 HV. As a result, conversion of the baseline sample reflects an extrapolation at the low range.

Table 6.10 Hardness conversions of 4043 baseline and processed samples from Vickers to Brinell

4043 Aluminum		
Sample ID	Vickers Hardness, HV	Brinell Hardness, HB
Baseline	36	34
Processed (3 passes)	68	60

Once Brinell hardness values were determined, approximate yield strength conversion values were obtained from material databases. Table 6.11 provides values obtained from material databases using O, H14, and H18 temper designations for 4043 aluminum alloy. These tempers reflect a fully annealed soft condition, a strain hardened state at ultimate tensile strengths half way between the O and H18 tempers, and the state with ultimate tensile strengths at approximately 75% cold work, respectively (American Society for Metals, 1979).

Table 6.11 Brinell hardness and yield strength values for O, H14, and H18 tempers for 4043 aluminum

4043 Aluminum		
Temper Designation	Brinell Hardness, HB	Yield Strength, MPa
O	39	70
H14	46	165
H18	77	270

Reference: <http://www.matweb.com/search/DataSheet>

A scatter plot is provided in Figure 6.51 on the following page to obtain approximate values of yield strength for both the baseline sample and processed sample exhibiting maximum hardness. As shown in the figure, a reference line for the processed sample was added at the converted Brinell hardness value of 60 in order to obtain a corresponding yield strength value of 212.4 MPa. This value, which represents a 203.4% increase in yield strength, would provide the critical input into the Hall-Petch Relation, thereby allowing calculation of the final grain size from the redesigned Ix-ECAP process.

Baseline material yield strength was also required in order to perform calculations and provide verification of material constants to be used with the Hall-Petch relation. Since the baseline material used in this research consisted of 4043 aluminum welding rods fully annealed to the O temper during the initial preparation phase of the study, the published database values in Table 6.11 were used. As noted in ASTM E140, the minimum Vickers hardness value for Equation 6.10 conversion was $HV = 44$. Extrapolations beyond the established range for Equation 6.10 were required for the baseline sample with $HV = 36$. Therefore, the value of 70 MPa associated with $HV = 39$ obtained from material databases was used for the yield strength of the baseline 4043

unprocessed material. The relationship for Brinell hardness versus yield strength for 4043 aluminum is shown in Figure 6.51 below. As discussed previously, each of the respective material properties representing hardness and yield strength for both the unprocessed baseline sample as well as the processed sample with maximum hardness is illustrated.

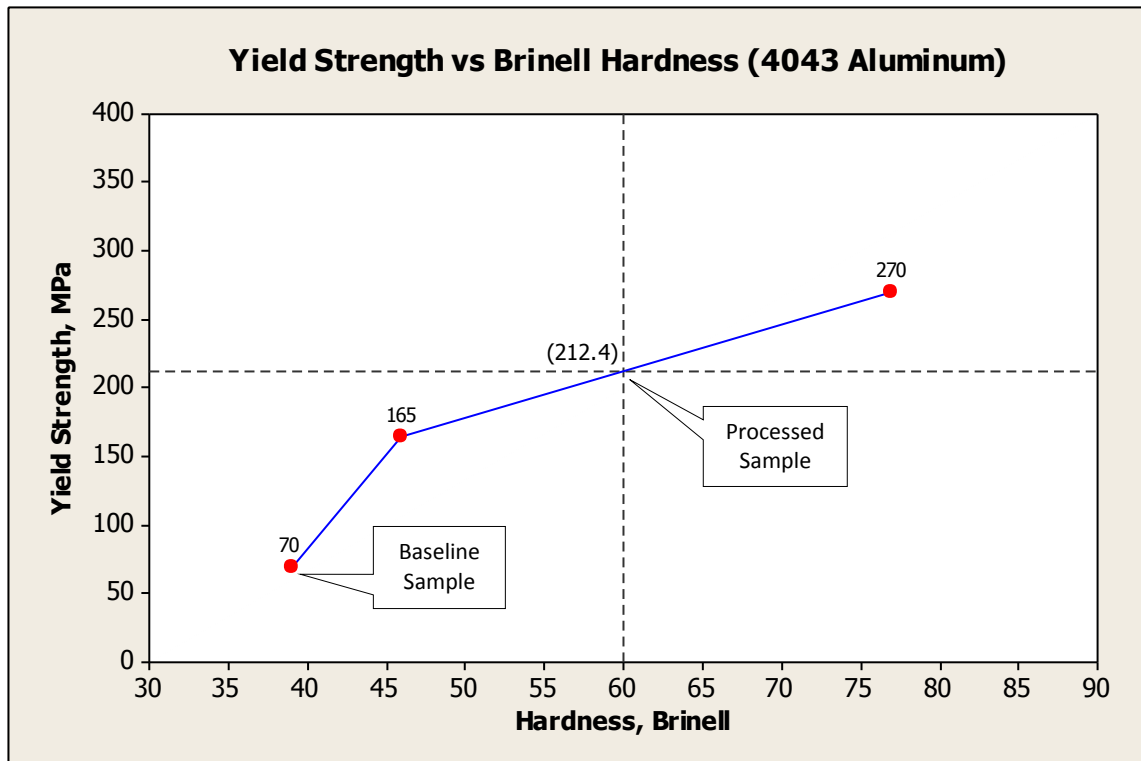


Figure 6.51 Yield strength versus Brinell hardness for 4043 aluminum

Prior to calculation of the final grain size for processed samples, actual measurements of the baseline material grain size were obtained. These values were used in conjunction with yield strength to further assess applicability of the Hall-Petch relation and to assess selected material constants required for computations. To obtain baseline

grain size measurements, transverse and longitudinal rod sections were mounted in epoxy and prepared using standard metallographic techniques for optical microscopy of aluminum per ASTM E3 and E407. Mounted sections with photomicrographs for the unprocessed baseline sample are shown in Figure 6.52 below.

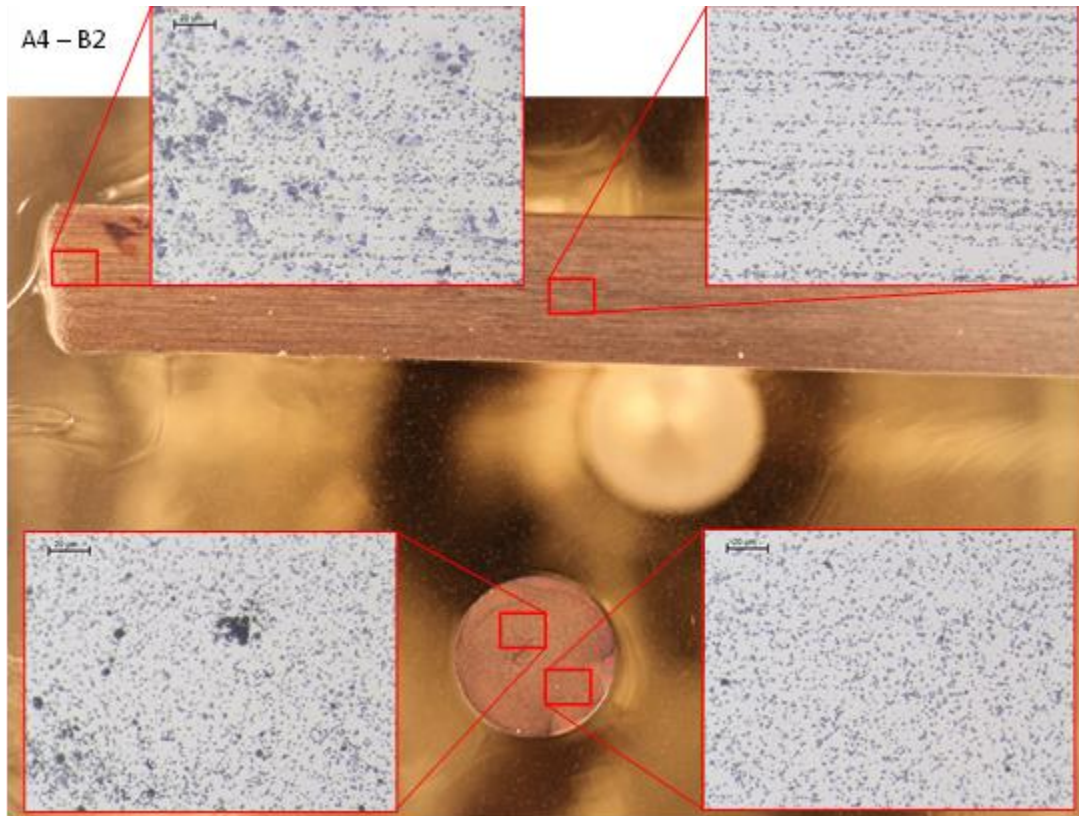


Figure 6.52 Microstructures of un-pressed 4043 aluminum. Sections from longitudinal and transverse directions (sample #A4B2)

A color tinted photomicrograph of the transverse section of baseline sample number A4B2 is shown in Figure 6.53 on the following page. Length and width grain size measurements were obtained on cross diagonals as well as counting grain intercepts

to obtain a mean lineal intercept distance to determine an average grain dimension of 7.0 microns (7,000 nanometers) (ASTM E 112, 1997).

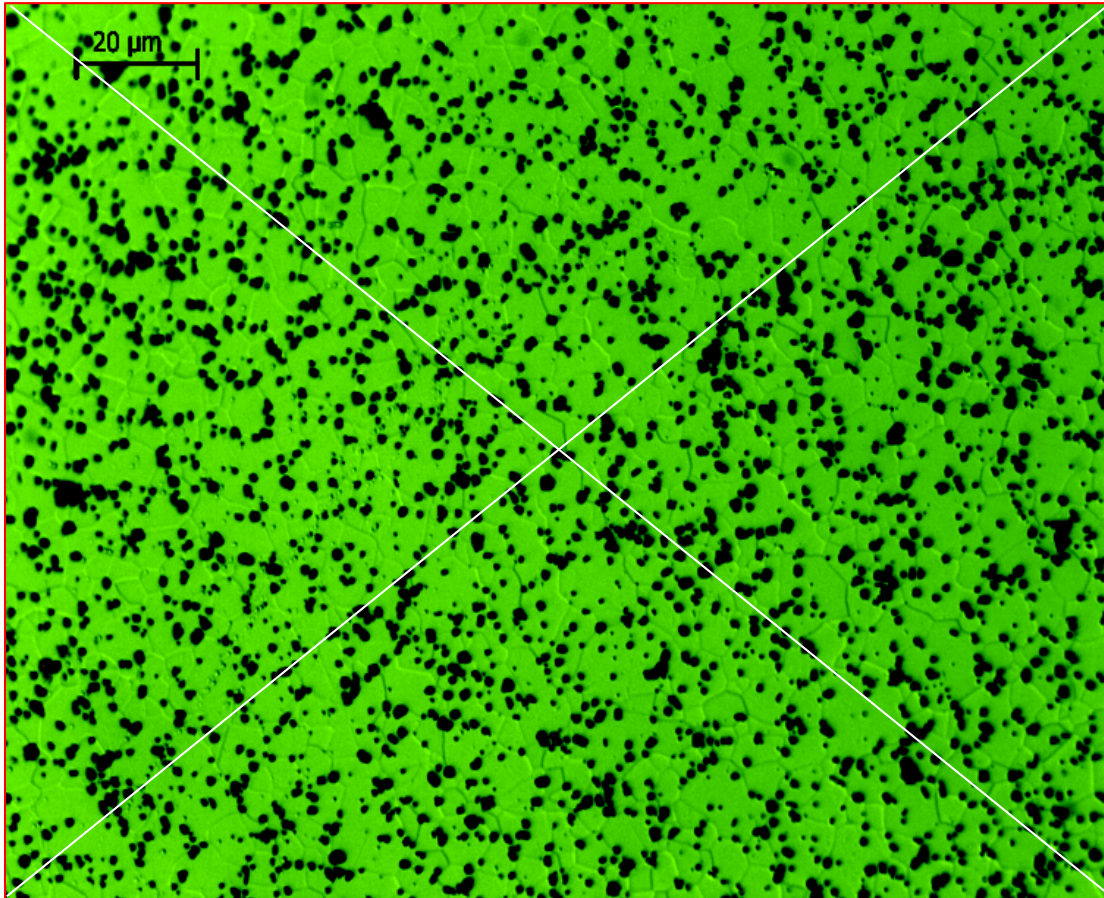


Figure 6.53 Etched microstructure of transverse section of un-pressed baseline 4043 aluminum rod (sample #A4B2) color tinted to reveal grain boundaries

Note: Grain boundaries visible at higher magnifications. Silicon particles indicated by dark areas within the microstructure.

As noted in step four of the analysis, the yield strength and measured grain size for the baseline sample #A4B2 were used to assess selected material constants in the Hall-Petch relationship. Material constants for 4043 aluminum were selected based on compositional ranges of similar aluminum-silicon alloys used in the Hall-Petch relation.

Determined material constants for σ_0 and k_y were successfully used to assess property relationships for a 7.0% silicon aluminum alloy during equal channel angular pressing (Gutierrez-Urrutia et al., 2008). With 4043 alloy containing 6.0% silicon at the upper range of the compositional limit, the values noted below were used in subsequent computations. The Hall-Petch relation is as follows (Valiev and Langdon, 2006):

$$\sigma_y = \sigma_0 + k_y d^{-1/2} \quad (6.11)$$

where,

σ_y is the material's yield strength = 70 MPa

σ_0 is the friction stress = 50 MPa

k_y is a material constant for yielding = 52 MPa $\mu\text{m}^{1/2}$

d is the material's internal grain size = 7 μm = 7,000 nm

Using the actual measured grain size for the baseline material, the Hall-Petch relation provided calculated yield strength of 70 MPa as noted in Table 6.12. This value is compared to the material database value of 70 MPa.

Table 6.12 Hall-Petch calculated yield strength for 4043 baseline aluminum sample

4043 Aluminum		
Sample ID	Yield Strength, MPa (Material Data Base)	Yield Strength, MPa (Hall-Petch)
Baseline	70	70

Even though the calculated and material database yield strength values are equal in this case, dispersion of values should be expected. Specifically, the Hall-Petch relation as noted in Equation 6.12 may include additional terms for aluminum-silicon alloys to

accommodate dislocation hardening within the aluminum matrix, σ_p , and the potential strengthening effect of the dispersed silicon particles, σ_{Orowan} , expressed as follows (Gutierrez-Urrutia et al., 2008):

$$\sigma_y = \sigma_0 + k_y d^{-1/2} + \sigma_p + \sigma_{\text{Orowan}} \quad (6.12)$$

where,

σ_y is the material's yield strength

σ_0 is the friction stress

k_y is a material constant for yielding

d is the material's internal grain size

σ_p is the dislocation hardening term

σ_{Orowan} is the silicon particle strengthening term based on the Orowan model

Each of these additional contributions, σ_p and σ_{Orowan} , vary in magnitude depending on processing parameters which activate each of the respective strengthening mechanisms. Such parameters include pressing or static annealing temperature, effective strain, etc. Specifically, the dislocation hardening term, σ_p , is quantified based on a measure of dislocation densities within the aluminum matrix after severe plastic deformation; whereas, the particle strengthening term, σ_{Orowan} , requires measures of the silicon particle precipitate size and interparticle spacing (Gutierrez-Urrutia et al., 2008). Since scanning and transmission electron microscopy (SEM and TEM) would be required to assess such microstructural features, quantification of each of these respective terms for the 4043 alloy processed through the specific manufacturing system developed in this research represents areas of future research.

The ultimate step in the analysis was a determination of final grain size to evaluate the manufacturing system's effectiveness in achieving nanocrystalline or ultrafine grains. Using Equation 6.13 with material constants noted previously and a yield strength of 212.4 MPa for the sample processed to maximum hardness, Table 6.13 reflects a final grain size of 103 nanometers which represents a 98.5% theoretical reduction in grain diameter.

$$\sigma_y = \sigma_0 + k_y d^{-1/2} \quad (6.13)$$

where,

σ_y is the material's yield strength = 212.4 MPa

σ_0 is referred to as the friction stress = 50 MPa

k_y is a material constant for yielding = 52 MPa $\mu\text{m}^{1/2}$

d is the material's internal grain size to be determined

Table 6.13 Hall-Petch calculated grain size, d , for 4043 processed maximum hardness aluminum sample

4043 Aluminum	
Sample ID	Grain Diameter (d), nm
Processed 3 passes Max Hardness, HV = 68	103

Manufacturing system performance regarding grain size reduction can also be constructed for the mean hardness values reported at the beginning of this section for number of passes through the system versus Vickers hardness at both high and low

temperatures. For example, Table 6.14 shows the results of performing a similar analysis for mean hardness values. A scatter plot of the data is presented in Figure 6.54.

Table 6.14 Hall-Petch grain size determination for 4043 aluminum mean hardness

4043 Aluminum					
Pressing Temperature	Sample ID	Mean Hardness (Vickers)	Mean Hardness (Brinell)	Yield Strength (MPa)	Grain Size (nm)
Low	Baseline	-	39	70	7,000
	1 Pass	61.5	55	196	127
	3 Passes	66.5	59	210	106
High	Baseline	-	39	70	7,000
	1 Pass	60.0	53	189	140
	3 Passes	62.5	55	196	127

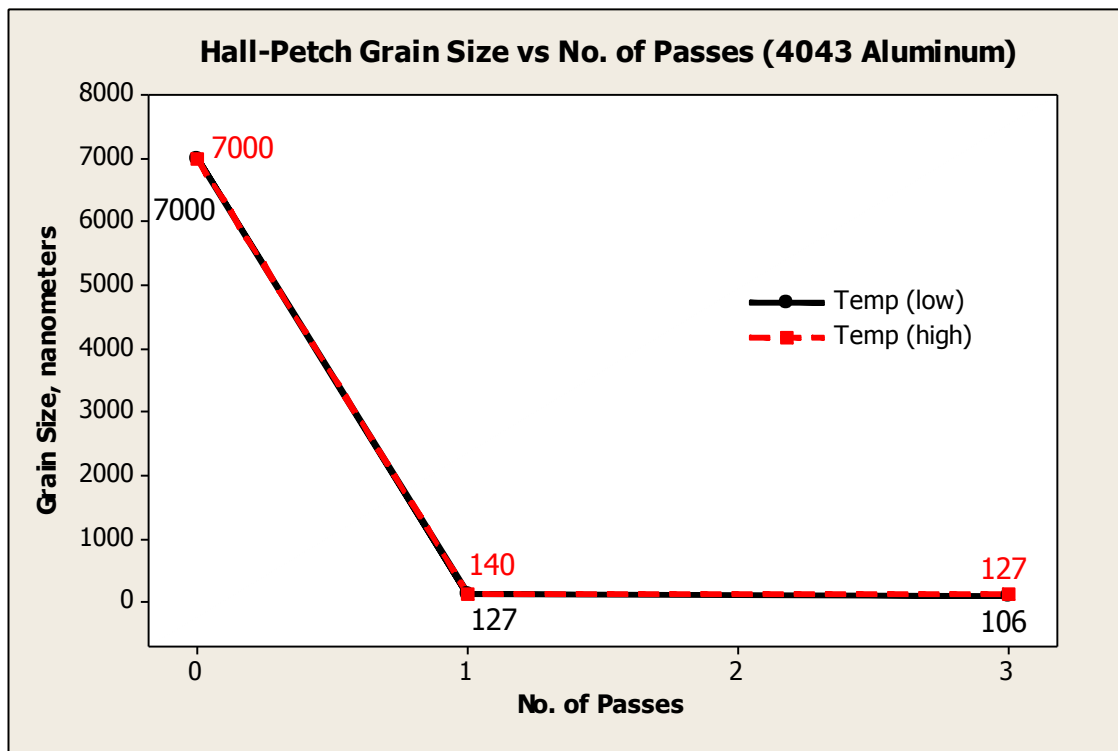


Figure 6.54 Scatter plot of Hall-Petch grain size versus number of passes at low and high temperature for 4043 aluminum based on converted mean hardness

1100 Aluminum

Commercial purity 1100 alloy was used to assess feasibility of the system during initial phases of performance testing. The material was run through the complete two-level five-factor $\frac{1}{4}$ fraction factorial split plot experimental trials employing three replicates over a three-day period to provide system output response regarding work piece surface integrity for cracking and distortion. These trials also provided experience in preparation for running 4043 designed experiments and to make necessary modifications to manufacturing system components. Based on completion of all experimental trials with the 1100 alloy, no surface cracking or distortion was encountered. Materials development regarding microhardness, yield strength conversions, and calculated Hall-Petch grain size were only completed for the 4043 alloy.

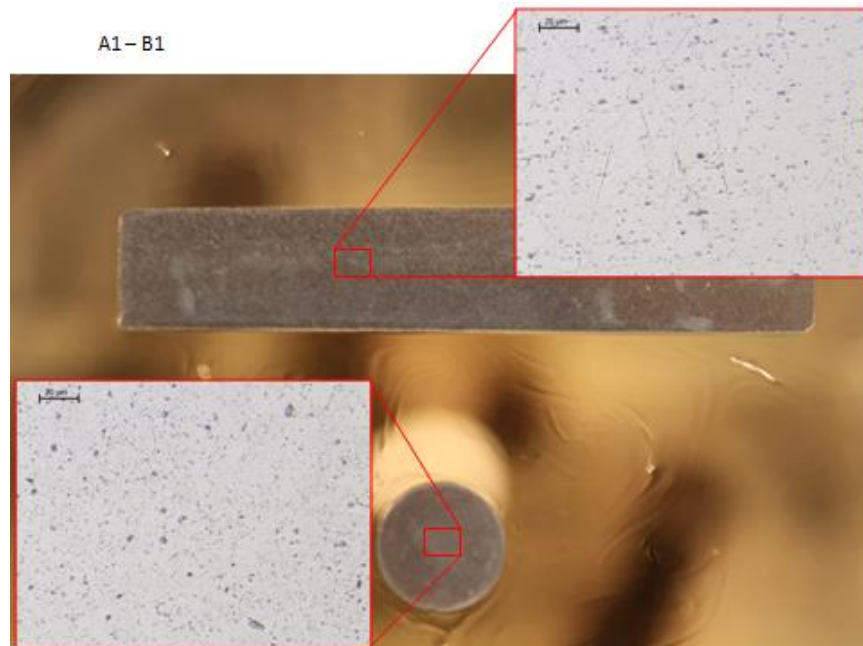


Figure 6.55 Microstructures of un-pressed 1100 aluminum. Sections from longitudinal and transverse directions (sample #A1B1)

CHAPTER VII

SUMMARY AND CONCLUSIONS

Summary

Nanotechnology continues to play a pivotal role in providing solutions to legacy engineering problems, offering improvements to existing engineering systems and designs, enabling breakthroughs in new fields of science and technology, and capturing opportunities in promoting sustainable engineering. This emphasis regarding an opportunity in sustainable engineering whereby waste or spent materials and resources from one industry or process provide essential components or resources to additional industries or processes provided the motivation for this research (Huang, 2010).

With nanotechnology, especially nanomanufacturing methods, being in the infancy stage of life cycle development for many industries, an opportunity existed to bridge the gap between process potential and actual manufacturing output by developing and building a top down nanomanufacturing prototype system referred to as Indexing Equal Channel Angular Pressing. This new process based on an extension of existing ECAP constructs was successful in transforming traditional bulk solid 4043 aluminum welding rods of discrete variable length into materials with theoretically determined ultrafine and nanostructure grains possessing significant actual mechanical property enhancements. An extension of the applicability to sustainable engineering involves the

capture, transformation, and re-use of spent or scrap welding rods in applications such as composite reinforcements, micro-machine elements, and other materials of construction.

The objective of the research was to extend the knowledge of nanotechnology by designing and building the proposed system to process continuous and discrete variable length metallic materials to impose severe plastic deformation resulting in property enhancements from strain hardening and grain refinement. Based on research findings, system redesigns are required for continuous processing; however, variable length discrete processing was very successful. To investigate and quantify processing parameters required for successful system performance, a five-factor $\frac{1}{4}$ fraction factorial split plot designed experiment was completed. Regression analysis was used to develop a predictive model for response variable output, microhardness, based on regressor variables which included pressing temperature, number of passes through the system, pressing speed, vibration, and back pressure. Quantification of material improvements were investigated through microhardness and microstructural analysis.

Conclusions

Manufacturing Process Development

I_x-ECAP represents a potentially viable manufacturing process for continuous length products. Redesigns are required for the reinforcing guides to prevent lateral expansion of the work piece material in the indexing gap during pressing. Sliding mechanisms identified in existing ECAP literature provide numerous options for redesign with closer tolerances and increased coverage of the work piece to accommodate normal pressing stresses.

I_x-ECAP represents a completely viable straightforward manufacturing process for discrete, yet variable, length products. The system is readily interchangeable using various die inserts and plungers to accommodate different cross-section diameter work pieces.

Clamping forces applied by the clamping die from the vertically mounted hydraulic cylinder were sufficient to prevent the work piece from slipping using slow pressing speeds. However, at the fast pressing speeds additional clamping forces were required by adding the clamping chuck at the rear of the clamping die. The combination of clamping chuck and clamping die were sufficient to accommodate all pressings.

Proper lubrication of the work piece and die cavities was critical to successful pressing. The system was unable to press samples completely through the entrance and exit channels of the die using motor oil as a lubricant. An extreme pressure molybdenum disulfide graphite based spray lubricant allowed successful pressing for all process parameter settings.

Back pressure also proved to be a critical parameter from a manufacturing process perspective. Using the spring loaded mechanism applying 48,918 psi of back pressure to the rods either buckled the plunger or allowed slippage of the rod in the clamping die. Employing the static loaded back pressure of 818 psi allowed successful pressing at all parameter settings.

Pressing temperature adjustments were readily accomplished by the heating elements and control unit. No noticeable manufacturing system performance differences were noted between the two pressing temperatures of 70 and 175 °F.

Vibration was, likewise, easily applied using the miniature pneumatic vibrator. No noticeable manufacturing system performance differences were noted between the two vibration settings of 0 and 9,498.6 vibrations per minute.

Even though the system is referred to as equal channel angular pressing with commonly identified equal entrance and exit channel dimensions, lateral expansion upon exit from the process precludes immediate re-insertion into the same pressing die for additional presses. Therefore, reductions to the dimensions of the exit channel are required to accommodate work piece lateral expansion.

The four basic indexing steps of the I_X-ECAP process (clamp, press, unclamp, retract) were very successful and readily processed work pieces through the system.

Statistical Methods

The two-level five-factor ¼ fraction split plot factorial experimental design offered tremendous efficiencies in running the actual experiments as compared to a full factorial design. Process factors included one hard-to-change factor, pressing temperature, thereby requiring the use of the split plot design. Three replicates were run which required the experiments to be conducted over a three-day period resulting in the additional consideration of blocking. All experiments were successfully run according to the design matrix.

Based on the analysis of variance at the 95% confidence level only one factor, number of passes through the system, was statistically significant with a p value of 0.001. Considered at the 90% confidence level two process factors, number of passes through the system and pressing temperature, were statistically significant with p values of 0.001 and 0.086, respectively.

With this research representing the development and build of a totally new prototype manufacturing process, statistical efforts were focused as screening experiments assessing the impact of main factors. Being a Resolution III design, main effects were confounded with two-way interactions as well as higher-order interactions, and additional two-way interactions were confounded with higher-order interactions. Therefore, the analysis focused on understanding the impact of main factors and precluded an assessment of factor interactions.

Multiple linear regression was used to develop a predictive model for the output response variable, microhardness, based on the five regressor variables noted previously. The coefficient of multiple determination, R^2 , at the sub-plot and whole-plot levels were 61.91 and 86.44 percent, respectively.

Materials Development

Materials development considered aluminum alloys 1100 and 4043. The 1100 alloy, however, was strictly used during initial preliminary trials to assess feasibility of the proposed manufacturing process. Aluminum 1100 was run through the complete two-level five-factor $\frac{1}{4}$ fraction factorial split plot experimental matrix employing three replicates over a three-day period. The output response, however, only involved visual inspection for external cracking and distortion. 4043 aluminum alloy was analyzed for materials development and property enhancements based on mechanical property and grain size considerations. Specifically, the discrete variable length rod with maximum microhardness, HV=68, was produced using a low temperature level and three passes through the system. This value represented an 88.88% increase in microhardness which

equated to an increase of 203.4% in yield strength and a 98.5% reduction in theoretical final grain size to 103 nanometers.

Future Research

Manufacturing Methods and Procedures

The primary focus of future research from a manufacturing system design perspective is a consideration of machine elements that promote continuous indexing of work pieces through the die channels. Improved sliding mechanisms or reinforcing guides could be employed to accommodate lateral expansion from normal stresses present in the work piece throughout the indexing gap.

Expected outcomes include a quantifiable difference between baseline 4043 aluminum work pieces and nanocrystalline or ultra-fine grain stock produced by I_x-ECAP. Knowledge of the material performance characteristics, in conjunction with the delineation of the processing variables required to achieve such outcomes, would provide critical knowledge towards the development of manufacturing systems required to reliably and consistently produce nanocrystalline material. Future research should include the design and development of expanded manufacturing systems by employing I_x-ECAP processing in parallel or series manufacturing cells for cost effectiveness and economies of scale.

Further research efforts regarding the development and implementation of product standardization through quality, reliability, and process engineering system elements within an actual nano-manufacturing environment should be considered in future research due to foundational knowledge provided within this study. As a consequence, critical alternatives available to design engineers regarding the selection of more advanced

materials and product forms enabling safer, more efficient, and economical engineering components and systems could be realized.

Statistical Methods

This research considers the effects of five processing factors, each considered at two levels. These factors include the number of times the work piece is passed through the die, pressing temperature, pressing speed, back pressure, and externally applied vibrational energy. To the best of the author's knowledge, this is the first time vibration has been considered in ECAP processing. Different factor levels could be considered or additional factors may become active within the process contributing to response outputs. For example, pressing friction and additional die design factors are of significant importance. The assumption was made within this study to use settings or levels for respective process parameters that have previously been successful in prior research or industrial settings involving equal channel angular pressing. Therefore, a progressive approach to statistical experimentation could be used in future research, whereby fewer predictor variables could be studied employing more than two factor level settings.

Additionally, interaction effects may play a key role in system performance. Therefore, statistical experimentation should be considered in future research to assess the impact of two-factor and, possibly, higher-order interactions.

Materials Development

As noted in Chapter VI, the basic Hall-Petch relation for aluminum-silicon alloys may include additional terms to accommodate dislocation hardening within the aluminum matrix, σ_p , and the potential strengthening effect, σ_{Orowan} , of the dispersed silicon

particles. Without quantifying and including these additional terms, the Hall-Petch theoretically determined reduction in grain size may be overstated. Therefore, future research should include specific quantifications for these additional terms based on actual processing parameters and resultant microstructural analysis involving SEM and TEM studies to measure grain sizes and dislocation densities within the final output materials.

This research represents one very specific dimension of nanotechnology, that being the production of a bulk structural material possessing nanoscale or ultra-fine grain constituents. Even though the manufacturing method devised, Indexing Equal Channel Angular Pressing, is based on the use of existing substantiated technologies, prior research indicates the potential for incremental or quantum leap performance improvements. Especially with the top-down approach whereby a traditional material is transformed into a material containing nanocrystalline or ultra-fine grain constituents, transformation limits exist. For example, a theoretical expression developed by Mohammed (2003) gives the relation for the minimum attainable grain size that could theoretically be possible based on the respective inherent and invariable physical characteristics within a material. In other words, regardless of efforts undertaken, there exists a limit that cannot be exceeded. Substantiation of this claim involving commercially available materials provides an area of future research.

An assumption that restricted the scope of this study involved the intended use of product forms manufactured by the I_x-ECAP process. In extrusion and pressing processes, the concept of mechanical anisotropy oftentimes results in very different mechanical properties based on the direction the bar or product form is stressed. The longitudinal direction may be very strong; whereas, the transverse direction could be very

weak. Within this study, it was assumed the extruded bars were to be subsequently used for wire drawing or shapes that had minimal cross section compared to their respective length. As a result, analyses were performed on transverse sections of the work pieces. Therefore, future studies with the I_X-ECAP process should incorporate three-dimensional analyses to substantiate anisotropic materials performance.

An additional limitation within this research relates to possible limiting capabilities of the ECAP process to produce grain sizes of extreme nanoscale dimensions. For example, grain sizes in the ultra-fine grain region (100 to 1,000 nm) may be the resultant norm of the ECAP process studied. Nanoscale dimensions (≤ 100 nm) may not be attained, especially the lower values such as ten or twenty nanometer grains. Smaller grain sizes, however, should be considered in future investigations in order to extend the current knowledge base regarding the limits of applicability and performance deviations from the Hall-Petch relation. This important theoretical construct provides the generalized relationship between grain size of a material and its respective strength. However, as grains become progressively smaller towards the nanoscale regime, departures from the Hall-Petch relation become evident (Haouaoui, 2005).

REFERENCES

- Andrews, R. and Weisenberger, M. (January 2004). Carbon nanotube polymer composites. *Current Opinion in Solid State and Materials Science*, Volume 8, Issue 1, 31-37.
- American Society for Metals (1979). *Metals Handbook. Volume 2, Properties and Selection: Nonferrous Alloys and Pure Metals, Ninth Edition*. Materials Park, OH: American Society for Metals.
- ASM International (1992). *ASM Handbook. Volume 3, Alloy Phase Diagrams*. Materials Park, OH: ASM International.
- ASTM (1997). ASTM Standard E 3, Standard Practice for Preparation of Metallographic Specimens. In *Annual Book of ASTM Standards. Volume 03.01 Metals – Mechanical Testing; Elevated and Low-Temperature Tests; Metallography*. West Conshohocken, PA: American Society for Testing and Materials.
- ASTM (1997). ASTM Standard E 92, Standard Test Method for Vickers Hardness of Metallic Materials. In *Annual Book of ASTM Standards. Volume 03.01 Metals – Mechanical Testing; Elevated and Low-Temperature Tests; Metallography*. West Conshohocken, PA: American Society for Testing and Materials.
- ASTM (1997). ASTM Standard E 112, Standard Test Method for Determining Average Grain Size. In *Annual Book of ASTM Standards. Volume 03.01 Metals – Mechanical Testing; Elevated and Low-Temperature Tests; Metallography*. West Conshohocken, PA: American Society for Testing and Materials.
- ASTM (1997). ASTM Standard E 140, Standard Hardness Conversion Tables for Metals. In *Annual Book of ASTM Standards. Volume 03.01 Metals – Mechanical Testing; Elevated and Low-Temperature Tests; Metallography*. West Conshohocken, PA: American Society for Testing and Materials.
- ASTM (1997). ASTM Standard E 384, Standard Test Method for Microhardness of Materials. In *Annual Book of ASTM Standards. Volume 03.01 Metals – Mechanical Testing; Elevated and Low-Temperature Tests; Metallography*. West Conshohocken, PA: American Society for Testing and Materials.

ASTM (1997). ASTM Standard E 407, Standard Practice for Microetching Metals and Alloys. In *Annual Book of ASTM Standards. Volume 03.01 Metals – Mechanical Testing; Elevated and Low-Temperature Tests; Metallography*. West Conshohocken, PA: American Society for Testing and Materials.

ASTM Standard A 1038, 2005, Standard Practice for Portable Hardness Testing by the Ultrasonic Contact Impedance Method, ASTM International, West Conshohocken, PA, 2005, DOI: 10.1520/A1038-2005, www.astm.org.

Azushima, A., Kopp, R., Korhonen, A., Yang, D.Y., Micari, F., Lahoti, G.D., Groche, P., Yanagimoto, J., Tsuji, N., Rosochowski, A., and Yanagida, A. (2008). Severe plastic deformation (SPD) processes for metals. *CIRP Annals - Manufacturing Technology*, 57(2), 716-735.

Balasundar, I. and T. Raghu. Effect of friction model in numerical analysis of equal channel angular pressing process. (2010). *Materials & Design*, 31(1), 449-457.

Brochu, M., Zimmerly, T., Ajdelsztajn, L., Lavernia, E., and Kim, G. (2007). Dynamic consolidation of nanostructured Al-7.5% Mg alloy powders. *Materials Science and Engineering A*, 466, 84-89.

Clark, C.T. and Schkade, L.L. (1979). *Statistical Analysis for Administrative Decisions*, 3rd Edition. Cincinnati, Ohio: South-Western Publishing Co.

Colombo G. The effect of equal channel angular extrusion (ECAE) and boron additions on the mechanical properties of a biomedical titanium-niobium-zirconium-tantalum (TNZT) alloy [Ph.D. dissertation]. United States -- Missouri: Washington University in St. Louis; 2010.

Dasgupta, T., Ma, C., Joseph, V., Wang, Z., and Wu, C. (2008). Statistical modeling and analysis for robust synthesis of nanostructures. *Journal of the American Statistical Association*, June, Vol. 103, No. 482, 594-603.

Delta T. Process Heating Application Examples. <http://www.deltat.com/sitemap.html>, 2014.

Dieter, G.F. (1986). *Mechanical Metallurgy*, 3rd Edition. New York, New York: Irwin McGraw-Hill.

Dobatkin, S.V., J. Zrnik, and I. Mamuzic. Nanostructure by severe plastic deformation of steels: Advantages and problems. (2006). *Metalurgija*, 45 (4), 313-321.

Gould, P. (May 2006). Nanomaterials face control measures. *Nanotoday*, Volume 1, No. 2, 34-39.

- Gutierrez-Urrutia, I., Munoz-Morris, M.A., Puertas, I., Luis, C., and Morris, D.G. (2008). Influence of processing temperature and die angle on the grain microstructure produced by severe deformation of an Al-7% Si alloy. *Materials Science and Engineering: A*, 475(1-2), 268-278.
- Haouaoui, Mohammed. An investigation of bulk nanocrystalline copper fabricated via severe plastic deformation and nanoparticle consolidation [Ph.D. dissertation]. United States -- Texas: Texas A&M University; 2005.
- Hatch, J. (1984). *Aluminum: Properties and Physical Metallurgy*. Metals Park, OH: American Society for Metals.
- Heilmann, R., Chen, C., Konkola, P., and Schattenburg, M. (2004). Dimensional metrology for nanometer-scale science and engineering: towards sub-nanometre accurate encoders. *Nanotechnology*, 15, S505-S511.
- Hertzberg, R. (1996). *Deformation and Fracture Mechanics of Engineering Materials*, 4th Edition. New York, New York: John Wiley & Sons, Inc.
- Higdon, A., Stiles, W., Davis, A., and Evces, C. (1976). *Engineering Mechanics: Statics and Dynamics*, 2nd Edition. Englewood Cliffs, New Jersey: Prentice-Hall, Inc.
- Huang, H., Moving to sustainability: Improving material flows in the iron casting industry [Ph.D. dissertation]. United States -- Pennsylvania: The Pennsylvania State University; 2010.
- Jin, Y., Son, II-Heon, and Im, Yong-Taek. Three-dimensional flow characteristics of aluminum alloy in multi-pass equal channel angular pressing. (2010). *Met. Mater. Int.*, 16, 3, 413-420.
- Kang, F, Liu, J., Wang, J., and Zhao, X. Equal channel angular pressing of a Mg-3Al-1Zn alloy with back pressure. (2010). *Advanced Engineering Materials*, 12(8), 730-734.
- Kochmann, W., Riebold, M., Goldberg, R., Hauffe, W., Levin, A.A., Meyer, D.C., Stephan, T., Muller, H., Belger, A., and Paufler, P. (2004). Nanowires in ancient Damascus steel. *Journal of Alloys and Compounds*, 372(1-2), L15-L19.
- Kossiakoff, A. and Sweet, W.N. (2003). *Systems Engineering: Principles and Practice*, 1st Edition. Hoboken, New Jersey: John Wiley & Sons, Inc.
- Kuo, W. (December 2007). IE in the nano era. *Industrial Engineer*, Volume 39, Issue 12, 24.

- Langdon, T.G. The principles of grain refinement in equal-channel angular pressing. (2007). *Materials Science and Engineering: A*, 462(1-2), 3-11.
- Lapovok, R.Y. The role of back-pressure in equal channel angular extrusion. (2005). *Journal of Materials Science*, 40, 341-346.
- Latysh, V., Krallics, G., Alexandrov, I., and Fodor, A. (2006). Application of bulk nanostructured materials in medicine. *Current Applied Physics*, 6(2), 262-266.
- Lau, K. and Hue, D. (August 2002). Effectiveness of using carbon nanotubes as nano-reinforcements for advanced composite structures. *Carbon*, Volume 40, Issue 9, 1605-1606.
- Lowe, T. Metals and alloys nanostructured by severe plastic deformation: Commercialization pathways. (2006). *JOM Journal of the Minerals, Metals and Materials Society*, 58(4), 28-32.
- Mamalis, A. (2005). Advanced manufacturing engineering. *Journal of Materials Processing Technology*, 161, 1-9.
- Miller, Mark Gregory. An analysis of the metallurgical effects of vibratory casting [M.S. thesis]. United States -- Georgia: Georgia Institute of Technology; 1982.
- Mohamed, F. (2003). A dislocation model for the minimum grain size obtainable by milling. *Acta Materialia*, 51, 4107-4119.
- Montgomery, D. and Runger, G. (2007). *Applied Statistics and Probability for Engineers*, 4th Edition. New York: John Wiley & Sons, Inc.
- Mukundan, G. (2004). What is nanotechnology? *Journal of Advanced Manufacturing Systems*, Volume 3, Number 1, 1-3.
- National Nanotechnology Initiative (2008). NNI Strategic Plan 2007. [http://www.nano.gov/NNI Strategic Plan 2007.pdf](http://www.nano.gov/NNI%20Strategic%20Plan%202007.pdf), accessed 9/29/08.
- Osman, T., Rardon, D.E., Friedman, L.B., and Vega, L.F. (2006). The commercialization of nanomaterials: Today and tomorrow. *JOM Journal of the Minerals, Metals and Materials Society*, 58(4), 21-24.
- Pérez, C.J. Luis and Luri, R. (2010). Upper bound analysis of the ECAE process by considering circular cross-section and strain hardening materials. *Journal of Manufacturing Science and Engineering*, 132, 041003-1 – 041003-14.
- Poole, Jr., C.P. and Owens, F.J. (2003). *Introduction to Nanotechnology*, 1st Edition. Hoboken, New Jersey: John Wiley & Sons, Inc.

- Qu, S., Huang, C.X., Gao, Y.L., Yang, G., Wu, S.D., Zang, Q.S., and Zhang, Z.F. (2008). Tensile and compressive properties of AISI 304L stainless steel subjected to equal channel angular pressing. *Materials Science and Engineering: A*, 475(1-2), 207-216.
- Roco, M. (2001). From vision to the implementation of the U.S. National Nanotechnology Initiative. *Journal of Nanoparticle Research*, 3, 5-11.
- Rue, B. (2006). Assuring product quality in the production of nanoelectronic components. *Quality Engineering*, 18, 477-489.
- Salerno, M., Landoni, P., and Verganti, R. (2008). Designing foresight studies for Nanoscience and Nanotechnology (NST) future developments. *Technological Forecasting & Social Change*, 75, 1202-1223.
- Segal, V.M. Equal channel angular extrusion: from macromechanics to structure formation. (1999). *Materials Science and Engineering A*, 271(1-2), 322-333.
- Segal, V.M. Engineering and commercialization of equal channel angular extrusion (ECAE). (2004). *Materials Science and Engineering A*, 386(1-2), 269-276.
- Sengul, H., Theis, T.L., and Ghosh, S. (2008). Toward sustainable nanoproducts. *Journal of Industrial Ecology*, Volume 12, Number 3, 329-358.
- Smith, W.F. (1993). *Foundations of Materials Science and Engineering*, 2nd Edition. New York, New York: Irwin McGraw-Hill.
- Smith, W.F. (1993). *Structure and Properties of Engineering Alloys*, 2nd Edition. New York, New York: Irwin McGraw-Hill.
- Stoica, G. and P. Liaw. Progress in equal-channel angular processing. (2001). *JOM Journal of the Minerals, Metals and Materials Society*, 53(3), 36-40.
- Sun, L., Keshoju, K., and Xing, H. (2008). Magnetic field mediated nanowire alignment in liquids for nanocomposite synthesis. *Nanotechnology*, 19, 1-6.
- Ueno, H., Kakihata, K., Kaneko, Y., Hashimoto, S., and Vinogradov, A. (2011). Nanostructurization assisted by twinning during equal channel angular pressing of metastable 316L stainless steel. *Journal of Materials Science*, 46, 4276-4283.
- Valiev, R.Z. (2001). Developing SPD Methods for Processing Bulk Nanostructured Materials with Enhanced properties. *Metals and Materials International*, 17(5), 413-420.

- Valiev, R.Z., Alexandrov, I.V., Zhu, Y.T., and Lowe, T.C. (2002). Paradox of strength and ductility in metals processed by severe plastic deformation. *Journal of Materials Research*, 17, 5-8.
- Valiev, R.Z. and T.G. Langdon. Principles of equal-channel angular pressing as a processing tool for grain refinement. (2006). *Progress in Materials Science*, 51(7), 881-981.
- Valiev, R., Lowe, T., and Mukherjee, A. (2000). Understanding the unique properties of SPD-induced microstructures. *JOM Journal of the Minerals, Metals and Materials Society*, 52(4), 37-40.
- Witkin, D. and Lavernia, E. (2006). Synthesis and mechanical behavior of nanostructured materials via cryomilling. *Progress in Materials Science*, 51, 1-60.
- Xu, C., Schroeder, S., Berbon, P.B., and Langdon, T. (2010). Principles of ECAP-Conform as a continuous process for achieving grain refinement: Application to an aluminum alloy. *Acta Materialia*, 58(4), 1379-1386.
- Yamashita, A., Yamaguchi, D., Horita, Z., and Langdon, T.G. (2000). Influence of pressing temperature on microstructural development in equal-channel angular pressing. *Materials Science and Engineering A*, 287(1), 100-106.
- Yoon, E.Y., Yoo, J.H., Yoon, S.C., Kim, Y.K., Baik, S.C., and Kim, H.S. (2010). Analyses of route Bc equal channel angular pressing and post-equal channel angular pressing behavior by the finite element method. *Journal of Materials Science*, 45(17), 4682-4688.
- Zhu, Y., Lowe, T., and Langdon, T. (2004). Performance and applications of nanostructured materials produced by severe plastic deformation. *Scripta Materialia*, 51, 825-830.
- Zhu, Y., Valiev, R.Z., Langdon, T.G., Tsuji, N., and Lu, K. (2010). Processing of nanostructured metals and alloys via plastic deformation. *MRS Bulletin*, 35(12), 977-981.

<http://www.aist.go.jp>

<http://www.ame-www.usc.edu>

http://www.engineeringtoolbox.com/hydraulic-force-calculator-d_1369.html

http://www.engineersedge.com/fluid_flow/cylinder_piston_velocity.html

<http://www.inweldcorporation.com/datasheets/Inweld%20LFB%20&%20LFBFC.pdf>

<http://www.ipam.ugatu.ac.ru>

<http://www.materialsminded.wordpress.com>

<http://www.matweb.com/search/DataSheet>

<http://www.nanospd.org>

ADDITIONAL BIBLIOGRAPHY

- Acharya, Navinchandra N. Missing observations and restrictions on randomization in nanomanufacturing experimentation [Ph.D. dissertation]. United States - Pennsylvania: The Pennsylvania State University; 2006.
- ASTM (1997). *Annual Book of ASTM Standards. Volume 01.05 Steel – Bars, Forgings, Bearing, Chain, Springs*. West Conshohocken, PA: American Society for Testing and Materials.
- ASTM (1997). *Annual Book of ASTM Standards. Volume 01.03 Steel – Plate, Sheet, Strip, Wire, Stainless Steel Bar*. West Conshohocken, PA: American Society for Testing and Materials.
- Balasundar, I., Rao, M.S., and Raghu, T.. Equal channel angular pressing die to extrude a variety of materials. (2009). *Materials & Design*, 30(4), 1050-1059.
- Berbon, Patrick B. Processing of ultrafine-grained materials using the equal-channel angular (ECA) pressing technique and optimization of the parameters to obtain superplasticity [Ph.D. dissertation]. United States -- California: University of Southern California; 1998.
- Bergmann, M., Bruzek, B., and Lang, H. Numerical studies of microstructurally optimized bolts with graded grain size. (2010). *Materials & Design*, 31(3), 1438-1443.
- Besley, J., Kramer, V., and Priest, S. (2008). Expert opinion on nanotechnology: risks, benefits, and regulation. *Journal of Nanoparticle Research*, 10, 549-558.
- Bozeman, B., Laredo, P., and Mangematin, V. (2007). Understanding the emergence and deployment of “nano” S&T. *Research Policy*, 36, 807-812.
- Beygelzimer, Y., et al. Planar Twist Extrusion versus Twist Extrusion. (2011). *Journal of Materials Processing Technology*, 211(3), 522-529.
- Box, G.E.P., Hunter, W.G., and Hunter, J. S. (1978). *Statistics for Experimenters: An Introduction to Design, Data Analysis, and Model Building*, 1st Edition. New York: John Wiley & Sons, Inc.

- Carnes T. Ultra fine grained production in RRR niobium for RF cavities by ECAE [M.S. thesis]. United States -- Florida: The Florida State University; 2009.
- Chin, K., Chong, G., Poh, C., Van, L., Sow, C., Lin, J., and Wee, A. (2007). Large-scale synthesis of Fe₃O₄ nanosheets at low temperature. *Journal of Physical Chemistry C*, 111, 9136-9141.
- Choi, J.S., Nawaz, S., Hwang, S.K., Lee, H.C., and Im, Y.T. (2010). Forgeability of ultra-fine grained aluminum alloy for bolt forming. *International Journal of Mechanical Sciences*, 52(10), 1269-1276.
- Dasgupta T. Robust parameter design for automatically controlled systems and nanostructure synthesis [Ph.D. dissertation]. United States -- Georgia: Georgia Institute of Technology; 2007.
- Devore, J.L. (2004). *Probability and Statistics for Engineering and the Sciences*, 6th Edition. Pacific Grove, California: Brooks/Cole.
- Djavanroodi, F. and Ebrahimi, M. Effect of die channel angle, friction and back pressure in the equal channel angular pressing using 3D finite element simulation. (2010). *Materials Science and Engineering: A*, 527(4-5), 1230-1235.
- Djavanroodi, F. and Ebrahimi, M. Effect of die parameters and material properties in ECAP with parallel channels. (2010). *Materials Science and Engineering: A*, 527(29-30), 7593-7599.
- Djavanroodi, F., Ebrahimi, M., Rajabifar, B., and Akramizadeh, S. (2010). Fatigue design factors for ECAPed materials. *Materials Science and Engineering: A*, 2010. 528(2), 745-750.
- Dobrzanski, L. (2006). Significance of materials science for the future development of societies. *Journal of Materials Processing Technology*, 175, 133-148.
- Duan Z. Investigation of the influence of severe plastic deformation on the microstructure and mechanical properties of aluminum-7136 alloy [Ph.D. dissertation]. United States -- California: University of Southern California; 2009.
- Eivani, A.R. and Taheri, A.K. A new method for producing bimetallic rods. (2007). *Materials Letters*, 61(19-20), 4110-4113.
- Fatemi-Varzaneh, S.M. and Zarei-Hanzaki, A. Processing of AZ31 magnesium alloy by a new noble severe plastic deformation method. (2011). *Materials Science and Engineering: A*, 528(3), 1334-1339.

- Ferrasse, S., V.M. Segal, and Alford, F. Effect of additional processing on texture evolution of Al0.5Cu alloy processed by equal channel angular extrusion (ECAE). (2004). *Materials Science and Engineering A*, 372(1-2), 44-55.
- Ferrasse, S., Segal, V.M., Kalidindi, S.R., and Alford, F. (2004). Texture evolution during equal channel angular extrusion: Part I. Effect of route, number of passes and initial texture. *Materials Science and Engineering A*, 368(1-2), 28-40.
- Ferrasse, S., V.M. Segal, and Alford, F. Texture evolution during equal channel angular extrusion (ECAE): Part II. An effect of post-deformation annealing. (2004). *Materials Science and Engineering A*, 372(1-2), 235-244.
- Ferrasse, S. Segal, V.M., Alford, F., Kardokus, J., and Strothers, S. (2008). Scale up and application of equal-channel angular extrusion for the electronics and aerospace industries. *Materials Science and Engineering: A*, 493(1-2), 130-140.
- Figueiredo, R.B., Cetlin, P.R., and Langdon, T.G. The evolution of damage in perfect-plastic and strain hardening materials processed by equal-channel angular pressing. (2009). *Materials Science and Engineering: A*, 518(1-2), 124-131.
- Figueiredo R. Processing of magnesium alloys with ultrafine grain structure [Ph.D. dissertation]. United States -- California: University of Southern California; 2009.
- Gleiter, H. Nanostructured materials: basic concepts and microstructure. (2000). *Acta Materialia*, 48(1), 1-29.
- Gregor, M., Vodarek, V., Dobrzanski, L.A., Kander, L., Kovick, R., and Kuretova, B. The structure of austenitic steel AISI 316 after ECAP and low-cycle fatigue. (2008). *Journal of Achievements in Materials and Manufacturing Engineering*, 28 (2), 151-158.
- Grigorieva, T., Barinova, A., and Lyakhov, N. (2003). Mechanosynthesis of nanocomposites. *Journal of Nanoparticle Research*, 5, 439-453.
- Guo, W.-G. and Nemat-Nasser, S. Flow stress of Nitronic-50 stainless steel over a wide range of strain rates and temperatures. (2006). *Mechanics of Materials*, 38(11), 1090-1103.
- Hamada, A.S. and Karjalainen, L.P. High-cycle fatigue behavior of ultrafine-grained austenitic stainless and TWIP steels. (2010). *Materials Science and Engineering: A*, 527(21-22), 5715-5722.
- Hattar K. Thermal and mechanical stability of nanograined FCC metals [Ph.D. dissertation]. United States -- Illinois: University of Illinois at Urbana-Champaign; 2009.

- Hester, M. (2004). In-situ structural member reinforcement via polymer/carbon nanotube nanocomposite deposition. Final Project – Nanoscale Science and Technology (MATL 7156). Auburn University, Auburn.
- Higdon, A., Ohlsen, E., Stiles, W., Weese, J., and Riley, W. (1976). *Mechanics of Materials*, 3rd Edition. New York, New York: John Wiley & Sons, Inc.
- Horita, Z., Fujinami, T., and Langdon, T.G. The potential for scaling ECAP: effect of sample size on grain refinement and mechanical properties. (2001). *Materials Science and Engineering A*, 318(1-2), 34-41.
- Hosseini Nedjad, S., Meidani, H., and Ahmadabadi, M. Nili. Effect of equal channel angular pressing on the microstructure of a semisolid aluminum alloy. (2008). *Materials Science and Engineering: A*, 475(1-2), 224-228.
- Hu, H.-j., Zhang, D.-f., and Pan, F. Die structure optimization of equal channel angular extrusion for AZ31 magnesium alloy based on finite element method. (2010). *Transactions of Nonferrous Metals Society of China*, 20(2), 259-266.
- Huang, C., Murthy, T.G., Shankar, M.R., M'Saoubi, R., and Chandrasekar, S. (2008). Temperature rise in severe plastic deformation of titanium at small strain-rates. *Scripta Materialia*, 58(8), 663-666.
- Huang, C.X., Yang, G., Wang, C., Zhang, Z.F., and Wu, S.D. (2011). Mechanical behaviors of ultrafine-grained 301 austenitic stainless steel produced by equal-channel angular pressing. *Metallurgical and Materials Transactions A*, 42A(July), 2061-2071.
- Im, J., Grain refinement and texture development of cast bismuth-antimony alloy via severe plastic deformation [Ph.D. dissertation]. United States -- Texas: Texas A&M University; 2007.
- Jeswiet, J., Geiger, M., Engel, U., Kleiner, M., Schikorra, M., Duflou, J., Neugebauer, R., Bariani, P., and Bruschi, S. (2008). Metal forming progress since 2000. *CIRP Journal of Manufacturing Science and Technology*, 1(1), 2-17.
- Jiang, H., Fan, Z., and Xie, C. Finite element analysis of temperature rise in CP-Ti during equal channel angular extrusion. (2009). *Materials Science and Engineering: A*, 513-514, 109-114.
- Jones, B. and Nachtsheim, C. Split-Plot Designs: What, Why, and How. (2009). *Journal of Quality Technology*, 41(4), 340-361.

- Jung, Byungin. Microstructural refinement of alpha-brass and titanium-aluminum-vanadium alloys by equal channel angular extrusion processing: Modeling and experimental validation [D.Sc. dissertation]. United States -- Missouri: Washington University; 2006.
- Kaculi, Xhemal. Integration of mechanical alloying and equal channel angular extrusion for production of nanostructured materials [D.E. dissertation]. United States -- Texas: Lamar University - Beaumont; 2002.
- Kamachi, M., Furukawa, M., Horita, Z., and Langdon, T.G. (2003). Equal-channel angular pressing using plate samples. *Materials Science and Engineering A*, 361(1-2), 258-266.
- Kaushik A. Analysis of powder compaction process through Equal Channel Angular Extrusion [Ph.D. dissertation]. United States -- Texas: Texas A&M University; 2007.
- Khoddam, S., Farhoumand, A., and Hodgson, P.D. Axi-symmetric forward spiral extrusion, a kinematic and experimental study. (2011). *Materials Science and Engineering: A*, 528(3), 1023-1029.
- Kim, E., Oh, S., Lee, Y., and Na, K. (2008). Backward can extrusion of ultra-fine-grained bulk Al-Mg alloy fabricated by cryomilling and hydrostatic extrusion. *Journal of Materials Processing Technology*, 201, 163-167.
- Kim, -H. Choi, M., Chung, C., and Shin, D. (2003). Fatigue properties of ultrafine grained low carbon steel produced by equal channel angular pressing. *Materials Science and Engineering A*, 340(1-2), 243-250.
- Kim, H.S. Analysis of thermal behavior during equal channel multi-angular pressing by the 3-dimensional finite volume method.(2009). *Materials Science and Engineering: A*, 503(1-2), 130-136.
- Kim, N. and Sankar, B. (2009). *Introduction to Finite Element Analysis and Design*, 1st Edition. New York, New York: John Wiley & Sons, Inc.
- Kim, W.J. and Sa, Y.K. Micro-extrusion of ECAP processed magnesium alloy for production of high strength magnesium micro-gears. (2006). *Scripta Materialia*, 54(7), 1391-1395.
- Kocich, R., Greger, M., Kursá, M., Szurman, I., and Machachova, A. (2010). Twist channel angular pressing (TCAP) as a method for increasing the efficiency of SPD. *Materials Science and Engineering: A*, 527(23), 6386-6392.

- Kostoff, R., Koytcheff, R., and Lau, C. (2007). Global nanotechnology research literature overview. *Technological Forecasting & Social Change*, 74, 1733-1747.
- Kostoff, R., Koytcheff, R., and Lau, C. (2007). Global nanotechnology research literature overview. *Journal of Nanoparticle Research*, 9, 701-724.
- Kostoff, R., Murday, J., Lau, C., and Tolles, W. (2006). The seminal literature of nanotechnology research. *Journal of Nanoparticle Research*, 8, 193-213.
- Kowalski, S., Borrer, C., and Montgomery, D. A Modified Path of Steepest Ascent for Split-Plot Experiments. (2005). *Journal of Quality Technology*, 37(1), 75-83.
- Kowalski, S. and Potcner, K. How to recognize a split-plot experiment. (2003). *Quality Progress*, November, 60-66.
- Kubota, M., Wu, X., Xu, W., and Xia, K. (2010). Mechanical properties of bulk aluminium consolidated from mechanically milled particles by back pressure equal channel angular pressing. *Materials Science and Engineering: A*, 527(24-25), 6533-6536.
- Kwan, C.-T. and Hsu, Y.-C. An analysis of pseudo equal-cross-section lateral extrusion through a curved channel. (2002). *Journal of Materials Processing Technology*, 122(2-3), 260-265.
- Labadie, J., Fontaine, D., and Ko, S. (February 1992). Multiobjective optimization of reservoir system operation. *Water Resources Bulletin*, American Water Resources Association, Volume 28, Number 1 Paper No. 91016, 111-112.
- Lane, N. (2001). The grand challenges of nanotechnology. *Journal of Nanoparticle Research*, 3, 95-103.
- Lavernia, E., Han, B., and Schoenung, J. (2008). Cryomilled nanostructured materials: Processing and properties. *Materials Science and Engineering A*, 493, 207-214.
- Lee, J.-H., Son, I.-H., Im, Y.-T., Chon, S.H., and Park, J.K. (2007). Design guideline of multi-pass equal channel angular extrusion for uniform strain distribution. *Journal of Materials Processing Technology*, 191(1-3), 39-43.
- Lee, Sangmok. Mechanical processing of two-phase alloys by severe plastic deformation [Ph.D. dissertation]. United States -- California: University of Southern California; 2001
- Lee, Z., Witkin, D., Radmilovic, V., Lavernia, E., and Nutt, S. (2005). Bimodal microstructure and deformation of cryomilled bulk nanocrystalline Al-7.5% Mg alloy. *Materials Science and Engineering A*, 410-411, 462-467.

- Li, G. Microstructure and mechanical properties of SPD processed nanocrystalline tantalum [Ph.D. dissertation]. United States -- North Carolina: The University of North Carolina at Charlotte; 2008.
- Li, H., S. Li, and Zhang, D. On the selection of outlet channel length and billet length in equal channel angular extrusion. (2010). *Computational Materials Science*, 49(2), 293-298.
- Li, X., Chen, H., Dang, Y., Lin, Y., Larson, C., and Roco, M. (2008). *Journal of Nanoparticle Research*, 10, 1007-11051.
- Lo, K.H., C.H. Shek, and Lai, J.K.L. . Recent developments in stainless steels. (2009). *Materials Science and Engineering: R: Reports*, 65(4-6), 39-104.
- Luri, R., Perez, C.J., Salcedo, I., Puertas, I., Leon, J., Perez, I., and Fuertes, J.P. (2011). Evolution of damage in AA-5083 processed by equal channel angular extrusion using different die geometries. *Journal of Materials Processing Technology*, 211(1), 48-56.
- Lynch, Donald Patrick. The application of response surface methodologies to microjoining of magnet wire without prior removal of insulation [Ph.D. dissertation]. United States -- Colorado: Colorado State University; 2001.
- Mamalis, A. (2007). Advanced manufacturing engineering. *Journal of Materials Processing Technology*, 181, 52-58.
- Mathieu, J.P., Suwas, S., Eberhardt, A., Toth, L.S., and Moll, P. (2006). A new design for equal channel angular extrusion. *Journal of Materials Processing Technology*, 173(1), 29-33.
- Mishin, O.V., Bowen, J.R., and Lathabai, S. Quantification of microstructure refinement in aluminium deformed by equal channel angular extrusion: Route A vs. route Bc in a 90° die. (2010). *Scripta Materialia*, 63(1), 20-23.
- Mishra A. Microstructural evolution in ultra-fine grained copper processed by severe plastic deformation [Ph.D. dissertation]. United States -- California: University of California, San Diego; 2007.
- Montgomery, D. (2001). *Design and Analysis of Experiments*, 5th Edition. New York: John Wiley & Sons, Inc.
- Moscoco, W. Severe plastic deformation and nanostructured materials by large strain extrusion machining [Ph.D. dissertation]. United States -- Indiana: Purdue University; 2008.

- Nagasekhar, A.V., Chakkingal, U., and Venugopal, P. Equal Channel Angular Extrusion of Tubular Aluminum Alloy Specimens--Analysis of Extrusion Pressures and Mechanical Properties. (2006). *Journal of Manufacturing Processes*, 8(2), 112-120.
- Nagasekhar, A.V., Chakkingal, U., and Venugopal, P. Candidature of equal channel angular pressing for processing of tubular commercial purity-titanium. (2006). *Journal of Materials Processing Technology*, 173(1), 53-60.
- Nakashima, K., Horita, Z., Nemoto, M., and Langdon, T.G. (2000). Development of a multi-pass facility for equal-channel angular pressing to high total strains. *Materials Science and Engineering A*, 281(1-2), 82-87.
- Narooei, K. and Taheri, A.K. A new model for prediction the strain field and extrusion pressure in ECAE process of circular cross section. (2010). *Applied Mathematical Modeling*, 34(7), 1901-1917.
- Nishida, Y., Ando, T., Nagase, M., Lim, S., Shigematsu, I., and Watazu, A. (2002). Billet temperature rise during equal-channel angular pressing. *Scripta Materialia*, 46(3), 211-216.
- Niu, H., Yang, Q., Tang, K., and Xie, Y. (2006). Large-scale synthesis of single-crystalline MgO with bone-like nanostructures. *Journal of Nanoparticle Research*, 8, 881-888.
- Orlov, D., Raab, G., Lamark, T.T., Popov, M., and Estrin, Y. (2011). Improvement of mechanical properties of magnesium alloy ZK60 by integrated extrusion and equal channel angular pressing. *Acta Materialia*, 59(1), 375-385.
- Ozdemir, Gultekin. Quality loss functions and signal-to-noise ratios for a trivariate response [Ph.D. dissertation]. United States -- Alabama: Auburn University; 2002.
- Pardis, N. and Ebrahimi, R. Different processing routes for deformation via simple shear extrusion (SSE). (2010). *Materials Science and Engineering: A*, 527(23), 6153-6156.
- Patil A. Mechanical and tribological properties of ultrafine grained zinc-copper-aluminum alloy obtained by Equal Channel Angular Extrusion [Ph.D. dissertation]. United States -- Michigan: Michigan Technological University; 2008.
- Paul, D. and Robeson, L. (2008). Polymer nanotechnology: Nanocomposites. *Polymer*, 49, 3187-3204.

- Paydar, M.H., Reilhanian, M., Ebrahimi, R., Dean, T.A., and Moshdsar, M.M. (2008). An upper-bound approach for equal channel angular extrusion with circular cross-section. *Journal of Materials Processing Technology*, 198(1-3), 48-53.
- Pei, Q.X., Hu, B.H., Lu, C., and Wang, Y.Y. (2003). A finite element study of the temperature rise during equal channel angular pressing. *Scripta Materialia*, 2003. 49(4), 303-308.
- Pérez, C.J. Luis. On the correct selection of the channel die in ECAP processes. (2004). *Scripta Materialia*, 50(3), 387-393.
- Pérez, C.J. Luis and Luri, R. (2008). Study of the ECAE process by the upper bound method considering the correct die design. *Mechanics of Materials*, 40(8), 617-628.
- Perig, A.V., Laptev, A.M., Golodenko, N.N., Erfort, Y.A., and Bondarenko, E.A. (2010). Equal channel angular extrusion of soft solids. *Materials Science and Engineering: A*, 527(16-17), 3769-3776.
- Pond, B. Analysis of strain distribution in equal channel angular extrusion by finite element method simulation and experimental validation [D.Sc. dissertation]. United States -- Missouri: Washington University in St. Louis; 2006.
- Potcner, K., and Kowalski, S. (2004). How to analyze a split-plot experiment. *Quality Progress*, December, 67-74.
- Quate, C. (1999). Nanoscience and engineering: The next five years. *Journal of Nanoparticle Research*, 1, 131-136.
- Rashba, E. and Gamota, D. (2003). Anticipatory standards and the commercialization of nanotechnology. *Journal of Nanoparticle Research*, 5, 401-407.
- Reihanian, M., Ebrahimi, R., and Moshksar, M.M. Upper-bound analysis of equal channel angular extrusion using linear and rotational velocity fields. (2009). *Materials & Design*, 30(1), 28-34.
- Roco, M. and Bainbridge, W. (2005). Societal implications of nanoscience and nanotechnology: Maximizing human benefit. *Journal of Nanoparticle Research*, 7, 1-13.
- Roco, M. (2003). Broader issues of nanotechnology. *Journal of Nanoparticle Research*, 5, 181-189.

- Roco, M. (2002). Coherence and divergence of megatrends in science and engineering. *Journal of Nanoparticle Research*, 4, 9-19.
- Romig Jr., A., Baker, A., Johannes, J., Zipperian, T., Eijkel, K., Kirchhoff, B., Mani, H., Rao, C., and Walsh, S. (2007). An introduction to nanotechnology policy: Opportunities and constraints for emerging and established economies. *Technological Forecasting & Social Change*, 74, 1634-1642.
- Scarlett, B. (2000). Standardization of nanoparticle measurements. *Journal of Nanoparticle Research*, 2, 1-2.
- Segal, V.M. Materials processing by simple shear. (1995). *Materials Science and Engineering A*, 197(2), 157-164.
- Segal, V.M. Severe plastic deformation: simple shear versus pure shear. (2002). *Materials Science and Engineering A*, 338(1-2), 331-344.
- Segal, V.M. Slip line solutions, deformation mode and loading history during equal channel angular extrusion. (2003). *Materials Science and Engineering A*, 345(1-2), 36-46.
- Segal, V.M. Deformation mode and plastic flow in ultra fine grained metals. (2005). *Materials Science and Engineering: A*, 406(1-2), 205-216.
- Segal, V.M. Equal channel angular extrusion of flat products. (2008). *Materials Science and Engineering: A*, 476(1-2), 178-185.
- Segal, V.M. Mechanics of continuous equal-channel angular extrusion. (2010). *Journal of Materials Processing Technology*, 210(3), 542-549.
- Segal, V.M., Ferrasse, S., and Alford, F. Tensile testing of ultra fine grained metals. (2006). *Materials Science and Engineering: A*, 422(1-2), 321-326.
- Segal, V.M., Hartwig, K.T., and Goforth, R.E. In situ composites processed by simple shear. (1997). *Materials Science and Engineering A*, 224(1-2), 107-115.
- Seiner, H., Bodnarova, L., Sedlak, P., Janecek, M., Srba, O., Kral, R., and Landa, M. (2010). Application of ultrasonic methods to determine elastic anisotropy of polycrystalline copper processed by equal-channel angular pressing. *Acta Materialia*, 58(1), 235-247.
- Semiatin, S.L., Berbon, P.B., and Langdon, T.G. Deformation heating and its effect on grain size evolution during equal channel angular extrusion. (2001). *Scripta Materialia*, 44(1), 135-140.

- Semiatin, S.L., DeLo, D.P., and Shell, E.B. The effect of material properties and tooling design on deformation and fracture during equal channel angular extrusion. (2000). *Acta Materialia*, 48(8), 1841-1851.
- Shin, D.H., Pak, J., Kim, Y.K., Park, K., and Kim, Y. (2002). Effect of pressing temperature on microstructure and tensile behavior of low carbon steels processed by equal channel angular pressing. *Materials Science and Engineering A*, 325(1-2), 31-37.
- Stoica G. Equal-channel-angular processing (ECAP) of materials: Experiment and theory [Ph.D. dissertation]. United States -- Tennessee: The University of Tennessee; 2007.
- Stolyarov, V.V., Zeipper, L., Mingler, B., and Zehetbauer, M. (2008). Influence of post-deformation on CP-Ti processed by equal channel angular pressing. *Materials Science and Engineering: A*, 476(1-2), 98-105.
- Stolyarov, V.V., Zhu, Y.T., Lowe, T.C., and Valiev, R.Z (2001). Microstructure and properties of pure Ti processed by ECAP and cold extrusion. *Materials Science and Engineering: A*, 303(1-2), 82-89.
- Stoneham, A. (2003). The challenges of nanostructures for theory. *Materials Science and Engineering C*, 23, 235-241.
- Tham, Y.W., Fu, M.W., Hng, H.H., Yong, M.S., and Lim, K.B. (2007). Bulk nanostructured processing of aluminum alloy. *Journal of Materials Processing Technology*, 192-193, 575-581.
- Venkateswarlu, K., Ghosh, M., Ray, A.K., Xu, C., and Langdon, T.G. (2008). On the feasibility of using a continuous processing technique incorporating a limited strain imposed by ECAP. *Materials Science and Engineering: A*, 485(1-2), 476-480.
- Vinogradov, A.Y., Stolyarov, V.V., Hashimoto, S., and Valiez, R.Z. (2001). Cyclic behavior of ultrafine-grain titanium produced by severe plastic deformation. *Materials Science and Engineering A*, 318(1-2), 163-173.
- Vollertsen, F., Biermann, D., Hansen, H.N., Jawahir, I.S., and Kuzman, K. (2009). Size effects in manufacturing of metallic components. *CIRP Annals - Manufacturing Technology*, 58(2), 566-587.
- Wang, S., Liang, W., Wang, Y., Bian, L., and Chen, K. (2009). A modified die for equal channel angular pressing. *Journal of Materials Processing Technology*, 209(7), 3182-3186.

- Wei, W., Zhang, W., Wei, K.X., Zhong, Y., Cheng, G., and Hu, J. (2009). Finite element analysis of deformation behavior in continuous ECAP process. *Materials Science and Engineering: A*, 516(1-2), 111-118.
- Wei, Z., Laizhu, J., Ning, L., Yuhu, W. (2008). Improvement of shape memory effect in an Fe-Mn-Si-Cr-Ni alloy fabricated by equal channel angular pressing. *Journal of Materials Processing Technology*, 208(1-3), 130-134.
- Xi, Xiaomei. Low-cost fabrication of ceramic-reinforced metal-matrix composites through rapid pressureless infiltration in air [Ph.D. dissertation]. United States -- Alabama: Auburn University; 1996.
- Xu, S., Zhao, G., Ma, X., and Ren, G. (2007). Finite element analysis and optimization of equal channel angular pressing for producing ultra-fine grained materials. *Journal of Materials Processing Technology*, 184(1-3), 209-216.
- Yamaguchi, D., Horita, Z., Nemoto, M., and Langdon, T.G. (1999). Significance of adiabatic heating in equal-channel angular pressing. *Scripta Materialia*, 41(8), 791-796.
- Yanagida, A., Joko, K., and Azushima, A. Formability of steels subjected to cold ECAE process. (2008). *Journal of Materials Processing Technology*, 201(1-3), 390-394.
- Yang, F., Saran, A., and Okazaki, K. Finite element simulation of equal channel angular extrusion. (2005). *Journal of Materials Processing Technology*, 166(1), 71-78.
- Yapici G. Investigation and modeling of processing-microstructure-property relations in ultra-fine grained hexagonal close packed materials under strain path changes [Ph.D. dissertation]. United States -- Texas: Texas A&M University; 2007.
- Yoon, S.C., Quang, P., Hong, S.I., and Kim, H.S. (2007). Die design for homogeneous plastic deformation during equal channel angular pressing. *Journal of Materials Processing Technology*, 187-188, 46-50.
- Yun, Su-Jin. An analysis by the finite element method of material deformation in equal channel angular extrusion [Ph.D. dissertation]. United States -- Texas: Texas A&M University; 1996.
- Zebardast, M. and Taheri, A.K. The cold welding of copper to aluminum using equal channel angular extrusion (ECAE) process. (2011). *Journal of Materials Processing Technology*, 211(6), 1034-1043.
- Zhang, X., Cheng, S., and Fang. (2004). Manufacturing at nanoscale: Top-down, bottom-up and system engineering. *Journal of Nanoparticle Research*, 6, 125-130.

Zhao, Q., Boxman, A., and Chowdhry, U. (2003). Nanotechnology in the chemical industry – opportunities and challenges. *Journal of Nanoparticle Research*, 5, 567-572.

Zhao, Z., Chen, Q., Chao, H., Hu, C., and Huang, S. (2011). Influence of equal channel angular extrusion processing parameters on the microstructure and mechanical properties of Mg-Al-Y-Zn alloy. *Materials & Design*, 32(2), 575-583.

Zhu, Y.T. and Lowe, T.C. Observations and issues on mechanisms of grain refinement during ECAP process. (2000). *Materials Science and Engineering A*, 291(1-2), 46-53.

APPENDIX A
EXPERIMENTAL DATA

4043 Aluminum Alloy - Research Data Sheets

Results from the 4043 aluminum alloy split plot $\frac{1}{4}$ fraction factorial experiments are illustrated in the following photographs. Photographs depict actual pressed rods.

Table A.1 Research data sheet – 4043 – sample 1

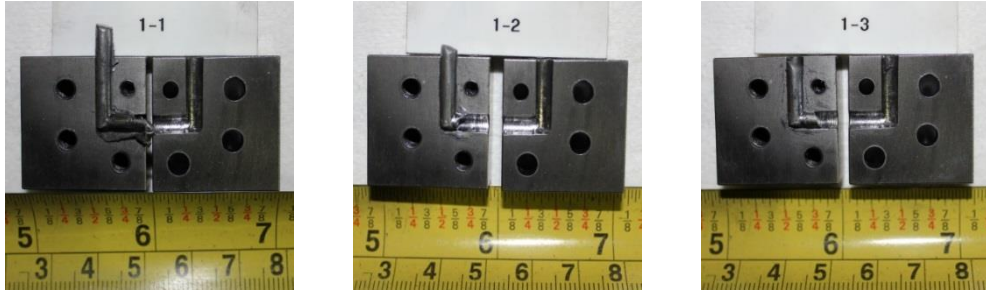
RESEARCH DATA SHEET						
Date	4-12-14				Process Type	<input checked="" type="checkbox"/> Discrete <input type="checkbox"/> Continuous
Block	1				Sample Type	<input checked="" type="checkbox"/> DOE <input type="checkbox"/> Test Run
Whole Plot	1				Base Alloy	4043 Aluminum
Sample ID (Run Order)	1				Hardness	36 HV ₁₀₀
					Grain Size	N/A
EXPERIMENTAL FACTORS	Level	Pass #1	Pass #2	Pass #3	Average	NOTES
(A) Temperature (°F)	Low	71	71	71	71	
(B) Number of Passes	High	1	1	1	3	Total no. of passes
(C) Back Pressure (lbs.)	High	10	10	10	10.0	
(D) Speed: (in./minute)	Low	0.9	0.8	0.7	0.8	
(E) Vibration (cpm)	Low	0	0	0	0.0	
PROCESS VARIABLES						NOTES
Indexing Distance (in.)	N/A	0.8125	0.6875	0.5000	N/A	
Indexing Time (seconds)	N/A	51.6	49.0	43.5	N/A	
Die Insert No.	N/A	1	1	1	N/A	
Test Rod Diameter (in.)	N/A	0.125	0.125	0.125	N/A	
Test Rod Length (in.)	N/A	0.875	0.875	0.875	N/A	Original rod length
Lubricant	N/A	Yes	Yes	Yes	N/A	EP Dri Slide
Pressing Die	N/A	Yes	Yes	Yes	N/A	
Clamping Die	N/A	Yes	Yes	Yes	N/A	
Clamping Chuck	N/A	Yes	Yes	Yes	N/A	
Push Rod	N/A	Yes	Yes	Yes	N/A	0.875 in. diam., 10 in. length
Pressing Route	N/A	Bc	Bc	Bc	N/A	
RESULTS						NOTES
Hardness (HV ₁₀₀)	N/A	N/A	N/A	66	N/A	
Grain Size	N/A	N/A	N/A	N/A	N/A	
Visual Inspection	N/A	Accept	Accept	Accept	N/A	No surface cracking or distortion
PHOTOGRAPHS						
						

Table A.2 Research data sheet – 4043 – sample 2

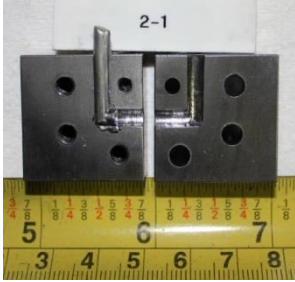
RESEARCH DATA SHEET						
Date:	4-12-14				Process Type:	[x] Discrete [] Continuous
Block	1				Sample Type:	[x] DOE [] Test Run
Whole Plot:	1				Base Alloy:	4043 Aluminum
Sample ID (Run Order):	2				Hardness	36 HV ₁₀₀
					Grain Size:	N/A
EXPERIMENTAL FACTORS	Level	Pass #1	Pass #2	Pass #3	Average	NOTES
(A) Temperature (°F)	Low	71	N/A	N/A	71	
(B) Number of Passes	Low	1	N/A	N/A	1	Total no. of passes
(C) Back Pressure (lbs.)	Low	0	N/A	N/A	0	
(D) Speed: (in./minute)	Low	0.9	N/A	N/A	0.9	
(E) Vibration (cpm)	High	9499	N/A	N/A	9499	
PROCESS VARIABLES						NOTES
Indexing Distance (in.)	N/A	0.8125	N/A	N/A	N/A	
Indexing Time (seconds)	N/A	53.8	N/A	N/A	N/A	
Die Insert No.	N/A	1	N/A	N/A	N/A	
Test Rod Diameter (in.)	N/A	0.125	N/A	N/A	N/A	
Test Rod Length (in.)	N/A	0.875	N/A	N/A	N/A	Original rod length
Lubricant	N/A	Yes	N/A	N/A	N/A	EP Dri Slide
Pressing Die	N/A	Yes	N/A	N/A	N/A	
Clamping Die	N/A	Yes	N/A	N/A	N/A	
Clamping Chuck	N/A	Yes	N/A	N/A	N/A	
Push Rod	N/A	Yes	N/A	N/A	N/A	0.875 in. diam., 10 in. length
Pressing Route	N/A	Bc	N/A	N/A	N/A	
RESULTS						NOTES
Hardness (HV ₁₀₀)	N/A	63	N/A	N/A	N/A	
Grain Size	N/A	N/A	N/A	N/A	N/A	
Visual Inspection	N/A	Accept	N/A	N/A	N/A	No surface cracking or distortion
PHOTOGRAPHS						
						

Table A.3 Research data sheet – 4043 – sample 3

RESEARCH DATA SHEET						
Date:	4-12-14				Process Type:	[x] Discrete [] Continuous
Block	1				Sample Type:	[x] DOE [] Test Run
Whole Plot:	1				Base Alloy:	4043 Aluminum
Sample ID (Run Order):	3				Hardness	36 HV ₁₀₀
					Grain Size:	N/A
EXPERIMENTAL FACTORS	Level	Pass #1	Pass #2	Pass #3	Average	NOTES
(A) Temperature (°F)	Low	71	71	71	71	
(B) Number of Passes	High	1	1	1	3	Total no. of passes
(C) Back Pressure (lbs.)	Low	0	0	0	0	
(D) Speed: (in./minute)	High	34.8	37.5	30.0	34.1	
(E) Vibration (cpm)	Low	0	0	0	0	
PROCESS VARIABLES						NOTES
Indexing Distance (in.)	N/A	0.8125	0.6250	0.500	N/A	
Indexing Time (seconds)	N/A	1.4	1.0	1.0	N/A	
Die Insert No.	N/A	1	1	1	N/A	
Test Rod Diameter (in.)	N/A	0.125	0.125	0.125	N/A	
Test Rod Length (in.)	N/A	0.875	0.875	0.875	N/A	Original rod length
Lubricant	N/A	Yes	Yes	Yes	N/A	EP Dri Slide
Pressing Die	N/A	Yes	Yes	Yes	N/A	
Clamping Die	N/A	Yes	Yes	Yes	N/A	
Clamping Chuck	N/A	Yes	Yes	Yes	N/A	
Push Rod	N/A	Yes	Yes	Yes	N/A	0.875 in. diam., 10 in. length
Pressing Route	N/A	Bc	Bc	Bc	N/A	
RESULTS						NOTES
Hardness (HV ₁₀₀)	N/A	N/A	N/A	65	N/A	
Grain Size	N/A	N/A	N/A	N/A	N/A	
Visual Inspection	N/A	Accept	Accept	Accept	N/A	No surface cracking or distortion
PHOTOGRAPHS						

Table A.4 Research data sheet – 4043 – sample 4


RESEARCH DATA SHEET						
Date:	4-12-14				Process Type:	[x] Discrete [] Continuous
Block	1				Sample Type:	[x] DOE [] Test Run
Whole Plot:	1				Base Alloy:	4043 Aluminum
Sample ID (Run Order):	4				Hardness	36 HV ₁₀₀
					Grain Size:	N/A
EXPERIMENTAL FACTORS	Level	Pass #1	Pass #2	Pass #3	Average	NOTES
(A) Temperature (°F)	Low	71	N/A	N/A	71	
(B) Number of Passes	Low	1	N/A	N/A	1	Total no. of passes
(C) Back Pressure (lbs.)	High	10	N/A	N/A	10	
(D) Speed: (in./minute)	High	45.0	N/A	N/A	45.0	
(E) Vibration (cpm)	High	9499	N/A	N/A	9499	
PROCESS VARIABLES						NOTES
Indexing Distance (in.)	N/A	0.7500	N/A	N/A	N/A	
Indexing Time (seconds)	N/A	1.0	N/A	N/A	N/A	
Die Insert No.	N/A	1	N/A	N/A	N/A	
Test Rod Diameter (in.)	N/A	0.125	N/A	N/A	N/A	
Test Rod Length (in.)	N/A	0.875	N/A	N/A	N/A	Original rod length
Lubricant	N/A	Yes	N/A	N/A	N/A	EP Dri Slide
Pressing Die	N/A	Yes	N/A	N/A	N/A	
Clamping Die	N/A	Yes	N/A	N/A	N/A	
Clamping Chuck	N/A	Yes	N/A	N/A	N/A	
Push Rod	N/A	Yes	N/A	N/A	N/A	0.875 in. diam., 10 in. length
Pressing Route	N/A	Bc	N/A	N/A	N/A	
RESULTS						NOTES
Hardness (HV ₁₀₀)	N/A	N/A	N/A	60	N/A	
Grain Size	N/A	N/A	N/A	N/A	N/A	
Visual Inspection	N/A	Accept	Accept	Accept	N/A	No surface cracking or distortion
PHOTOGRAPHS						
						

Table A.5 Research data sheet – 4043 – sample 5


RESEARCH DATA SHEET						
Date:	4-12-14				Process Type:	[x] Discrete [] Continuous
Block	1				Sample Type:	[x] DOE [] Test Run
Whole Plot:	2				Base Alloy:	4043 Aluminum
Sample ID (Run Order):	5				Hardness	36 HV ₁₀₀
					Grain Size:	N/A
EXPERIMENTAL FACTORS	Level	Pass #1	Pass #2	Pass #3	Average	NOTES
(A) Temperature (°F)	High	175.2	175.3	175.1	175.2	
(B) Number of Passes	High	1	1	1	3	Total no. of passes
(C) Back Pressure (lbs.)	Low	0	0	0	0	
(D) Speed: (in./minute)	Low	0.9	0.9	0.8	0.87	
(E) Vibration (cpm)	High	9499	9499	9499	9499	
PROCESS VARIABLES						NOTES
Indexing Distance (in.)	N/A	0.8125	0.6875	0.5625	N/A	
Indexing Time (seconds)	N/A	54.5	45.0	40.2	N/A	
Die Insert No.	N/A	1	1	1	N/A	
Test Rod Diameter (in.)	N/A	0.125	0.125	0.125	N/A	
Test Rod Length (in.)	N/A	0.875	0.875	0.875	N/A	Original rod length
Lubricant	N/A	Yes	Yes	Yes	N/A	EP Dri Slide
Pressing Die	N/A	Yes	Yes	Yes	N/A	
Clamping Die	N/A	Yes	Yes	Yes	N/A	
Clamping Chuck	N/A	Yes	Yes	Yes	N/A	
Push Rod	N/A	Yes	Yes	Yes	N/A	0.875 in. diam., 10 in. length
Pressing Route	N/A	Bc	Bc	Bc	N/A	
RESULTS						NOTES
Hardness (HV ₁₀₀)	N/A	N/A	N/A	64	N/A	
Grain Size	N/A	N/A	N/A	N/A	N/A	
Visual Inspection	N/A	Accept	Accept	Accept	N/A	No surface cracking or distortion
PHOTOGRAPHS						
						

Table A.6 Research data sheet – 4043 – sample 6

RESEARCH DATA SHEET						
Date:	4-12-14				Process Type:	[x] Discrete [] Continuous
Block	1				Sample Type:	[x] DOE [] Test Run
Whole Plot:	2				Base Alloy:	4043 Aluminum
Sample ID (Run Order):	6				Hardness	36 HV ₁₀₀
					Grain Size:	N/A
EXPERIMENTAL FACTORS	Level	Pass #1	Pass #2	Pass #3	Average	NOTES
(A) Temperature (°F)	High	175.2	175.2	175.5	175.4	
(B) Number of Passes	High	1	1	1	3	Total no. of passes
(C) Back Pressure (lbs.)	High	10	10	10	10	
(D) Speed: (in./minute)	High	17.4	22.9	21.1	20.5	
(E) Vibration (cpm)	High	9499	9499	9499	9499	
PROCESS VARIABLES						NOTES
Indexing Distance (in.)	N/A	0.8125	.6875	.5625	N/A	
Indexing Time (seconds)	N/A	2.8	1.8	1.6	N/A	
Die Insert No.	N/A	1	1	1	N/A	
Test Rod Diameter (in.)	N/A	0.125	0.125	0.125	N/A	
Test Rod Length (in.)	N/A	0.875	0.875	0.875	N/A	Original rod length
Lubricant	N/A	Yes	Yes	Yes	N/A	EP Dri Slide
Pressing Die	N/A	Yes	Yes	Yes	N/A	
Clamping Die	N/A	Yes	Yes	Yes	N/A	
Clamping Chuck	N/A	Yes	Yes	Yes	N/A	
Push Rod	N/A	Yes	Yes	Yes	N/A	0.875 in. diam., 10 in. length
Pressing Route	N/A	Bc	Bc	Bc	N/A	
RESULTS						NOTES
Hardness (HV ₁₀₀)	N/A	N/A	N/A	60	N/A	
Grain Size	N/A	N/A	N/A	N/A	N/A	
Visual Inspection	N/A	Accept	Accept	Accept	N/A	No surface cracking or distortion
PHOTOGRAPHS						

Table A.7 Research data sheet – 4043 – sample 7


RESEARCH DATA SHEET						
Date:	4-12-14				Process Type:	[x] Discrete [] Continuous
Block	1				Sample Type:	[x] DOE [] Test Run
Whole Plot:	2				Base Alloy:	4043 Aluminum
Sample ID (Run Order):	7				Hardness	36 HV ₁₀₀
					Grain Size:	N/A
EXPERIMENTAL FACTORS	Level	Pass #1	Pass #2	Pass #3	Average	NOTES
(A) Temperature (°F)	High	175.3	N/A	N/A	175.3	
(B) Number of Passes	Low	1	N/A	N/A	1	Total no. of passes
(C) Back Pressure (lbs.)	Low	0	N/A	N/A	0.0	
(D) Speed: (in./minute)	High	22.2	N/A	N/A	22.2	
(E) Vibration (cpm)	Low	0	N/A	N/A	0	
PROCESS VARIABLES						NOTES
Indexing Distance (in.)	N/A	0.8125	N/A	N/A	N/A	
Indexing Time (seconds)	N/A	2.2	N/A	N/A	N/A	
Die Insert No.	N/A	1	N/A	N/A	N/A	
Test Rod Diameter (in.)	N/A	0.125	N/A	N/A	N/A	
Test Rod Length (in.)	N/A	0.875	N/A	N/A	N/A	Original rod length
Lubricant	N/A	Yes	N/A	N/A	N/A	EP Dri Slide
Pressing Die	N/A	Yes	N/A	N/A	N/A	
Clamping Die	N/A	Yes	N/A	N/A	N/A	
Clamping Chuck	N/A	Yes	N/A	N/A	N/A	
Push Rod	N/A	Yes	N/A	N/A	N/A	0.875 in. diam., 10 in. length
Pressing Route	N/A	Bc	N/A	N/A	N/A	
RESULTS						NOTES
Hardness (HV ₁₀₀)	N/A	59	N/A	N/A	N/A	
Grain Size	N/A	N/A	N/A	N/A	N/A	
Visual Inspection	N/A	N/A	N/A	Accept	N/A	No surface cracking or distortion
PHOTOGRAPHS						
						

Table A.8 Research data sheet – 4043 – sample 8


RESEARCH DATA SHEET						
Date:	4-12-14				Process Type:	[x] Discrete [] Continuous
Block	1				Sample Type:	[x] DOE [] Test Run
Whole Plot:	2				Base Alloy:	4043 Aluminum
Sample ID (Run Order):	8				Hardness	36 HV ₁₀₀
					Grain Size:	N/A
EXPERIMENTAL FACTORS	Level	Pass #1	Pass #2	Pass #3	Average	NOTES
(A) Temperature (°F)	High	175.5	N/A	N/A	175.5	
(B) Number of Passes	Low	1	N/A	N/A	1	Total no. of passes
(C) Back Pressure (lbs.)	High	10	N/A	N/A	10	
(D) Speed: (in./minute)	Low	0.9	N/A	N/A	0.9	
(E) Vibration (cpm)	Low	0	N/A	N/A	0	
PROCESS VARIABLES						NOTES
Indexing Distance (in.)	N/A	0.8125	N/A	N/A	N/A	
Indexing Time (seconds)	N/A	53.5	N/A	N/A	N/A	
Die Insert No.	N/A	1	N/A	N/A	N/A	
Test Rod Diameter (in.)	N/A	0.125	N/A	N/A	N/A	
Test Rod Length (in.)	N/A	0.875	N/A	N/A	N/A	Original rod length
Lubricant	N/A	Yes	N/A	N/A	N/A	EP Dri Slide
Pressing Die	N/A	Yes	N/A	N/A	N/A	
Clamping Die	N/A	Yes	N/A	N/A	N/A	
Clamping Chuck	N/A	Yes	N/A	N/A	N/A	
Push Rod	N/A	Yes	N/A	N/A	N/A	0.875 in. diam., 10 in. length
Pressing Route	N/A	Bc	N/A	N/A	N/A	
RESULTS						NOTES
Hardness (HV ₁₀₀)	N/A	60	N/A	N/A	N/A	
Grain Size	N/A	N/A	N/A	N/A	N/A	
Visual Inspection	N/A	Accept	N/A	N/A	N/A	No surface cracking or distortion
PHOTOGRAPHS						
						

Table A.9 Research data sheet – 4043 – sample 9


RESEARCH DATA SHEET						
Date:	4-13-14				Process Type:	[x] Discrete [] Continuous
Block	2				Sample Type:	[x] DOE [] Test Run
Whole Plot:	3				Base Alloy:	4043 Aluminum
Sample ID (Run Order):	9				Hardness	36 HV ₁₀₀
					Grain Size:	N/A
EXPERIMENTAL FACTORS	Level	Pass #1	Pass #2	Pass #3	Average	NOTES
(A) Temperature (°F)	Low	73	73	73	73	
(B) Number of Passes	High	1	1	1	3	Total no. of passes
(C) Back Pressure (lbs.)	Low	0	0	0	0	
(D) Speed: (in./minute)	High	24.4	22.9	30.0	25.8	
(E) Vibration (cpm)	Low	0	0	0	0	
PROCESS VARIABLES						NOTES
Indexing Distance (in.)	N/A	0.8125	0.6875	0.500	N/A	
Indexing Time (seconds)	N/A	2.0	1.8	1.0	N/A	
Die Insert No.	N/A	1	1	1	N/A	
Test Rod Diameter (in.)	N/A	0.125	0.125	0.125	N/A	
Test Rod Length (in.)	N/A	0.875	0.875	0.875	N/A	Original rod length
Lubricant	N/A	Yes	Yes	Yes	N/A	EP Dri Slide
Pressing Die	N/A	Yes	Yes	Yes	N/A	
Clamping Die	N/A	Yes	Yes	Yes	N/A	
Clamping Chuck	N/A	Yes	Yes	Yes	N/A	
Push Rod	N/A	Yes	Yes	Yes	N/A	0.875 in. diam., 10 in. length
Pressing Route	N/A	Bc	Bc	Bc	N/A	
RESULTS						NOTES
Hardness (HV ₁₀₀)	N/A	N/A	N/A	67	N/A	
Grain Size	N/A	N/A	N/A	N/A	N/A	
Visual Inspection	N/A	Accept	Accept	Accept	N/A	No surface cracking or distortion
PHOTOGRAPHS						
						

Table A.10 Research data sheet – 4043 – sample 10


RESEARCH DATA SHEET						
Date:	4-13-14				Process Type:	[x] Discrete [] Continuous
Block	2				Sample Type:	[x] DOE [] Test Run
Whole Plot:	3				Base Alloy:	4043 Aluminum
Sample ID (Run Order):	10				Hardness	36 HV ₁₀₀
					Grain Size:	N/A
EXPERIMENTAL FACTORS	Level	Pass #1	Pass #2	Pass #3	Average	NOTES
(A) Temperature (°F)	Low	73	N/A	N/A	73	
(B) Number of Passes	Low	1	N/A	N/A	1	Total no. of passes
(C) Back Pressure (lbs.)	High	10	N/A	N/A	10	
(D) Speed: (in./minute)	High	24.4	N/A	N/A	24.4	
(E) Vibration (cpm)	High	9499	N/A	N/A	9499	
PROCESS VARIABLES						NOTES
Indexing Distance (in.)	N/A	0.8125	N/A	N/A	N/A	
Indexing Time (seconds)	N/A	2.0	N/A	N/A	N/A	
Die Insert No.	N/A	1	N/A	N/A	N/A	
Test Rod Diameter (in.)	N/A	0.125	N/A	N/A	N/A	
Test Rod Length (in.)	N/A	0.875	N/A	N/A	N/A	Original rod length
Lubricant	N/A	Yes	N/A	N/A	N/A	EP Dri Slide
Pressing Die	N/A	Yes	N/A	N/A	N/A	
Clamping Die	N/A	Yes	N/A	N/A	N/A	
Clamping Chuck	N/A	Yes	N/A	N/A	N/A	
Push Rod	N/A	Yes	N/A	N/A	N/A	0.875 in. diam., 10 in. length
Pressing Route	N/A	Bc	N/A	N/A	N/A	
RESULTS						NOTES
Hardness (HV ₁₀₀)	N/A	64	N/A	N/A	N/A	
Grain Size	N/A	N/A	N/A	N/A	N/A	
Visual Inspection	N/A	Accept	Accept	Accept	N/A	No surface cracking or distortion
PHOTOGRAPHS						
						

Table A.11 Research data sheet – 4043 – sample 11

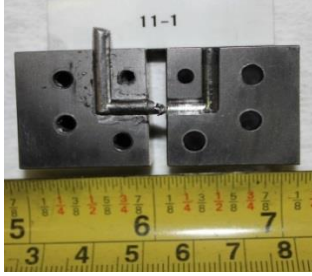
RESEARCH DATA SHEET						
Date:	4-13-14				Process Type:	[x] Discrete [] Continuous
Block	2				Sample Type:	[x] DOE [] Test Run
Whole Plot:	3				Base Alloy:	4043 Aluminum
Sample ID (Run Order):	11				Hardness	36 HV ₁₀₀
					Grain Size:	N/A
EXPERIMENTAL FACTORS	Level	Pass #1	Pass #2	Pass #3	Average	NOTES
(A) Temperature (°F)	Low	73	N/A	N/A	73	
(B) Number of Passes	Low	1	N/A	N/A	1	Total no. of passes
(C) Back Pressure (lbs.)	Low	0	N/A	N/A	0	
(D) Speed: (in./minute)	Low	0.9	N/A	N/A	0.9	
(E) Vibration (cpm)	High	9499	N/A	N/A	9499	
PROCESS VARIABLES						NOTES
Indexing Distance (in.)	N/A	0.8125	N/A	N/A	N/A	
Indexing Time (seconds)	N/A	52.5	N/A	N/A	N/A	
Die Insert No.	N/A	1	N/A	N/A	N/A	
Test Rod Diameter (in.)	N/A	0.125	N/A	N/A	N/A	
Test Rod Length (in.)	N/A	0.875	N/A	N/A	N/A	Original rod length
Lubricant	N/A	Yes	N/A	N/A	N/A	EP Dri Slide
Pressing Die	N/A	Yes	N/A	N/A	N/A	
Clamping Die	N/A	Yes	N/A	N/A	N/A	
Clamping Chuck	N/A	Yes	N/A	N/A	N/A	
Push Rod	N/A	Yes	N/A	N/A	N/A	0.875 in. diam., 10 in. length
Pressing Route	N/A	Bc	N/A	N/A	N/A	
RESULTS						NOTES
Hardness (HV ₁₀₀)	N/A	60	N/A	N/A	N/A	
Grain Size	N/A	N/A	N/A	N/A	N/A	
Visual Inspection	N/A	Accept	N/A	N/A	N/A	No surface cracking or distortion
PHOTOGRAPHS						
						

Table A.12 Research data sheet – 4043 – sample 12

RESEARCH DATA SHEET						
Date:	4-13-14				Process Type:	[x] Discrete [] Continuous
Block	2				Sample Type:	[x] DOE [] Test Run
Whole Plot:	3				Base Alloy:	4043 Aluminum
Sample ID (Run Order):	12				Hardness	36 HV ₁₀₀
					Grain Size:	N/A
EXPERIMENTAL FACTORS	Level	Pass #1	Pass #2	Pass #3	Average	NOTES
(A) Temperature (°F)	Low	73	73	73	73	
(B) Number of Passes	High	1	1	1	3	Total no. of passes
(C) Back Pressure (lbs.)	High	10	10	10	10.0	
(D) Speed: (in./minute)	Low	1.0	1.0	0.9	1.0	
(E) Vibration (cpm)	Low	0	0	0	0.0	
PROCESS VARIABLES						NOTES
Indexing Distance (in.)	N/A	0.8125	0.6875	0.5625	N/A	
Indexing Time (seconds)	N/A	50.0	40.8	39.0	N/A	
Die Insert No.	N/A	1	1	1	N/A	
Test Rod Diameter (in.)	N/A	0.125	0.125	0.125	N/A	
Test Rod Length (in.)	N/A	0.875	0.875	0.875	N/A	Original rod length
Lubricant	N/A	Yes	Yes	Yes	N/A	EP Dri Slide
Pressing Die	N/A	Yes	Yes	Yes	N/A	
Clamping Die	N/A	Yes	Yes	Yes	N/A	
Clamping Chuck	N/A	Yes	Yes	Yes	N/A	
Push Rod	N/A	Yes	Yes	Yes	N/A	0.875 in. diam., 10 in. length
Pressing Route	N/A	Bc	Bc	Bc	N/A	
RESULTS						NOTES
Hardness (HV ₁₀₀)	N/A	N/A	N/A	66	N/A	
Grain Size	N/A	N/A	N/A	N/A	N/A	
Visual Inspection	N/A	Accept	Accept	Accept	N/A	No surface cracking or distortion
PHOTOGRAPHS						

Table A.13 Research data sheet – 4043 – sample 13

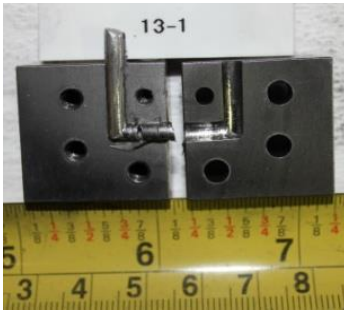
RESEARCH DATA SHEET						
Date:	4-13-14				Process Type:	[x] Discrete [] Continuous
Block	2				Sample Type:	[x] DOE [] Test Run
Whole Plot:	4				Base Alloy:	4043 Aluminum
Sample ID (Run Order):	13				Hardness	36 HV ₁₀₀
					Grain Size:	N/A
EXPERIMENTAL FACTORS	Level	Pass #1	Pass #2	Pass #3	Average	NOTES
(A) Temperature (°F)	High	174.8	N/A	N/A	174.8	
(B) Number of Passes	Low	1	N/A	N/A	1	Total no. of passes
(C) Back Pressure (lbs.)	Low	0	N/A	N/A	0.0	
(D) Speed: (in./minute)	High	32.5	N/A	N/A	32.5	
(E) Vibration (cpm)	Low	0	N/A	N/A	0	
PROCESS VARIABLES						NOTES
Indexing Distance (in.)	N/A	0.8125	N/A	N/A	N/A	
Indexing Time (seconds)	N/A	1.5	N/A	N/A	N/A	
Die Insert No.	N/A	1	N/A	N/A	N/A	
Test Rod Diameter (in.)	N/A	0.125	N/A	N/A	N/A	
Test Rod Length (in.)	N/A	0.875	N/A	N/A	N/A	Original rod length
Lubricant	N/A	Yes	N/A	N/A	N/A	EP Dri Slide
Pressing Die	N/A	Yes	N/A	N/A	N/A	
Clamping Die	N/A	Yes	N/A	N/A	N/A	
Clamping Chuck	N/A	Yes	N/A	N/A	N/A	
Push Rod	N/A	Yes	N/A	N/A	N/A	0.875 in. diam., 10 in. length
Pressing Route	N/A	Bc	N/A	N/A	N/A	
RESULTS						NOTES
Hardness (HV ₁₀₀)	N/A	61	N/A	N/A	N/A	
Grain Size	N/A	N/A	N/A	N/A	N/A	
Visual Inspection	N/A	N/A	N/A	Accept	N/A	No surface cracking or distortion
PHOTOGRAPHS						
						

Table A.14 Research data sheet – 4043 – sample 14

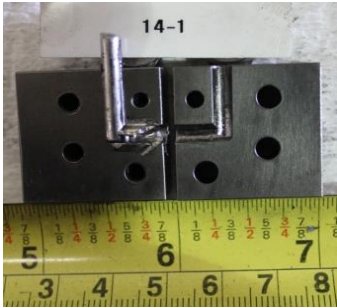
RESEARCH DATA SHEET						
Date:	4-13-14				Process Type:	[x] Discrete [] Continuous
Block	2				Sample Type:	[x] DOE [] Test Run
Whole Plot:	4				Base Alloy:	4043 Aluminum
Sample ID (Run Order):	14				Hardness	36 HV ₁₀₀
					Grain Size:	N/A
EXPERIMENTAL FACTORS	Level	Pass #1	Pass #2	Pass #3	Average	NOTES
(A) Temperature (°F)	High	175.0	N/A	N/A	175.0	
(B) Number of Passes	Low	1	N/A	N/A	1	Total no. of passes
(C) Back Pressure (lbs.)	High	10	N/A	N/A	10	
(D) Speed: (in./minute)	Low	0.9	N/A	N/A	0.9	
(E) Vibration (cpm)	Low	0	N/A	N/A	0	
PROCESS VARIABLES						NOTES
Indexing Distance (in.)	N/A	0.8125	N/A	N/A	N/A	
Indexing Time (seconds)	N/A	55.0	N/A	N/A	N/A	
Die Insert No.	N/A	1	N/A	N/A	N/A	
Test Rod Diameter (in.)	N/A	0.125	N/A	N/A	N/A	
Test Rod Length (in.)	N/A	0.875	N/A	N/A	N/A	Original rod length
Lubricant	N/A	Yes	N/A	N/A	N/A	EP Dri Slide
Pressing Die	N/A	Yes	N/A	N/A	N/A	
Clamping Die	N/A	Yes	N/A	N/A	N/A	
Clamping Chuck	N/A	Yes	N/A	N/A	N/A	
Push Rod	N/A	Yes	N/A	N/A	N/A	0.875 in. diam., 10 in. length
Pressing Route	N/A	Bc	N/A	N/A	N/A	
RESULTS						NOTES
Hardness (HV ₁₀₀)	N/A	57	N/A	N/A	N/A	
Grain Size	N/A	N/A	N/A	N/A	N/A	
Visual Inspection	N/A	Accept	N/A	N/A	N/A	No surface cracking or distortion
PHOTOGRAPHS						
						

Table A.15 Research data sheet – 4043 – sample 15

RESEARCH DATA SHEET						
Date:	4-13-14				Process Type:	[x] Discrete [] Continuous
Block	2				Sample Type:	[x] DOE [] Test Run
Whole Plot:	4				Base Alloy:	4043 Aluminum
Sample ID (Run Order):	15				Hardness	36 HV ₁₀₀
					Grain Size:	N/A
EXPERIMENTAL FACTORS	Level	Pass #1	Pass #2	Pass #3	Average	NOTES
(A) Temperature (°F)	High	175.6	175.2	175.4	175.4	
(B) Number of Passes	High	1	1	1	3	Total no. of passes
(C) Back Pressure (lbs.)	Low	0	0	0	0	
(D) Speed: (in./minute)	Low	0.9	1.0	0.8	0.9	
(E) Vibration (cpm)	High	9499	9499	9499	9499	
PROCESS VARIABLES						NOTES
Indexing Distance (in.)	N/A	0.8125	0.6875	0.500	N/A	
Indexing Time (seconds)	N/A	56.0	42.8	35.5	N/A	
Die Insert No.	N/A	1	1	1	N/A	
Test Rod Diameter (in.)	N/A	0.125	0.125	0.125	N/A	
Test Rod Length (in.)	N/A	0.875	0.875	0.875	N/A	Original rod length
Lubricant	N/A	Yes	Yes	Yes	N/A	EP Dri Slide
Pressing Die	N/A	Yes	Yes	Yes	N/A	
Clamping Die	N/A	Yes	Yes	Yes	N/A	
Clamping Chuck	N/A	Yes	Yes	Yes	N/A	
Push Rod	N/A	Yes	Yes	Yes	N/A	0.875 in. diam., 10 in. length
Pressing Route	N/A	Bc	Bc	Bc	N/A	
RESULTS						NOTES
Hardness (HV ₁₀₀)	N/A	N/A	N/A	59	N/A	
Grain Size	N/A	N/A	N/A	N/A	N/A	
Visual Inspection	N/A	Accept	Accept	Accept	N/A	No surface cracking or distortion
PHOTOGRAPHS						
						

Table A.16 Research data sheet – 4043 – sample 16

RESEARCH DATA SHEET						
Date:	4-13-14				Process Type:	[x] Discrete [] Continuous
Block	2				Sample Type:	[x] DOE [] Test Run
Whole Plot:	4				Base Alloy:	4043 Aluminum
Sample ID (Run Order):	16				Hardness	36 HV ₁₀₀
					Grain Size:	N/A
EXPERIMENTAL FACTORS	Level	Pass #1	Pass #2	Pass #3	Average	NOTES
(A) Temperature (°F)	High	175.7	175.4	175.4	175.5	
(B) Number of Passes	High	1	1	1	3	Total no. of passes
(C) Back Pressure (lbs.)	High	10	10	10	10	
(D) Speed: (in./minute)	High	24.4	20.6	15.3	20.1	
(E) Vibration (cpm)	High	9499	9499	9499	9499	
PROCESS VARIABLES						NOTES
Indexing Distance (in.)	N/A	0.8125	0.6875	0.5625	N/A	
Indexing Time (seconds)	N/A	2.0	2.0	2.2	N/A	
Die Insert No.	N/A	1	1	1	N/A	
Test Rod Diameter (in.)	N/A	0.125	0.125	0.125	N/A	
Test Rod Length (in.)	N/A	0.875	0.875	0.875	N/A	Original rod length
Lubricant	N/A	Yes	Yes	Yes	N/A	EP Dri Slide
Pressing Die	N/A	Yes	Yes	Yes	N/A	
Clamping Die	N/A	Yes	Yes	Yes	N/A	
Clamping Chuck	N/A	Yes	Yes	Yes	N/A	
Push Rod	N/A	Yes	Yes	Yes	N/A	0.875 in. diam., 10 in. length
Pressing Route	N/A	Bc	Bc	Bc	N/A	
RESULTS						NOTES
Hardness (HV ₁₀₀)	N/A	N/A	N/A	63	N/A	
Grain Size	N/A	N/A	N/A	N/A	N/A	
Visual Inspection	N/A	Accept	Accept	Accept	N/A	No surface cracking or distortion
PHOTOGRAPHS						
<p>The photographs show three views of a metal part, labeled 16-1, 16-2, and 16-3. Each view shows the part with a yellow ruler placed below it for scale. The ruler shows inches from 3 to 8. The part is a rectangular block with a central slot and two circular holes on each side. The part is shown from different angles to illustrate its geometry and the results of the process.</p>						

Table A.17 Research data sheet – 4043 – sample 17

RESEARCH DATA SHEET						
Date:	4-14-14				Process Type:	[x] Discrete [] Continuous
Block	3				Sample Type:	[x] DOE [] Test Run
Whole Plot:	5				Base Alloy:	4043 Aluminum
Sample ID (Run Order):	17				Hardness	36 HV ₁₀₀
					Grain Size:	N/A
EXPERIMENTAL FACTORS	Level	Pass #1	Pass #2	Pass #3	Average	NOTES
(A) Temperature (°F)	Low	73	73	73	73.0	
(B) Number of Passes	High	1	1	1	3	Total no. of passes
(C) Back Pressure (lbs.)	High	10	10	10	10.0	
(D) Speed: (in./minute)	Low	1.0	1.0	0.8	0.9	
(E) Vibration (cpm)	Low	0	0	0	0.0	
PROCESS VARIABLES						NOTES
Indexing Distance (in.)	N/A	0.8125	0.6875	0.5000	N/A	
Indexing Time (seconds)	N/A	50.8	42.5	37.8	N/A	
Die Insert No.	N/A	1	1	1	N/A	
Test Rod Diameter (in.)	N/A	0.125	0.125	0.125	N/A	
Test Rod Length (in.)	N/A	0.875	0.875	0.875	N/A	Original rod length
Lubricant	N/A	Yes	Yes	Yes	N/A	EP Dri Slide
Pressing Die	N/A	Yes	Yes	Yes	N/A	
Clamping Die	N/A	Yes	Yes	Yes	N/A	
Clamping Chuck	N/A	Yes	Yes	Yes	N/A	
Push Rod	N/A	Yes	Yes	Yes	N/A	0.875 in. diam., 10 in. length
Pressing Route	N/A	Bc	Bc	Bc	N/A	
RESULTS						NOTES
Hardness (HV ₁₀₀)	N/A	N/A	N/A	67	N/A	
Grain Size	N/A	N/A	N/A	N/A	N/A	
Visual Inspection	N/A	Accept	Accept	Accept	N/A	No surface cracking or distortion
PHOTOGRAPHS						

Table A.18 Research data sheet – 4043 – sample 18


RESEARCH DATA SHEET						
Date:	4-14-14				Process Type:	[x] Discrete [] Continuous
Block	3				Sample Type:	[x] DOE [] Test Run
Whole Plot:	5				Base Alloy:	4043 Aluminum
Sample ID (Run Order):	18				Hardness	36 HV ₁₀₀
					Grain Size:	N/A
EXPERIMENTAL FACTORS	Level	Pass #1	Pass #2	Pass #3	Average	NOTES
(A) Temperature (°F)	Low	73	N/A	N/A	73	
(B) Number of Passes	Low	1	N/A	N/A	1	Total no. of passes
(C) Back Pressure (lbs.)	High	10	N/A	N/A	10	
(D) Speed: (in./minute)	High	24.4	N/A	N/A	24.4	
(E) Vibration (cpm)	High	9499	N/A	N/A	9499	
PROCESS VARIABLES						NOTES
Indexing Distance (in.)	N/A	0.8125	N/A	N/A	N/A	
Indexing Time (seconds)	N/A	2.0	N/A	N/A	N/A	
Die Insert No.	N/A	1	N/A	N/A	N/A	
Test Rod Diameter (in.)	N/A	0.125	N/A	N/A	N/A	
Test Rod Length (in.)	N/A	0.875	N/A	N/A	N/A	Original rod length
Lubricant	N/A	Yes	N/A	N/A	N/A	EP Dri Slide
Pressing Die	N/A	Yes	N/A	N/A	N/A	
Clamping Die	N/A	Yes	N/A	N/A	N/A	
Clamping Chuck	N/A	Yes	N/A	N/A	N/A	
Push Rod	N/A	Yes	N/A	N/A	N/A	0.875 in. diam., 10 in. length
Pressing Route	N/A	Bc	N/A	N/A	N/A	
RESULTS						NOTES
Hardness (HV ₁₀₀)	N/A	61	N/A	N/A	N/A	
Grain Size	N/A	N/A	N/A	N/A	N/A	
Visual Inspection	N/A	Accept	Accept	Accept	N/A	No surface cracking or distortion
PHOTOGRAPHS						
						

Table A.19 Research data sheet – 4043 – sample 19


RESEARCH DATA SHEET						
Date:	4-14-14				Process Type:	[x] Discrete [] Continuous
Block	3				Sample Type:	[x] DOE [] Test Run
Whole Plot:	5				Base Alloy:	4043 Aluminum
Sample ID (Run Order):	19				Hardness	36 HV ₁₀₀
					Grain Size:	N/A
EXPERIMENTAL FACTORS	Level	Pass #1	Pass #2	Pass #3	Average	NOTES
(A) Temperature (°F)	Low	73	N/A	N/A	73	
(B) Number of Passes	Low	1	N/A	N/A	1	Total no. of passes
(C) Back Pressure (lbs.)	Low	0	N/A	N/A	0	
(D) Speed: (in./minute)	Low	0.8	N/A	N/A	0.8	
(E) Vibration (cpm)	High	9499	N/A	N/A	9499	
PROCESS VARIABLES						NOTES
Indexing Distance (in.)	N/A	0.8125	N/A	N/A	N/A	
Indexing Time (seconds)	N/A	61.8	N/A	N/A	N/A	
Die Insert No.	N/A	1	N/A	N/A	N/A	
Test Rod Diameter (in.)	N/A	0.125	N/A	N/A	N/A	
Test Rod Length (in.)	N/A	0.875	N/A	N/A	N/A	Original rod length
Lubricant	N/A	Yes	N/A	N/A	N/A	EP Dri Slide
Pressing Die	N/A	Yes	N/A	N/A	N/A	
Clamping Die	N/A	Yes	N/A	N/A	N/A	
Clamping Chuck	N/A	Yes	N/A	N/A	N/A	
Push Rod	N/A	Yes	N/A	N/A	N/A	0.875 in. diam., 10 in. length
Pressing Route	N/A	Bc	N/A	N/A	N/A	
RESULTS						NOTES
Hardness (HV ₁₀₀)	N/A	61	N/A	N/A	N/A	
Grain Size	N/A	N/A	N/A	N/A	N/A	
Visual Inspection	N/A	Accept	N/A	N/A	N/A	No surface cracking or distortion
PHOTOGRAPHS						
						

Table A.20 Research data sheet – 4043 – sample 20

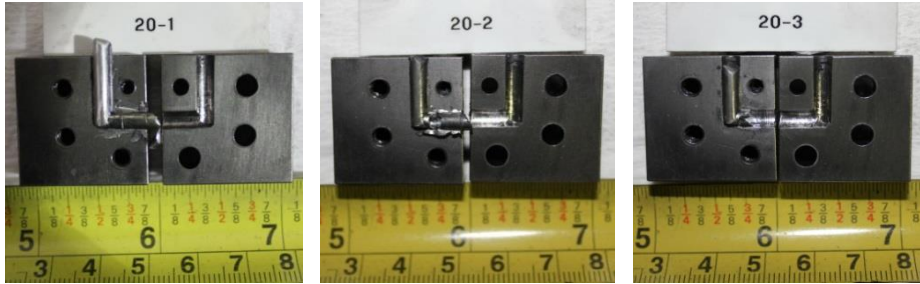
RESEARCH DATA SHEET						
Date:	4-14-14				Process Type:	[x] Discrete [] Continuous
Block	3				Sample Type:	[x] DOE [] Test Run
Whole Plot:	5				Base Alloy:	4043 Aluminum
Sample ID (Run Order):	20				Hardness	36 HV ₁₀₀
					Grain Size:	N/A
EXPERIMENTAL FACTORS	Level	Pass #1	Pass #2	Pass #3	Average	NOTES
(A) Temperature (°F)	Low	73	73	73	73	
(B) Number of Passes	High	1	1	1	3	Total no. of passes
(C) Back Pressure (lbs.)	Low	0	0	0	0	
(D) Speed: (in./minute)	High	24.4	25.0	25.0	24.8	
(E) Vibration (cpm)	Low	0	0	0	0	
PROCESS VARIABLES						NOTES
Indexing Distance (in.)	N/A	0.8125	0.7500	0.500	N/A	
Indexing Time (seconds)	N/A	2.0	1.8	1.2	N/A	
Die Insert No.	N/A	1	1	1	N/A	
Test Rod Diameter (in.)	N/A	0.125	0.125	0.125	N/A	
Test Rod Length (in.)	N/A	0.875	0.875	0.875	N/A	Original rod length
Lubricant	N/A	Yes	Yes	Yes	N/A	EP Dri Slide
Pressing Die	N/A	Yes	Yes	Yes	N/A	
Clamping Die	N/A	Yes	Yes	Yes	N/A	
Clamping Chuck	N/A	Yes	Yes	Yes	N/A	
Push Rod	N/A	Yes	Yes	Yes	N/A	0.875 in. diam., 10 in. length
Pressing Route	N/A	Bc	Bc	Bc	N/A	
RESULTS						NOTES
Hardness (HV ₁₀₀)	N/A	N/A	N/A	68	N/A	
Grain Size (nm)	N/A	N/A	N/A	103	N/A	Hall-Petch calculation
Visual Inspection	N/A	Accept	Accept	Accept	N/A	No surface cracking or distortion
PHOTOGRAPHS						
 <p>The photographs show three metal samples, labeled 20-1, 20-2, and 20-3, which appear to be small metal rods or inserts. Each sample is placed on a yellow ruler for scale. The ruler shows inches and centimeters. The samples are dark in color and have a complex, somewhat rectangular shape with a central protrusion. The labels 20-1, 20-2, and 20-3 are printed above each respective sample.</p>						

Table A.21 Research data sheet – 4043 – sample 21

RESEARCH DATA SHEET						
Date:	4-14-14				Process Type:	[x] Discrete [] Continuous
Block	3				Sample Type:	[x] DOE [] Test Run
Whole Plot:	6				Base Alloy:	4043 Aluminum
Sample ID (Run Order):	21				Hardness	36 HV ₁₀₀
					Grain Size:	N/A
EXPERIMENTAL FACTORS	Level	Pass #1	Pass #2	Pass #3	Average	NOTES
(A) Temperature (°F)	High	175.6	175	175	175.2	
(B) Number of Passes	High	1	1	1	3	Total no. of passes
(C) Back Pressure (lbs.)	Low	0	0	0	0	
(D) Speed: (in./minute)	Low	0.9	1.2	1.0	1.0	
(E) Vibration (cpm)	High	9499	9499	9499	9499	
PROCESS VARIABLES						NOTES
Indexing Distance (in.)	N/A	0.8125	0.7500	0.6250	N/A	
Indexing Time (seconds)	N/A	55.5	39.0	37.8	N/A	
Die Insert No.	N/A	1	1	1	N/A	
Test Rod Diameter (in.)	N/A	0.125	0.125	0.125	N/A	
Test Rod Length (in.)	N/A	0.875	0.875	0.875	N/A	Original rod length
Lubricant	N/A	Yes	Yes	Yes	N/A	EP Dri Slide
Pressing Die	N/A	Yes	Yes	Yes	N/A	
Clamping Die	N/A	Yes	Yes	Yes	N/A	
Clamping Chuck	N/A	Yes	Yes	Yes	N/A	
Push Rod	N/A	Yes	Yes	Yes	N/A	0.875 in. diam., 10 in. length
Pressing Route	N/A	Bc	Bc	Bc	N/A	
RESULTS						NOTES
Hardness (HV ₁₀₀)	N/A	N/A	N/A	61	N/A	
Grain Size	N/A	N/A	N/A	N/A	N/A	
Visual Inspection	N/A	Accept	Accept	Accept	N/A	No surface cracking or distortion
PHOTOGRAPHS						

Table A.22 Research data sheet – 4043 – sample 22

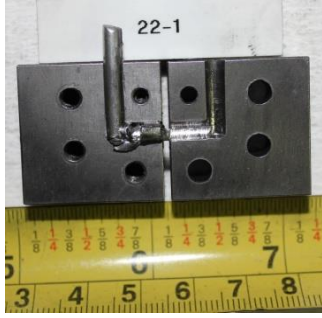

RESEARCH DATA SHEET						
Date:	4-14-14				Process Type:	[x] Discrete [] Continuous
Block	3				Sample Type:	[x] DOE [] Test Run
Whole Plot:	6				Base Alloy:	4043 Aluminum
Sample ID (Run Order):	22				Hardness	36 HV ₁₀₀
					Grain Size:	N/A
EXPERIMENTAL FACTORS	Level	Pass #1	Pass #2	Pass #3	Average	NOTES
(A) Temperature (°F)	High	175.4	N/A	N/A	175.4	
(B) Number of Passes	Low	1	N/A	N/A	1	Total no. of passes
(C) Back Pressure (lbs.)	High	10	N/A	N/A	10	
(D) Speed: (in./minute)	Low	0.9	N/A	N/A	0.9	
(E) Vibration (cpm)	Low	0	N/A	N/A	0	
PROCESS VARIABLES						NOTES
Indexing Distance (in.)	N/A	0.8125	N/A	N/A	N/A	
Indexing Time (seconds)	N/A	54.0	N/A	N/A	N/A	
Die Insert No.	N/A	1	N/A	N/A	N/A	
Test Rod Diameter (in.)	N/A	0.125	N/A	N/A	N/A	
Test Rod Length (in.)	N/A	0.875	N/A	N/A	N/A	Original rod length
Lubricant	N/A	Yes	N/A	N/A	N/A	EP Dri Slide
Pressing Die	N/A	Yes	N/A	N/A	N/A	
Clamping Die	N/A	Yes	N/A	N/A	N/A	
Clamping Chuck	N/A	Yes	N/A	N/A	N/A	
Push Rod	N/A	Yes	N/A	N/A	N/A	0.875 in. diam., 10 in. length
Pressing Route	N/A	Bc	N/A	N/A	N/A	
RESULTS						NOTES
Hardness (HV ₁₀₀)	N/A	62	N/A	N/A	N/A	
Grain Size	N/A	N/A	N/A	N/A	N/A	
Visual Inspection	N/A	Accept	N/A	N/A	N/A	No surface cracking or distortion
PHOTOGRAPHS						
						

Table A.23 Research data sheet – 4043 – sample 23

RESEARCH DATA SHEET						
Date:	4-14-14				Process Type:	[x] Discrete [] Continuous
Block	3				Sample Type:	[x] DOE [] Test Run
Whole Plot:	6				Base Alloy:	4043 Aluminum
Sample ID (Run Order):	23				Hardness	36 HV ₁₀₀
					Grain Size:	N/A
EXPERIMENTAL FACTORS	Level	Pass #1	Pass #2	Pass #3	Average	NOTES
(A) Temperature (°F)	High	175.1	175.2	175.2	175.2	
(B) Number of Passes	High	1	1	1	3	Total no. of passes
(C) Back Pressure (lbs.)	High	10	10	10	10	
(D) Speed: (in./minute)	High	27.1	27.5	18.8	24.4	
(E) Vibration (cpm)	High	9499	9499	9499	9499	
PROCESS VARIABLES						NOTES
Indexing Distance (in.)	N/A	0.8125	0.6875	0.5625	N/A	
Indexing Time (seconds)	N/A	1.8	1.5	1.8	N/A	
Die Insert No.	N/A	1	1	1	N/A	
Test Rod Diameter (in.)	N/A	0.125	0.125	0.125	N/A	
Test Rod Length (in.)	N/A	0.875	0.875	0.875	N/A	Original rod length
Lubricant	N/A	Yes	Yes	Yes	N/A	EP Dri Slide
Pressing Die	N/A	Yes	Yes	Yes	N/A	
Clamping Die	N/A	Yes	Yes	Yes	N/A	
Clamping Chuck	N/A	Yes	Yes	Yes	N/A	
Push Rod	N/A	Yes	Yes	Yes	N/A	0.875 in. diam., 10 in. length
Pressing Route	N/A	Bc	Bc	Bc	N/A	
RESULTS						NOTES
Hardness (HV ₁₀₀)	N/A	N/A	N/A	68	N/A	
Grain Size (nm)	N/A	N/A	N/A	103	N/A	Hall-Petch calculation
Visual Inspection	N/A	Accept	Accept	Accept	N/A	No surface cracking or distortion
PHOTOGRAPHS						

Table A.24 Research data sheet – 4043 – sample 24

RESEARCH DATA SHEET						
Date:	4-14-14				Process Type:	[x] Discrete [] Continuous
Block	3				Sample Type:	[x] DOE [] Test Run
Whole Plot:	6				Base Alloy:	4043 Aluminum
Sample ID (Run Order):	24				Hardness	36 HV ₁₀₀
					Grain Size:	N/A
EXPERIMENTAL FACTORS	Level	Pass #1	Pass #2	Pass #3	Average	NOTES
(A) Temperature (°F)	High	175.4	N/A	N/A	175.4	
(B) Number of Passes	Low	1	N/A	N/A	1	Total no. of passes
(C) Back Pressure (lbs.)	Low	0	N/A	N/A	0.0	
(D) Speed: (in./minute)	High	27.1	N/A	N/A	27.1	
(E) Vibration (cpm)	Low	0	N/A	N/A	0	
PROCESS VARIABLES						NOTES
Indexing Distance (in.)	N/A	0.8125	N/A	N/A	N/A	
Indexing Time (seconds)	N/A	1.8	N/A	N/A	N/A	
Die Insert No.	N/A	1	N/A	N/A	N/A	
Test Rod Diameter (in.)	N/A	0.125	N/A	N/A	N/A	
Test Rod Length (in.)	N/A	0.875	N/A	N/A	N/A	Original rod length
Lubricant	N/A	Yes	N/A	N/A	N/A	EP Dri Slide
Pressing Die	N/A	Yes	N/A	N/A	N/A	
Clamping Die	N/A	Yes	N/A	N/A	N/A	
Clamping Chuck	N/A	Yes	N/A	N/A	N/A	
Push Rod	N/A	Yes	N/A	N/A	N/A	0.875 in. diam., 10 in. length
Pressing Route	N/A	Bc	N/A	N/A	N/A	
RESULTS						NOTES
Hardness (HV ₁₀₀)	N/A	61	N/A	N/A	N/A	
Grain Size	N/A	N/A	N/A	N/A	N/A	
Visual Inspection	N/A	N/A	N/A	Accept	N/A	No surface cracking or distortion
PHOTOGRAPHS						
						

1100 Aluminum Alloy - Research Data Sheets

Results from the 1100 aluminum alloy split plot $\frac{1}{4}$ fraction factorial experiments are illustrated in the following photographs. The figures depict actual pressed rods as well as the associated metallographic photomicrographs in the longitudinal directions.

Table A.25 Research data sheet – 1100 – sample 1

RESEARCH DATA SHEET						
Date:	4-5-14				Process Type:	<input checked="" type="checkbox"/> Discrete <input type="checkbox"/> Continuous
Block	1				Sample Type:	<input checked="" type="checkbox"/> DOE <input type="checkbox"/> Test Run
Whole Plot:	1				Base Alloy:	1100 Aluminum
Sample ID (Run Order):	1				Hardness	23 Brinell
					Grain Size:	N/A
EXPERIMENTAL FACTORS	Level	Pass #1	Pass #2	Pass #3	Average	NOTES
(A) Temperature (°F)	Low	65	65	65	65	
(B) Number of Passes	High	1	1	1	3	Total no. of passes
(C) Back Pressure (lbs.)	High	10	10	10	10.0	
(D) Speed: (in./minute)	Low	1.7	1.2	1.6	1.5	
(E) Vibration (cpm)	Low	0	0	0	0.0	
PROCESS VARIABLES						NOTES
Indexing Distance (in.)	N/A	0.7500	0.6875	0.5000	N/A	
Indexing Time (seconds)	N/A	27.0	35.5	19.0	N/A	
Die Insert No.	N/A	1	1	1	N/A	
Test Rod Diameter (in.)	N/A	0.125	0.125	0.125	N/A	
Test Rod Length (in.)	N/A	0.875	0.875	0.875	N/A	Original rod length
Lubricant	N/A	Yes	Yes	Yes	N/A	EP Dri Slide
Pressing Die	N/A	Yes	Yes	Yes	N/A	
Clamping Die	N/A	Yes	Yes	Yes	N/A	
Clamping Chuck	N/A	Yes	Yes	Yes	N/A	
Push Rod	N/A	Yes	Yes	Yes	N/A	0.875 in. diam., 10 in. length
Pressing Route	N/A	Bc	Bc	Bc	N/A	
RESULTS						NOTES
Hardness (HRB)	N/A	N/A	N/A	N/A	N/A	
Grain Size	N/A	N/A	N/A	N/A	N/A	
Visual Inspection	N/A	Accept	Accept	Accept	N/A	No surface cracking or distortion
PHOTOGRAPHS						

Table A.26 Research data sheet – 1100 – sample 2

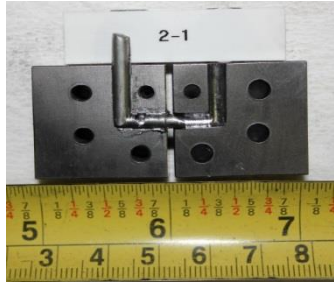
RESEARCH DATA SHEET						
Date:	4-5-14				Process Type:	[x] Discrete [] Continuous
Block	1				Sample Type:	[x] DOE [] Test Run
Whole Plot:	1				Base Alloy:	1100 Aluminum
Sample ID (Run Order):	2				Hardness	23 Brinell
					Grain Size:	N/A
EXPERIMENTAL FACTORS	Level	Pass #1	Pass #2	Pass #3	Average	NOTES
(A) Temperature (°F)	Low	65	N/A	N/A	65	
(B) Number of Passes	Low	1	N/A	N/A	1	Total no. of passes
(C) Back Pressure (lbs.)	Low	0	N/A	N/A	0	
(D) Speed: (in./minute)	Low	0.9	N/A	N/A	0.9	
(E) Vibration (cpm)	High	9499	N/A	N/A	9499	
PROCESS VARIABLES						NOTES
Indexing Distance (in.)	N/A	0.7500	N/A	N/A	N/A	
Indexing Time (seconds)	N/A	48.0	N/A	N/A	N/A	
Die Insert No.	N/A	1	N/A	N/A	N/A	
Test Rod Diameter (in.)	N/A	0.125	N/A	N/A	N/A	
Test Rod Length (in.)	N/A	0.875	N/A	N/A	N/A	Original rod length
Lubricant	N/A	Yes	N/A	N/A	N/A	EP Dri Slide
Pressing Die	N/A	Yes	N/A	N/A	N/A	
Clamping Die	N/A	Yes	N/A	N/A	N/A	
Clamping Chuck	N/A	Yes	N/A	N/A	N/A	
Push Rod	N/A	Yes	N/A	N/A	N/A	0.875 in. diam., 10 in. length
Pressing Route	N/A	Bc	N/A	N/A	N/A	
RESULTS						NOTES
Hardness (HRB)	N/A	N/A	N/A	N/A	N/A	
Grain Size	N/A	N/A	N/A	N/A	N/A	
Visual Inspection	N/A	Accept	N/A	N/A	N/A	No surface cracking or distortion
PHOTOGRAPHS						
						

Table A.27 Research data sheet – 1100 – sample 3

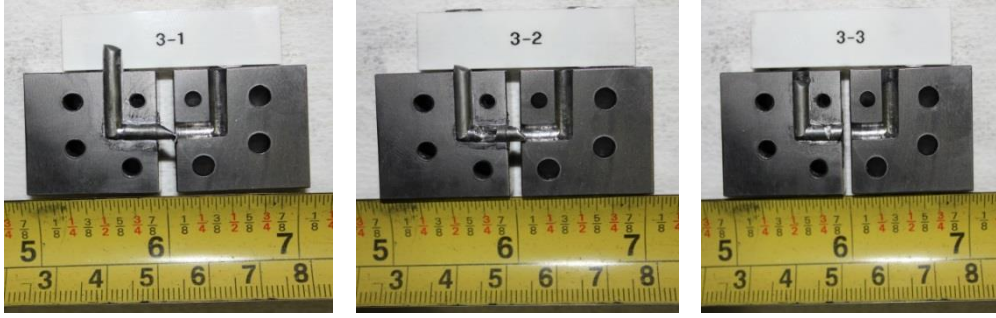
RESEARCH DATA SHEET						
Date:	4-5-14				Process Type:	[x] Discrete [] Continuous
Block	1				Sample Type:	[x] DOE [] Test Run
Whole Plot:	1				Base Alloy:	1100 Aluminum
Sample ID (Run Order):	3				Hardness	23 Brinell
					Grain Size:	N/A
EXPERIMENTAL FACTORS	Level	Pass #1	Pass #2	Pass #3	Average	NOTES
(A) Temperature (°F)	Low	65	65	65	65	
(B) Number of Passes	High	1	1	1	3	Total no. of passes
(C) Back Pressure (lbs.)	Low	0	0	0	0	
(D) Speed: (in./minute)	High	24.4	30.0	30.0	28.1	
(E) Vibration (cpm)	Low	0	0	0	0	
PROCESS VARIABLES						NOTES
Indexing Distance (in.)	N/A	0.8125	0.7500	0.500	N/A	
Indexing Time (seconds)	N/A	2.0	1.5	1.0	N/A	
Die Insert No.	N/A	1	1	1	N/A	
Test Rod Diameter (in.)	N/A	0.125	0.125	0.125	N/A	
Test Rod Length (in.)	N/A	0.875	0.875	0.875	N/A	Original rod length
Lubricant	N/A	Yes	Yes	Yes	N/A	EP Dri Slide
Pressing Die	N/A	Yes	Yes	Yes	N/A	
Clamping Die	N/A	Yes	Yes	Yes	N/A	
Clamping Chuck	N/A	Yes	Yes	Yes	N/A	
Push Rod	N/A	Yes	Yes	Yes	N/A	0.875 in. diam., 10 in. length
Pressing Route	N/A	Bc	Bc	Bc	N/A	
RESULTS						NOTES
Hardness (HRB)	N/A	N/A	N/A	N/A	N/A	
Grain Size	N/A	N/A	N/A	N/A	N/A	
Visual Inspection	N/A	Accept	Accept	Accept	N/A	No surface cracking or distortion
PHOTOGRAPHS						
						

Table A.28 Research data sheet – 1100 – sample 4


RESEARCH DATA SHEET						
Date:	4-5-14				Process Type:	[x] Discrete [] Continuous
Block	1				Sample Type:	[x] DOE [] Test Run
Whole Plot:	1				Base Alloy:	1100 Aluminum
Sample ID (Run Order):	4				Hardness	23 Brinell
					Grain Size:	N/A
EXPERIMENTAL FACTORS	Level	Pass #1	Pass #2	Pass #3	Average	NOTES
(A) Temperature (°F)	Low	65	N/A	N/A	65	
(B) Number of Passes	Low	1	N/A	N/A	1	Total no. of passes
(C) Back Pressure (lbs.)	High	10	N/A	N/A	10	
(D) Speed: (in./minute)	High	24.4	N/A	N/A	24.4	
(E) Vibration (cpm)	High	9499	N/A	N/A	9499	
PROCESS VARIABLES						NOTES
Indexing Distance (in.)	N/A	0.8125	N/A	N/A	N/A	
Indexing Time (seconds)	N/A	2.0	N/A	N/A	N/A	
Die Insert No.	N/A	1	N/A	N/A	N/A	
Test Rod Diameter (in.)	N/A	0.125	N/A	N/A	N/A	
Test Rod Length (in.)	N/A	0.875	N/A	N/A	N/A	Original rod length
Lubricant	N/A	Yes	N/A	N/A	N/A	EP Dri Slide
Pressing Die	N/A	Yes	N/A	N/A	N/A	
Clamping Die	N/A	Yes	N/A	N/A	N/A	
Clamping Chuck	N/A	Yes	N/A	N/A	N/A	
Push Rod	N/A	Yes	N/A	N/A	N/A	0.875 in. diam., 10 in. length
Pressing Route	N/A	Bc	N/A	N/A	N/A	
RESULTS						NOTES
Hardness (HRB)	N/A	N/A	N/A	N/A	N/A	
Grain Size	N/A	N/A	N/A	N/A	N/A	
Visual Inspection	N/A	Accept	N/A	N/A	N/A	No surface cracking or distortion
PHOTOGRAPHS						
						

Table A.29 Research data sheet – 1100 – sample 5


RESEARCH DATA SHEET						
Date:	4-5-14				Process Type:	[x] Discrete [] Continuous
Block	1				Sample Type:	[x] DOE [] Test Run
Whole Plot:	2				Base Alloy:	1100 Aluminum
Sample ID (Run Order):	5				Hardness	23 Brinell
					Grain Size:	N/A
EXPERIMENTAL FACTORS	Level	Pass #1	Pass #2	Pass #3	Average	NOTES
(A) Temperature (°F)	High	175	175	175	175	
(B) Number of Passes	High	1	1	1	3	Total no. of passes
(C) Back Pressure (lbs.)	Low	0	0	0	0	
(D) Speed: (in./minute)	Low	1.2	1.4	1.1	1.2	
(E) Vibration (cpm)	High	9499	9499	9499	9499	
PROCESS VARIABLES						NOTES
Indexing Distance (in.)	N/A	0.8125	0.7500	0.6250	N/A	
Indexing Time (seconds)	N/A	40.0	33.0	33.0	N/A	
Die Insert No.	N/A	1	1	1	N/A	
Test Rod Diameter (in.)	N/A	0.125	0.125	0.125	N/A	
Test Rod Length (in.)	N/A	0.875	0.875	0.875	N/A	Original rod length
Lubricant	N/A	Yes	Yes	Yes	N/A	EP Dri Slide
Pressing Die	N/A	Yes	Yes	Yes	N/A	
Clamping Die	N/A	Yes	Yes	Yes	N/A	
Clamping Chuck	N/A	Yes	Yes	Yes	N/A	
Push Rod	N/A	Yes	Yes	Yes	N/A	0.875 in. diam., 10 in. length
Pressing Route	N/A	Bc	Bc	Bc	N/A	
RESULTS						NOTES
Hardness (HRB)	N/A	N/A	N/A	N/A	N/A	
Grain Size	N/A	N/A	N/A	N/A	N/A	
Visual Inspection	N/A	Accept	Accept	Accept	N/A	No surface cracking or distortion
PHOTOGRAPHS						
						

Table A.30 Research data sheet – 1100 – sample 6

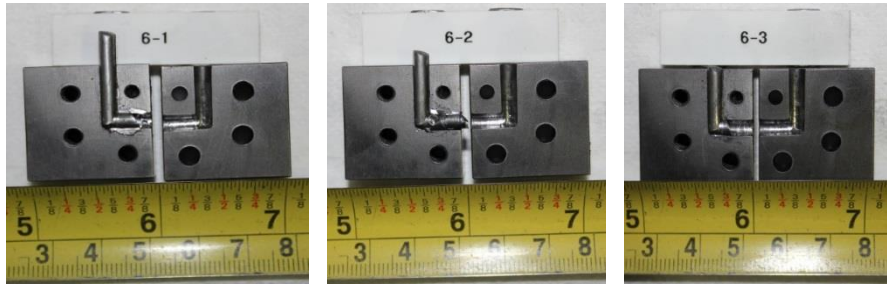
RESEARCH DATA SHEET						
Date:	4-5-14				Process Type:	[x] Discrete [] Continuous
Block	1				Sample Type:	[x] DOE [] Test Run
Whole Plot:	2				Base Alloy:	1100 Aluminum
Sample ID (Run Order):	6				Hardness	23 Brinell
					Grain Size:	N/A
EXPERIMENTAL FACTORS	Level	Pass #1	Pass #2	Pass #3	Average	NOTES
(A) Temperature (°F)	High	172	173	175	173.3	
(B) Number of Passes	High	1	1	1	3	Total no. of passes
(C) Back Pressure (lbs.)	High	10	10	10	10	
(D) Speed: (in./minute)	High	16.3	30.0	28.1	24.8	
(E) Vibration (cpm)	High	9499	9499	9499	9499	
PROCESS VARIABLES						NOTES
Indexing Distance (in.)	N/A	0.8125	0.7500	0.5625	N/A	
Indexing Time (seconds)	N/A	3.0	1.5	1.2	N/A	
Die Insert No.	N/A	1	1	1	N/A	
Test Rod Diameter (in.)	N/A	0.125	0.125	0.125	N/A	
Test Rod Length (in.)	N/A	0.875	0.875	0.875	N/A	Original rod length
Lubricant	N/A	Yes	Yes	Yes	N/A	EP Dri Slide
Pressing Die	N/A	Yes	Yes	Yes	N/A	
Clamping Die	N/A	Yes	Yes	Yes	N/A	
Clamping Chuck	N/A	Yes	Yes	Yes	N/A	
Push Rod	N/A	Yes	Yes	Yes	N/A	0.875 in. diam., 10 in. length
Pressing Route	N/A	Bc	Bc	Bc	N/A	
RESULTS						NOTES
Hardness (HRB)	N/A	N/A	N/A	N/A	N/A	
Grain Size	N/A	N/A	N/A	N/A	N/A	
Visual Inspection	N/A	Accept	Accept	Accept	N/A	No surface cracking or distortion
PHOTOGRAPHS						
						

Table A.31 Research data sheet – 1100 – sample 7


RESEARCH DATA SHEET						
Date:	4-5-14				Process Type:	[x] Discrete [] Continuous
Block	1				Sample Type:	[x] DOE [] Test Run
Whole Plot:	2				Base Alloy:	1100 Aluminum
Sample ID (Run Order):	7				Hardness	23 Brinell
					Grain Size:	N/A
EXPERIMENTAL FACTORS	Level	Pass #1	Pass #2	Pass #3	Average	NOTES
(A) Temperature (°F)	High	172	N/A	N/A	172	
(B) Number of Passes	Low	1	N/A	N/A	1	Total no. of passes
(C) Back Pressure (lbs.)	Low	0	N/A	N/A	0.0	
(D) Speed: (in./minute)	High	30.5	N/A	N/A	30.5	
(E) Vibration (cpm)	Low	0	N/A	N/A	0	
PROCESS VARIABLES						NOTES
Indexing Distance (in.)	N/A	0.8125	N/A	N/A	N/A	
Indexing Time (seconds)	N/A	1.6	N/A	N/A	N/A	
Die Insert No.	N/A	1	N/A	N/A	N/A	
Test Rod Diameter (in.)	N/A	0.125	N/A	N/A	N/A	
Test Rod Length (in.)	N/A	0.875	N/A	N/A	N/A	Original rod length
Lubricant	N/A	Yes	N/A	N/A	N/A	EP Dri Slide
Pressing Die	N/A	Yes	N/A	N/A	N/A	
Clamping Die	N/A	Yes	N/A	N/A	N/A	
Clamping Chuck	N/A	Yes	N/A	N/A	N/A	
Push Rod	N/A	Yes	N/A	N/A	N/A	0.875 in. diam., 10 in. length
Pressing Route	N/A	Bc	N/A	N/A	N/A	
RESULTS						NOTES
Hardness (HRB)	N/A	N/A	N/A	N/A	N/A	
Grain Size	N/A	N/A	N/A	N/A	N/A	
Visual Inspection	N/A	Accept	Accept	Accept	N/A	No surface cracking or distortion
PHOTOGRAPHS						
						

Table A.32 Research data sheet – 1100 – sample 8

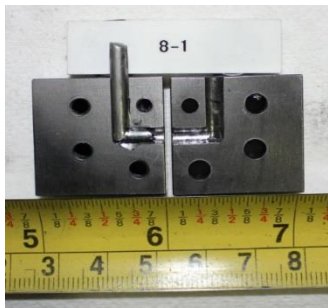
RESEARCH DATA SHEET						
Date:	4-5-14				Process Type:	[x] Discrete [] Continuous
Block	1				Sample Type:	[x] DOE [] Test Run
Whole Plot:	2				Base Alloy:	1100 Aluminum
Sample ID (Run Order):	8				Hardness	23 Brinell
					Grain Size:	N/A
EXPERIMENTAL FACTORS	Level	Pass #1	Pass #2	Pass #3	Average	NOTES
(A) Temperature (°F)	High	172	N/A	N/A	172	
(B) Number of Passes	Low	1	N/A	N/A	1	Total no. of passes
(C) Back Pressure (lbs.)	High	10	N/A	N/A	10	
(D) Speed: (in./minute)	Low	1.1	N/A	N/A	1.1	
(E) Vibration (cpm)	Low	0	N/A	N/A	0	
PROCESS VARIABLES						NOTES
Indexing Distance (in.)	N/A	0.8125	N/A	N/A	N/A	
Indexing Time (seconds)	N/A	45.0	N/A	N/A	N/A	
Die Insert No.	N/A	1	N/A	N/A	N/A	
Test Rod Diameter (in.)	N/A	0.125	N/A	N/A	N/A	
Test Rod Length (in.)	N/A	0.875	N/A	N/A	N/A	Original rod length
Lubricant	N/A	Yes	N/A	N/A	N/A	EP Dri Slide
Pressing Die	N/A	Yes	N/A	N/A	N/A	
Clamping Die	N/A	Yes	N/A	N/A	N/A	
Clamping Chuck	N/A	Yes	N/A	N/A	N/A	
Push Rod	N/A	Yes	N/A	N/A	N/A	0.875 in. diam., 10 in. length
Pressing Route	N/A	Bc	N/A	N/A	N/A	
RESULTS						NOTES
Hardness (HRB)	N/A	N/A	N/A	N/A	N/A	
Grain Size	N/A	N/A	N/A	N/A	N/A	
Visual Inspection	N/A	Accept	Accept	Accept	N/A	No surface cracking or distortion
PHOTOGRAPHS						
						

Table A.33 Research data sheet – 1100 – sample 9

RESEARCH DATA SHEET						
Date:	4-8-14				Process Type:	[x] Discrete [] Continuous
Block	2				Sample Type:	[x] DOE [] Test Run
Whole Plot:	3				Base Alloy:	1100 Aluminum
Sample ID (Run Order):	9				Hardness	23 Brinell
					Grain Size:	N/A
EXPERIMENTAL FACTORS	Level	Pass #1	Pass #2	Pass #3	Average	NOTES
(A) Temperature (°F)	Low	65	65	65	65	
(B) Number of Passes	High	1	1	1	3	Total no. of passes
(C) Back Pressure (lbs.)	Low	0	0	0	0	
(D) Speed: (in./minute)	High	40.6	31.3	30.0	34.0	
(E) Vibration (cpm)	Low	0	0	0	0	
PROCESS VARIABLES						NOTES
Indexing Distance (in.)	N/A	0.8125	0.6250	0.500	N/A	
Indexing Time (seconds)	N/A	1.2	1.2	1.0	N/A	
Die Insert No.	N/A	1	1	1	N/A	
Test Rod Diameter (in.)	N/A	0.125	0.125	0.125	N/A	
Test Rod Length (in.)	N/A	0.875	0.875	0.875	N/A	Original rod length
Lubricant	N/A	Yes	Yes	Yes	N/A	EP Dri Slide
Pressing Die	N/A	Yes	Yes	Yes	N/A	
Clamping Die	N/A	Yes	Yes	Yes	N/A	
Clamping Chuck	N/A	Yes	Yes	Yes	N/A	
Push Rod	N/A	Yes	Yes	Yes	N/A	0.875 in. diam., 10 in. length
Pressing Route	N/A	Bc	Bc	Bc	N/A	
RESULTS						NOTES
Hardness (HRB)	N/A	N/A	N/A	N/A	N/A	
Grain Size	N/A	N/A	N/A	N/A	N/A	
Visual Inspection	N/A	Accept	Accept	Accept	N/A	No surface cracking or distortion
PHOTOGRAPHS						
<p>The photographs show three metal samples, labeled 9-1, 9-2, and 9-3, positioned above a yellow ruler. Each sample is a rectangular block with a central slot and four circular holes. The ruler shows measurements in inches and centimeters, with the samples appearing to be approximately 2.5 inches long.</p>						

Table A.34 Research data sheet – 1100 – sample 10


RESEARCH DATA SHEET						
Date:	4-8-14				Process Type:	[x] Discrete [] Continuous
Block	2				Sample Type:	[x] DOE [] Test Run
Whole Plot:	3				Base Alloy:	1100 Aluminum
Sample ID (Run Order):	10				Hardness	23 Brinell
					Grain Size:	N/A
EXPERIMENTAL FACTORS	Level	Pass #1	Pass #2	Pass #3	Average	NOTES
(A) Temperature (°F)	Low	65	N/A	N/A	65	
(B) Number of Passes	Low	1	N/A	N/A	1	Total no. of passes
(C) Back Pressure (lbs.)	High	10	N/A	N/A	10	
(D) Speed: (in./minute)	High	24.4	N/A	N/A	24.4	
(E) Vibration (cpm)	High	9499	N/A	N/A	9499	
PROCESS VARIABLES						NOTES
Indexing Distance (in.)	N/A	0.8125	N/A	N/A	N/A	
Indexing Time (seconds)	N/A	2.0	N/A	N/A	N/A	
Die Insert No.	N/A	1	N/A	N/A	N/A	
Test Rod Diameter (in.)	N/A	0.125	N/A	N/A	N/A	
Test Rod Length (in.)	N/A	0.875	N/A	N/A	N/A	Original rod length
Lubricant	N/A	Yes	N/A	N/A	N/A	EP Dri Slide
Pressing Die	N/A	Yes	N/A	N/A	N/A	
Clamping Die	N/A	Yes	N/A	N/A	N/A	
Clamping Chuck	N/A	Yes	N/A	N/A	N/A	
Push Rod	N/A	Yes	N/A	N/A	N/A	0.875 in. diam., 10 in. length
Pressing Route	N/A	Bc	N/A	N/A	N/A	
RESULTS						NOTES
Hardness (HRB)	N/A	N/A	N/A	N/A	N/A	
Grain Size	N/A	N/A	N/A	N/A	N/A	
Visual Inspection	N/A	Accept	Accept	Accept	N/A	No surface cracking or distortion
PHOTOGRAPHS						
						

Table A.35 Research data sheet – 1100 – sample 11

RESEARCH DATA SHEET						
Date:	4-8-14				Process Type:	[x] Discrete [] Continuous
Block	2				Sample Type:	[x] DOE [] Test Run
Whole Plot:	3				Base Alloy:	1100 Aluminum
Sample ID (Run Order):	11				Hardness	23 Brinell
					Grain Size:	N/A
EXPERIMENTAL FACTORS	Level	Pass #1	Pass #2	Pass #3	Average	NOTES
(A) Temperature (°F)	Low	65	N/A	N/A	65	
(B) Number of Passes	Low	1	N/A	N/A	1	Total no. of passes
(C) Back Pressure (lbs.)	Low	0	N/A	N/A	0	
(D) Speed: (in./minute)	Low	1.1	N/A	N/A	1.1	
(E) Vibration (cpm)	High	9499	N/A	N/A	9499	
PROCESS VARIABLES						NOTES
Indexing Distance (in.)	N/A	0.8125	N/A	N/A	N/A	
Indexing Time (seconds)	N/A	43.6	N/A	N/A	N/A	
Die Insert No.	N/A	1	N/A	N/A	N/A	
Test Rod Diameter (in.)	N/A	0.125	N/A	N/A	N/A	
Test Rod Length (in.)	N/A	0.875	N/A	N/A	N/A	Original rod length
Lubricant	N/A	Yes	N/A	N/A	N/A	EP Dri Slide
Pressing Die	N/A	Yes	N/A	N/A	N/A	
Clamping Die	N/A	Yes	N/A	N/A	N/A	
Clamping Chuck	N/A	Yes	N/A	N/A	N/A	
Push Rod	N/A	Yes	N/A	N/A	N/A	0.875 in. diam., 10 in. length
Pressing Route	N/A	Bc	N/A	N/A	N/A	
RESULTS						NOTES
Hardness (HRB)	N/A	N/A	N/A	N/A	N/A	
Grain Size	N/A	N/A	N/A	N/A	N/A	
Visual Inspection	N/A	Accept	Accept	Accept	N/A	No surface cracking or distortion
PHOTOGRAPHS						
						

Table A.36 Research data sheet – 1100 – sample 12

RESEARCH DATA SHEET						
Date:	4-8-14				Process Type:	[x] Discrete [] Continuous
Block	2				Sample Type:	[x] DOE [] Test Run
Whole Plot:	3				Base Alloy:	1100 Aluminum
Sample ID (Run Order):	12				Hardness	23 Brinell
					Grain Size:	N/A
EXPERIMENTAL FACTORS	Level	Pass #1	Pass #2	Pass #3	Average	NOTES
(A) Temperature (°F)	Low	65	65	65	65	
(B) Number of Passes	High	1	1	1	3	Total no. of passes
(C) Back Pressure (lbs.)	High	10	10	10	10.0	
(D) Speed: (in./minute)	Low	1.1	1.0	1.2	1.1	
(E) Vibration (cpm)	Low	0	0	0	0	
PROCESS VARIABLES						NOTES
Indexing Distance (in.)	N/A	0.8125	0.7500	0.5625	N/A	
Indexing Time (seconds)	N/A	44.0	46.0	32.5	N/A	
Die Insert No.	N/A	1	1	1	N/A	
Test Rod Diameter (in.)	N/A	0.125	0.125	0.125	N/A	
Test Rod Length (in.)	N/A	0.875	0.875	0.875	N/A	Original rod length
Lubricant	N/A	Yes	Yes	Yes	N/A	EP Dri Slide
Pressing Die	N/A	Yes	Yes	Yes	N/A	
Clamping Die	N/A	Yes	Yes	Yes	N/A	
Clamping Chuck	N/A	Yes	Yes	Yes	N/A	
Push Rod	N/A	Yes	Yes	Yes	N/A	0.875 in. diam., 10 in. length
Pressing Route	N/A	Bc	Bc	Bc	N/A	
RESULTS						NOTES
Hardness (HRB)	N/A	N/A	N/A	N/A	N/A	
Grain Size	N/A	N/A	N/A	N/A	N/A	
Visual Inspection	N/A	Accept	Accept	Accept	N/A	No surface cracking or distortion
PHOTOGRAPHS						
<p>The photographs show three views of a metal part, labeled 12-1, 12-2, and 12-3. Each view shows the part with a yellow ruler placed below it for scale. The ruler has markings in inches and centimeters. The part appears to be a small metal component with a central slot and several holes. The views show different angles of the part, highlighting its geometry and the placement of the ruler for measurement.</p>						

Table A.37 Research data sheet – 1100 – sample 13

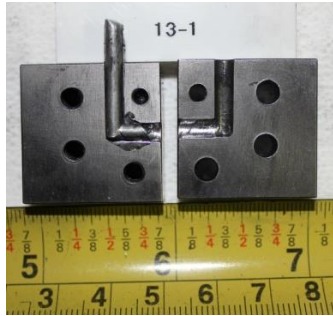
RESEARCH DATA SHEET						
Date:	4-8-14				Process Type:	[x] Discrete [] Continuous
Block	2				Sample Type:	[x] DOE [] Test Run
Whole Plot:	4				Base Alloy:	1100 Aluminum
Sample ID (Run Order):	13				Hardness	23 Brinell
					Grain Size:	N/A
EXPERIMENTAL FACTORS	Level	Pass #1	Pass #2	Pass #3	Average	NOTES
(A) Temperature (°F)	High	175	N/A	N/A	175	
(B) Number of Passes	Low	1	N/A	N/A	1	Total no. of passes
(C) Back Pressure (lbs.)	Low	0	N/A	N/A	0.0	
(D) Speed: (in./minute)	High	32.5	N/A	N/A	32.5	
(E) Vibration (cpm)	Low	0	N/A	N/A	0	
PROCESS VARIABLES						NOTES
Indexing Distance (in.)	N/A	0.8125	N/A	N/A	N/A	
Indexing Time (seconds)	N/A	1.5	N/A	N/A	N/A	
Die Insert No.	N/A	1	N/A	N/A	N/A	
Test Rod Diameter (in.)	N/A	0.125	N/A	N/A	N/A	
Test Rod Length (in.)	N/A	0.875	N/A	N/A	N/A	Original rod length
Lubricant	N/A	Yes	N/A	N/A	N/A	EP Dri Slide
Pressing Die	N/A	Yes	N/A	N/A	N/A	
Clamping Die	N/A	Yes	N/A	N/A	N/A	
Clamping Chuck	N/A	Yes	N/A	N/A	N/A	
Push Rod	N/A	Yes	N/A	N/A	N/A	0.875 in. diam., 10 in. length
Pressing Route	N/A	Bc	N/A	N/A	N/A	
RESULTS						NOTES
Hardness (HRB)	N/A	N/A	N/A	N/A	N/A	
Grain Size	N/A	N/A	N/A	N/A	N/A	
Visual Inspection	N/A	Accept	Accept	Accept	N/A	No surface cracking or distortion
PHOTOGRAPHS						
						

Table A.38 Research data sheet – 1100 – sample 14


RESEARCH DATA SHEET						
Date:	4-8-14				Process Type:	[x] Discrete [] Continuous
Block	2				Sample Type:	[x] DOE [] Test Run
Whole Plot:	4				Base Alloy:	1100 Aluminum
Sample ID (Run Order):	14				Hardness	23 Brinell
					Grain Size:	N/A
EXPERIMENTAL FACTORS	Level	Pass #1	Pass #2	Pass #3	Average	NOTES
(A) Temperature (°F)	High	175	N/A	N/A	175	
(B) Number of Passes	Low	1	N/A	N/A	1	Total no. of passes
(C) Back Pressure (lbs.)	High	10	N/A	N/A	10	
(D) Speed: (in./minute)	Low	1.0	N/A	N/A	1.0	
(E) Vibration (cpm)	Low	0	N/A	N/A	0	
PROCESS VARIABLES						NOTES
Indexing Distance (in.)	N/A	0.8125	N/A	N/A	N/A	
Indexing Time (seconds)	N/A	49.5	N/A	N/A	N/A	
Die Insert No.	N/A	1	N/A	N/A	N/A	
Test Rod Diameter (in.)	N/A	0.125	N/A	N/A	N/A	
Test Rod Length (in.)	N/A	0.875	N/A	N/A	N/A	Original rod length
Lubricant	N/A	Yes	N/A	N/A	N/A	EP Dri Slide
Pressing Die	N/A	Yes	N/A	N/A	N/A	
Clamping Die	N/A	Yes	N/A	N/A	N/A	
Clamping Chuck	N/A	Yes	N/A	N/A	N/A	
Push Rod	N/A	Yes	N/A	N/A	N/A	0.875 in. diam., 10 in. length
Pressing Route	N/A	Bc	N/A	N/A	N/A	
RESULTS						NOTES
Hardness (HRB)	N/A	N/A	N/A	N/A	N/A	
Grain Size	N/A	N/A	N/A	N/A	N/A	
Visual Inspection	N/A	Accept	Accept	Accept	N/A	No surface cracking or distortion
PHOTOGRAPHS						
						

Table A.39 Research data sheet – 1100 – sample 15

RESEARCH DATA SHEET						
Date:	4-8-14				Process Type:	<input checked="" type="checkbox"/> Discrete <input type="checkbox"/> Continuous
Block	2				Sample Type:	<input checked="" type="checkbox"/> DOE <input type="checkbox"/> Test Run
Whole Plot:	4				Base Alloy:	1100 Aluminum
Sample ID (Run Order):	15				Hardness	23 Brinell
					Grain Size:	N/A
EXPERIMENTAL FACTORS	Level	Pass #1	Pass #2	Pass #3	Average	NOTES
(A) Temperature (°F)	High	174.0	174.0	173.7	173.9	
(B) Number of Passes	High	1	1	1	3	Total no. of passes
(C) Back Pressure (lbs.)	Low	0	0	0	0	
(D) Speed: (in./minute)	Low	1.0	1.0	1.2	1.1	
(E) Vibration (cpm)	High	9499	9499	9499	9499	
PROCESS VARIABLES						NOTES
Indexing Distance (in.)	N/A	0.8125	N/A	N/A	N/A	
Indexing Time (seconds)	N/A	47.0	43.0	35.0	N/A	
Die Insert No.	N/A	1	1	1	N/A	
Test Rod Diameter (in.)	N/A	0.125	0.125	0.125	N/A	
Test Rod Length (in.)	N/A	0.875	0.875	0.875	N/A	Original rod length
Lubricant	N/A	Yes	Yes	Yes	N/A	EP Dri Slide
Pressing Die	N/A	Yes	Yes	Yes	N/A	
Clamping Die	N/A	Yes	Yes	Yes	N/A	
Clamping Chuck	N/A	Yes	Yes	Yes	N/A	
Push Rod	N/A	Yes	Yes	Yes	N/A	0.875 in. diam., 10 in. length
Pressing Route	N/A	Bc	Bc	Bc	N/A	
RESULTS						NOTES
Hardness (HRB)	N/A	N/A	N/A	N/A	N/A	
Grain Size	N/A	N/A	N/A	N/A	N/A	
Visual Inspection	N/A	Accept	Accept	Accept	N/A	No surface cracking or distortion
PHOTOGRAPHS						

Table A.40 Research data sheet – 1100 – sample 16


RESEARCH DATA SHEET						
Date:	4-8-14				Process Type:	[x] Discrete [] Continuous
Block	2				Sample Type:	[x] DOE [] Test Run
Whole Plot:	4				Base Alloy:	1100 Aluminum
Sample ID (Run Order):	16				Hardness	23 Brinell
					Grain Size:	N/A
EXPERIMENTAL FACTORS	Level	Pass #1	Pass #2	Pass #3	Average	NOTES
(A) Temperature (°F)	High	174.9	175.0	174.0	174.6	
(B) Number of Passes	High	1	1	1	3	Total no. of passes
(C) Back Pressure (lbs.)	High	10	10	10	10	
(D) Speed: (in./minute)	High	34.8	30.0	37.5	34.1	
(E) Vibration (cpm)	High	9499	9499	9499	9499	
PROCESS VARIABLES						NOTES
Indexing Distance (in.)	N/A	0.8125	0.7500	0.6250	N/A	
Indexing Time (seconds)	N/A	1.4	1.5	1.0	N/A	
Die Insert No.	N/A	1	1	1	N/A	
Test Rod Diameter (in.)	N/A	0.125	0.125	0.125	N/A	
Test Rod Length (in.)	N/A	0.875	0.875	0.875	N/A	Original rod length
Lubricant	N/A	Yes	Yes	Yes	N/A	EP Dri Slide
Pressing Die	N/A	Yes	Yes	Yes	N/A	
Clamping Die	N/A	Yes	Yes	Yes	N/A	
Clamping Chuck	N/A	Yes	Yes	Yes	N/A	
Push Rod	N/A	Yes	Yes	Yes	N/A	0.875 in. diam., 10 in. length
Pressing Route	N/A	Bc	Bc	Bc	N/A	
RESULTS						NOTES
Hardness (HRB)	N/A	N/A	N/A	N/A	N/A	
Grain Size	N/A	N/A	N/A	N/A	N/A	
Visual Inspection	N/A	Accept	Accept	Accept	N/A	No surface cracking or distortion
PHOTOGRAPHS						
						

Table A.41 Research data sheet – 1100 – sample 17


RESEARCH DATA SHEET						
Date:	4-10-14				Process Type:	[x] Discrete [] Continuous
Block	3				Sample Type:	[x] DOE [] Test Run
Whole Plot:	5				Base Alloy:	1100 Aluminum
Sample ID (Run Order):	17				Hardness	23 Brinell
					Grain Size:	N/A
EXPERIMENTAL FACTORS	Level	Pass #1	Pass #2	Pass #3	Average	NOTES
(A) Temperature (°F)	Low	83.2	83.2	83.2	83.2	
(B) Number of Passes	High	1	1	1	3	Total no. of passes
(C) Back Pressure (lbs.)	High	10	10	10	10.0	
(D) Speed: (in./minute)	Low	1.2	1.2	1.1	1.1	
(E) Vibration (cpm)	Low	0	0	0	0.0	
PROCESS VARIABLES						NOTES
Indexing Distance (in.)	N/A	0.8125	0.7500	0.5625	N/A	
Indexing Time (seconds)	N/A	41.0	38.6	31.8	N/A	
Die Insert No.	N/A	1	1	1	N/A	
Test Rod Diameter (in.)	N/A	0.125	0.125	0.125	N/A	
Test Rod Length (in.)	N/A	0.875	0.875	0.875	N/A	Original rod length
Lubricant	N/A	Yes	Yes	Yes	N/A	EP Dri Slide
Pressing Die	N/A	Yes	Yes	Yes	N/A	
Clamping Die	N/A	Yes	Yes	Yes	N/A	
Clamping Chuck	N/A	Yes	Yes	Yes	N/A	
Push Rod	N/A	Yes	Yes	Yes	N/A	0.875 in. diam., 10 in. length
Pressing Route	N/A	Bc	Bc	Bc	N/A	
RESULTS						NOTES
Hardness (HRB)	N/A	N/A	N/A	N/A	N/A	
Grain Size	N/A	N/A	N/A	N/A	N/A	
Visual Inspection	N/A	Accept	Accept	Accept	N/A	No surface cracking or distortion
PHOTOGRAPHS						
 <p>The photographs show three metal samples, labeled 17-1, 17-2, and 17-3, which are U-shaped components. Each sample is placed on a yellow ruler for scale. The ruler shows inches from 5 to 8. The samples appear to be made of a dark metal, possibly aluminum, and have a consistent shape and size across the three images.</p>						

Table A.42 Research data sheet – 1100 – sample 18

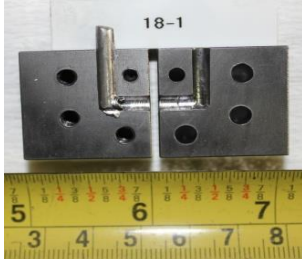
RESEARCH DATA SHEET						
Date:	4-10-14				Process Type:	[x] Discrete [] Continuous
Block	3				Sample Type:	[x] DOE [] Test Run
Whole Plot:	5				Base Alloy:	1100 Aluminum
Sample ID (Run Order):	18				Hardness	23 Brinell
					Grain Size:	N/A
EXPERIMENTAL FACTORS	Level	Pass #1	Pass #2	Pass #3	Average	NOTES
(A) Temperature (°F)	Low	83.2	N/A	N/A	83.2	
(B) Number of Passes	Low	1	N/A	N/A	1	Total no. of passes
(C) Back Pressure (lbs.)	High	10	N/A	N/A	10	
(D) Speed: (in./minute)	High	32.5	N/A	N/A	32.5	
(E) Vibration (cpm)	High	9499	N/A	N/A	9499	
PROCESS VARIABLES						NOTES
Indexing Distance (in.)	N/A	0.8125	N/A	N/A	N/A	
Indexing Time (seconds)	N/A	1.5	N/A	N/A	N/A	
Die Insert No.	N/A	1	N/A	N/A	N/A	
Test Rod Diameter (in.)	N/A	0.125	N/A	N/A	N/A	
Test Rod Length (in.)	N/A	0.875	N/A	N/A	N/A	Original rod length
Lubricant	N/A	Yes	N/A	N/A	N/A	EP Dri Slide
Pressing Die	N/A	Yes	N/A	N/A	N/A	
Clamping Die	N/A	Yes	N/A	N/A	N/A	
Clamping Chuck	N/A	Yes	N/A	N/A	N/A	
Push Rod	N/A	Yes	N/A	N/A	N/A	0.875 in. diam., 10 in. length
Pressing Route	N/A	Bc	N/A	N/A	N/A	
RESULTS						NOTES
Hardness (HRB)	N/A	N/A	N/A	N/A	N/A	
Grain Size	N/A	N/A	N/A	N/A	N/A	
Visual Inspection	N/A	Accept	Accept	Accept	N/A	No surface cracking or distortion
PHOTOGRAPHS						
						

Table A.43 Research data sheet – 1100 – sample 19


RESEARCH DATA SHEET						
Date:	4-10-14				Process Type:	[x] Discrete [] Continuous
Block	3				Sample Type:	[x] DOE [] Test Run
Whole Plot:	5				Base Alloy:	1100 Aluminum
Sample ID (Run Order):	19				Hardness	23 Brinell
					Grain Size:	N/A
EXPERIMENTAL FACTORS	Level	Pass #1	Pass #2	Pass #3	Average	NOTES
(A) Temperature (°F)	Low	83.2	N/A	N/A	83.2	
(B) Number of Passes	Low	1	N/A	N/A	1	Total no. of passes
(C) Back Pressure (lbs.)	Low	0	N/A	N/A	0	
(D) Speed: (in./minute)	Low	1.0	N/A	N/A	1.0	
(E) Vibration (cpm)	High	9499	N/A	N/A	9499	
PROCESS VARIABLES						NOTES
Indexing Distance (in.)	N/A	0.8125	N/A	N/A	N/A	
Indexing Time (seconds)	N/A	47.0	N/A	N/A	N/A	
Die Insert No.	N/A	1	N/A	N/A	N/A	
Test Rod Diameter (in.)	N/A	0.125	N/A	N/A	N/A	
Test Rod Length (in.)	N/A	0.875	N/A	N/A	N/A	Original rod length
Lubricant	N/A	Yes	N/A	N/A	N/A	EP Dri Slide
Pressing Die	N/A	Yes	N/A	N/A	N/A	
Clamping Die	N/A	Yes	N/A	N/A	N/A	
Clamping Chuck	N/A	Yes	N/A	N/A	N/A	
Push Rod	N/A	Yes	N/A	N/A	N/A	0.875 in. diam., 10 in. length
Pressing Route	N/A	Bc	N/A	N/A	N/A	
RESULTS						NOTES
Hardness (HRB)	N/A	N/A	N/A	N/A	N/A	
Grain Size	N/A	N/A	N/A	N/A	N/A	
Visual Inspection	N/A	Accept	Accept	Accept	N/A	No surface cracking or distortion
PHOTOGRAPHS						
						

Table A.44 Research data sheet – 1100 – sample 20

RESEARCH DATA SHEET						
Date:	4-10-14				Process Type:	[x] Discrete [] Continuous
Block	3				Sample Type:	[x] DOE [] Test Run
Whole Plot:	5				Base Alloy:	1100 Aluminum
Sample ID (Run Order):	20				Hardness	23 Brinell
					Grain Size:	N/A
EXPERIMENTAL FACTORS	Level	Pass #1	Pass #2	Pass #3	Average	NOTES
(A) Temperature (°F)	Low	83.2	83.2	83.2	83.2	
(B) Number of Passes	High	1	1	1	3	Total no. of passes
(C) Back Pressure (lbs.)	Low	0	0	0	0	
(D) Speed: (in./minute)	High	40.6	25.0	33.8	33.1	
(E) Vibration (cpm)	Low	0	0	0	0	
PROCESS VARIABLES						NOTES
Indexing Distance (in.)	N/A	0.8125	0.7500	0.5625	N/A	
Indexing Time (seconds)	N/A	1.2	1.8	1.0	N/A	
Die Insert No.	N/A	1	1	1	N/A	
Test Rod Diameter (in.)	N/A	0.125	0.125	0.125	N/A	
Test Rod Length (in.)	N/A	0.875	0.875	0.875	N/A	Original rod length
Lubricant	N/A	Yes	Yes	Yes	N/A	EP Dri Slide
Pressing Die	N/A	Yes	Yes	Yes	N/A	
Clamping Die	N/A	Yes	Yes	Yes	N/A	
Clamping Chuck	N/A	Yes	Yes	Yes	N/A	
Push Rod	N/A	Yes	Yes	Yes	N/A	0.875 in. diam., 10 in. length
Pressing Route	N/A	Bc	Bc	Bc	N/A	
RESULTS						NOTES
Hardness (HRB)	N/A	N/A	N/A	N/A	N/A	
Grain Size	N/A	N/A	N/A	N/A	N/A	
Visual Inspection	N/A	Accept	Accept	Accept	N/A	No surface cracking or distortion
PHOTOGRAPHS						
 <p>The photographs show three metal samples, labeled 20-1, 20-2, and 20-3, which are rectangular blocks with a central slot and four circular holes on each side. Each sample is placed on a yellow ruler for scale. The ruler shows inches and centimeters. The samples appear to be made of a dark metal, possibly aluminum, and have a smooth, machined surface.</p>						

Table A.45 Research data sheet – 1100 – sample 21

RESEARCH DATA SHEET						
Date:	4-10-14				Process Type:	[x] Discrete [] Continuous
Block	3				Sample Type:	[x] DOE [] Test Run
Whole Plot:	6				Base Alloy:	1100 Aluminum
Sample ID (Run Order):	21				Hardness	23 Brinell
					Grain Size:	N/A
EXPERIMENTAL FACTORS	Level	Pass #1	Pass #2	Pass #3	Average	NOTES
(A) Temperature (°F)	High	174.8	174.5	175.0	174.8	
(B) Number of Passes	High	1	1	1	3	Total no. of passes
(C) Back Pressure (lbs.)	Low	0	0	0	0	
(D) Speed: (in./minute)	Low	1.0	0.9	0.9	0.9	
(E) Vibration (cpm)	High	9499	9499	9499	9499	
PROCESS VARIABLES						NOTES
Indexing Distance (in.)	N/A	0.8125	0.7500	0.6250	N/A	
Indexing Time (seconds)	N/A	48.5	49.5	42.0	N/A	
Die Insert No.	N/A	1	1	1	N/A	
Test Rod Diameter (in.)	N/A	0.125	0.125	0.125	N/A	
Test Rod Length (in.)	N/A	0.875	0.875	0.875	N/A	Original rod length
Lubricant	N/A	Yes	Yes	Yes	N/A	EP Dri Slide
Pressing Die	N/A	Yes	Yes	Yes	N/A	
Clamping Die	N/A	Yes	Yes	Yes	N/A	
Clamping Chuck	N/A	Yes	Yes	Yes	N/A	
Push Rod	N/A	Yes	Yes	Yes	N/A	0.875 in. diam., 10 in. length
Pressing Route	N/A	Bc	Bc	Bc	N/A	
RESULTS						NOTES
Hardness (HRB)	N/A	N/A	N/A	N/A	N/A	
Grain Size	N/A	N/A	N/A	N/A	N/A	
Visual Inspection	N/A	Accept	Accept	Accept	N/A	No surface cracking or distortion
PHOTOGRAPHS						
<p>The photographs show three metal samples, labeled 21-1, 21-2, and 21-3, which are U-shaped components. Each sample is placed on a yellow ruler for scale. The ruler shows markings from 3 to 8 inches. The samples appear to be made of a dark metal and have a consistent U-shaped profile with two circular holes on each side.</p>						

Table A.46 Research data sheet – 1100 – sample 22

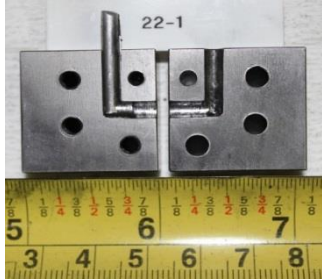
RESEARCH DATA SHEET						
Date:	4-10-14				Process Type:	[x] Discrete [] Continuous
Block	3				Sample Type:	[x] DOE [] Test Run
Whole Plot:	6				Base Alloy:	1100 Aluminum
Sample ID (Run Order):	22				Hardness	23 Brinell
					Grain Size:	N/A
EXPERIMENTAL FACTORS	Level	Pass #1	Pass #2	Pass #3	Average	NOTES
(A) Temperature (°F)	High	175.7	N/A	N/A	175.7	
(B) Number of Passes	Low	1	N/A	N/A	1	Total no. of passes
(C) Back Pressure (lbs.)	High	10	N/A	N/A	10	
(D) Speed: (in./minute)	Low	0.9	N/A	N/A	0.9	
(E) Vibration (cpm)	Low	0	N/A	N/A	0	
PROCESS VARIABLES						NOTES
Indexing Distance (in.)	N/A	0.8125	N/A	N/A	N/A	
Indexing Time (seconds)	N/A	53.5	N/A	N/A	N/A	
Die Insert No.	N/A	1	N/A	N/A	N/A	
Test Rod Diameter (in.)	N/A	0.125	N/A	N/A	N/A	
Test Rod Length (in.)	N/A	0.875	N/A	N/A	N/A	Original rod length
Lubricant	N/A	Yes	N/A	N/A	N/A	EP Dri Slide
Pressing Die	N/A	Yes	N/A	N/A	N/A	
Clamping Die	N/A	Yes	N/A	N/A	N/A	
Clamping Chuck	N/A	Yes	N/A	N/A	N/A	
Push Rod	N/A	Yes	N/A	N/A	N/A	0.875 in. diam., 10 in. length
Pressing Route	N/A	Bc	N/A	N/A	N/A	
RESULTS						NOTES
Hardness (HRB)	N/A	N/A	N/A	N/A	N/A	
Grain Size	N/A	N/A	N/A	N/A	N/A	
Visual Inspection	N/A	Accept	Accept	Accept	N/A	No surface cracking or distortion
PHOTOGRAPHS						
						

Table A.47 Research data sheet – 1100 – sample 23

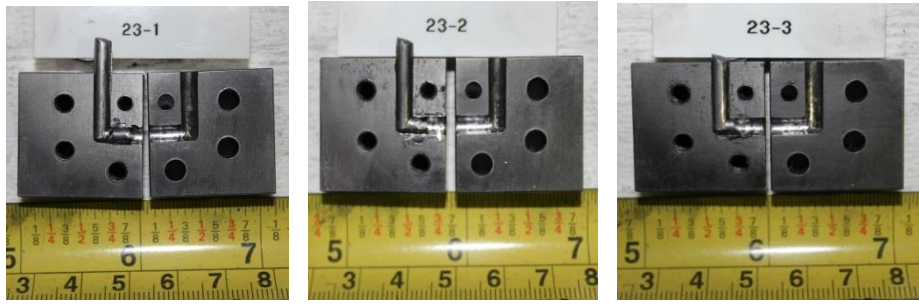
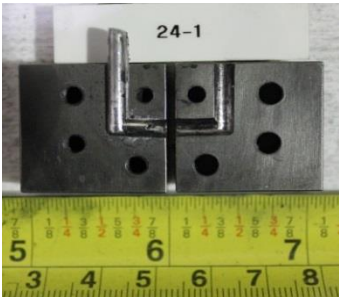
RESEARCH DATA SHEET						
Date:	4-10-14				Process Type:	[x] Discrete [] Continuous
Block	3				Sample Type:	[x] DOE [] Test Run
Whole Plot:	6				Base Alloy:	1100 Aluminum
Sample ID (Run Order):	23				Hardness	23 Brinell
					Grain Size:	N/A
EXPERIMENTAL FACTORS	Level	Pass #1	Pass #2	Pass #3	Average	NOTES
(A) Temperature (°F)	High	175.5	175.0	176.2	176.2	
(B) Number of Passes	High	1	1	1	3	Total no. of passes
(C) Back Pressure (lbs.)	High	10	10	10	10	
(D) Speed: (in./minute)	High	32.5	1.0	13.5	15.7	
(E) Vibration (cpm)	High	9499	9499	9499	9499	
PROCESS VARIABLES						NOTES
Indexing Distance (in.)	N/A	0.8125	0.7500	0.5625	N/A	
Indexing Time (seconds)	N/A	1.5	45.0	2.5	N/A	
Die Insert No.	N/A	1	1	1	N/A	
Test Rod Diameter (in.)	N/A	0.125	0.125	0.125	N/A	
Test Rod Length (in.)	N/A	0.875	0.875	0.875	N/A	Original rod length
Lubricant	N/A	Yes	Yes	Yes	N/A	EP Dri Slide
Pressing Die	N/A	Yes	Yes	Yes	N/A	
Clamping Die	N/A	Yes	Yes	Yes	N/A	
Clamping Chuck	N/A	Yes	Yes	Yes	N/A	
Push Rod	N/A	Yes	Yes	Yes	N/A	0.875 in. diam., 10 in. length
Pressing Route	N/A	Bc	Bc	Bc	N/A	
RESULTS						NOTES
Hardness (HRB)	N/A	N/A	N/A	N/A	N/A	
Grain Size	N/A	N/A	N/A	N/A	N/A	
Visual Inspection	N/A	Accept	Accept	Accept	N/A	No surface cracking or distortion
PHOTOGRAPHS						
						

Table A.48 Research data sheet – 1100 – sample 24

RESEARCH DATA SHEET						
Date:	4-10-14				Process Type:	[x] Discrete [] Continuous
Block	3				Sample Type:	[x] DOE [] Test Run
Whole Plot:	6				Base Alloy:	1100 Aluminum
Sample ID (Run Order):	24				Hardness	23 Brinell
					Grain Size:	N/A
EXPERIMENTAL FACTORS	Level	Pass #1	Pass #2	Pass #3	Average	NOTES
(A) Temperature (°F)	High	175.7	N/A	N/A	175.7	
(B) Number of Passes	Low	1	N/A	N/A	1	Total no. of passes
(C) Back Pressure (lbs.)	Low	0	N/A	N/A	0.0	
(D) Speed: (in./minute)	High	40.6	N/A	N/A	40.6	
(E) Vibration (cpm)	Low	0	N/A	N/A	0	
PROCESS VARIABLES						NOTES
Indexing Distance (in.)	N/A	0.8125	N/A	N/A	N/A	
Indexing Time (seconds)	N/A	1.2	N/A	N/A	N/A	
Die Insert No.	N/A	1	N/A	N/A	N/A	
Test Rod Diameter (in.)	N/A	0.125	N/A	N/A	N/A	
Test Rod Length (in.)	N/A	0.875	N/A	N/A	N/A	Original rod length
Lubricant	N/A	Yes	N/A	N/A	N/A	EP Dri Slide
Pressing Die	N/A	Yes	N/A	N/A	N/A	
Clamping Die	N/A	Yes	N/A	N/A	N/A	
Clamping Chuck	N/A	Yes	N/A	N/A	N/A	
Push Rod	N/A	Yes	N/A	N/A	N/A	0.875 in. diam., 10 in. length
Pressing Route	N/A	Bc	N/A	N/A	N/A	
RESULTS						NOTES
Hardness (HRB)	N/A	N/A	N/A	N/A	N/A	
Grain Size	N/A	N/A	N/A	N/A	N/A	
Visual Inspection	N/A	Accept	Accept	Accept	N/A	No surface cracking or distortion
PHOTOGRAPHS						
						

APPENDIX B
THERMAL REQUIREMENTS

Thermal requirements for design and selection of cartridge heaters are determined using the following engineering analysis (<http://www.deltat.com/sitemap.html>):

Process Description

Heating requirements are needed for two steel dies, one being the clamping die and the other being the pressing die. Both dies, however, are 2" x 3" x 3.25" rectangular blocks of 4340 alloy steel as shown in Figure 13. Therefore, wattage requirements will be the same for both. The process will be designed to accommodate pressing of 1/8" and 5/32" diameter metal rods. Thermal design calculations will be made for the 316 stainless steel which will provide sufficient wattage for both the stainless steel and aluminum materials being studied. Pressing speeds used to move the rods through the dies will be 12 mm/minute (0.4724 inches/minute) and 60 mm/minute (2.3622 inches/minute), respectively. During die heat up, both dies will be positioned together with their respective face plates in contact with each other. With the exception of the vertical surfaces of each die faceplate where the rod will pass through, all remaining die surfaces will be coated with an Envirotrol[®] insulating layer. Based on the manufacturer's specifications, applying a 0.060" thick coating at process temperatures operating at 320 °F will reduce surface temperatures on the exterior side of the coating by 50%. In other words, heat loss will be cut in half allowing the exposed coated surfaces of the Ix-ECAP dies to be operating at approximately 150 to 160 °F.

Even though the die face plates will contact each other at the end of each indexing cycle, the contact time is extremely small compared to the overall cycle time. Therefore, an assumption is made that the non-insulated vertical contact surfaces of the pressing and

clamping dies are exposed emitting heat during the actual indexing process once a pre-heat of the dies has been established.

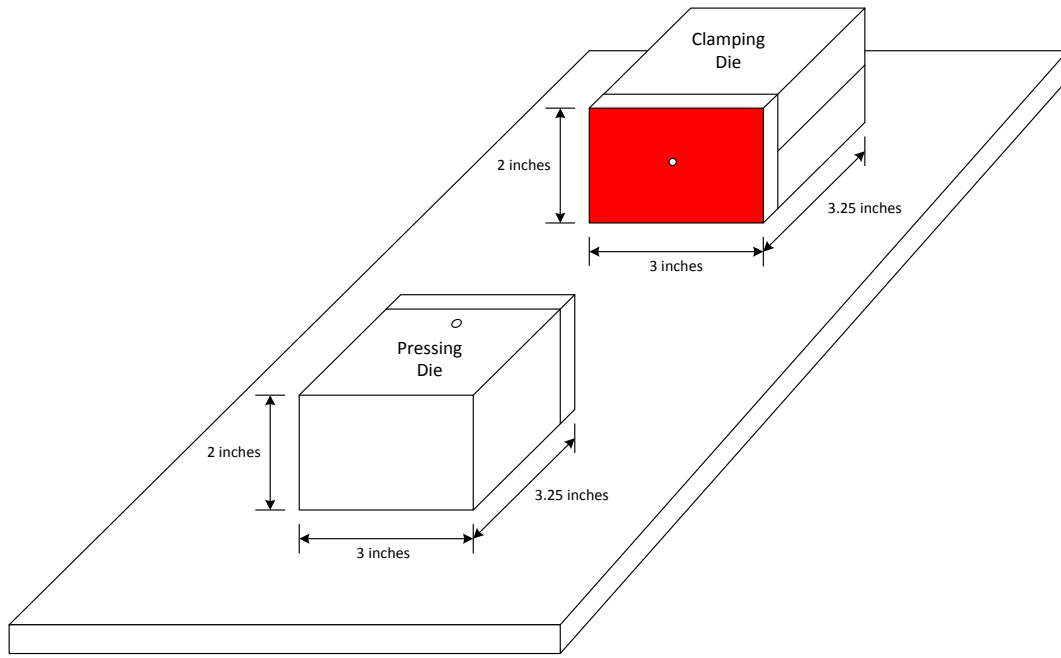


Figure B.1 Pressing and clamping die dimensions

Note: Red area represents non-insulated surface of die

Considerations

Beginning to final temperature: 70 - 302 °F (21 – 150 °C)

Time available for process start-up: 1 hour

Process cycle time:

37 seconds = 0.617 minutes = 0.0103 hour (for pressing speed at 0.4724 inches/minute)

12 seconds = 0.106 minutes = 0.00176 hour (for pressing speed at 2.3622 inches/minute)

Material weight and thermal properties:

Specific heat of die steel: 0.12 Btu/lb/°F

Specific heat of 316 stainless steel rod: 0.116 Btu/lb/°F

Density of die steel (ρ): 0.28 lbs/in³

Weight of each die: (2" x 3" x 3.25")(0.28 lbs/in³) = 5.04 lbs

Weight of 0.25" long, 5/32" diam. rod: $\pi^2 h \rho$
= $\pi(0.078125 \text{ in.})^2(0.25 \text{ in.})(0.28 \text{ lbs/in}^3)$
= 0.00134 lbs.

Exposed surface areas and heat losses:

No insulation on vertical face plate contact areas (red area in Figure B.1).

All remaining exterior surfaces insulated.

50% heat loss reduction for insulated surfaces.

Non-insulated die face plate area: 2" x 3" = 6 in.² = 0.04167 ft.²

Insulated die surface areas: 1(2" x 3") + 2(3.25" x 2") + 2(3" x 3.25") = 38.5 in.²
= 0.2673 ft²

Heat losses from non-insulated metal surfaces: 275 watts/ ft² at 350 °F

Heat losses from insulated metal surfaces: 50% (275 watts/ ft²) = 137.5 watts/ ft²

Contingency or Safety Factor: CF = 30%

Wattage Requirement Calculations

Q_{ha} = heat absorbed during process start up, kwh

Q_{ls} = system heat losses, kwh

CF = contingency or safety factor, %

kwh = required kilowatt hours

kw = required kilowatts

Q_{ha} :

$$= \frac{(\text{weight, lbs}) (\text{specific heat, Btu/lb/}^\circ\text{F})(\text{final} - \text{starting temperature, }^\circ\text{F})}{3412 \text{ Btu/kwh}}$$

$$Q_{ls} = \frac{(\text{exposed surface area, sq. ft.}) \left(\text{loss at final temp., } \frac{\text{watts}}{\text{sq ft}} \right) (\text{time to start up, hrs})(0.5)}{1,000 \text{ w/kw}}$$

$$CF = \%(Q_{ha} + Q_{ls})$$

$$\text{kwh} = Q_{ha} + Q_{ls} + CF$$

$$\text{kw} = \frac{Q_{ha} + Q_{ls} + CF}{\text{hours allowed for process start up}}$$

Step 1: Wattage Required for Process Start Up:

Since both the clamping and pressing dies are closed during process start up, no heat loss occurs on the vertical face plate contact surfaces of the dies. Heat losses on all remaining protected surfaces, however, must be considered.

Q_{ha} = heat absorbed during process start up to heat die from 70 to 302 °F

$$Q_{ha} = \frac{(5.04 \text{ lbs}) (0.12 \text{ Btu/lb/}^\circ\text{F})(302 - 70 \text{ }^\circ\text{F})}{3412 \text{ Btu/kwh}} = 0.04112 \text{ kwh}$$

Q_{ls} = system heat losses by each die at insulated surfaces

$$Q_{ls} = \frac{(0.26736 \text{ sq.ft.}) \left(137.5 \frac{\text{watts}}{\text{sq ft}} \right) (1 \text{ hr})(0.5)}{1,000 \text{ w/kw}} = 0.01838 \text{ kwh}$$

CF = contingency or safety factor, 30%

$$CF = \%(Q_{ha} + Q_{ls}) = 0.30(0.04112 + 0.01838) = 0.01785 \text{ kwh}$$

kwh = required kilowatt hours

$$\text{kwh} = Q_{\text{ha}} + Q_{\text{ls}} + \text{CF} = 0.04112 + 0.01838 + 0.01785 = 0.07735 \text{ kwh}$$

kw = required kilowatts

$$\text{kw} = \frac{Q_{\text{ha}} + Q_{\text{ls}} + \text{CF}}{\text{hours allowed for process start up}} = \frac{0.07735 \text{ kwh}}{1 \text{ hour}} = 0.07735 \text{ kw}$$
$$= 77.35 \text{ watts}$$

Total wattage required for process start up = 77.35 watts

Step 2: Wattage Required for Process Operation:

The indexing cycle begins by clamping the metal rod in place while the pressing die is in the backmost position. The pressing die is then moved forward until both die face plates contact each other. The clamping force is released, and the pressing die is indexed backwards to begin the process again. Based on this scenario, the portion of the cycle time when the die face plates actually contact one another is very small compared to the total cycle time. Thermal requirements will be based on the assumption that heat is continuously emitted from the die face plate vertical surfaces throughout the process cycle. Heat losses through the die face plate, therefore, must be considered in the calculation of wattage requirements. Additional heat losses must also consider the exposed insulated coated surface areas as noted in Step 1. Maximum thermal requirements will be determined from the weight of the larger 5/32" diameter metal rods 0.250" long being processed at the higher pressing speed of 2.3633 inches/minute. This

length of 0.250” for the metal rod represents the indexing length for each cycle of the Ix-ECAP process.

Q_{ha2} = heat absorbed by new rods being processed or heated from 70 to 302 °F

$$Q_{ha2} = \frac{(0.00134 \text{ lbs}) (0.12 \text{ Btu/lb/°F})(302 - 70 \text{ °F})}{3412 \text{ Btu/kwh}} = 0.0000109 \text{ kwh}$$

Q_{Is2a} = system heat losses of the die at the insulated surfaces

$$Q_{Is2a} = \frac{(0.26736 \text{ sq.ft.}) \left(137.5 \frac{\text{watts}}{\text{sq ft}}\right) (0.00176 \text{ hr})}{1,000 \text{ w/kw}} = 0.0000647 \text{ kwh}$$

Q_{Is2b} = system heat losses by non insulated die face plate surface

$$Q_{Is2b} = \frac{(0.04167 \text{ sq. ft.}) \left(275 \frac{\text{watts}}{\text{sq ft}}\right) (0.00176 \text{ hr})}{1,000 \text{ w/kw}} = 0.0000202 \text{ kwh}$$

CF = contingency or safety factor, 30%

$$CF = 0.30(0.0000109 + 0.0000647 + 0.0000202) = 0.0000582 \text{ kwh}$$

kwh = required kilowatt hours for the 60 mm/minute pressing speed cycle time

$$\text{kwh} = 0.0000109 + 0.0000647 + 0.0000202 + 0.0000582 = 0.0000154 \text{ kwh}$$

kw = required kilowatts

$$\text{kw} = \frac{\text{kwh}}{\text{cycle time, hours}} = \frac{0.0000154 \text{ kwh}}{0.00176 \text{ hr}} = 0.0875 \text{ kw} = 87.50 \text{ watts}$$

Total wattage required for process operation = 87.50 watts

Step 3: Cartridge Heater Selection:

As can be seen from the thermal calculations in Steps 1 & 2, the wattage requirements for both the process start up and process operation are very close. To heat the dies from 70 to 302 °F during process start up requires 77.35 watts; whereas, process operation requires 87.50 watts. The increased wattage requirement for actually running the process at this elevated temperature is due to the higher heat losses at the exposed die face plate surfaces. Therefore, to simplify die heater design, the size and number of cartridge heaters will be selected to equally provide at least 87.5 watts to each of the clamping and pressing dies. This criterion will be met by using four 65 watt 4” long cartridge heaters per die. Total wattage will be 260 watts per die which provides a large contingency in the event additional heat is required for higher temperatures or one of the heaters fails during operation. Additionally, this particular size cartridge heater operates at a low wattage density of 34 watts/in.² which provides improved heat distribution and reduced potential for overheating of the cartridge heaters resulting in sticking to the die. A cartridge heater is shown in Figure 14.



Figure B.2 Cartridge heater